University of Southampton

Faculty of Engineering and Physical Sciences

School of Chemistry

Exploring the Cytotoxicity of DNA Nanopores for Treatment of Melanoma

Volume 1 of 1

by

Lauren Lucinda Entwistle

Thesis for the degree of Doctor of Philosophy

May 2020

University of Southampton

Abstract

Faculty of Engineering and Physical Sciences

School of Chemistry

Thesis for the degree of Doctor of Philosophy

Exploring the Cytotoxicity of DNA Nanopores for Treatment of Melanoma

by

Lauren Lucinda Entwistle

According to Cancer Research UK "incidence rates for melanoma skin cancer are projected to rise by 7% in the UK between 2014 and 2035, to 32 cases per 100,000 people by 2035"[1], showing there will be an increased need for therapeutics for melanoma in the coming years. Current treatments such as chemo- and radiation therapy are nonspecific and carry undesirable side effects, thus new targeted therapies are in dire need. This thesis proposed to use a deoxyribonucleic acid (DNA) nanopore – peptide hybrid that will target melanoma cells, with little collateral damage to surrounding tissues. It has been shown that DNA nanopores produce a cytotoxic effect when embedded into the cell membrane[2]. By conjugating DNA nanopores with the known receptor targeting peptide, NAP-amide, a novel melanoma targeted therapy for advanced disease was proposed.

DNA nanopores are a simple form of DNA origami, where DNA strands fold into a predetermined shape, utilising the specific interactions of Watson-Crick DNA base pairing. The nanosized particles are formed by combining a custom-designed set of single stranded DNA, some of which can be modified during or after solid phase synthesis. We have modified two different sized (2 nm and 0.8 nm) nanopore constructs which were previously published[3, 4] using the hydrophobic compounds, cholesterol and palmitate, and investigated these for cytotoxicity in HEK293T, B16-F10 and FM55-P cells in a proof-of-concept study. Further modifications of a tetraphenyl porphyrin were made for a bi-modal photodynamic therapeutic, not only as hydrophobic anchors but also as photosensitizers in a human melanoma cell line.

Table of Contents

Table of Tables

Table of Figures

Table of Figures

Table of Figures

Table of Figures

Table of Figures

Table of Figures

Table of Figures

Research Thesis: Declaration of Authorship

Print name:	Lauren Lucinda Entwistle

Title of thesis:	Exploring the Cytotoxicity of DNA Nanopores for Treatment of Melanoma

I declare that this thesis and the work presented in it are my own and has been generated by me as the result of my own original research.

I confirm that:

1. This work was done wholly or mainly while in candidature for a research degree at this University;
2. Where any part of this thesis has previously been submitted for a degree or any other qualification at this University or any other institution, this has been clearly stated;
3. Where I have consulted the published work of others, this is always clearly attributed;
4. Where I have quoted from the work of others, the source is always given. With the exception of such quotations, this thesis is entirely my own work;
5. I have acknowledged all main sources of help;
6. Where the thesis is based on work done by myself jointly with others, I have made clear exactly what was done by others and what I have contributed myself;
7. None of this work has been published before submission

Signature:		Date:	19/05/2020

Acknowledgements

I would like to extend my thanks to my supervisors throughout my studies; Associate professor Eugen Stulz, Associate professor Paul Bigliardi, Associate professor David Leavesley and Dr Bhimsen Rout, for their academic support and guiding me through my studies.

I have been a part of many different lab groups throughout my PhD which means that I have a lot of people to thank for their support in different stages of my studies. From the original Stulz group, Jo, James, Iwona and our adopted Matt to my final year lab buddies Andrea and Christina, I thank you for all your emotional and chemical support. For all the biological skills I have gained I have to express thanks to Christine Newmann, Akanksha Pant and to my dear friend Alicia Yap who showed me friendship can last years and distance.

Finally, and most importantly I must thank my family. The Sargisson, Swatton and Entwistle clans I love you all. Bob you are everything to me. Words cannot express how much I owe you for your love and support through this all.

For Mum – who always believed in me

Abbreviations

UV	-	Ultra violet
BCC	-	Basal cell carcinoma
SCC	-	Squamous cell carcinoma
DNA	-	Deoxyribonucleic acid
A	-	Adenosine
T	-	Thymidine
C	-	Cytosine
G	-	Guanine
Å	-	Angstrom
DMT	-	Dimethoxytrityl chloride
CPG	-	Controlled pore glass
HPLC	-	High performance liquid chromatography
PAGE	-	Poly acrylamide gel electrophoresis
RP-HPLC	-	Reverse phrase high performance liquid chromatography
AE-HPLC	-	Anion exchange high performance liquid chromatography
KDa	-	Kilodalton
GUV	-	Giant unilamellar vesicle
HEK293	-	Human embryonic kidney cells 293
SDS	-	Sodium dodecyl sulphate
PBS	-	Phosphate buffered saline
DMSO	-	Dimethyl sulfoxide
MB	-	Methylene blue

Abbreviations

HPPH	-	2-(1-hexyloxyethyl)-2-devinyl pyropheophorbide-a
µM	-	Micro molar
SRIS	-	Skin Research Institute of Singapore
IMB	-	Institute of molecular biology
A*STAR	-	Agency for Science, Technology and Research
ANOVA	-	Analysis of variance
CO_2	-	Carbon dioxide
RPMI	-	Roswell Park Memorial Institute
FBS	-	Fetal bovine serum
Pen/strep	-	Penicillin/streptomycin
NHS	-	N-Hydoxysuccinimide
DDQ	-	2,3-Dichloro-5,6-dicyano-1,4-benzoquinone
SD	-	Standard deviation
PDT	-	Photodynamic therapy
EtOAc	-	Ethyl acetate
NMR	-	Nuclear magnetic resonance
DCM	-	Dichloromethane
MeOH	-	Methanol
Equiv.	-	Equivalent
NaOMe	-	Sodium methoxide
Na_2SO_4	-	Sodium sulphate
DMF	-	Dimethyl formamide
HCl	-	Hydrochloric acid

HATU	-	1-[Bis(dimethylamino)methylene]-1*H*-1,2,3-triazolo[4,5-*b*]pyridinium 3-oxid hexafluorophosphate
DIPEA	-	N,N-Diisopropylethylamine
$MgCl_2$	-	Magnesium chloride

Chapter 1 Introduction

1.1 An introduction to deoxyribonucleic acid

Deoxyribonucleic acid (DNA) was first precipitated from the nuclei of leucocytes in 1869 by Johann Miescher as a substance he termed nuclein. In 1872 he also showed that the novel compound contained carbon, oxygen, nitrogen and phosphorus; however, at the time no structure was proposed. Further work with nuclein obtained from salmon sperm provided Miesher with the indication that nuclein was a multibasic acid[5]. This led to the evolution of the term nucleic acid.

Work by Albrecht Kossel between the years of 1885 and 1901 identified the 4 bases of DNA, adenosine, guanine, thymidine and cytosine. They can be split into two groups: purines and pyrimidines respectively[6], shown in **Figure 1**.

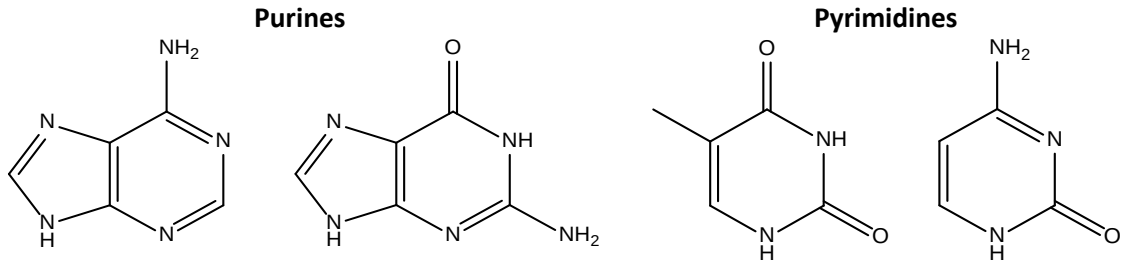

Figure 1 (Left) Purine dna bases adenine and guanine, (Right) Pyrimidines DNA bases thymine and cytosine.

This was further built on by Phoebus Levene who identified another component of DNA, the deoxyribose sugar[7].

This encouraged many theories of the three-dimensional structure of DNA, none of which were accurate until Watson and Crick combined all the evidence provided in the previous 90 years. Perhaps the most important data were Chargaff's rule and the x-ray crystallography data produced by a variety of scientists discussed below.

Chargaff showed that purines and pyrimidines could be separated using chromatography paper and a variety of solvent mixtures which were visualized by forming mercury salts which were then characterized by UV-Vis curves[8]. Later development abolished the need to form mercury salts when a Ultra Violet (UV) lamp alone was used to locate the areas of interest on the chromatography paper[9]. Quantification of these results led to the discovery that there are always equal ratios of purines and pyrimidines in double stranded DNA samples

X-ray diffraction played a vital role in the development of the theory of the structure of DNA. Bell and Astbury were first to measure the distance between stacked bases as 3.3 Å but wrongly showed the ribose rings to lie in the same plane as the purine and pyrimidine bases[10]. This was adapted by Furberg who proposed that the ribose sugars were in fact 'roughly parallel to the long access of the molecule'[11]. Whilst Franklin proposed three space groups of DNA, it was Hodgkin who, by process of elimination, narrowed it down to face centred monoclinic. Franklin, along with Gosling and Wilkins, also produced the famous photo #51 which was pivotal in Watson and Crick's conclusion of the double helix structure of DNA. Where Franklin focused her efforts on the A form of DNA, Watson and Crick turned their attention on the hydrated B form of DNA observed in photo#51.

This led to Watson and Crick unveiling the three dimensional structure of DNA that we all recognise today, the double helix, in 1953[12]. Along with Wilkins, they received a Nobel Prize for their discovery in 1962. They determined that a single strand of DNA is formed through a phosphate bond between nucleosides [13] seen below in **Figure 2**.

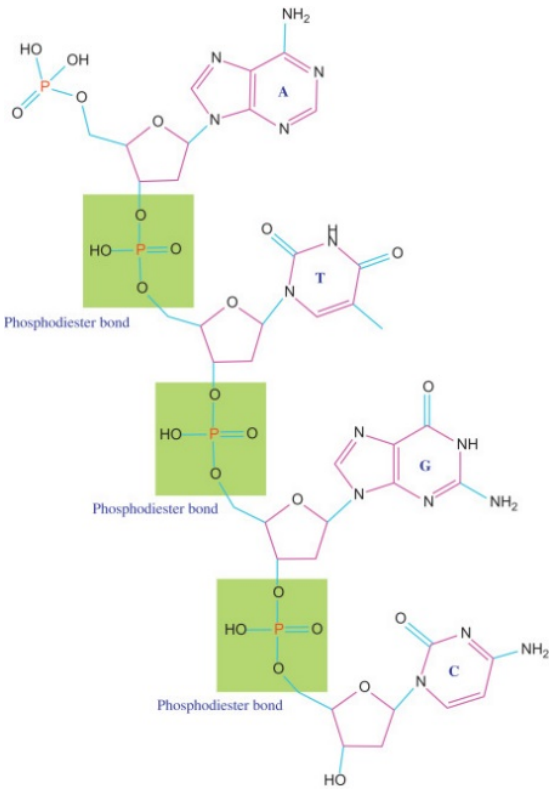

Figure 2 Strand of DNA showing nucleotides linked by phosphodiester bonds. Reprinted with permission[i].

[i] Bhagavan, N. V.; Ha, C.-E., Chapter 21 - Structure and Properties of DNA. In Essentials of Medical Biochemistry (Second Edition), Bhagavan, N. V.; Ha, C.-E., Eds. Academic Press: San Diego, 2015; pp 381-400. Copyright Elsevier Books 2015

The single stranded primary structures lie antiparallel to each other and the bases form base pairs: adenosine with thymidine (A·T), and cytosine with guanine (C·G) through hydrogen bonds (**Figure 3**).

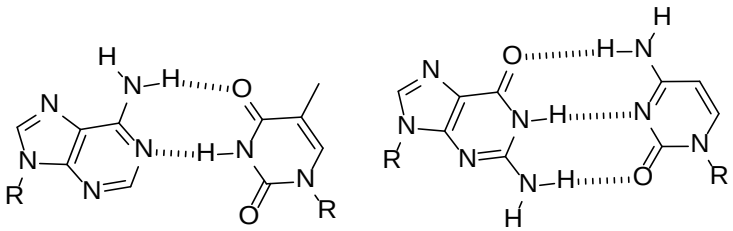

Figure 3 Watson crick base pairs, (left) adenosine and thymine form two hydrogen bonds, (right) guanine and cytosine form three hydrogen bonds.

For B-DNA, which is the structure most commonly found in nature, this secondary structure twists to from an alpha helix where the negatively charged phosphate backbones sit on the outside of the helix and the hydrophobic bases are on the inside. One helical turn was calculated to be equivalent to 10. 5 bases with a pitch of 3.4 nm[12 13] (**Figure 4**).

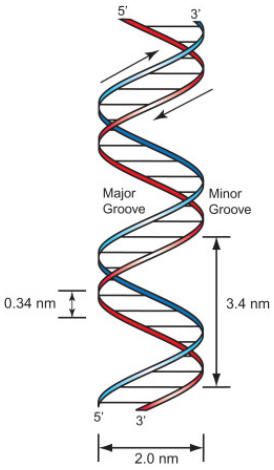

Figure 4 Structure of the double helix, 10.5 bases make up one helical turn with a pitch of 3.4 nm. Reprinted with permission[ii].

Other secondary structures, not so commonly found in nature, are A-DNA and Z-DNA which can be seen in **Figure 5**.

[ii] Bhagavan, N. V.; Ha, C.-E., Chapter 21 - Structure and Properties of DNA. In Essentials of Medical Biochemistry (Second Edition), Bhagavan, N. V.; Ha, C.-E., Eds. Academic Press: San Diego, 2015; pp 381-400. Copyright Elsevier Books 2015

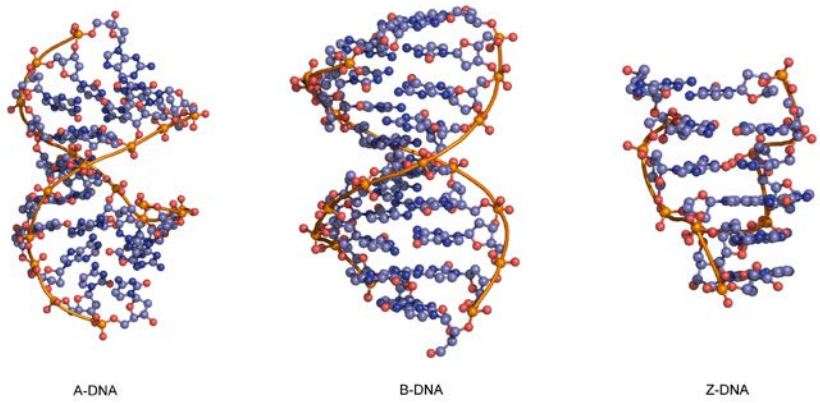

Figure 5 Secondary structures of DNA image taken from ATDBio nucleic acid book[14] (Left) α-DNA occurs readily in humidity less than 75%, 11 base pairs form one helical turn with a pitch of 2.86 nm, (Middle) β-DNA most commonly found structure of DNA where 10.5 base pairs form one helical turn with a pitch of 3.4 nm, (Right) Z-DNA is found in some bacteria and viruses and is a left handed double helix where 12 base pairs form one helical turn with a pitch of 4.56 nm.

1.1.1 DNA origami

Although the structure of DNA was determined in 1953 it was not until much later that using DNA as a programmable material was discussed. Due to the specificity of the base pairing it was noted that the secondary structure of DNA could be easily predicted and manipulated.

Ned Seeman was the first to bring this to the attention of the scientific community. He based his work on a structure formed in the genetic recombination of DNA where four strands of DNA form four helices that branch out around a central point[15], a Holliday junction.

Figure 6 (Left) Immobilised junction constructed by Seeman *et al* Reprinted with permission[iii], (Middle) Extended Holliday junction with sticky ends. Sticky ends are designed to be complementary and therefore hybridise to form a lattice. (Right) Lattice formed when complementary strands on single tiles hybridise.

It was from this that an immobilised junction was constructed through reduction of base symmetry[16, 17] see **Figure 6**. This was then extended by leaving 'sticky ends' (single stranded extensions to the junctions which are complimentary) so that the single tiles self-arranged into a 2D lattice. Junctions with increasing numbers of branches were also constructed. Three-armed junctions worked to terminate sticky ends and produced planar nanostructures. Using ten DNA strands and a system of hybridisation and ligation these junctions were used to build a cube where a three arm branch was formed at each corner[18].

However, it was realised that the number of arms contained in the branches limited the connectivity of the vertices therefore the connectivity was increased by exploring 5 and 6 armed branches. Although this did increase the connectivity and therefore an opportunity to extend the lattice in more directions, it was shown to be less stable than the previous 3 and 4 armed junctions. This was partially combatted by increasing the length of the arms which increased stability.

Another way of building larger nanostructures without having such large junctions was brought forward by Seeman. Further work by Seeman detailed how strands from two different double helices can be crossed over. These can be split into two different types, parallel and antiparallel crossovers[19]. Parallel crossovers connect to the adjacent strand and continue in the direction they were originally travelling. Antiparallel crossovers cross over to adjacent strands and reverse the direction they were going in. When this occurred twice between two helices, a double crossover, the strands are bound together. It was found that antiparallel cross overs were more stable than

[iii] Kallenbach, N. R.; Ma, R.-I.; Seeman, N. C., An immobile nucleic acid junction constructed from oligonucleotides. Nature 1983, 305 (5937), 829-831. Copyright Springer Nature 1983

parallel crossovers. This technique was the basis for work started by Rothemund to make large DNA nanostructures termed DNA origami: the folding of DNA into a predetermined shape.

First DNA origami structures were made from a combination of single strands that folded to a predetermined shape. However, this technique had disadvantages, for example the strands had to be in equimolar ratios which was difficult when aliquoting many strands. This would have led to high error levels. Therefore, this technique evolved to one long strand of DNA combined with small 'helper strands'[20] and then to finally working with a long single strand of circular DNA with small 'staple strands'[21]. The long circular DNA used was plasmid DNA such as pUC1983[22] or M13[23] treated with endo- and exo- nucleases to form a single stranded circular piece of DNA. This negated the need to synthesise long strands of DNA with solid phase synthesis.

Using computer programs such Cadnano, the single strand was programmed into the users' desired shape[24]. Short strands of DNA were used to cross over between helical domains (antiparallel cross overs), thereby holding the structure in place. The crossover positions are of great importance as placed wrongly, they will cause strain the system causing it to fall apart. This is explained in more detail in further sections.

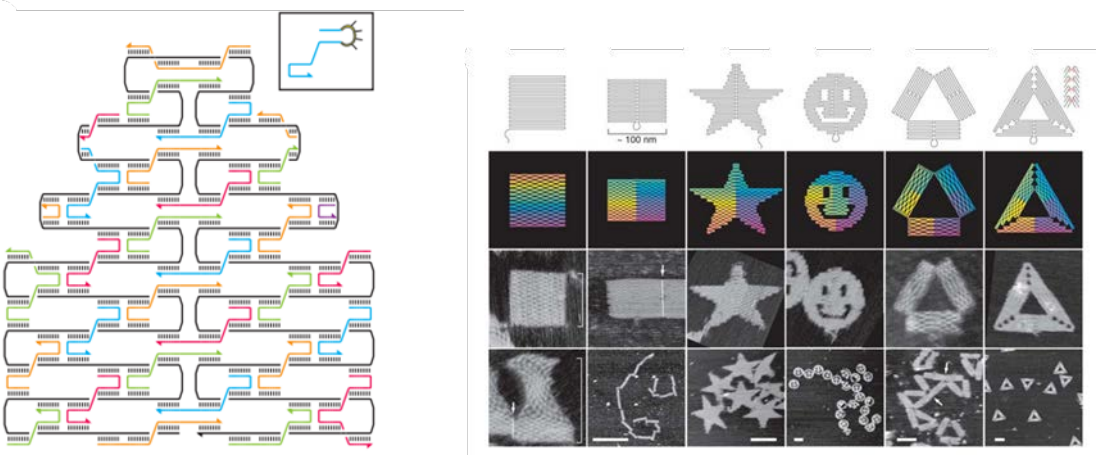

Figure 7 (Left) Simplified image of planned structure of DNA origami tile. Black long single strand represents the long single scaffold DNA strand and the coloured short strands represent the staple strands crossing over between helical domains (Right) Top two rows shows the desired design; bottom two rows show atomic force microscopy images of formed nanostructures. Reprinted with permission[iv].

Rothemund showed the true versatility of DNA origami by creating many different shaped such as smiley faces, stars and also 3-D structures shown in **Figure 7** [21]. This has given rise to DNA origami

[iv] Rothemund, P. W. K., Folding DNA to create nanoscale shapes and patterns. Nature 2006, 440 (7082), 297-302. Copyright Springer Nature 2006.

being used as a platform for drug delivery[25-29], enzyme reactions[30-33] and biomolecular machines[34, 35].

1.1.1.1 Cross overs

There are two standard different lattice types that a DNA nanostructure can be based on, a honeycomb lattice or a square lattice.

1.1.1.1.1 Honeycomb lattice

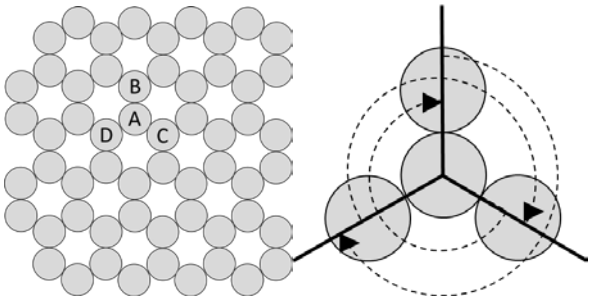

Figure 8 (Left) Honeycomb lattice packing. Each circle represents a helical domain. (Right) Each helical domain has three nearest neighbours spaced evenly around it therefore cross overs occur every 7 bases, represented by an arrow head.

In a honeycomb lattice, a helical domain has three nearest neighbours and therefore it has the opportunity to create antiparallel crossovers with each of these helical domains. This can be seen in **Figure 8** (Left) where, for example, helical domain A can form crossovers with domains B, C and D. To reduce strain in the system, crossovers only occur at points where the backbones of the strands arrive at points of closest proximity. Each of the three neighbouring domains is spaced evenly around the central helical domain. Therefore, each segment between strands measures 3.5 bases (10.5 bases in a helical turn divided by 3). As a fraction of a base cannot exist, there is an opportunity to crossover every seven bases (two segments). This is depicted in **Figure 8** (Right).

1.1.1.1.2 Square lattice

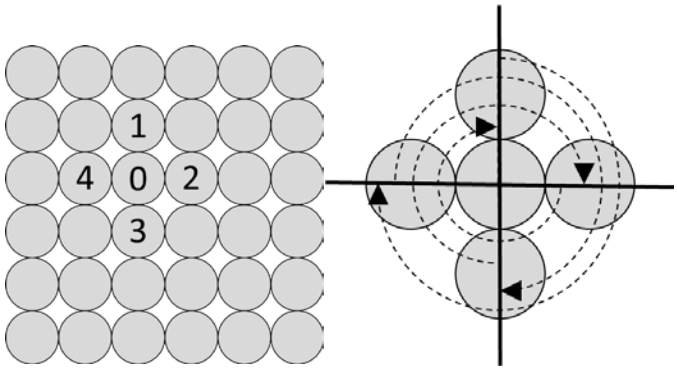

Figure 9 (Left) Square lattice packing. Each circle represents a helical domain. (Right) Each helical domain has four nearest neighbours spaced evenly around it therefore cross overs occur every 8 bases, represented by an arrow head.

A nanostructure based on a square lattice is where a helical domain is surrounded by four nearest neighbours with which it can form antiparallel crossovers. This is depicted in **Figure 9**. As discussed above, strand crossovers can only occur at certain points in the structure to reduce strain. As a full turn in the helix is approximately 10.5 bases, ~8 bases equate to ¾ of a turn which correlates with the four evenly spaced neighbouring helical domains[36].

1.1.2 DNA nanopores

1.1.2.1 Nanopores in nature

Nanopores play a key role in nature for allowing molecules and ions to pass through lipid bilayers in cell membranes. There are many types which can be classified into 5 families: Channels/pores, electrochemical potential-driven transporters, primary active transporters, group translocators, transmembrane electron carriers[37]. The most applicable to this project are channels/ pores. This is because they act purely through passive diffusion which is the proposed method for the DNA nanopores discussed in this work. Examples of pores that fall into this class are porins, ionophores, toxin channels, colicins and peptides.

Porins are a class of pore found in gram negative bacteria. They can be split into two different groups, general and specific. General porins allow the passive diffusion of any solute under 600 KDa with no discrimination. Specific porins on the other hand, only allow passive diffusion of particular solutes as they have a low affinity to particular compounds due to channel architecture. They are of particular interest as they still allow diffusion at temperatures as low as 0 °C and occur in high abundance in cells (10^5 per cell) in different varieties depending on the environment[38]. Most porins are made up of trimers of β - sheet cylinders which each form a pore. Amino acid sequences

between species vary, yet hydrophilic and hydrophobic residues follow a similar trend in location within the structure where a cylindrical pore contains a hydrophobic belt[39].

Toxin channels such as those which cause anthrax, cholera and diphtheria typically follow the AB model. This is where there are different parts of the compound with a different function. In its simplest form, the B function acts as a catalyst to attach the structure to the cell membrane. The A part carries out the translocation. However some molecules, such as those which cause anthrax, have three different domains with additional functionality[38].

Colicins are a class of antibiotic peptides that are expressed by certain strains of ecoli. They function by attacking similar strains of bacteria. They do this by forming pores in the cytoplasmic membrane and inhibiting protein synthesis[40].

Ionophores are molecules that form channels across cell membranes. They are lipid soluble since they are hydrophobic on the outside and contain a hydrophilic core, therefore they can sit in lipid bilayers. They transport ions across lipid bilayers with both specific and nonspecific properties. As an example, Nystatin transports both monovalent cations and anions, whereas Valinomycin and Monoensin each exhibit a high selectivity for potassium and sodium ions respectively[41]. Ionophores are commonly used for their antibiotic properties[42].

1.1.2.2 Designed and synthesised nanopores interacting with lipid bilayers

Many researchers have tried to mimic the structure and activity of membrane bound pores. This work focuses on pores formed using DNA as a building material. The DNA nanostructures are generally designed with the inclusion of DNA modified with hydrophobic components to enhance the hydrophobic character of the structures.

Langecker *et al* based a DNA nanostructure on the well-known protein α-hemolysin. The channel consisted of two modules where an internal core protruded from the outer sleeve which anchored the structure to cell membrane using 26 cholesterol moieties (**Figure 10**). The overall structure measured 47 nm in length and was made up of 54 helical domains where the internal pore size measured 2 nm. Using transmission electron microscopy (TEM) it was shown that the structures inserted into small unilaminer vesicles made from phosphatidylcholine (POPC) and demonstrated electrical conductivity[43].

The Langecker construction, although one of the first of its kind, was a large structure compared to later designs of the pore. This could be seen as a disadvantage as it makes the structure a lot more expensive to make and also a lot more complicated to fold. The simpler the structure, the faster it can be annealed and folded.

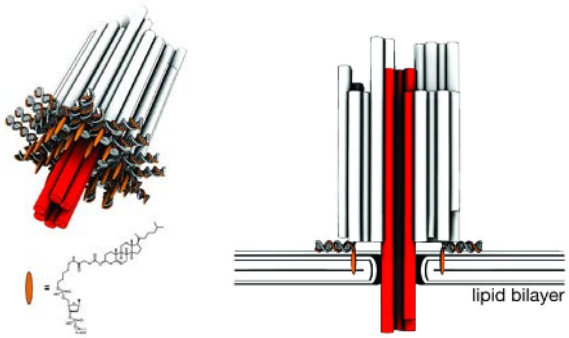

Figure 10 Schematic of Langecker nanopore where cholesterol modifications point directly down into the lipid bilayer. The system was made up of two components, an outer sheath containing cholesterol modifications surrounding a stem able to puncture the membrane. Reprinted with permission[v].

Interestingly, the cholesterol modifications pointed perpendicular to the membrane and inserted downwards into the bilayers. This differed from later pores where the modifications either formed a belt like band of hydrophobicity around the pore or lay parallel within the plane of the membrane.

There are two of advantages to the perpendicular approach. Firstly, it is more likely to only insert fully into the membrane in one direction. Therefore, the end of the pore not in the membrane can be identified and modified, whereas the pores with modifications parallel to the membrane can sit in the membrane either way up. Secondly, the perpendicular pore is more likely to fully insert into the membrane as it would be unable to partially insert due to the position of the multiple modifications. This is compares favourably with the pores which contain the modifications that stick out parallel to the membrane and could in theory insert sideways onto the membrane and not create the pore through the membrane. Researchers have tried to combat this by increasing the amount of modifications around the pore.

The main disadvantages to the Langecker pore, as previously discussed, is its large size. This means that more hydrophobic compounds were included in the structure. This reduces the solubility of the pore and there is more likely to be aggregation at high concentrations.

Burns *et al* simplified this structure to the equivalent of the internal core used by Langecker. Fourteen oligonucleotide strands were used to form a six helical bundle measuring 5.5 nm across and 14 nm long. The oligonucleotides were modified with twelve ethylthiophosphate groups partially replacing the native backbone so that when folded, the nanostructure contained a

[v] Langecker, M.; Arnaut, V.; Martin, T. G.; List, J.; Renner, S.; Mayer, M.; Dietz, H.; Simmel, F. C., Synthetic Lipid Membrane Channels Formed by Designed DNA Nanostructures. Science 2012, 338 (6109), 932-936. Copyright 2012 The American Association for the Advancement of Science.

hydrophobic belt of 72 ethylthiophophate groups (**Figure 11**). This was shown to insert into a lipid bilayer by measuring a change in current flow across a membrane when in the presence of the modified pores[44].

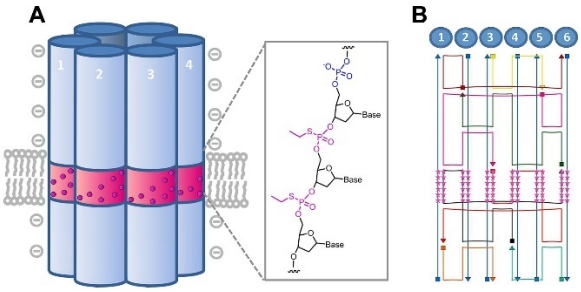

Figure 11 A) Schematic representations of DNA nanopore where each cylinder represents a duplex. The pink band is where the native DNA backbone has been substituted by phosphorothioate-ethyl groups forming a hydrophobic belt. B) Map of DNA strands showing crossovers between helical domains, modifications are represented by stars. Reprinted and adapted with permission[vi].

This design was further simplified by Burns, firstly to only two porphyrin modifications, and also in number of oligonucleotide strands[45]. Six strands were designed to fold into six helices with two internal tetra phenyl porphyrin modifications (**Figure 12**). This allowed fluorescence studies in giant luminlamiar vesicles to show that the structures interacted with the lipid bilayers. This supported the observation of the change in ionic current between GUV with and without the modified pore.

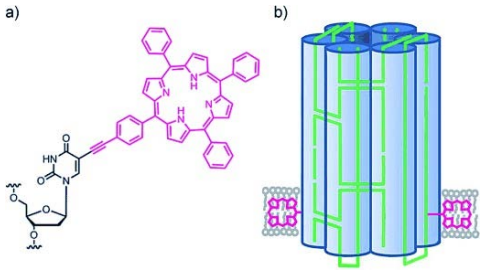

Figure 12 A) Deoxyuridine modified with tetraphenylporphyrin at 5 position acts as hydrophobic anchor for the nanopore. B) DNA nanopore formed of six helical domains shown anchored in a lipid bilayer by the porphyrin modifications. Reprinted with permission[vii].

A similar pore made up of six strands but modified with an ethyl thiophophate backbone was used for cellular experiments[2]. The ethylphosphiothiaoate molecules were an interesting modification.

[vi] Burns, J. R.; Stulz, E.; Howorka, S., Self-Assembled DNA Nanopores That Span Lipid Bilayers. Nano Letters 2013, 13 (6), 2351-2356. Copyright 2013 American Chemical Society.

[vii] Burns, J. R.; Gopfrich, K.; Wood, J. W.; Thacker, V. V.; Stulz, E.; Keyser, U. F.; Howorka, S., Lipid-Bilayer-Spanning DNA Nanopores with a Bifunctional Porphyrin Anchor. Angewandte Chemie-International Edition 2013, 52 (46), 12069-12072. Copyright John Wiley and Sons 2013.

Compared to a cholesterol molecule an ethyl chain is a far less hydrophobic molecule which is why 72 modifications needed to be included to guarantee a belt of hydrophobicity. They showed that when incubated with HeLa cells for 24 hours at 60 μg mL^{-1}, a 20% decrease in cell viability was observed.

The same group of researchers continued work with the six helical pores, still evolving the pore design. The most recent was a simple structure where the crossovers occurred at the both ends of the helices, linking each domain to its neighbour[3]. It was shown that this 2 nm pore was able to transport small molecules across a lipid bilayer. Gating was then introduced using temperature dependent dissociation of one strand to open and close the pore allowing small molecules to pass through **Figure 13**[46].

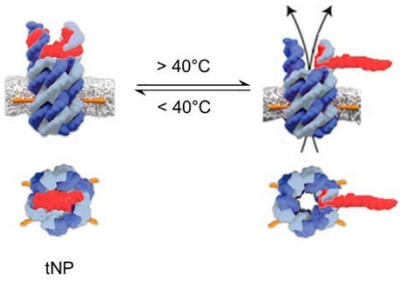

Figure 13 Temperature dependant gating of 6-duplex nanopore with four cholesterol modifications. Images on the left show the pore is closed at temperatures lower than 40 °C, Images on the right show that at 40 °C a single strand dissociates therefore opening the pore. Top images represent the side view of the nanopore inserted in the membrane whereas the bottom images show the nanopore end on. Reprinted with permission[viii].

All of the above examples were based on the hexagonal lattice design earlier discussed. A different approach was shown by Göpfrich *et al* in 2015 where they created a much smaller pore based on the square lattice where a bundle of four helices created a pore measuring 0.8 nm in diameter compared to the 2 nm pore formed by the hexagonal lattice[4].

[viii] Arnott, P. M.; Howorka, S., A Temperature-Gated Nanovalve Self-Assembled from DNA to Control Molecular Transport across Membranes. ACS Nano 2019, 13 (3), 3334-3340. Copyright 2019 American Chemical Society

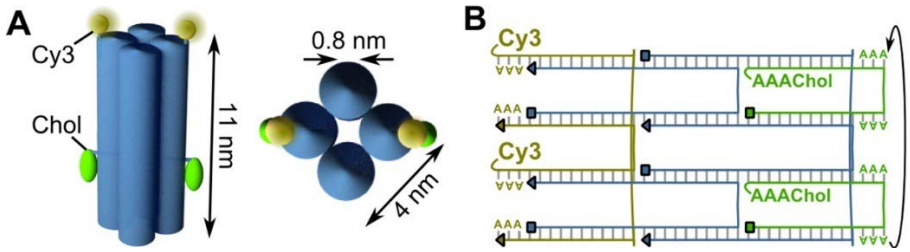

Figure 14 A) Schematic representation of DNA nanopore based on the square lattice where each cylinder represents a helical domain, B) Map of DNA strands showing the cross over of strands between helical domains. Reprinted with permission[ix].

Through tagging with two cholesterol modifications and two Cy3 fluorescent tags it was shown that the structure inserted into giant unilaminner vesicles by showing an ionic conductance measured across a membrane. This was the first step towards the design of smaller pores which were more similar to ion channels found in nature.

Although this thesis is focused on nanopores interacting with membranes, the interaction of other DNA structures cannot be overlooked. An example of this is lattice growth on a membrane where the anchoring of DNA origami tiles onto a lipid bilayer with cholesterol modified strands was used to promote lattice growth[47]. Another example is a simple prism shaped DNA cage which was tagged with fluorescent probes. It was shown to insert into artificial lipid bilayers and could be displaced by the addition of new DNA strands. Again, using cholesterol as an anchor for the structure, they showed that the structure could be displaced from the membrane when using a complementary cholesterol modified strand[48].

Although arguably not DNA nanostructures, single duplexes of DNA have also been shown to interact with lipid bilayers. A DNA duplex with multiple porphyrin modifications was shown to present pore like properties where a flow on ions was measured across a lipid bilayer[49]. The other most interesting pieces of work were published in the 1990's[50, 51]. A group working on the inhibition of the hepatitis B virus (HBV) surface antigen stumbled upon the cytotoxic effects of a self-complementary single strand of DNA modified with a cholesterol molecule. After primary findings on hepatic cell lines they continued to screen 60 cell lines of varying origin and found that not all cell lines responded to treatment. Colon and breast cell lines were shown to be most susceptible. The disadvantage to this work was that it only monitored the cells through cell morphology; observing the formation of large vacuoles, the blebbing of plasma membrane and floating cells. Although cell morphology does indicate cell death, there was no measure of cell activity which could

[ix] Göpfrich, K.; Zettl, T.; Meijering, A. E. C.; Hernández-Ainsa, S.; Kocabey, S.; Liedl, T.; Keyser, U. F., DNA-Tile Structures Induce Ionic Currents through Lipid Membranes. Nano Letters 2015, 15 (5), 3134-3138. . Copyright 2015 American Chemical Society

have benefited the study greatly. However this did show that even the simplest of DNA structures modified with hydrophobic compounds could interact with cells.

1.2 Scope of project

This project planned to use deoxyribonucleic acid (DNA) nanostructures as a therapy for cancer. It has been shown that DNA nanostructures, with hydrophobic modifications, insert into artificial lipid bilayers[3, 4, 43-45, 52, 53]. There has been evidence that this applies to cell membranes and produced a cytotoxic effect to HeLa cells[2].

DNA makes a suitable building material for a nanopore for a plethora of reasons. Firstly, it is highly programmable due to specific base pairing. It is also soluble in aqueous media therefore does not need to be dissolved in organic solvents which can be incompatible with living organisms. This also means it increases the solubility of hydrophobic compounds, e.g. porphyrin, in aqueous media when conjugated together. It is readily available commercially or can be synthesised in a short period of time using a DNA synthesiser. Hence, depending on the size of the nanostructure, they can be relatively cost effective to synthesise.

Cell membranes, although far more complex than artificial lipid bilayers due to the inclusion of proteins, receptors and carbohydrates on the surface, are lipid bilayers. A lipid bilayer consists of amphiphilic lipids which form the bilayer by forming two distinct areas, a hydrophobic centre where the fatty acid tails point inwards to each other, and a hydrophilic area which consist of the charged head groups.

It is suggested that the DNA nanostructures insert into cell membranes and sit in the lipid bilayer therefore disrupting the cell membrane. DNA has a negatively charged backbone and therefore would interact with the hydrophilic area and the addition of the hydrophobic modification would interact with the hydrophobic internal belt. This would therefore create a channel through which ions and matter could flow, shown in **Figure 15**.

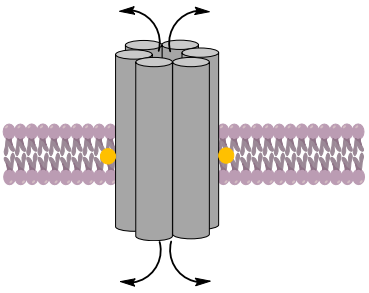

Figure 15 An example DNA nanostructure modified with two hydrophobic compounds (represented as circles) inserted into a lipid bilayer, arrows represent the predicted flow of ions.

It is thought that this would then cause disturbance to the cell that would either cause osmotic differences leading to cell death or start the cell's natural mechanism to destroy diseased cells.

This mechanism is proposed to be coupled with photodynamic therapy through attachment of hydrophobic photosensitisers to the DNA to act as the anchors in the cell membrane and to be used for PDT.

Photodynamic therapy (PDT) is a lesser used therapy in treatment of cancer that has successfully shown to lead to cell death in some cancer tumours and is also applied as a treatment for age-related macular degeneration[54]. The first drug clinically approved was Photofrin®, a complex mixture of monomeric and oligomers[55], which is now used to treat a wide range of tumours[56]. However, it is limited by its low wavelength absorbance which means that the light does not penetrate very far into the tissues and also induces prolonged skin sensitivity[57]. Second generation drugs generally absorb at longer wavelengths, 650 – 850 nm[58], which penetrate further into tumours[59]. Third generation drugs aim to increase the cellular uptake by reducing hydrophobicity and directing the drug through conjugation with sugars[55, 60], liposome[61] or antibodies[62].

This project planned to utilise the phototoxic and hydrophobic properties of porphyrins to create a dual therapy where the porphyrins not only anchor a nanopore into a cell membrane, but also used for PDT. Although PDT has been used to successfully treat melanoma in studies[63-67] there are also some difficulties. Part of the problem with using PDT as a treatment is the absorption of light by melanin[68]. Melanin absorbs light strongly at short wavelengths and this has been combatted by using the second-generation photosensitisers which absorb light at longer wavelengths[69]. However, it is also hindered by the antioxidant effect of melanin acting as a reactive oxygen species scavenger[70, 71]. Therefore, the dual therapy approach of the nanopore and the photosensitizer would increase the therapeutic effect present treatments. Tetraphenyl porphyrin (TTP) was chosen to be used in this project due to the extensive work previously carried by the Stulz group with the compound.

The tetrapyrrole ring of the porphyrin absorbs a photon which promotes an electron from the ground state S0 to an excited singlet Sn state[72]. The fast decay from this state occurs via different routes; the two main being fluorescence and intersystem crossing to a triplet state[57]. Fluorescence can be used as a useful tool for diagnostics of tumours whereas the latter can be utilised for photodynamic therapy when the compound is taken up by a cell.

From the excited triplet state the porphyrin can undergo two further reaction routes. Type I reactions react with the substrate leading to free radicles which further react with oxygen to form free radicals such as $O_2^{\cdot-}$, $OH^{\cdot}$ and H_2O_2 which result in cell death[54, 73]. In Type II reactions the excited

triplet state of the porphyrin reacts with molecular oxygen ($^3O_2$) to form an excited state singlet oxygen ($^1O_2$)[54, 57, 72], a highly reactive species. These reactive oxygen species cause cell death.

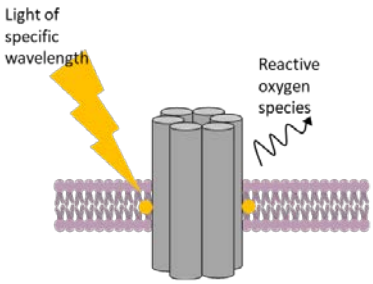

Figure 16 A DNA structure in a lipid bilayer can be modified with hydrophobic photosensitisers which can be excited at a specific wavelength to release reactive oxygen species.

Finally, a goal that was not reached during the time frame of this PhD; targeted therapy would be achieved by the attachment of a peptide that would target an overexpressed receptor in a type of cancer cell, **Figure 17**.

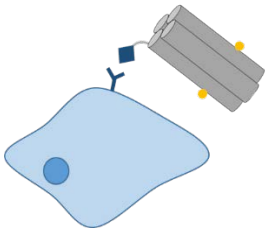

Figure 17 DNA nanostructure modified with peptide to target receptor on cell surface.

1.3 Choosing a target - skin cancer

1.3.1 The structure of skin

The human skin is a versatile organ in the human body that has many uses, all of critical importance: prevention of water loss, immune defence, protection against ultra violet (UV) light damage, temperature regulation, sensation and social interactions[74, 75]. It is made up of three main layers: the epidermis, the dermis and the subcutaneous layer as show in **Figure 18**. The epidermis is the outmost layer of the skin and is made up of five sublayers: basal, squamous, stratum granulosum, stratum lucidum and the stratum corneum.

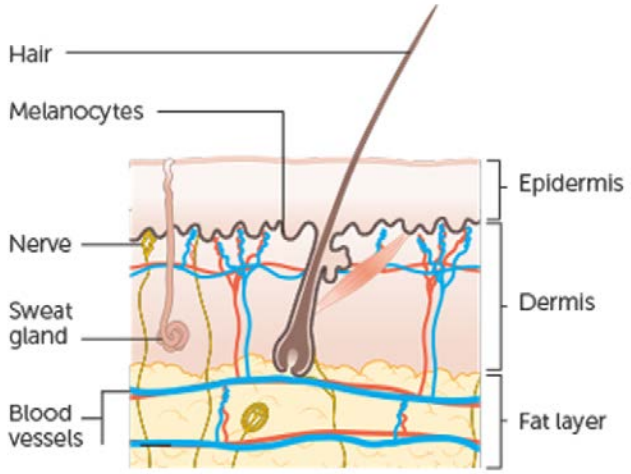

Figure 18 The structure of skin is made up of three main layers: the epidermis, the dermis and the subcutaneous fat layer. Image taken from Cancer Research UK[76].

The basal layer contains melanocytes and basal cells. Basal cells are keratinocytes attached through hemidesmosomes to the basement membrane[74]. As they divide and differentiate, they move up through the epidermis layers; squamous fat layer, stratum granulosum and stratum lucidum, where they eventually become flat in shape as they dehydrate and die. They then fuse together into layers which migrate through the final layer of the epidermis, the stratum corneum[77]. This layer is made up of 10-30 layers of dead keratinocytes which are continually shed and replaced by new cells moving through the cycle[77]. The stratum corneum is also the layer of skin which prevents water loss as the cells overlap and release intercellular lipids. This not only provides a water proof layer, but also a physical barrier to allergens and pathogens[74]. The melanocytes located in the basal layer provide the body with UV protection. They produce melanin which is then transported to the keratinocytes which protects the nuclei from UV radiation[74].

The second layer of the skin is the dermis which is made up of two sublayers, the papillary and reticular layers[77]. The reticular layer of the dermis is home to proteins, collagen and elastin, synthesised by fibroblasts[74], and many different types of structures: blood and lymph vessels, hair follicles, sweat and sebaceous glands, and nerve endings[77]. These structures ensure a supply of nutrients to the epidermis through blood flow. Vasoconstriction and dilation of blood vessels and the activation of the sweat glands in the dermis provide a regulation mechanism for body heat[74].

Finally, the innermost layer is the subcutaneous layer. This is a store of fat for the body and therefore varies in thickness within the population. It consists of fat and collagen cells which blood vessels, nerves, lymph vessels and hair follicles all pass through to reach the dermis[77].

Due to the movement of the keratinocytes through the epidermis, the skin is classed as self-healing as cells are constantly renewed. However, this mechanism is not completely reliable as various skin diseases still arise for example, highlighted in this project, skin cancer.

1.3.2 Non-melanoma skin cancers

The most common type of non-melanoma skin cancer is basal cell carcinoma (BCC) which accounts for nearly 80% of cases[78]. BCC occurs in the basal layer of the skin and as the name suggests, effects the basal cells. Although it is currently the most common type of skin cancer, it is known to be the least dangerous as few cases metastasise[78]. However, if left untreated, tumours can cause extensive local damage and increase the need for skin grafts and plastic surgery after treatment. The second most common form of non-melanoma skin cancer is squamous cell carcinoma (SCC)[79]. Unlike BCC, this is type of carcinoma is more likely to metastasise but this is largely dependant on size, location and depth of the tumour[80].

Tumours are more commonly found on patients' upper bodies, with approximately 80% of BCC cases being found on the head and most others on the trunk or lower limbs[81]. This could be due to many researchers defining the major risk factor for both diseases as UV-exposure, specifically increased when sunburn has occurred in childhood[78, 79, 81]. Other risk factors include arsenic exposure, patients on immunosuppressant therapy (e.g. after organ transplant) and various genetic diseases such as albinism where there is no pigment to protect the cells, and Gorlin's syndrome[79, 81].

The most common treatment for non-melanoma skin cancers is surgical intervention. Excision, cryogenic therapy, electro dissection and curettage are all common methodologies, each with advantages and disadvantages. Cryogenic therapy, electro dissection and curettage all destroy removed tissue and directly surrounding tissue therefore clear boundaries of removal cannot be established. In comparison, excision provides clear boundaries that can be examined through histological techniques. However, the former techniques are less expensive than the latter. Another technique used is Moh's micrographic surgery: A technique of excision where the tissue is removed layer by layer and analysed for disease, minimalizing the extent of the wound left on the patient. This is however also costly.

Patients for whom excision is not appropriate, may undertake other treatments including radiation therapy for both BCC and SCC, and photodynamic therapy and topically applied chemotherapy for BCC.

5-fluorouricil is a chemotherapy drug used in a large variety of cancers. The most common application is through an intravenous drip wherethe drug enters the blood stream which means that it circulates around the body and causes uncomfortable side effects for the patient. However, for skin cancer the drug can be applied topically and therefore although the treatment site is painful, there are fewer off-target side effects.

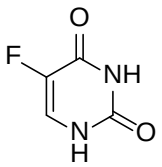

Figure 19 5-Fluorouricil is a commonly used drug for the treatment of a variety of cancers. It has a similar structure to thymine and is therefore incorporated into DNA and RNA which interferes with cell nucleoside metabolism[82].

Photodynamic therapy has also shown to be successful in treating BCC [81]. δ-aminolevulininc acid (5-ALA) is a termed a prodrug as it converts to protoporphyrin IX (PpIX), a photoactive compound, in the body. The structures of these compounds can be seen in **Figure 20**. PpIX is naturally occurring in the body however the synthesis is limited by the availability of aminolevulininc acid. Therefore, the addition of this compound increases the amount of photoactive compound in the body. This is allows high levels of reactive oxygen species to be released when the treated area is irradiated with a light source at specific wavelengths.

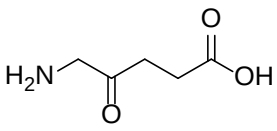

5 - Aminolevulinic Acid

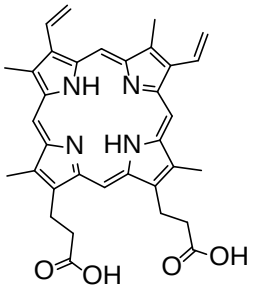

Protoporphyrin IX

Figure 20 (Left) 5 – Aminolevulinic acid is a converted to protoporphyrin IX in the body through the heme synthesis cycle. Administration of the prodrug leads to an increase of PpIX and can subsequently be used for photodynamic therapy, (Right) Protoporphyrin IX can be excited with either blue light, 410 to 420 nm, or red light 630 nm to produce a photodynamic effect[83, 84].

1.3.3 Melanoma

Melanoma is cancer of the melanocytes located most commonly in the epidermis of the skin. They are also located in various other parts of the body; the eyes and various mucus membranes. This project focuses on cutaneous melanoma.

Although melanoma is one of the least common types of skin cancer (it represents only 1% of the cases diagnosed in the US) it has the lowest survival rate compared to non-melanoma skin cancers[85]. The risk of contracting this cancer and it becoming invasive has increased over the last century[86].

The high mortality rate of melanoma can be accredited to the high risk of melanoma metastasising. As melanoma grows downwards into the skin (commonly measured by the Clark scale), the further it infiltrates, the more likely it is to travel around the rest of the body. It is also notoriously difficult to treat due to its chemo- and radiation resistance[87].

Currently the success rates of treatment for melanoma depends highly on the stage it is at. The stages described by the National Cancer Institute are summarised in Table 1[88].

Table 1 Data summarised from the National Cancer Institute detailing the different stages of Melanoma[88].

Stage	Symptoms
Stage 0 or melanoma in situ	Abnormal melanocytes found in the epidermis
Stage I	**Stage IA**: tumour ≤1 mm thick with or without ulceration Stage IB: 1 mm < tumour < 2mm thick without ulceration
Stage II	**Stage IIA**: 1 mm < tumour < 2 mm thick with ulceration or 2 mm < tumour < 4 mm thick without ulceration **Stage IIB**: 2 mm < tumour > 4 mm thick with ulceration or 4 mm < tumour without ulceration Stage IIC: 4 mm < tumour thick with ulceration
Stage III	**Stage IIIA**: tumour < 1mm thick with ulceration or tumour < 2 mm thick without ulceration. Cancer in 1 to 3 lymph nodes by sentinel lymph node biopsy **Stage IIIB**: primary unknown and cancer in 1 lymph node or microsatellite, satellite or in-transit metastases on or under skin or Tumour < 1 mm thick with ulceration or tumour < 2 mm thick without ulceration and cancer in 1 to 3 lymph nodes or microsatellite, satellite or in-transit metastases on or under skin or

	1 mm < tumour < 2 mm thick with ulceration or 2 mm< tumour<4 mm thick without ulceration and cancer in 1 to 3 lymph nodes or microsatellite, satellite or in-transit metastases on or under skin Stage IIIC: Primary tumour unknown or unseen and cancer found in either (2 or 3 lymph nodes) or (in 1 lymph node and microsatellite, satellite or in-transit metastases on or under skin) or (in ≥ 4 lymph nodes or any number lymph nodes matted together) or (in ≥ 2 lymph nodes or in any number of lymph nodes matted together and microsatellite, satellite or in-transit metastases on or under skin) or tumour < 2 mm thick with or without ulceration or tumour <4 mm thick without ulceration and cancer is found in either; (1 lymph node and microsatellite, satellite or in-transit metastases on or under skin) or (in ≥4 mm or any number of lymph nodes matted together) or (in ≥2 lymph nodes or in any number of lymph nodes matted together and microsatellite, satellite or in-transit metastases on or under skin) or tumour > 4 mm thick with ulceration or > 4 mm thick without ulceration and cancer is found in ≥ 1 lymph nodes or in any number matted together. Possibly microsatellite, satellite or in-transit metastases on or under skin or tumour > 4 mm thick with ulceration and cancer in ≥1 lymph nodes or microsatellite, satellite or in-transit metastases on or under skin **Stage IIID**: tumour > 4 mm thick with ulceration and cancer either; (in ≥ 4 lymph nodes or lymph nodes matted together) or (in ≥ 2 lymph nodes or lymph nodes matted together and microsatellite, satellite or in-transit metastases on or under skin)
Stage IV	Cancer has spread to other parts of the body e.g. Liver, brain etc or distant lymph nodes or skin
Recurrent	Cancer has recurred after treatment either in primary area or other locations in the body

Treatment options include surgery, chemotherapy, radiation, immunotherapy and photodynamic therapy depending on the stage of the disease.

Surgery is almost always used to remove the primary tumour with a wide local excision to ensure that all the damaged tissue is removed. This can also include removal of the effected lymphocytes and combined with other therapy options.

Chemotherapy is regularly used for later stages of the disease where metastasis has occurred. Although melanoma is fairly resistant to radiation, both internal and external radiation therapy is useful for the treatment of metastatic melanoma in the central nervous system[87].

However, these treatments come with side effects and still the survival rate for melanoma is low. With cases of melanoma increasing, there is room in the market for a new melanoma treatment.

1.3.4 Targeting melanoma

Melanocortin type-1 receptors (MC1Rs) have been shown to be overexpressed in melanoma cells and tissues[89-92] and are therefore a suitable target for treatments for melanoma. Multiple studies have used an octapeptide derivative of the alpha - melanocyte stimulating hormone named NAP-amide, **Figure 21**, to target the MC1R for imaging melanoma[93, 94].

.

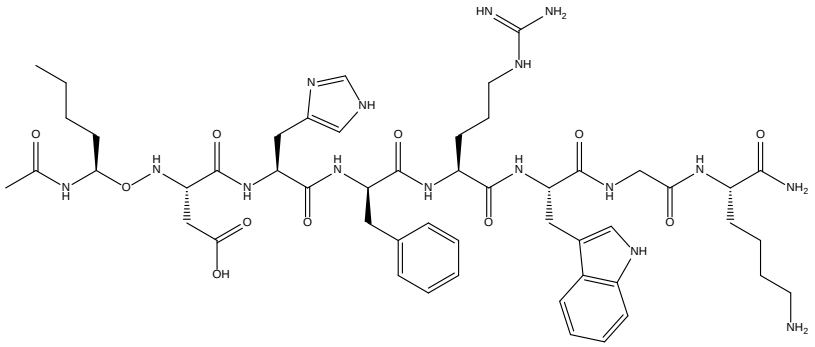

Figure 21 The peptide NAP-amide is an agonist for the melanocortin 1 receptor[93, 94].

It has also been used to target melanoma cells for photodynamic therapy (PDT) using methylene blue and HPPH as photosensitisers[95]. This paper utilised an amine on the NAP-amide molecule to attach the photosensitizers modified with an NHS group.

Chapter 2 Methodology

This research project took place between two research facilities; the University of Southampton and the Agency of Science Technology and Research (A*STAR) Singapore in both the Institute of Molecular Biology (IMB) and the Skin Research Institute of Singapore (SRIS). All chemical and DNA synthesis took place at the University of Southampton whereas all cell testing took place in Singapore. Alternating years of the project were spent in each location therefore allowing for optimisation of structures and experiments.

2.1 DNA synthesis

DNA synthesis, commonly descried as oligonucleotide synthesis, is a largely automated process that is now widely available commercially. In the formation of unmodified oligonucleotides, the first base is attached to controlled glass beads which the reagents flow over to complete the reactions. The sections below detail the steps involved in the synthesis.

2.1.1.1 Detritylation

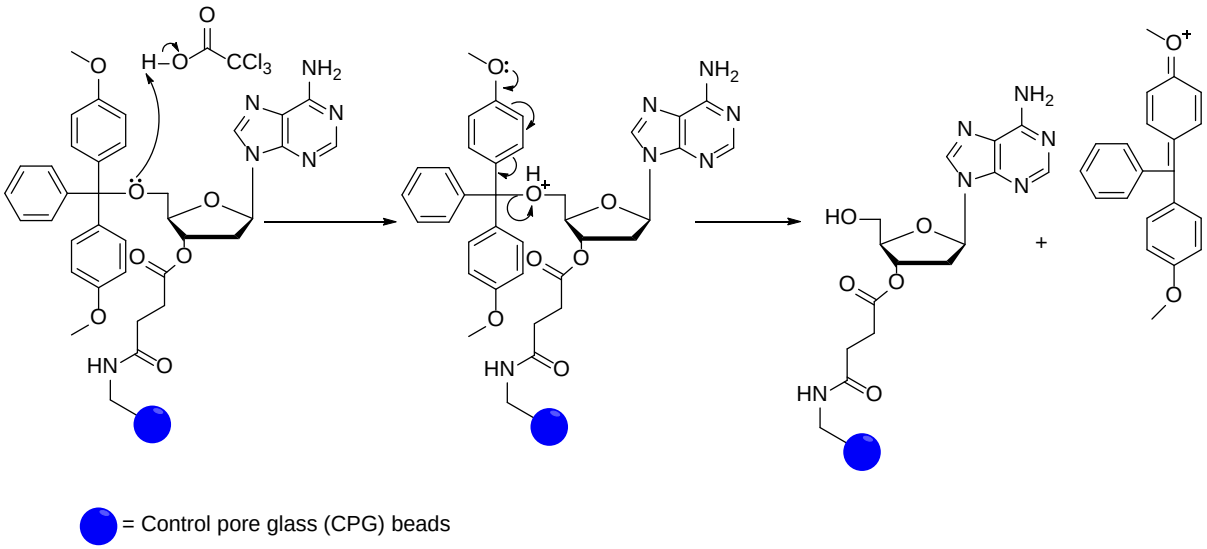

Figure 22 Mechanism of detritylation of adenine with trichloroacetic acid, forming a bright orange cation biproduct which is commonly used for monitoring the synthesis efficiency.

The first step in the reaction is the deprotection of the 5' oxygen on the pre-loaded base through acid catalysis using dilute trichloroacetic acid (3%) in dichloromethane. The protonation of the bridging oxygen encourages the readily available lone pair of electrons on the conjugated oxygen to resonate down and create the perfect leaving group therefore cleaving the protecting group from the sugar. The resonance form of the dimethyoxytrityl (DMT) leaving group results in a bright

orange colour which provides a method of observing the efficiency of the reaction by measuring the absorbance at 498 nm throughout the synthesis.

2.1.1.2 Activation and coupling

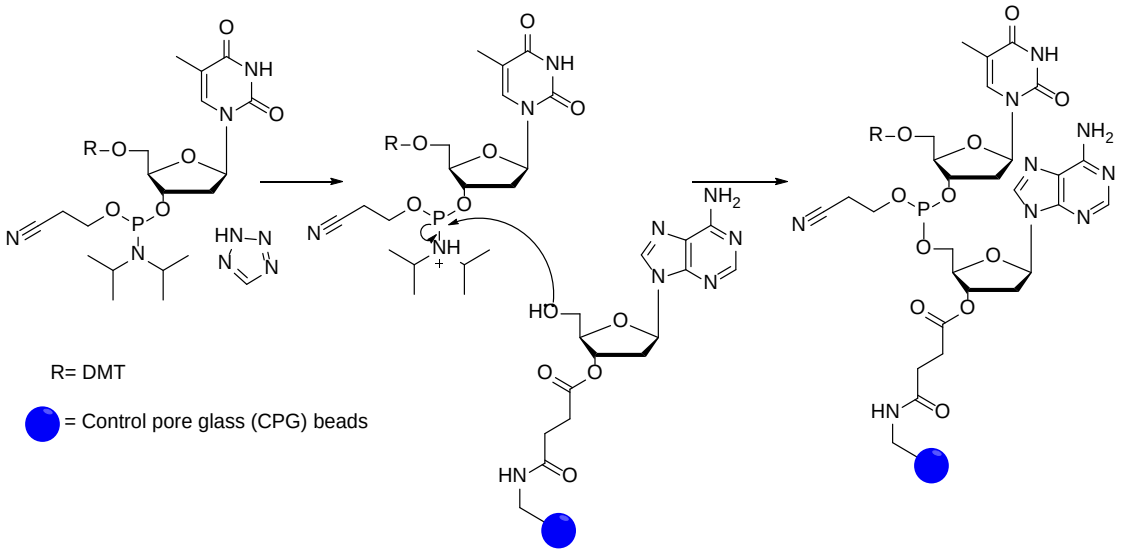

Figure 23 Mechanism showing the activation of thymine with tetrazole coupling in solid phase synthesis of DNA.

The previous deprotection step leaves the hydroxyl group of the ribose sugar free to react with any introduced phosphoramidite monomer. The monomer is first activated by protonation by a tetrazole catalyst. The 5' hydroxyl group then displaces the protonated diisopropyl group forming a new oxygen phosphorus bond. It is essential that this step is conducted under an anhydrous inert atmosphere as the phosphoramidite monomer is easily oxidised which renders it useless for synthesis.

2.1.1.3 Capping

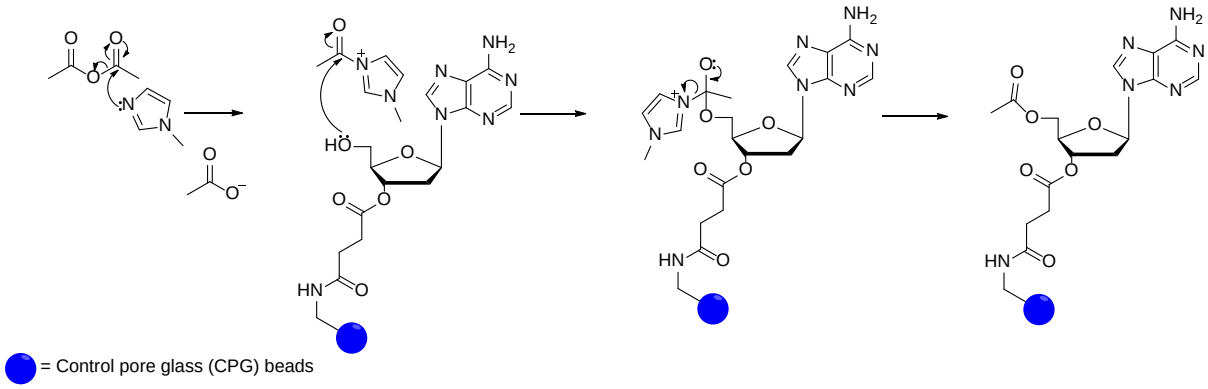

Figure 24 Mechanism showing capping of adenine using acetic anhydride and N-methylimidazole in oligonucleotide synthesis.

Any unreacted monomers on the growing DNA strand are then capped by acetylation of the unreacted alcohol groups making them unable to react to any further monomer additions.

2.1.1.4 Oxidation

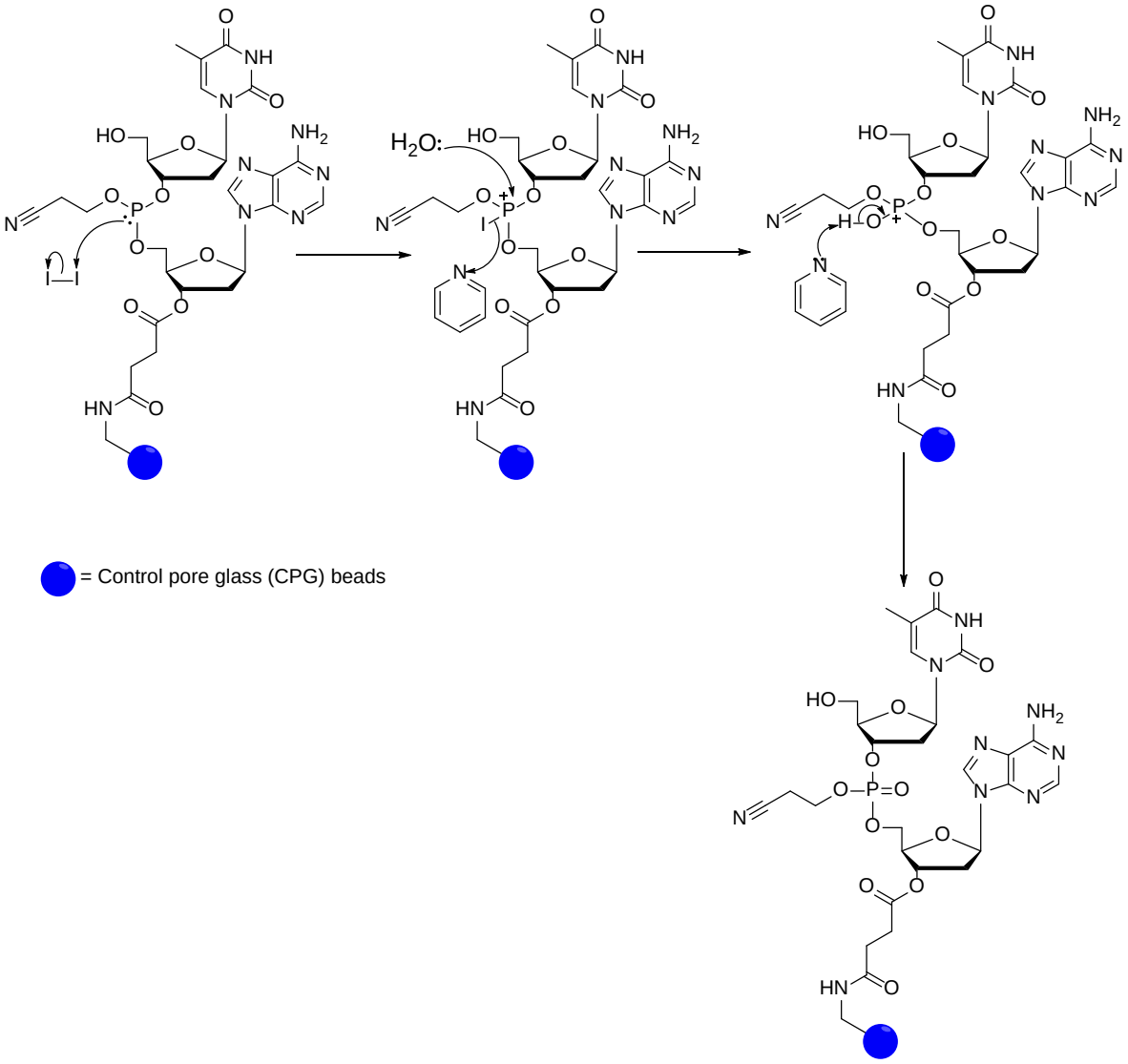

Figure 25 Mechanism showing the oxidation step of thymine using iodine and pyridine in oligonucleotide synthesis.

A mixture of iodine, water and pyridine is used to oxidise the phosphate-triester to an acid stable P(V) species for future detritlyation steps.

2.1.1.5 Cleavage

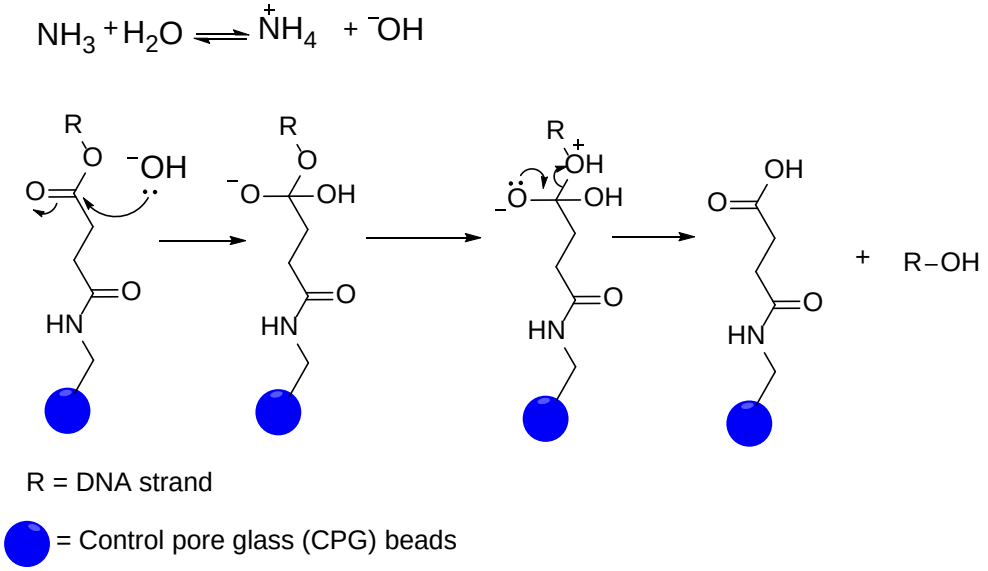

Figure 26 Cleavage of the DNA strand from the CPG bead using aqueous ammonia.

Cleavage from the bead occurs through the addition of aqueous ammonia to the beads. The ammonia deprotonates the water in the solution giving a negatively charged hydroxyl group which is able to attack the ester that links the DNA strand to the CPG bead.

2.1.1.6 Deprotection

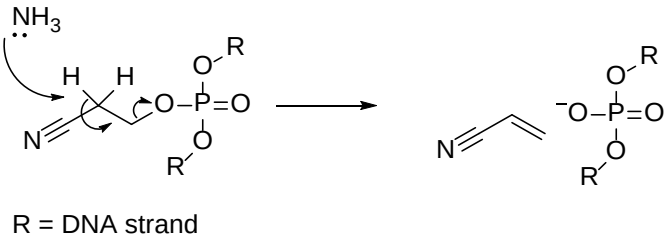

Figure 27 Deprotection of the cyanoethyl protected DNA backbone using aqueous ammonia.

The aqueous ammonia used in the cleavage step is not only used for cleavage from the solid support. It also provides adequate conditions for both the deprotection of the cyanoethly ester protected phosphate backbone and the protecting groups on the DNA bases that would have been susceptible to attack throughout the solid phase synthesis cycle. This is most commonly done at 55 °C for 5 hours but can also take place at lower temperatures for prolonged periods of time.

2.1.1.7 Purification

There are three main methods for the purification of oligonucleotides, high performance liquid chromatography (HPLC), polyacrylamide gel electrophoresis (PAGE) and gel filtration. Each technique has its advantages and disadvantages.

Gel filtration is by far the simplest of the three methods. Commonly used for the removal of small molecules from the sample, rather than failure sequences, it separates the molecules in the mixture by size. Columns are made up of a matrix that small molecules such as salts or cleaved protecting groups bind to which allows the oligonucleotide to pass through the column and be collected. The disadvantage of this technique is that it does not remove similar size molecules. It is routinely used after both HPLC and PAGE as a clean-up method to remove buffer salts and urea.

There are two main types of HPLC used for oligonucleotide purification: reversed phase HPLC (RP-HPLC) and anion exchange HPLC (AE-HPLC). Each works by separating the oligonucleotides using different methods. Reverse phase HPLC uses columns made up of hydrocarbon chains bound to silica as a stationary phase and the change from an aqueous solution to a hydrophobic solvent as the mobile phase. This separates the mixture by hydrophobicity. This technique is especially useful for hydrophobically modified strands or strands synthesised DMT-on. This is when the final DMT group is not removed in solid phase synthesis, thus only the correct strand will contain the DMT group. This therefore increases its hydrophobic properties compared to failure sequences. The disadvantage of this technique is that as the length of the strand increases, the difficulty in strand separation from failure sequences also increases.

AE-HPLC uses the characteristic of a charged backbone to separate out failure sequences. The column used is made up of a tertiary amine which the oligonucleotides originally bind to and slowly release as the ionic strength of the mobile phase is increased. Longer strands are more highly charged as they have a longer backbone, and they therefore bind to the column more strongly and therefore elute later than the shorter failure sequences.

In both AE-HPLC and RP-HPLC, secondary structures of DNA strands can cause broad peaks in the spectrum, making it hard to collect clean fractions. However, both techniques have methods of combating this. A column heater can be used in RP-HPLC which breaks the hydrogen bonds and AE-HPLC can tolerate a high pH which also stops hydrogen bonding therefore eluting clean fractions.

Finally, polyacrylamide gels can be used for purification. Similar to AE-HPLC, they separate by charge but are also affected by hydrodynamic properties. An advantage of this technique is that it is very good at purifying hydrophobic strands. A disadvantage is that a lot of material can be lost in the process, therefore leading to low yields. It also requires the use of large electrophoresis equipment that is expensive, and the technique can be time consuming.

This project used a simple purification technique of a miniaturised version of RP-HPLC. Different brands are available commercially, but this project used GlenPaks. This involved synthesising the DNA with the final DMT group left on which allowed the fully synthesised strand to bind to the

GlenPak resin when treated with triethylammonuim acetate. The failure sequences were then washed through the column as they did not contain the DMT group to bind them to the column. This was followed by the cleaving of the trityl group with a weak acid which was further diluted by washing the column with water. The strand was then eluted in a water acetonitrile mix. A small amount of ammonium hydroxide was also included in the final elution to neutralise any remaining acid.

2.1.1.8 Concentration determination

DNA absorbs light at 260 nm due to the heterocyclic bases therefore using the absorbance spectra of a DNA sample, the concentration can be determined using the Beer Lamberts Law see Equation 1. Where A is the absorbance, c is the concentration, l is path length and ε is the extinction coefficient.

$$A = cl\varepsilon$$

Equation 1 Beer Lamberts Law. A is the absorbance, c is the concentration, l is path length and ε is the extinction coefficient.

2.2 Hydrophobic modifications

Three modifications were chosen to modify the DNA nanopores . Two were commercially available: cholesterol and palmitate. The third, porphyrin, was synthesised using published procedures[96].

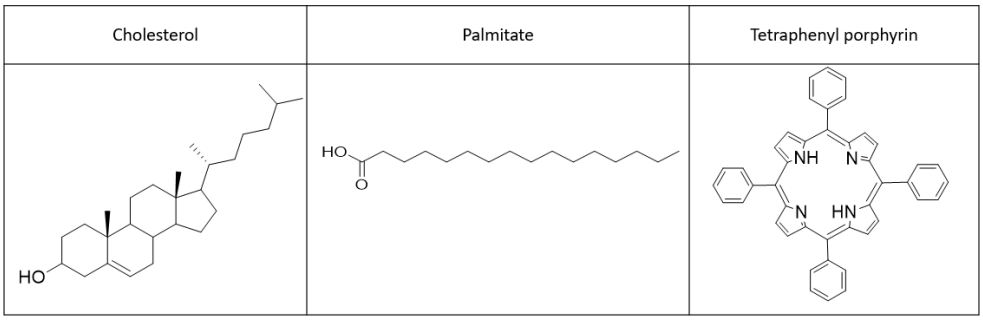

Figure 28 Cholesterol, palmitate and tetraphenyl porphyrin modifications were used in this project. Cholesterol and palmitate were commercially available whereas tetraphenyl porphyrin was synthesised in the lab.

2.2.1 Cholesterol

Cholesterol is a compound readily found in the human body. It is part of the steroid family thus its primary structure is made up of 4 cyclohexane rings and a singular cyclopentane ring (**Figure 29**).

Two sources of cholesterol in the body are dietary intake and biosynthesis which occurs mainly in the hepatic cells in the liver. Although cholesterol is a key component of the human body, too much can lead to many diseases. High cholesterol leads to atherosclerosis, a condition where plaque builds up in the artery and it narrows in diameter. This results in a rise in blood pressure and increases the likelihood of a clot forming which in turn causes life threatening situations such as heart attacks and strokes.

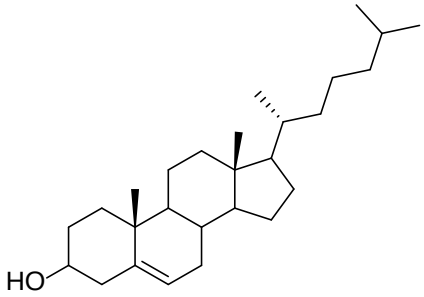

Figure 29 Structure of cholesterol.

Not only is cholesterol the biological precursor to steroid hormones, bile salts and vitamin D, it also is a key component of the plasma membranes. Up to 50% of the membrane lipids is thought to consist of cholesterol[97]. Therefore, it is widely used as a modification to oligonucleotides to aid delivery of the oligonucleotides to cells for antisense therapy[98, 99], transfection[100, 101] etc. Consequently it is a prime candidate for enabling the insertion of a DNA nanostructure into a cell membrane.

2.2.2 Palmitic acid

Palmitic acid is a long saturated fatty acid chain containing 16 carbons, see **Figure 30**. It is found in the human body and enters either through diet or synthesised via *de novo* lipogenesis and makes up 20 – 30% of all fatty acids in the body[102]. It is one of the many fatty acids that is used in membranes within cells.

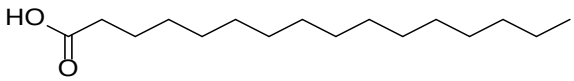

Figure 30 Structure of palmitic acid.

This modification was chosen for a variety of reasons. As the length of fatty acid chains increases the solubility decreases. Chains of C20 and above are known to be insoluble in water whereas short chains of C4 and below are known to be infinitely soluble see **Figure 31**[103]. It can be seen that the solubility between C6 and C8 drops dramatically yet the melting point is still fairly low. The solubility

of palmitate is known to be 0.007 g/L at 20 °C. This value would change when attached to DNA, however it can still give an indication of expected solubility.

Systematic name	Trivial name	Structure	Melting point (°C)	Water solubility (g/L, 20 °C)
Acetic	Acetic	2:0	16.7	Infinite
Butanoic	Butyric	4:0	-7.9	Infinite
Hexanoic	Caproic	6:0	-3.4	9.7
Octanoic	Caprylic	8:0	16.7	0.7
Decanoic	Capric	10:0	31.6	0.15
Dodecanoic	Lauric	12:0	44.2	0.055
Tetradecanoic	Myristic	14:0	53.9	0.02
Hexadeconoic	Palmitic	16:0	63.1	0.007
Octadecanoic	Stearic	18:0	69.6	0.003
Eicosanoic	Arachidic	20:0	75.3	Insoluble
Docosanoic	Behenic	22:0	79.9	Insoluble
Tetracosanoic	Lignoceric	24:0	84.2	Insoluble

Figure 31 Table showing the melting point and water solubility of saturated fatty acids C-2 to C-24. Reprinted with permission[X].

Previous works had used multiple ethyl modifications to act as anchors for DNA nanostructures; they used 72 modifications into total[2]. Therefore, as this project planned to reduce this number to two modifications, a longer chain of 16 carbons (palmitate) was chosen. This modification was also readily available commercially for the attachment to DNA through Link Technologies (3'-Palmitate SynBase™ CPG 1000/110) for use in delivery of DNA into cells. Hence, the palmitate modification was deemed to be appropriate for use in this project.

2.2.3 Porphyrin

Porphyrins are planar macrocyclic compounds consisting of 4 pyrrole units joined at the alpha position by methylene bridges, **Figure 32** left. This gives an aromatic system containing 22 pi electrons, of which, 18 of the electrons are included in a conjugated system therefore satisfying Huckles law of aromaticity. Modifications are commonly made at the meso and B'-positions. The type of modifications made can play a large part in the compound properties. Charged side groups increase the hydrophilicity, whereas large aromatic side groups increase the hydrophobic character.

[X] Stillwell, W., Chapter 4 - Membrane Lipids: Fatty Acids. In An Introduction to Biological Membranes (Second Edition), Stillwell, W., Ed. Elsevier: 2016; pp 49-62. Copyright (2013) Elsevier.

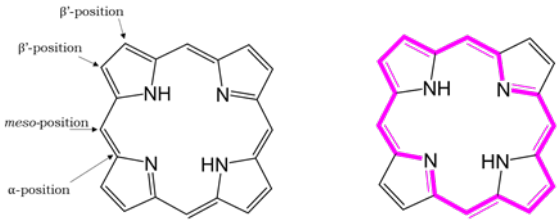

Figure 32 (Left) Porphyrin structure showing different positions, (Right) Aromatic system in porphyrins contain 22 pi electrons of which 18 are in a conjugated system.

The cavity formed is available for the chelation of metal ions. The amines' protons in the ring deprotonate so that the lone pairs then become Lewis acids. Therefore allowing the compounds to become tetradentate chelators to ions such as iron, copper, nickel and cobalt. Larger ligands are also known to sit just out of the plane of the porphyrin[104].

Porphyrins have a very distinct UV-vis profile. The main band with the highest peak is the Soret band which occurs between 380 and 500 nm[105]. This represents the transition from the ground state to the second excited state, S0 to S2, and has an extinction coefficient in the magnitude of 10^5 $M^{-1}cm^{-1}$ [104]. The much smaller bands, the Q bands, occur between 500 and 750 nm which have an extinction coefficient in the magnitude of 10^4 $M^{-1}cm^{-1}$ [104]. They represent a forbidden transition of electrons from the ground state to the first excited state, S0 to S1.

The spectrum varies depending on a variety of factors. For example, in a free base porphyrin, where no metal ion occupies the cavity, there are four Q-bands. This is due to the symmetry in the orbitals being disrupted by the protonated amines. In metallated porphyrins the symmetry is regained and therefore only two Q bands are seen. This is explained with the Gouterman four orbital model which is the widely excepted theorem for this occurrence[106, 107].

Another factor of spectrum appearance is aggregation. Due to the highly hydrophobic character of porphyrins, they easily form aggregates in solution. These aggregates lead to a shift in the Soret band. J- aggregates lead to a red shift and H aggregates lead to a blue shift[108].

2.2.3.1 Porphyrins in nature

Porphyrins play a key role in nature. One of the main examples given is heme, the structure of which is shown in **Figure 33** (right). Heme contains chelated iron (II) which binds oxygen. At high carbon dioxide concentrations, (low pH), oxygen is released whereas at low carbon dioxide concentrations (higher pH), oxygen is bound to the heme[109]. This allows oxygen to be carried around the body and delivered to areas that need it.

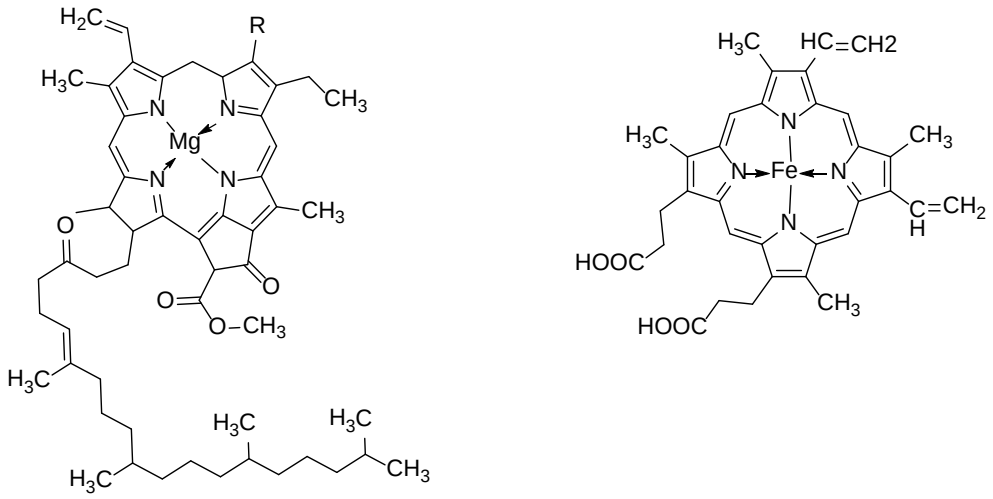

Figure 33 (Left) Structure of chlorophyll, (Right) Structure of heme.

Another commonly known example is chlorophyll, whose centre contains a chlorin which is a reduced form of porphyrin. Chlorophyll, found in plants, contains a magnesium ion and is key in the process photosynthesis; the conversion of water, sunlight and carbon dioxide into glucose and oxygen.

2.2.3.2 Synthesis and attachment to DNA

Rothemund first successfully synthesised porphyrins by reacting pyrrole with an aldehyde in methanol and pyridine for either a prolonged period of time (several weeks) or refluxing at high temperatures for 15 to 25 hours[110, 111]. Benzaldehyde was then used to modify the porphin at the meso position focusing on using high temperatures of 220 °C for 48 hours[112]. These conditions were adapted by Alder and Longo by changing the solvent to propionic acid and refluxing for a shorter period of time (30 minutes) in atmospheric oxygen which led to the oxidation of the porphyrinogen intermediate to porphyrin[113]. This led to conclusions that the rate and yield of the reaction was dependent on acidity, solvent, temperature and concentration of reagents. This was further confirmed by Lindsey *et al.* in 1986[114, 115]. They optimised the equilibrium conditions to give high yields of tetraphenyl porphyrin (between 30 and 40%) by using an aprolar solvent at room temperature and introducing Lewis acids; either boron trifluoride etherate or trifluoroacetic acid. Two oxidants were compared, DDQ and p-chloranil. The former gave lower yields but reaction times were faster, whereas the latter gave notably higher yields yet needed longer reaction times. This gave a synthesis route that used less harsh conditions, in both temperature and acidity, which broadened the variety of side groups that the porphin structure could be modified with.

Although perfect for symmetrical porphyrins, the Lindsey synthesis route did not account for asymmetric porphyrin synthesis. Work by Stulz *et al*[116-121] showed that using specific ratio of 6:6:1 of pyrrole, aldehyde and desired aldehyde modification gave a single point modification on the

compound. The disadvantage for this method is that a large amount of unsubstituted tetraphenyl porphyrin is also formed. However, this did allow for further single point modification of the porphyrin such as the attachment of DNA either post or on solid phase synthesis. Therefore the Stulz method, discussed further in Chapter 4, was used in this project.

2.3 Nanopores

Three different nanopores were used in this project with different modifications, summarised in **Figure 34** and described in detail below.

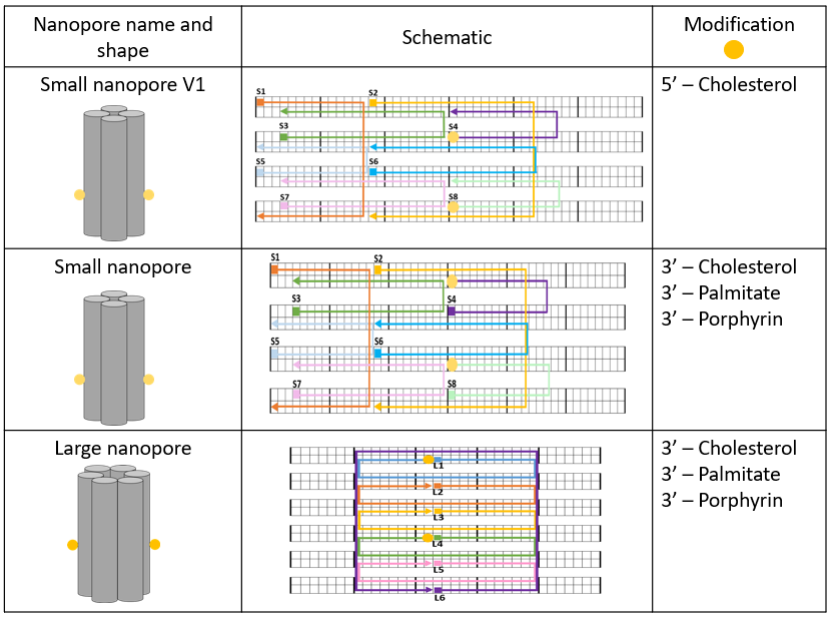

Figure 34 Summary image of nanopores and modifications used in this project.

2.3.1 Small nanopore

The small nanopore design used in this project was that published by Göpfrich *et al.* in 2015. Built on the square lattice, it provided an analysed nanopore with a pore width of 0.8 nm and length of 11 nm.

Göpfrich's nanopore was modified on the 3' terminus of two strands of DNA with cholesterol molecules. In initial experiments the modifications were moved to the 5' terminus using a phosphoramidite of cholesterol purchased through LinkTechnologies, shown in **Figure 35**. This was done as the materials for the 5' modification were less expensive than that of the 3' modified beads. It was also noted that the 5' phosphoramidite could be used in multiple synthesises whereas the CGP beads could only be used for one synthesis. The optimal method of purification of hydrophobically modified DNA is through PAGE. HPLC is also a viable method but the risk of the

hydrophobic DNA blocking the column is high. Therefore, PAGE was first used to purify these products.

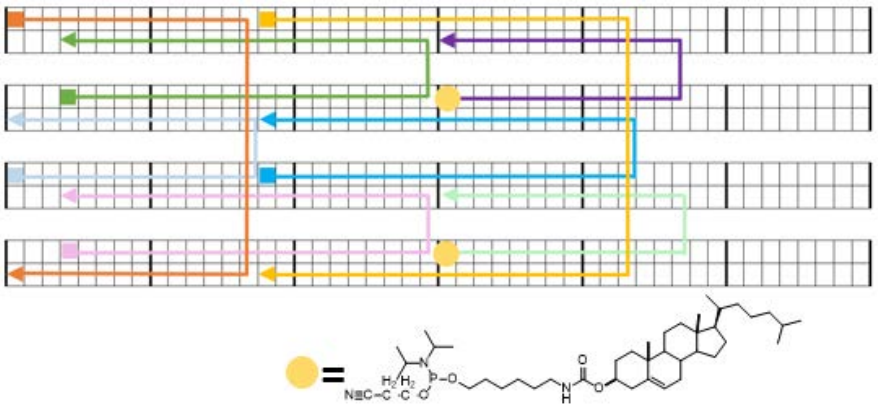

Figure 35 Design of the small nanopore V1 based on Göpfrich nanopore. Modifications were moved from 3' to 5'.

Although PAGE is a useful and widely used method in the purification of oligonucleotides, it can lead to low yields because a lot of material can be lost during the process. Another limiting factor was access to the large gel kits needed for PAGE. It was also noted that even after PAGE there was still unmodified DNA remaining. However, due to time constraints the impure strands were used in initial cell tests in the first visit to Singapore described in Chapter 3.

Due to the purification issues described above, it was decided that for secondary cell experiments, that took place during the second instalment of work in Singapore, the project would revert to the original design by Göpfrich *et al.* CPG beads were purchased from LinkTechnologies modified with a cholesterol compound so that a modification at the 3' terminus occurred. This would ensure that all DNA strands synthesised would contain a modification, even the failure sequences. Although it would be very difficult to remove failure sequences from the desired sequence, it meant that all DNA strands synthesised had a cholesterol modification on them. Any failure sequences were less likely to be included in the nanostructures since the longer the strand, the more likely they would displace any shorter strand in the nanostructures and therefore form full structures. This was also ensured by including the modified strands in a 2x excess compared to unmodified strands. This was a slight decrease from that used in literature but conserved material.

One small alteration from the published nanopore was a base change in S6 from G to A base and in S7 from C to T. This was due to initial experiments were the modification was moved to be internal in these strands. This one base change was carried forward so not to waste material previously made.

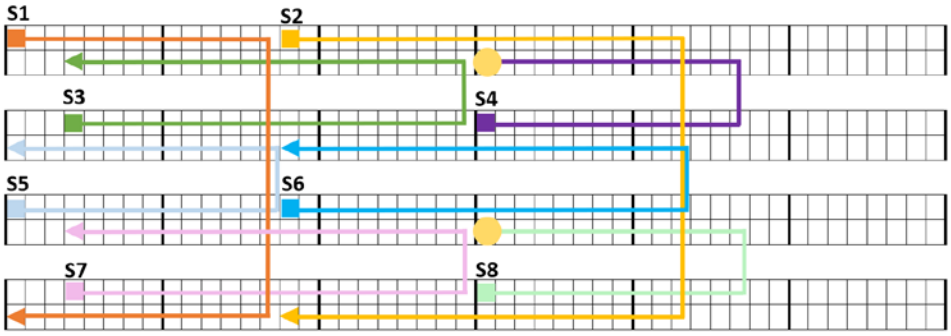

Figure 36 A schematic of the small nanopore in a form used by Cadnano, each squared grid represents a helical domain with each individual square representing a nucleotide. The solid filled squares represent the 5' terminus of the DNA and the solid triangles, the 3' terminus. DNA strands and crossovers are clearly shown by the different coloured arrows.

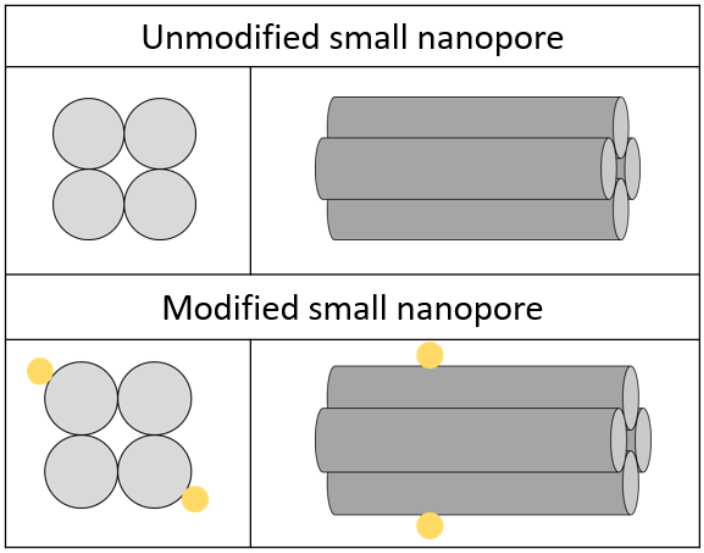

Figure 37 A simplified image of the small nanopore both with and without modifications. Each helical domain is represented by a cylinder. The strand sequences can be seen in Table 2. (Upper left) End view of unmodified small nanopore, (Upper right) Length view of unmodified small nanopore, (Bottom left) End on view of modified nanopore, (Bottom right) Side view of modified small nanopore.

Table 2 Small nanopore DNA sequences.

Stand label	Sequence 5' to 3'
S1	AAACTCCCGGAGTCCGCTGCTGATCAAA
S2	GTCCCGTCTTTGGATCCGAAAGCCATAATATATCGAGACGGG

S3	GGATCTAAAGGACTTCTATCAAAGACGGGACGACTCCGGGAG
S4	GGCATCGTTGGAAAAAATTTCGGATCCA
S5	AAAACGCTAAGCCACCTTTAGATCCAAA
S6	GGTCGTGCAGACTGTCGAACACCAACGATGCCTGATAGAAGT
S7	GATCAGCAGCGCCCGTCTCGACTGCACGACCTGGCTTAGCGT
S8	TATATTATGGCAAAAAATGTTCGACAGT
S4 cholesterol modified	GGCATCGTTGGAAAAAATTTCGGATCCAAAA – Cholesterol
S8 cholesterol modified	TATATTATGGCAAAAAATGTTCGACAGTAAA – Cholesterol
S4 palmitate modified	GGCATCGTTGGAAAAAATTTCGGATCCAAAA – Palmitate
S8 palmitate modified	TATATTATGGCAAAAAATGTTCGACAGTAAA – Palmitate
S4 tetraphenyl porphyrin modified	GGCATCGTTGGAAAAAATTTCGGATCCAAAA – Porphyrin
S8 tetraphenyl porphyrin modified	TATATTATGGCAAAAAATGTTCGACAGTAAA – Porphyrin

2.3.2 Large nanopore

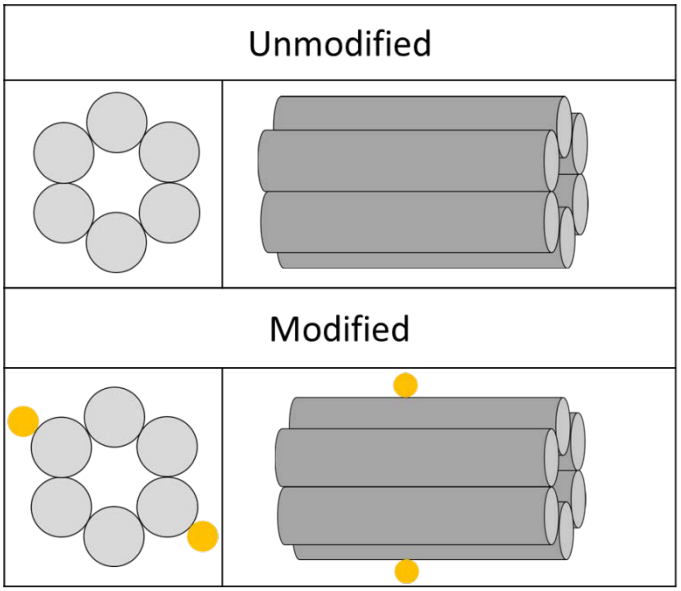

Figure 38 A simplified image of the large nanopore both with and without modifications. Each helical domain is represented by a cylinder. The strand sequences can be seen in Table 3. (Upper left) End view of unmodified large nanopore, (Upper right) Length view of unmodified large nanopore, (Bottom left) End on view of modified nanopore, (Bottom right) Side view of modified large nanopore.

Early versions of a nanopore based on the hexagonal lattice were shown to successfully insert into artificial membranes and show a current passing through when modified with porphyrin[45] (**Figure 39**) or ethyl thiophosphate molecules[44]. These structures were made up of 8 strands of DNA varying in length which crossed over between helical domains.

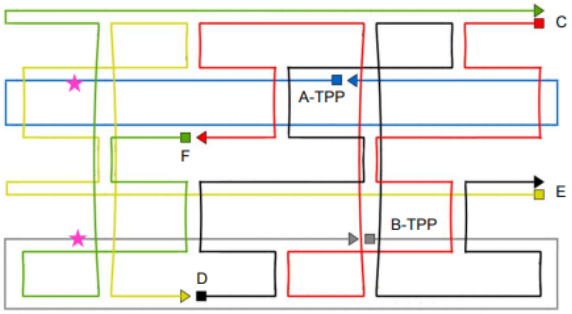

Figure 39 Original large nanopore published by Burns *et al.* modified with tetraphenyl porphyrin represented by purple star. Reprinted with permission[XI]. The system was made up of long strands of DNA with multiple crossovers.

The porphyrin modifications were placed in strands which were 92 bases in length. This was undesirable for a variety of reasons. Firstly, the modification was made in the middle of the strand. This meant that if the coupling efficiency was low yielding, the resultant strand would be very low yielding due to additional couplings decreasing the yield further. This could be easily combatted by shifting the break in the strand so that the position coincides with either the 5' or 3' terminus. This would ensure that any modification was in the same position but would combat the difficulty of an internal modification.

Secondly, long strands of DNA are difficult to synthesise because the yield decreases as the length of the strand increases. Finally, long strands are also more difficult to purify. This could be combatted by shortening the modified strand. However this may have led to instability in the structure.

[XI] Burns, J. R.; Gopfrich, K.; Wood, J. W.; Thacker, V. V.; Stulz, E.; Keyser, U. F.; Howorka, S., Lipid-Bilayer-Spanning DNA Nanopores with a Bifunctional Porphyrin Anchor. Angewandte Chemie-International Edition 2013, 52 (46), 12069-12072. Copyright John Wiley and Sons 2013.

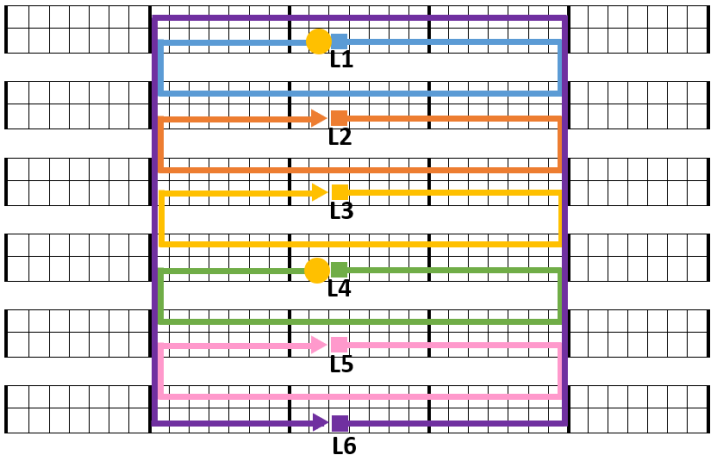

Figure 40 Schematic of the large nanopore, each squared grid represents a helical domain with each individual square representing a base. The solid filled squares represent the 5' terminus of the DNA and the solid triangles, the 3' terminus.

Further work provided by Burns *et al* showed a much simpler system[3], shown in **Figure 40**. Although shorter in length, it also provided an easy to modify structure that was well studied. The disadvantage of this structure was that there were no strand breaks at either end of the pore therefore there are fewer chances of extending the system, however again, as said before with the previous system, the break in the strands could be repositioned if desired. Therefore, the latter system was taken forward as a structure for the large nanopore in this project, for which the DNA sequences can be found in Table 3.

Table 3 DNA sequences for the large nanopore.

Stand label	Sequence 5' to 3'
L1	AGCGAACGTGGATTTTGTCCGACATCGGCAAGCTCCCTTTTTCGACTATT
L2	CCGATGTCGGACTTTTACACGATCTTCGCCTGCTGGGTTTTGGGAGCTTG
L3	CGAAGATCGTGTTTTTCCACAGTTGATTGCCCTTCACTTTTCCCAGCAGG
L4	AATCAACTGTGGTTTTTCTCACTGGTGATTAGAATGCTTTTGTGAAGGGC
L5	TCACCAGTGAGATTTTTGTCGTACCAGGTGCATGGATTTTTGCATTCTAA
L6	CCTGGTACGACATTTTTCCACGTTCGCTAATAGTCGATTTTATCCATGCA
L1 cholesterol modified	AGCGAACGTGGATTTTGTCCGACATCGGCAAGCTCCCTTTTTCGACTATT – Cholesterol

L4 cholesterol modified	AATCAACTGTGGTTTTTCTCACTGGTGATTAGAATGCTTTTGTGAAGGGC – Cholesterol
L1 palmitate modified	AGCGAACGTGGATTTTGTCCGACATCGGCAAGCTCCCTTTTTCGACTATT – Palmitate
L4 palmitate modified	AATCAACTGTGGTTTTTCTCACTGGTGATTAGAATGCTTTTGTGAAGGGC – Palmitate
L1 tetraphenyl porphyrin modified	AGCGAACGTGGATTTTGTCCGACATCGGCAAGCTCCCTTTTTCGACTATT – Porphyrin
L4 tetraphenyl porphyrin modified	AATCAACTGTGGTTTTTCTCACTGGTGATTAGAATGCTTTTGTGAAGGGC – Porphyrin

2.4 Cell lines tested

Four different cell lines were tested throughout this project. Each was selected for their suitability and availability during the project.

2.4.1 HEK293

HEK293 cells are human embryonic kidney cells of which there are many variants. Due to availability, two different variants were used at different stages of the project; HEK293T and HEK293FT. HEK293T cells contain a SV40 large T antigen, therefore any plasmid that contains SV40 has increased protein production when transfected. The HEK293FT variant also contains the SV40 large T antigen, but is a faster growing variant[122].

2.4.2 B16-F10

B16-F10 cells are an adherent mouse melanoma cell line commonly used for investigations with melanoma. They are a fast-growing cell line therefore suitable for a high throughput of cell tests.

2.4.3 FM55-P

FM55-P cells are an adherent human melanoma cell line established from a primary malignant melanoma therefore was highly relevant to this project. It is commonly used for modelling melanoma cell assays and was readily available for use.

2.5 Measuring cytotoxicity

There are many methods of monitoring cell viability and proliferation of cells. This project utilised a variety of methods depending on availability of equipment and reagents.

2.5.1 Confluence

Cell confluence is a measure of the area taken up by the cells in the vessel they are contained in. A change confluence gives an indication of how the cells are proliferating. A way of measuring the confluence of many cells is by using an IncuCyte. The IncuCyte is a useful machine as it allows the cells to be monitored without disturbing them from cell culture conditions. For confluence measurements it takes a set number of photos in a well (four for a 96 well plate) and applies a specified cell mask which recognises cell material and calculates the area covered by cells in the photo. This data can then be plotted as a confluence curve.

2.5.2 MTS

The MTS assay is a cell viability assay. This utilised the mitochondrial activity in viable cells where multiple redox reaction occur which can be used to reduce the MTS compound formazan. This produces a colorimetric change, **Figure 41**. The absorbance of solutions can be measured at 490 nm and the higher the value, the greater number of viable cells in the sample.

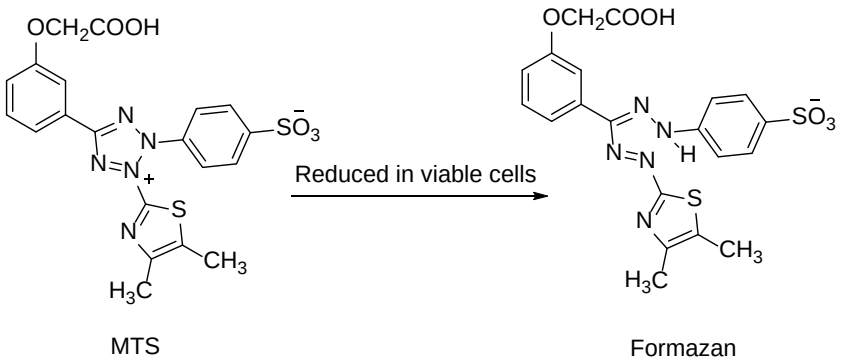

Figure 41 Reduction of MTS tetrazolium to formazan.

2.5.3 Alamar Blue

Alamar blue is an assay that measures cell viability by monitoring the reduction of resazurin through absorbance or fluorescence. Resazurin is readily reduced in viable cells to resorufin, **Figure 42**, providing a colorimetric change, blue to pink, which can be measured by absorbance. Resorufin is also highly fluorescent (excitation 560 nm, emission 590 nm). Therefore, the higher the fluorescence signal the more viable cells are in the sample. For the purpose of this project the fluorescence was used as a measurement do to the greater sensitivity than absorbance[123].

Whereas the previously mentioned MTS assay involved the use of an intermediate electron acceptor in the reaction chain to reduce the tetrazolium compound, the resazurin salt is directly reduced by FMNH2, FADH2, NADH, NADPH and cytochromes[124]. Some argue, that as it does not interfere with the electron chain reaction, this can allow the assay to be used for continuous cell monitoring, however for the purpose of this project it was used as an end point assay.

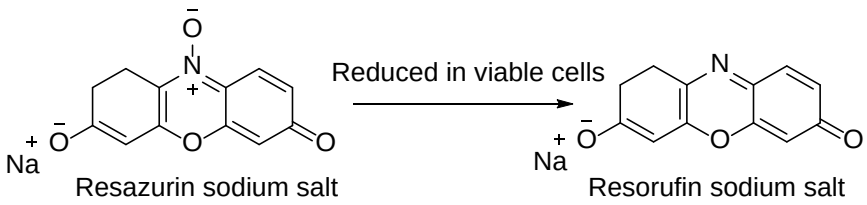

Figure 42 Alamar blue assay resazurin reduction.

2.5.4 Crystal violet

The crystal violet assay utilises the fact that when cells die, they are no longer adherent and therefore detach from the well plate[125]. Crystal violet, the structure of which can be seen in **Figure 43**, binds to DNA and peptides and therefore the remaining cells in the monitored population. In this project the crystal violet assay was conducted after the alamar blue assay. Excess dye was washed off and the remaining stain was dissolved in acetic acid and the resulting purple solution's absorbance was read using a well plate reader. The higher the absorbance reading, the more viable cells there were in the sample.

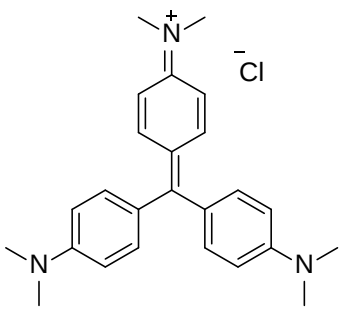

Figure 43 Structure of crystal violet.

2.6 Normalising data

Data was normalised to negative controls within the experiments. This varied between using the vehicle control of PBS or cells treated only with media depending on the experiment. This has been clearly indicated in each experiment. These cells were taken as healthy cells and therefore are taken as 100% cell viability. In some experiments this led to values being classed as over 100% cell viability or biomass in well as these samples produced results higher than that of the control.

Chapter 3 Experimental details

3.1 General experimental details

3.1.1 Suppliers

Chemicals were supplied by, Sigma Aldrich, Fischer Scientific, Glen Research, Link Technologies and Cambio and used as instructed by supplier. Deionised water was filtered by a Milli-Q gradient A1-filter.

3.1.2 Colum chromatography and TLC

Silica gel (40 – 60 μm particle size) and silica gel type H (10 – 40 μm particle size) where specified were supplied from Sigma Aldrich and basic aluminium oxide (50 – 200 μm, Brockmann activity I) supplied from Acros Organics were used to conduct column chromatography.

TLC silica gel 60 F_{254} on aluminium backed sheets supplied by Merk were used to visualise compounds using UV light of wavelengths 254 nm and 365 nm.

3.1.3 UV-Visible spectroscopy

A Varian Cary 300 Bio spectrometer with quartz cells (supplied by Hellma and Starna) with a path length of 1 cm were used for scans at room temperature.

3.1.4 Fluorescence Spectroscopy

A Varian Cary Eclipse spectrometer with quartz cells (supplied by Hellma and Starna) were used for scans at room temperature.

3.1.5 NMR Spectroscopy

NMR was carried out at room temperature using a Brucker Advance DPX-400 spectrometer.

3.1.6 DNA experimental details

3.1.6.1 DNA Synthesis

DNA synthesis was carried out on either an Applied Biosystems Expedite machine or an Applied Biosystems 392 DNA/RNA Synthesizer using 1000 Å CPG beads on a 1 μmol scale. Standard coupling

times were used for the bases unless otherwise stated for modified beads. The deblock used was 3% TCA in DCM. Activator used was 0.3 M Benzylthio-1 *H*-tetrazol in acetonitrile. Cap A, acetic anhydride in THF and Cap B, 10% methylimidazole in THF/pyridine (8:1), were used for capping steps. 0.02 M iodine in THF/pyridine/water were used for oxidation.

DNA was cleaved from the beads through passing concentrated ammonium hydroxide (1 mL) at room temperature for 2 hours followed by washing the beads with additional concentrated ammonium hydroxide (0.5 mL). The DNA was then deprotected by heating in the concentrated ammonium hydroxide solution at 55 °C for a minimum of 5 hours with agitation in an Eppendorf thermomixer compact.

The oligonucleotide was then purified and desalted using GlenPak cartridges purchased from Glen research.

3.1.6.2 GlenPak procedure

The cartridge was first prepared by treating with acetonitrile (1 mL) followed by 2.0 M TEAA (2 mL). The sample was made up to a concentration of 50 mg /mL sodium chloride solution and a volume of 2 mL. This was then loaded onto the column by syringe at a pressure that equated to the liquid exiting the column in a dropwise fashion. The column was then treated with a solution containing 5% Acetonitrile in 100 mg/mL sodium chloride solution (2 mL). Followed by 2% trifluoacetic acitic (2 mL). Finally, the column was washed with water (2 mL) before the elution of the sample in acetonitrile/water (50:50) containing 5% aqueous ammonia hydroxide solution (1 mL).

3.1.6.3 DNA drying

Samples were dried using an Eppendorf Concentrator 5301 using appropriate solvent settings.

3.1.6.4 Cholesterol and Palmitate modified DNA synthesis

Strands were synthesised using modified CPG beads (3’ Cholesterol SynBase™ CPG 1000/110 Link Technologies item number 2394, 3’ Palmitate SynBase™ CPG 1000/110 Link Technologies item number 2393) and synthesised on a 1 µM scale. Synthesis was modified for the synthesis of these strands as recommended by the manufacturers. The initial detritylation step was doubled from the usual 85 seconds to 170 seconds. The first coupling was held on the beads for 5 minutes as opposed to the normal 25 seconds coupling time. The strands were synthesised DMT off and were desalted using NAP columns.

3.1.6.5 Amino modified DNA synthesis

Strands were synthesised using a modified CPG bead (3'-Amino-Modifier C7 CPG 1000 item number Link Technologies 2350) on an Expedite Nuclei Acid synthesis system. The DNA synthesiser was set to do two detritylations before the first coupling followed by an extended coupling time of the first base of 5 minutes. Synthesis was continued on a 1 µM scale DMT on. Before cleavage from the solid support the strand was treated to deprotect the amine. The column was first washed with 20% Diisopropylamine in acetonitrile (1 mL) followed by acetonitrile (1 mL). 20% Piperidine in DMF (1 mL) was pushed through the column for 10 minutes before being washed with acetonitrile (2 mL). Three wash steps were then prefomed on the DNA synthesiser followed by three gas purging steps to dry the beads. The oligonucleotide was then cleaved from the beads in the normal manner, deprotected and purified by GlenPak.

3.1.6.6 Porphyrin modified DNA

This was conducted by the university of Southampton undergraduate 4th Year chemistry student Andrew Peddie.

Amino-SynBase™ CPG (1000/110) (LCAA) resin (250 mg, Link Technologies, 64 µmol/g loading) was measured into two 1.5 mL Eppendorf tubes. To each Eppendorf tube, Succinic anhydride (25 mg, 0.25 mmol, 1 equiv), 4-dimethylaminopyridine (3 mg, 0.025 mmol, 0.1 equiv) and anhydrous pyridine (6 mL) was added and the solutions were shaken overnight at room temperature. The liquid was removed by filtration and the beads were combined and washed with anhydrous pyridine (1.2 mL), methanol (3 mL) and dichloromethane (6 mL) before being left to dry. Qualitative analysis of the reaction was measured with ninhydrin.

The succinylated beads were split between two 1.5 mL Eppendorf tubes and 5'-DMT-(5''-p¬-ethynylphenyl)-10'',15'',20''-triphenyl-Zn (II)-porphyrin-dU (15 mg, 0.0125 mmol 1 equiv) was added to each. DMAP (1.5 mg, 0.0125 mmol, 1 equiv), triethylamine (10 µL, 7.26 µmol, 0.9 equiv), N,N'-Diisopropylcarbodiimide (19 µL, 0.0153 mmol, 1.2 equiv) and anhydrous pyridine (0.6 mL) were added to each Eppendorf tube and the reaction was shaken for 18 hours.

Pentachlorophenol (17mg, 63.8 nmol, 0.005 equiv) was added to each Eppendorf tube and shaken for 24 hours. Piperidine (0.6 mL, 6.07 µMol, 0.5 equivalents) was added to each shaking suspension for less than five minutes. The beads were collected by filtration and washed with anhydrous pyridine (1.2 mL), methanol (3 mL) and dichloromethane (6 mL) and left to dry.

The beads were returned to Eppendorf tubes and a 1:1 mixture of Capping solution A and Capping solution B (0.6 mL) was added to each and shaken for 2 hours. The beads were collected by filtration and dried by air.

Functionalised beads (5 mg) were treated with detritylating solution (3% trifluoroacetic acid in DCM, 500 µL). Absorbance at 505 nm was measured Equation 2 was used to determine bead loading.

$$Loading = \frac{volume \times absorbance}{\varepsilon} \times \frac{1000}{weight}$$

Equation 2 Equation to determine the loading of functionalised beads. Loading (µmol g-1), for a cuvette pathlength of 1 cm, volume (mL), support weight (mg), Ɛ = 76 mL cm-1 µmol-1

Where loading (µmol g^{-1}), for a cuvette pathlength of 1 cm, volume (mL), support weight (mg), DMT Ɛ = 76 mL cm^{-1} µmol^{-1}.

3.1.6.7 Formation of nanopore

DNA strands (0.2 nmol) were pipetted into an Eppendorf tube to a final volume of 100 mL in a buffer of 1 x PBS to make a solution of concentration 2 µM. The mixture was heated to 90 °C then cooled 1 °C per minute to 4 °C using one of three thermocyclers; BioRad T-100 thermal cycler, Applied Biosystems Veriti 96 well thermal Cycler or Applied Biosystems ProFlex PCR System. Before cell treatment, nanopores were sterilised with a Millex®-GV 0.22 µm filter unit (Hydrophilic durapore® PVDF membrane).

Unmodified small nanopore strand combination: S1, S2, S3, S4, S5, S6, S7, S8

Cholesterol modified small nanopore strand combination: S1, S2, S3, S5, S6, S7 and S4 cholesterol modified and S8 cholesterol modified (Cholesterol strands added in x 2 excess 0.4 nmol)

Palmitate modified small nanopore combination: S1, S2, S3, S5, S6, S7 and S4 palmitate modified and S8 palmitate modified (palmitate strands added in x 2 excess 0.4 nmol)

Porphyrin modified small nanopore strand combinations: S1, S2, S3, S5, S6, S7 and S4 porphyrin modified and S8 porphyrin modified (porphyrin strands added in x 2 excess 0.4 nmol)

Unmodified large nanopore strand combination: L1, L2, L3, L4, L5, L6

Cholesterol modified small nanopore strand combination: L2, L3, L5, L6 and L1 cholesterol modified and L4 cholesterol modified (Cholesterol strands added in x 2 excess 0.4 nmol)

Palmitate modified small nanopore combination: L2, L3, L5, L6, L1 palmitate modified and L4 palmitate modified (palmitate strands added in x 2 excess 0.4 nmol)

Porphyrin modified small nanopore strand combinations: L2, L3, L5, L6 and L1 porphyrin modified and L4 porphyrin modified (porphyrin strands added in x 2 excess 0.4 nmol)

3.1.6.8 Agarose gel electrophoresis

Agarose (1.5 g, 1.5% gel) was dissolved in 1 x TAE buffer supplemented with 11 mM $MgCl_2$ (100 mL) by heating by microwave and swirling regularly until solution was clear. The molten solution was poured into a gel cast and sybr Safe (10 µL) was added and mixed evenly in the gel. A comb was then inserted and the gel was left to set. The solid gel was transferred to the gel tank and the gel was run at the indicated voltage for the desired time. Gels were imaged using a BioRad molecular Imager Gel Doc™ using SyBr safe setting.

3.1.7 Chemical synthesis

3.1.7.1 Synthesis of 4-(3-hydroxy-3-methylbut-1-ynyl)benzaldehyde[96]

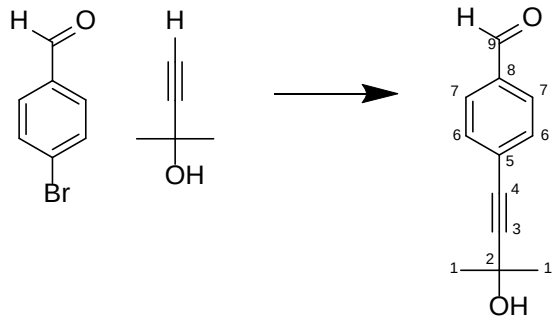

4-Bromobenzaldehyde (6.0 g, 30 mmol, 1 equiv.) 10% palladium on carbon (1.26 g, 12.0 mmol, 0.40 equiv.), triphenylphosphine (1.28 g, 4.8 mmol, 0.16 equiv.), copper iodide (0.46 g, 2.4 mmol, 0.08 equiv.) and potassium carbonate (20.58 g, 150 mmol, 5 equiv.) were dissolved in 1,2-Dimethoxyethane water mixture (1:1, 120 mL) which resulted in a black solution. This was purged with argon for 30 minutes. Methyl-3-2-ol (14.7 mL, 150 mmol, 5 equiv.) was then added to the reaction mixture. The reaction was heated at 90 °C and stirred for 18 hours.

The reaction mixture was filtered through celite twice and extracted with ethyl acetate (400 mL. The reaction was further washed with Brine (3 x 50 mL). The reaction mixture was collected and dried with Sodium sulphate and concentrated *in vacuo*.

The reaction was then purified by column chromatography (Silica, 12.5% EtOAc in petroleum ether to 20% EtOAc in petroleum ether). This resulted in a brown oil (3.4429 g, 18.3 mmol, 61% yield).

This was further purified by column chromatography (Silica, 12.5% Ethyl acetate in petroleum ether to 20% Ethyl acetate in petroleum ether) which resulted in a yellow oil which further dried to form a yellow solid. NMR showed slight decomposition of the product but further purification would lead to further reduced yields therefore the product was carried forward. 2.1689 g (0.015 mol, 36% yield). Analytical data were consistent with literature values.[96]

^{1}H NMR (Chloroform-d 400 MHz): δ = 10.00 (s, 1H, H-9), 7.82 (d, J = 8.2, 2H, H-7), 7.56 (d, J = 8.2, 2H, H-6), 1.64 (s, 6H, H-1)

3.1.7.2 Synthesis of 5-p-(3-methyl-3-hydroxyl-1-butynl)phenyl – 10,15,20-triphenyl porphyrin[96]

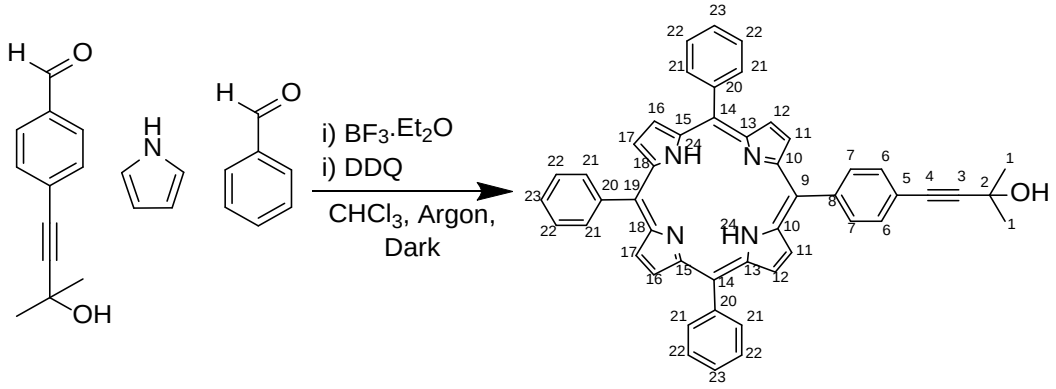

Chloroform was purged with argon for 15 minutes. Pyrrole, first purified by silica, (2.1 mL, 30 mmol, 6 equiv.), benzaldehyde (3.05 mL, 30.0 mmol, 6 equiv.) and 4-(3-hydroxy-3-methylbut-1-ynyl)benzaldehyde (0.931 g, 5.0 mmol, 1equiv.) were added to the reaction and stirred for 30 minutes under argon and in darkness. Boron trifluoride dietyletherate (0.57 mL, 4.5 mmol,0.9 equiv.) was added to the reaction and stirred for a further one hour. DDQ (6.81 g, 30.0 mmol, 6 equiv.) was added to the reaction and the argon was removed. The reaction was left to stir for a final 18 hours in the dark.

The reaction was concentrated *in vacuo* and re-dissolved in DCM (200 mL) to be purified by column chromatography, firstly (silica/basic alumina, DCM to 5% MeOH), secondly (silica/basic alumina, 100 % DCM to 5% MeOH) and finally (silica, DCM). This resulted in dark purple crystals (384.5 mg, 0.55 mmol, 11% yield). Analytical data were consistent with literature values.[96]

RF (10% MeOH in DCM): 0.84

^{1}H NMR (Chloroform-d 400 MHz): δ = 8.91 (d, J =5.6, 6H, H-17/16/12), 8.87 (d, J =4.8, 2H, H-11), 8.27 (d, J =1.5, 6H, H-21), 8.22 (d, J =8, 2H, H-7), 7.86 (d, J =8, 2H, H-6), 7.80 (m, 9H, H-22/23), 1.81 (s, 6H, H-1), -2.712 (s, 2H, H-24)

ESI+ ($C_{49}H_{36}N_4O$): Monoisotopic mass: 696.29, Observed m/z = 697 $[M + H]^+$

3.1.7.3 Synthesis of Zn(II) 5-p-(3-methyl-3-hydroxyl-1-butynl)phenyl – 10,15,20-triphenyl porphyrin[96]

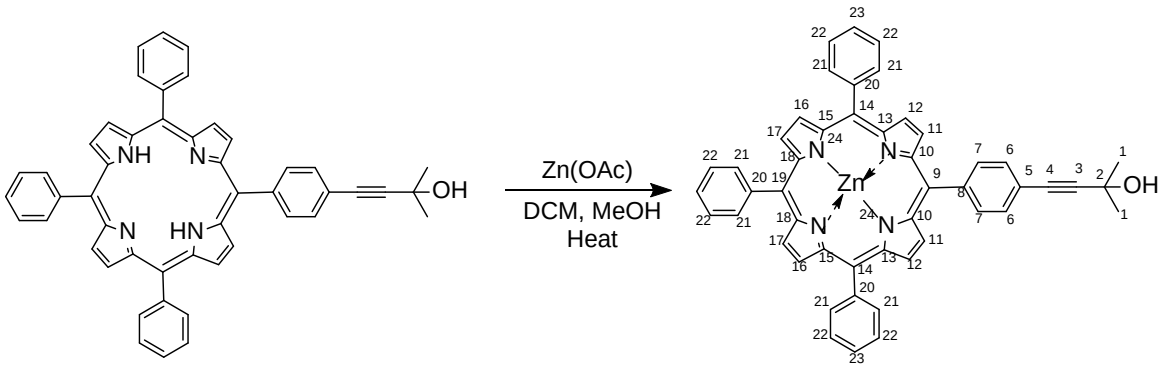

5-p-(3-methyl-3-hydroxyl-1-butynl)phenyl – 10,15,20-triphenyl porphyrin (370 mg, 0.530 mmol, 1 equiv.) and zinc acetate dehydrate (4.64 g, 21 mmol, 40 equiv.) were dissolved in DCM : MeOH (80 mL:10 mL). The reaction was heated gently whilst swirling for 15 minutes. The solvent was removed *in vacuo* and the solid re-dissolved in Dichloromethane (20 mL). The insoluble zinc was then removed by filtration and the solvent in vacuo.

The product was then purified by column chromatography (Silica, 100% DCM) which resulted in purple/pink crystals (393 mg, 0.52 mmol, 93%). Analytical data were consistent with literature values.[96]

RF (10% MeOH in DCM): 0.84

^{1}H NMR (Chloroform-d, 400 MHz): δ = 9.00 (d, J = 4.1, 6H, H12/16/17), 8.95 (d, J = 4.7, H11), 8.25 (d, J = 6.3, 6H, H21), 8.20 (d, J = 8, 2H, H-7), 7.83 (d, J = 7.9H, 2H, H6), 7.79 (m, 9H, H22/23), 1.67 (s, 6H, H1)

^{13}C NMR (Chloroform-d, 100 MHz): δ = 150.30 (C-12), 150.20 (C-17), 149.79 (C-7), 14.55 (C-6), 142.74 (C-18), 134.42 (C-19), 134.35 (C-5), 132.20 (C-10/9), 132.06 (C-15/14), 130.36 (C-4), 127.52 (C-21), 121.37 (C-16), 121.26 (C-13), 119.92 (C-8), 83.77 (C-1), 78.11 (C-2)

ESI+ ($C_{49}H_{34}N_4OZn$): Monoisotopic mass: 700.16 observed m/z 701 $[M+H]^+$

3.1.7.5 Synthesis of 5-DMT-5-Iodo-deoxyuridine[96]

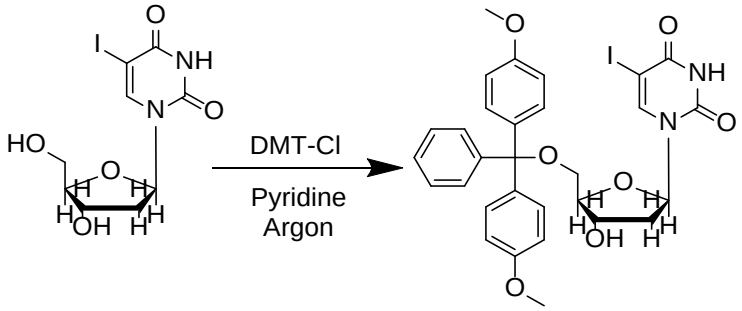

5-Iodo-deoxyuridine (2.5 g, 7.06 mmol, 1.0 equiv.) was dried by co-evaporation with pyridine (3 x 5 mL) before dissolving in anhydrous pyridine (20 mL) and purging for 10 minutes with Argon. 4, 4' dimethoxytrityl chloride (2.6 g, 7.77 mmol, 1.1 equiv.) was added portion wise over 4 hours as the reaction was stirred. After the last addition of dimethoxytrityl chloride the reaction was stirred for a further 30 minutes. The reaction was then quenched with 1:1 methanol water mix (5mL) and stirring for 15 minutes. The solvent was removed *in vacuo* to leave a yellow oil.

The oil was dissolved in DCM (50 mL) and washed with water (2 x 50 mL), Brine (3 x 60 mL) and dried with Na_2SO_4. The reaction was concentrated *in vacuo* and co evaporated first with toluene (3 x 20 mL) followed by neutralised chloroform (3 x 20 mL) to remove residual pyridine. Analytical data were consistent with literature values.[96]

RF(10% MeOH in DCM): 0.61

MS ESI+: mass 656.47 observed m/z 679.4 $[M+Na]^+$

^{1}H NMR (Chloroform-d, 400 MHz): δ = 8.07 (s, 1H, H16), 7.25 (m, 12H, H4,8,9,10), 6.79 (d, J = 8.7 4H, gH3), 6.25 (t, J = 7.4, 1H, H15a), 4.48 (t, J = 2.7, 1H, H13a), 4.03 (d, J = 2.6, 1H, H12a), 3.73 (s, 6H, H1), 3.32 (dd, J = 1.6, 10.8, 2H, H11), 2.43 (dd, J = 2.3, 10.6, 1H, H14a/b), 2.23 (m, 1H, H14a,b)

3.1.7.6 Synthesis of Zn(II) -5-P-ethylnylphenyl-10,15,20-triphenyl porphyrin[96]

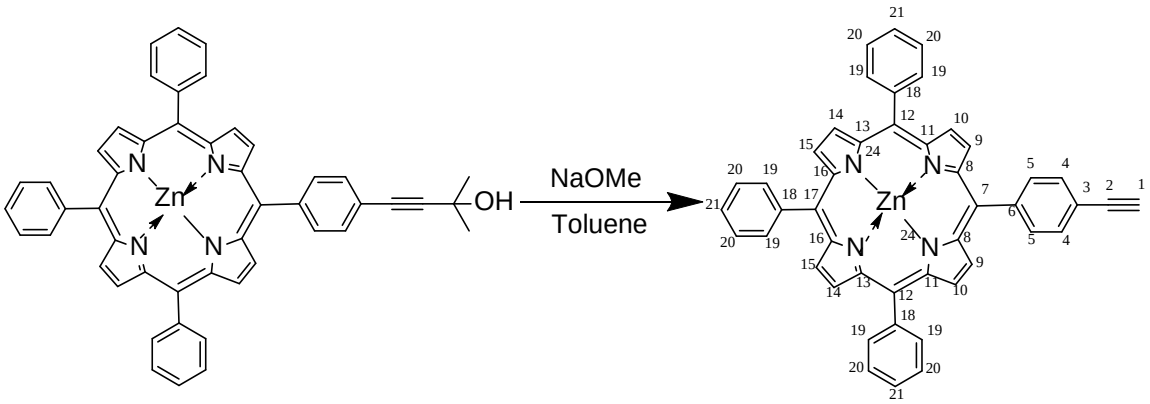

Zn(II) 5-p-(3-methyl-3-hydroxyl-1-butynl)phenyl – 10,15,20-triphenyl porphyrin (302.4 mg, 0.390 mmol, 1 equiv.) was dissolved in toluene (100 mL) and purged with argon for 10 minutes. Sodium methoxide (0.643 g, 0.1198 mol, 30 equiv.) was added to the stirring reaction. The reaction was then heated to reflux, 125 °C, for 24 hours. The solvent was removed *in vacuo*. The product was re-dissolved in DCM and washed with brine (3 x 50 mL) before drying with Na_2SO_4. This resulted in a purple solid powder 0.265 g (0.378 mmol, 97%). Analytical data were consistent with literature values.[96]

RF (10% MeOH in DCM): 0.92

^{1}H NMR (Chloroform-d, 400 MHz): δ = 9.00 (m, 6H, H15, 14, 10), 8.96 (m, 2H, H9), 8.24 (m, 7H, H21, 20), 7.91 (d, J= 8.1, 2H, H4, 5), 7.79 (m, 10H, H19, 5), 3.32 (s, 1H, H1)

^{13}C NMR (Chloroform-d, 100 MHz): δ = 150.30 (C-12), 150.20 (C-17), 149.79 (C-7), 14.55 (C-6), 142.74 (C-18), 134.42 (C-19), 134.35 (C-5), 132.20 (C-10/9), 132.06 (C-15/14), 130.36 (C-4), 127.52 (C-21), 121.37 (C-16), 121.26 (C-13), 119.92 (C-8), 83.77 (C-1), 78.11 (C-2)

MS ESI+: mass 700.16 observed m/z 701 [M+H]+

UV-Vis (CH_2Cl_2, x 10^{-6} M)λ: 419 (1.23), 548 (0.066), 578 (0.029)

Emission (CH_2Cl_2, x 10^{-6} M, λex= 419 nm) λem (relative intensity) = 597.94 (0.90), 643.04 (1)

3.1.7.7 Synthesis of 5'-DMT-(5''-p¬-ethynylphenyl)-10'',15'',20''-triphenyl-Zn (II)-porphyrin-dU[96]

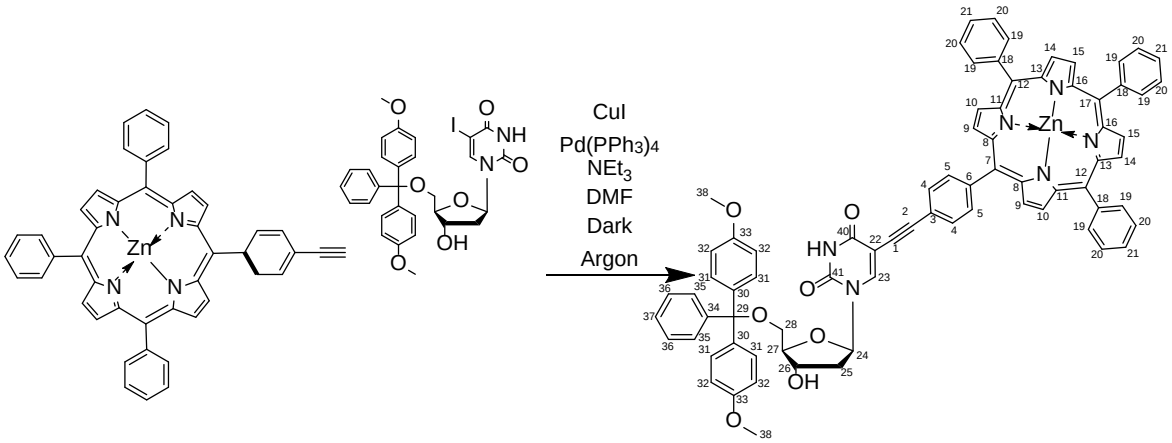

Zn (II)-5-P-ethylnylphenyl-10,15,20-triphenyl porphyrin (0.1 g, 0.142 mmol, 1 equiv.) was dissolved in DMF (5 mL) in an oven dried round bottomed flask and purged for 10 minutes. 5-DMT -5-Iodo-deoxyuridine (0.124 g, 0.189 mmol, 1.3 equiv.), Copper iodide (36 mg, 0.19 mmol, 1.3 equiv.) and triethylamine (35 µL) and molecular sieves were added. The reaction was further purged for 20 minutes before tetrakis(triphenylphosphine) palladium (0) (63 mg, 0.06 mmol, 0.38 equiv.) was added to the reaction.

The reaction was stirred under argon in the dark overnight. Although a small amount of starting material was detected by TLC the reaction was worked up. The reaction was diluted in EtOAc (50 mL) and washed with brine (3 x 50 mL). The organic layer was dried Na_2SO_4 and the solvent removed by rotary evaporation. The resulting solid was co-evaporated with toluene (20 mL x3) and neutralised chloroform (20 mL x 3) to remove residual triethylamine.

Three rounds of column chromatography were conducted. Firstly neutralised silica (DCM to DCM, 5% MeOH), secondly neutralised silica (DCM, 5% MeOH 1%, EtOAc). And finally neutralised silica (DCM, 5% MeOH, 1% EtOAc) which was run very slowly to aid separation of the nucleoside and the coupled nucleoside. This yielded a purple solid (64 mg, 0.052 mmol, 37%). Analytical data were consistent with literature values.[96]

RF (10% MeOH in DCM): 0.68

^{1}H NMR (Chloroform-d 400 MHz): δ = 8.93 (d, J = 4.8, 2H, H10), 8.91 (s, 4H, H14,15), 8.86 (d, J = 4.7, 2H, H9), 8.19 (m, 6H, H19), 7.98 (d, J = 8.2, 2H, H5), 7.83 (s, 1H, H23), 7.73 (m, 11H H20,21), 7.36 (d, J = 7.5, 2H, H35), 7.27 (m, 4H, H31), 7.25 (m, 4H, H4,36), 7.18 (m 1H, H37), 6.77 (dd, J =1.1, 8.8, 4H, H32), 5.55 (m, 1H, H24), 4.15 (s, 1H, H26), 3.66 (d, J= 2.2, 6H, H38,39), 3.29 (s, 1H, H27), 2.98 (m, 6H, H28), 1.98-1.93 (m, 1H, H25), 1.40 (m, 1H, H25)

UV-Vis (CH_2Cl_2, 2.90 x 10^{-6} M)λ: 419 (0.958), 548 (0.0410), 585 (0.0125)

Emission (CH_2Cl_2, 2.90 x 10^{-6} M, λex= 419 nm) λem (relative intensity) = 596.02 (1), 645.07 (0.98)

3.1.7.8 Synthesis of methyl 4-(10,15,20-triphenylporphyrin-5-yl)benzoate[96]

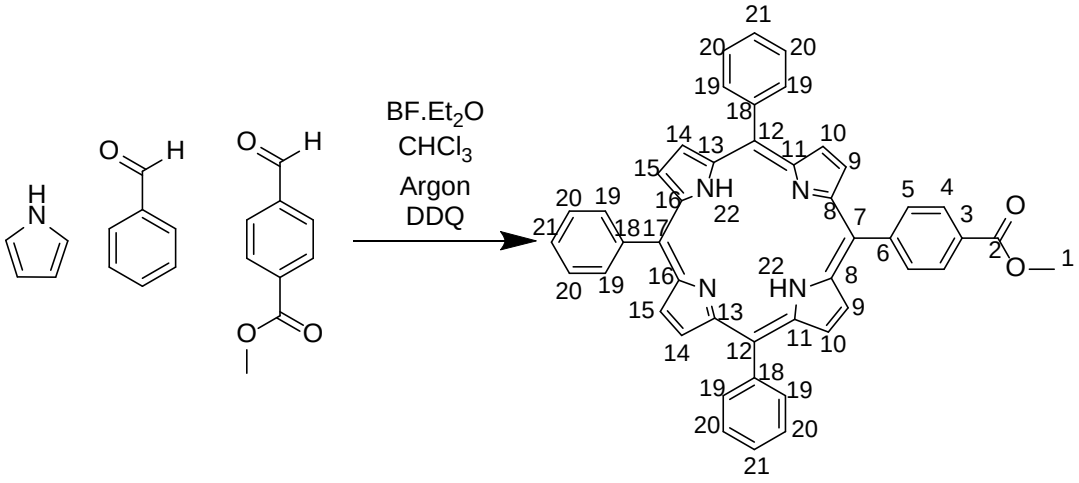

Chloroform (500 mL) was purged with argon for 45 minutes before pyrrole (2.52 mL, 36 mmol, 6 equiv.), benzaldehyde (3.6 mL, 36 mmol, 6 equiv.) and methyl-p-formybenzaoate (0.985 g, 6 mmol, 1 equiv.) were added to the reaction. The reaction was then stirred for 45 minutes under argon in the dark. Borontrifluoride diethyl etherate (0.69 mL, 5.4 mmol, 0.9 equiv.) was added to the reaction and stirred for 1 hour. The argon line was removed and DDQ (8.14 g, 36 mmol, 6 equiv.) was added. The reaction was then left to stir overnight.

The solvent was removed by rotary evaporation and the crude product was purified by three rounds of column chromatography. Firstly silica/alumina using DCM as an eluent, Secondly silica/alumina using toluene as an eluent and finally silica/sand using toluene as an eluent. Fractions were then co-evaporated with chloroform to remove traces of toluene. This yielded a purple solid (602.8 mg, 0.890 mmol, 14%). Analytical data were consistent with literature values.[96]

RF (10% MeOH in DCM): 0.88

^{1}H NMR (Chloroform-d 400 MHz): δ = 8.93 – 8.91 (m, 6H, H15, 14, 10), 8.85 – 8.84 (d, J = 4.6, 2H, H9), 8.50 – 8.47 (d, J = 8.1, 2H, H5), 8.37 – 8.35 (d, J = 8.1 2H, H4), 8.27 – 8.25 (m, 6H, H19), 7.82 – 7.76 (m, 9H, H21, 20), 4.15 (s, 3H, H1), -2.70 (s, 2H, H22)

UV-Vis (CH_2Cl_2, 5.96 x 10-6 M)λ: 417 (3.73), 514 (0.173), 549 (0.077), 590 (0.055), 645 (0.0407)

Emission (CH_2Cl_2, 5.96 x 10^{-6} M, λex= 417 nm) λem (relative intensity) = 650 (1) 718.05 (0.31)

3.1.7.9 Synthesis of 4-(10,15,20-triphenylporphyrin-5-yl)benzoic acid[96]

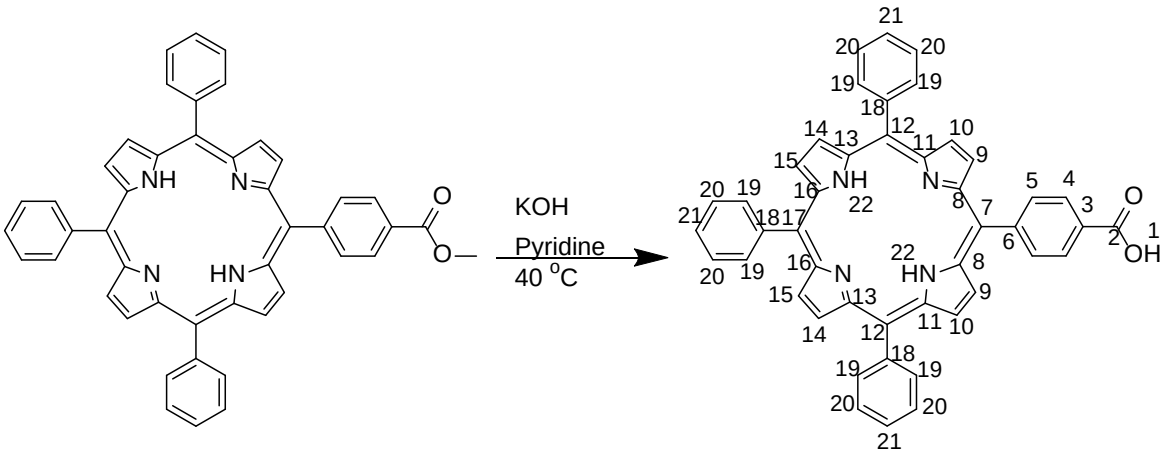

Methyl 4-(10,15,20-triphenylporphyrin-5-yl)benzoate (0.317 g, 0.47 mmol, 1 equiv.) was dissolved in pyridine (10 mL). Potassium hydroxide (1.33 g, 23.7 mmol, 50 equiv.) was dissolved in minimum amount of MQ water (~1.5 mL) and added to reaction. The reaction was heated to 40 °C and stirred overnight. The pyridine was removed on the rotary evaporator and the crude material was dissolved in DCM and washed with water (3 x 50 mL), 1 M HCl (~15 mL) was added slowly to aid separation with care taken not to acidify the porphyrin. The organic layer was removed and dried with Na_2SO_4. The crude material was purified by column chromatography with silica using a gradient of DCM to 10% MeOH in DCM. The fractions were then coevaporated with toluene (3 x 20 mL) followed by chloroform (3 x 20 mL). This yielded a purple solid (0.1632 g, 0.248 mmol, 53%). Analytical data were consistent with literature values.[96]

RF (10% MeOH in DCM): 0.56

^{1}H NMR (Chloroform-d 400 MHz): δ = 8.86 (m, 6H, H15, 14, 10), 8.82 – 8.81(d, J = 4.0, 2H, H9), 8.53 – 8.51 (d, J = 7.5, 2H, H4), 8.35 – 8.33 (d, J = 7.8, 2H, H5), 8.22 (m, 6H, H19), 7.78 – 7.76 (m, 9H, H21, 20), -2.76 (s, 2H, H22)

UV-Vis (CH2Cl2, 3.56 x 10-6 M)λ: 417 (1.98), 515 (0.078), 549 (0.031), 589 (0.021), 647 (0.012)

Emission (CH2Cl2, 3.56 x 10-6 M, λex= 417 nm) λem (relative intensity) = 651 (1), 714.02 (0.31)

3.1.7.10 Synthesis of (9H-fluoren-9-yl)methyl (3-(4-(10,15,20-triphenylporphyrin-5-yl)benzamido)propyl)carbamate[96]

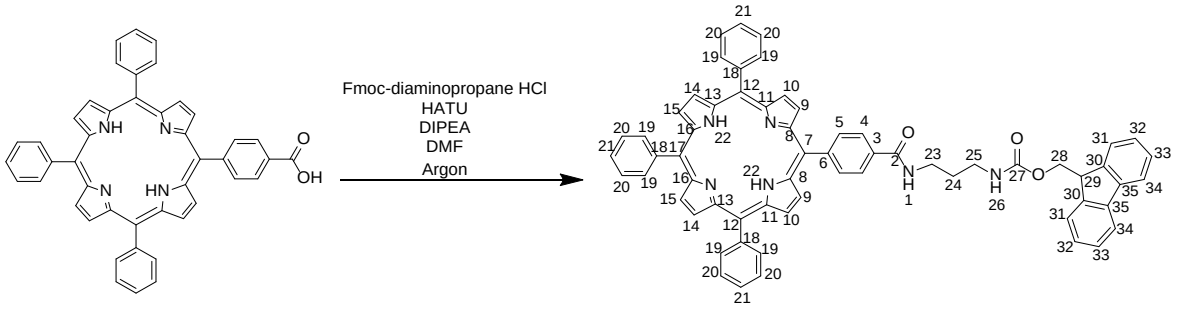

4-(10,15,20-triphenylporphyrin-5-yl)benzoic acid (0.03 g, 0.045 mmol, 1 equiv.) was dissolved in DMF (2 mL) in an oven dried flask containing molecular sieves. The reaction was purged for 10 minutes before the addition of HATU (34.2 mg, 0.090 mmol, 2 equiv.), DIPEA (15.7 µL, 0.090 mmol, 2 equiv.) in DMF (1 mL). The reaction was stirred and purged with argon for a 10 minutes.

Fmoc-diaminopropane HCl (30.3 mg, 0.090 mmol, 2 equiv.) was added and the reaction was stirred in the dark for 2 hours. The reaction was diluted with EtOAc (10 mL) and washed with brine (5 x 20 mL) with no back extraction. The crude material was purified by column chromatography, silica using a gradient of 100% DCM to 10% MeOH in DCM. This yielded a purple solid (60.4 mg, 0.068 mmol, 151%). Although showing too higher yield, the product was taken forward due to time restraints as the ^{1}H NMR showed mainly DMF solvent impurities. Analytical data were consistent with literature values.[96]

RF (10% MeOH in DCM): 0.76

^{1}H NMR (Chloroform-d 400 MHz): δ = 8.87 (d, J = 4.2, 6H, H15, 14, 10), 8.82 (d, J = 4.6, 2H, H9), 8.31 (d, J = 8.1, 2H, H4), 8.26 – 8.22 (m, 8H, H19, 5), 7.82 – 7.74 (m, 11H, H34, 21, 20), 7.64 (d, J = 7.2, 2H, H31), 7.50 (t, J = 5.2, 1H, H1), 7.39 (t, J = 7.3, 2H, H33), 7.31 (t, J = 7.3, 2H, H32), 5.43 (t, J = 6.1, 1H, H26), 4.52 (d, J = 6.8, 2H, H28), 4.25 (t, J = 6.6, 1H, H29), 3.65 (d, J = 5.5, 2H, H23), 3.45 (d, J = 5.1, 2H, H25), 1.88 (s, 2H, H24), -2.75 (s, 2H,H22)

3.1.7.11 Synthesis of N-(3-aminopropyl)-4-(10,15,20-triphenylporphyrin-5-yl)benzamide[96]

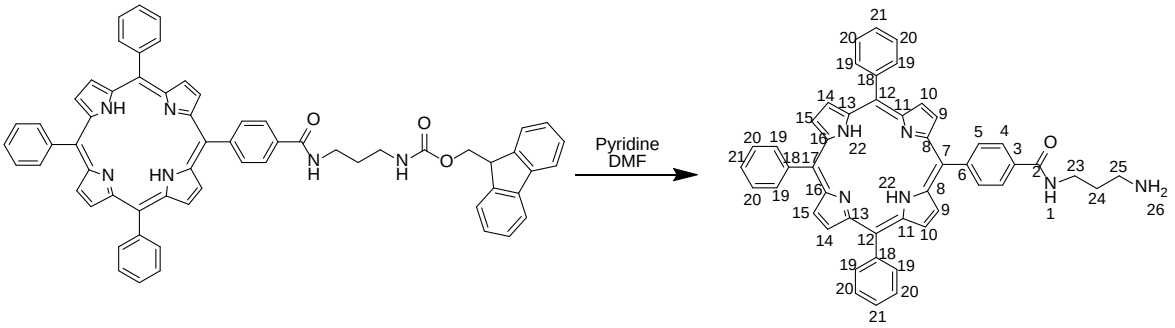

9H-fluoren-9-yl)methyl(3-(4-(10,15,20-triphenylporphyrin-5-yl)benzamido)propyl)carbamate (30.2 mg, 0.032 mmol) was dissolved in 20% piperidine in DMF (3 mL) and stirred in the dark for 1.5 hours. The reaction was diluted with EtOAc (20 mL) and washed with Brine (5 x 20 mL) with no back extraction of the aqueous layer. The organic layer was taken and purified by column chromatography, using silica and a gradient of 2% MeOH in DCM to 15% MeOH in DCM. This yielded a purple solid (19.6 mg, 0.027 mmol, 84%).

Due to time restraints a clear NMR was not obtained however due to a clear change being observed by TLC the reaction mixture was taken forward.

3.1.8 Cell culture experimental details

HEK293FT cell line was acquired from the Bigliardi Laboratory Institute of Molecular Biology (IMB). HEK293T cell line was acquired from the Skin Research Institute of Singapore (SRIS). FM55-P and B16-F10 cell lines were acquired from ZUDL laboratory Skin research institute of Singapore.

Unless otherwise specified, cells were cultured at 37 °C, 5% CO_2.

All treatments in chapter 4 were conducted in 96 well plates (Thermo scientific, Nunclon™Delta Surface, sterile) and cells were kept in culture in T75 flasks (Thermo Scientific Nunc™ EasyFlask 75 cm^2).

3.1.8.1 Treatment sterilisation

All treatments eg. Nanopore solutions, were filtered through a Millex®-GV 0.22 µm filter unit (Hydrophilic durapore® PVDF membrane)

3.1.8.2 HEK 293T Media

DMEM (1 x) + Glutamax™ + 4.5 g/L D- Glucose, + 110 mg/L Sodium Pyruvate (445 mL), FBS (50 mL), Penicillin/Streptomycin (5 mL) were combined and filtered through a 0.22 µM filter.

3.1.8.3 B16-F10 Media

DMEM (1 x) + Glutamax™ + 4.5 g/L D- Glucose, + 110 mg/L Sodium Pyruvate (445 mL), FBS (50 mL), Penicillin/Streptomycin (5 mL) were combined and filtered through a 0.22 µM filter.

3.1.8.4 FM55-P Media

RPMI Medium 1640 (1 x) + L- Glutamine, + 25 mM HEPES (Gibco) (440 mL), FBS (50 mL), Penicillin/Streptomycin (5 mL), Sodium pyruvate 100 nM (Gibco) (5 mL) were combined and filtered through a 0.22 µM filter.

3.1.8.5 HEK293FT Media

DMEM Media, High glucose, pyruvate (Gibo.11995) (500 mL), FBS (10 mL), penicillin/streptomycin 10,000 µg/mL (5 mL), NEAA (5 mL), Glutamax (5 mL).

3.1.8.6 Thawing cells

The cells were removed from the freezer and placed in the water bath for approximately 1 minute. The cells were added dropwise to pre-warmed media. The solution was centrifuged at 2.0 RCF for

3 minutes to make a pellet. The supernant was discarded and the cells were re-suspended in media (5 mL). Cells were then counted, and calculation was made to passage cells into T-75 flask. Cells were passaged at least once before any further experiments were conducted.

3.1.8.7 Passaging cells

Cells were passaged when they reached approximately 80% confluence in a T-75 flask. After removal of the media they were washed with DPBS (5 mL) and trypsinized with TripLE (2 mL) for 3 minutes. Media (8 mL) was added to quench the TripLE action and the cells were then centrifuged at 1500 RMP for 5 mins so they formed a cell pellet. The pellet was dissolved in media (5 mL) and cells counted.

3.1.8.8 Cell counting

Cells were either counted manually using a C-Chip or a using an automatic cell counter (Life technologies Countess II FL and Countess™ cell counting chamber slides).

For manual counting, after pellet formation when passaging, the supernant was discarded and the resulting pellet was dissolved in Media (3 mL). Cell solution (15 µL) was mixed with Trypan blue (15 µL) and pipetted onto a C-Chip slide to be visualized under microscope 10 X magnification. Cells were then counted in each quadrant using a manual cell counter. Calculation:

$$\frac{Number\ of\ cells\ counted}{Number\ of\ quadrants\ counted} \times Dilution\ factor = Number\ of\ cells\ in\ 1\ mL\ \times 10^4$$

Cells were then divided into T-75 flasks in media (10 mL) at desired cell number.

3.1.8.9 Alamar Blue assay

Stock solution 6 mM Alamar Blue was diluted 100x using relevant cell media. Cell treatment was removed from the well and replaced with Alamar Blue working solution (200 µL). Cells were returned to incubator (37 °C, 8% CO2) for 90 minutes. Resulting solution was transferred to a black flat bottomed 96 well plate suitable for microplate reader (Greiner bio-one 96 well PS chimney well). Fluorescence was read at 590 nm after excitation at 560 nm.

3.1.8.10 Crystal violet assay

Cells were washed with Dulbecco's phosphate-buffered saline (100 µL x 3). They were then fixed with 10% Neutral Buffered Formalin (50 µL) for 15 minutes. This was then removed and the cells were treated with 0.1% Crystal Violet solution for 20 minutes, followed by washing with tap water (2 x 100 µL) and leaving to dry for at least 24 hours. Resulting stained cells were dissolved in 10%

Acetic acid (100 µL) and left to shake for 20 minutes. The absorbance of each of the wells was then read at 595 nm using a microplate reader.

3.1.8.11 MTS Assay

Cells were cultured for required amount of time. The cell media was then replaced with a mixture of media (100 µL) and CellTiter 96® AQueous One Solution Cell Proliferation Assay (20 µL). The cells were incubated at 37 ˚C and 5% CO2 for 2 hours and the absorbance at 490 nm was measured.

3.1.8.12 IncuCyte

IncuCuyte was used with 10 x optical zoom. First photos were taken were taken within 30 minutes of the treatment giving a time point of 0 hours.

Chapter 4 Results

4.1 Nanopore synthesis and formation

A 1.5% agarose gel, **Figure 44**, was used to monitor the formation of the small nanopore. Lane 1 contained a standard 100 bp ladder to act as a control to make sure that the gel ran and stained adequately. It did not act as an indication of molecular weight of the nanopore. The tertiary structure of the nanopore meant that although it was larger in molecular weight, it was more compact in size. Therefore, the combined single strands in the nanopore travelled differently through the gel compared to a single stand of DNA of the same molecular weight meaning that the ladder could not be used as an indication of molecular weight.

It can be ascertained that the structure of the nanopore has formed by comparing the single strand in lane 1 and the unmodified nanopore in lane 4. The single strand moved further through the gel than the fully formed nanopore which formed a clear band higher in the gel. The hydrophobically modified structures (cholesterol modified small nanopore in lane 5 and palmitate modified small nanopore in lane 6) were shown also travel a shorter distance through the gel which indicated formation. These samples were also seen to streak due to the hydrophobic nature of the modifications (**Figure 45**) which has been commonly seen in literature[2, 43, 52].

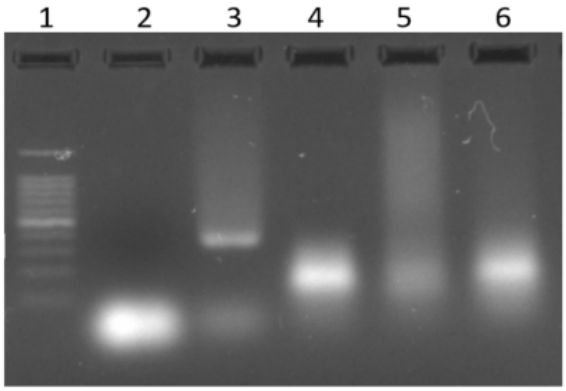

Figure 44 1.5% Agarose gel (60V 60 mins 1 x TAE supplemented with 11mM $MgCl_2$), lane 1:100 bp ladder, lane 2: single strand of DNA, lane 3: cholesterol single strand of DNA, lane 4: unmodified small nanopore, lane 5: cholesterol modified small nanopore, lane 6: palmitate modified small nanopore.

This was also seen in **Figure 45** which showed the formation of the porphyrin modified small nanopore.

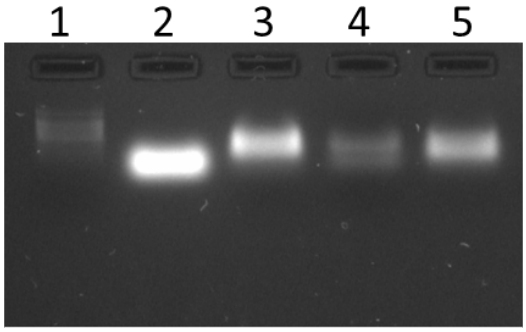

Figure 45 1.5% Agarose gel (60V 30 mins 1 x TAE supplemented with 11mM $MgCl_2$), lane 1:100 bp ladder, lane 2: single strand of DNA, lane 3: unmodified small nanopore, lane 4: porphyrin modified single strand, lane 5: porphyrin modified small nanopore

A 2% agarose gel was used to determine the formation of the large nanopore (**Figure 46**). Lanes 8 through to 10 contained single strands of DNA and therefore travel further through the gel than lanes 11 through to 13 which contained fully formed nanopore. Like the hydrophobically modified small nanopores, the hydrophobically modified large nanopores also streaked through the gel. This was also seen with the porphyrin modified large nanopore (**Figure 47**).

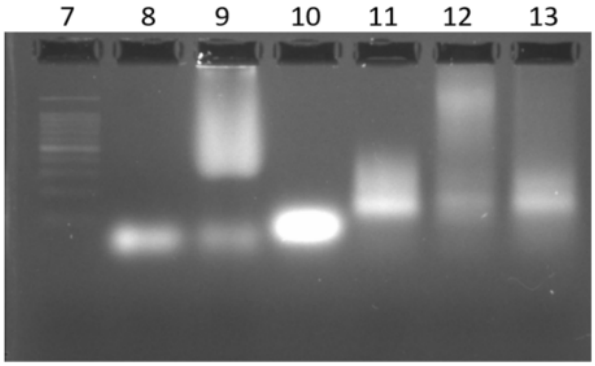

Figure 46 2% Agarose gel (60 V, 60 minutes 1 x TAE supplemented with 11 mM $MgCl_2$), lane 7: 100bp ladder, lane 8: single strand of unmodified DNA, lane 9: cholesterol modified single strand of DNA, lane 10: palmitate modified single strand of DNA, lane 11: unmodified large nanopore, lane 12: cholesterol modified large nanopore, lane 13: palmitate modified large nanopore.

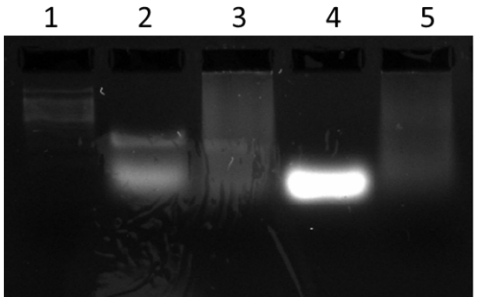

Figure 47 2% Agarose gel (60V 40 mins 1 x TAE supplemented with 11mM $MgCl_2$), lane 1:100 bp ladder, lane 2: single strand of unmodified DNA, lane 3: unmodified large nanopore, lane 4: porphyrin modified single strand, lane 5: porphyrin modified large nanopore.

4.2 Cytotoxicity of the small nanopore V1 in HEK293FT cells

These experiments were conducted with an earlier version of the small nanopore, labelled as small nanopore v1, still based on the structure published by Göpfrich *et al*[4]. This only differed from the nanopore used throughout the rest of the project by the location of the cholesterol modification. The modification was moved from the 3' to the 5' terminus of the DNA strands using a phosphoramidite purchased from Link Technologies (5' Cholesterol-CE Phosphoramidite).

HEK293FT cells were first used to test the hypothesis that the nanopores were cytotoxic. HEK293FT cells are human embryonic kidney cells which are a tumour cell line. Although very different to the skin system, they are similar in the fact that they are epithelial and form monolayers of cells. The fact that they are very fast growing, and a robust cell line[126] was also of use in the project. The cells are also regularly used for transfection[127] therefore it was predicted that the cell membrane maybe more susceptible to interaction with the hydrophobically modified nanopore. It was hypothesised that the hydrophobically modified nanopores would have a negative impact on the growth of the HEK293FT cells.

Cells were initially seeded at 10,000 cells per well in a 96 well plate. However, early results showed that the cholesterol modified small nanopore had no effect on the HEK293FT cell proliferation. It was considered that the seeding density of cells may have had an effect as this led to a high starting confluence of cells and therefore the ratio of nanopore to cell would be low.

Therefore, the cells were seeded at various densities into a 96 well plate; 5000, 2000 and 1000 cells per well. The cells were then left to acclimatise in an incubator at 37 °C, 5% CO_2, for 48 hours which was then followed by a change of media containing the small cholesterol modified nanopore at 0.5 µM in phosphate buffered saline (PBS). The cells were incubated with the nanopore for 48 hours and the cell confluence was monitored. Control experiments were also conducted: firstly, a vehicle

control of PBS and secondly a negative control of unmodified nanopore was also used. It was hypothesised that the cholesterol modified nanopore would have a negative effect on the proliferation of cells compared to the vehicle control and unmodified nanopore. A technical duplicate was run on the plate instead of a technical triplicate due to a lack of materials and the experiments were initially repeated 3 times. However, due to an anomalous result in the 3rd repetition, the experiment was run a further 2 times. The cells were monitored using an IncuCyte for 48 hours. **Figure 48**, **Figure 49** and **Figure 50** are split into two and show the results of these tests: the (Left) which show the full 5 biological repeats, and (Right) which omit the 3rd biological repeat. This omission only affected the error bars in **Figure 49** where cells were seeded at 2000 cells per well and the most activity was seen. Data for each biological repeat can be found in the appendix.

Cells seeded at higher densities, 5000 cells per well, were not affected by the addition of the cholesterol modified small nanopore. This can be seen in the confluence plot, **Figure 48**, where the proliferation curves of the cells treated with each of the treatment groups follow a similar pattern. The cell growth can be seen to increase and reach a plateau close to 100% confluence for each of the treatment groups.

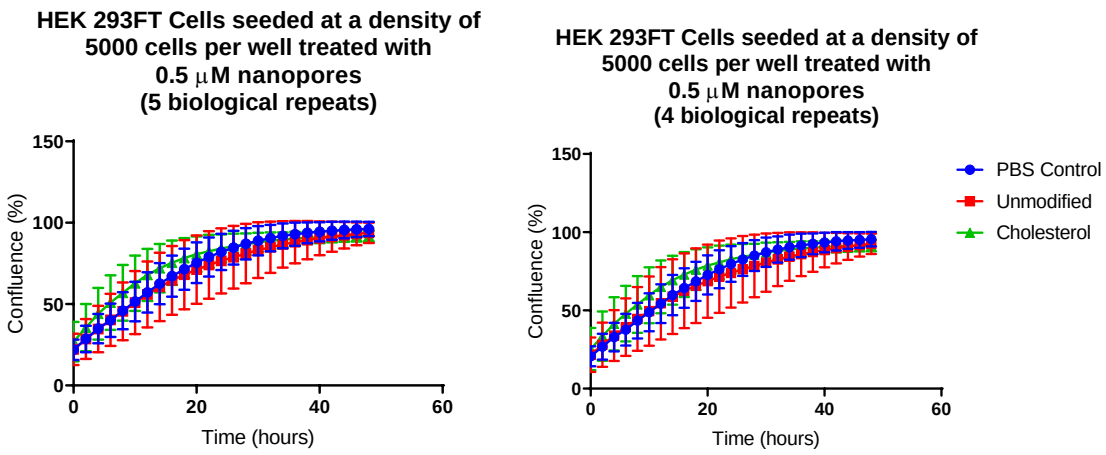

Figure 48 (Left) At high seeding densities of 5000 cells per well the proliferation of HEK293FT cells was not negatively affected by the cholesterol modified small nanopore V1. (Right) Omitting the 3rd biological repeat had no effect on the high seeding density results. Individual traces can be found in the appendix.

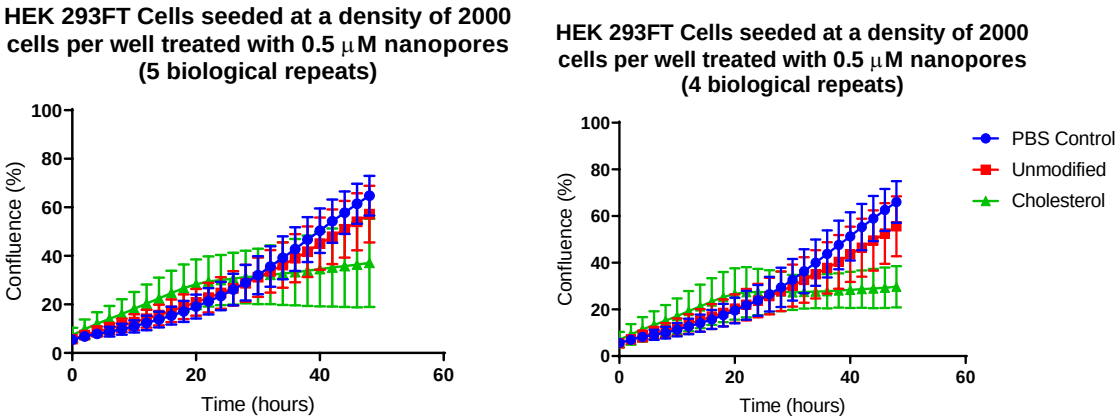

Figure 49 At a seeding density of 2000 cells per well, a decrease in proliferation was seen in HEK293FT cells treated with 0.5 μM cholesterol modified small nanopore V1. (Left) The data of 5 biological repeats which showed a large SD error in the cells treated with the cholesterol modified small nanopore V1 due to an anomalous result in the 3rd biological repeat. (Right) The data omitting the anomalous result from the 3rd biological repeat leading to smaller SD error. Individual traces can be found in the appendix.

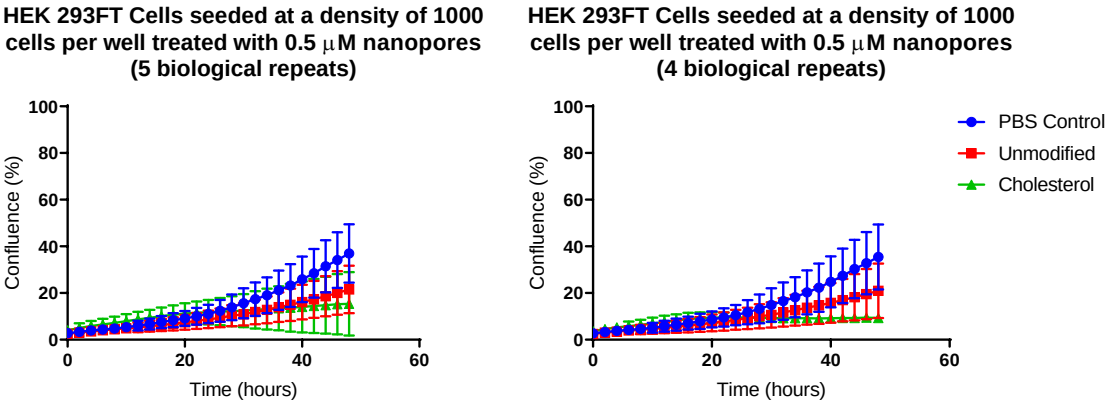

Figure 50 At a seeding density of 1000 cells per well a negative effect on the proliferation was observed in HEK293FT cells treated with 0.5 μM cholesterol modified small nanopore V1 (Left) Data of 5 biological repeats showed a large SD error due to an anomalous result in the 3rd biological repeat, (Right) The data omitting the anomalous result from the 3rd biological repeat leading to small SD error. Individual traces can be found in the appendix.

When seeded at 2000 cells per well, shown in **Figure 49**, the unmodified nanopore treated cells were seen to follow a similar proliferation curve to the PBS control which indicated that it had no effect on the proliferation of the cells. Whereas, at the same seeding density, the cells treated with the cholesterol modified nanopore showed a proliferation curve that formed a plateau after 24 hours signifying no further proliferation of cells. This experiment was repeated 5 times because the

3rd run of the experiment showed different trends to that seen in the first two. **Figure 49** (Right) shows by the omitting this data from the data set, the trends in the results are clearer and the standard deviation error is less.

At even lower starting confluences when the cells were seeded at 1000 cells per well, shown in **Figure 50**, the cells treated with the unmodified nanopore did not reach as high confluence as the control treatment group indicating an effect on the proliferation of the cells. However, the trajectory of the unmodified and cholesterol modified treated cells plots can be seen to be different. Where the unmodified treated cells seem to be set to continue to proliferate, the cholesterol modified nanopore treated cells reached a plateau; indicating cell death. This could be confirmed in future experiments by monitoring the cells for a longer period of time.

The issue with using such low starting confluences was that a small difference in starting confluence led to a large change in the curve of the graph. This led to large error bars being observed making the data seem to be unreliable and not significant. Therefore, another way of interpreting the data was plotting the difference in starting and ending confluence which would indicate the change in number of cells in the sample and therefore would show how much the cells were affected by the treatments. This can be seen in **Figure 51**.

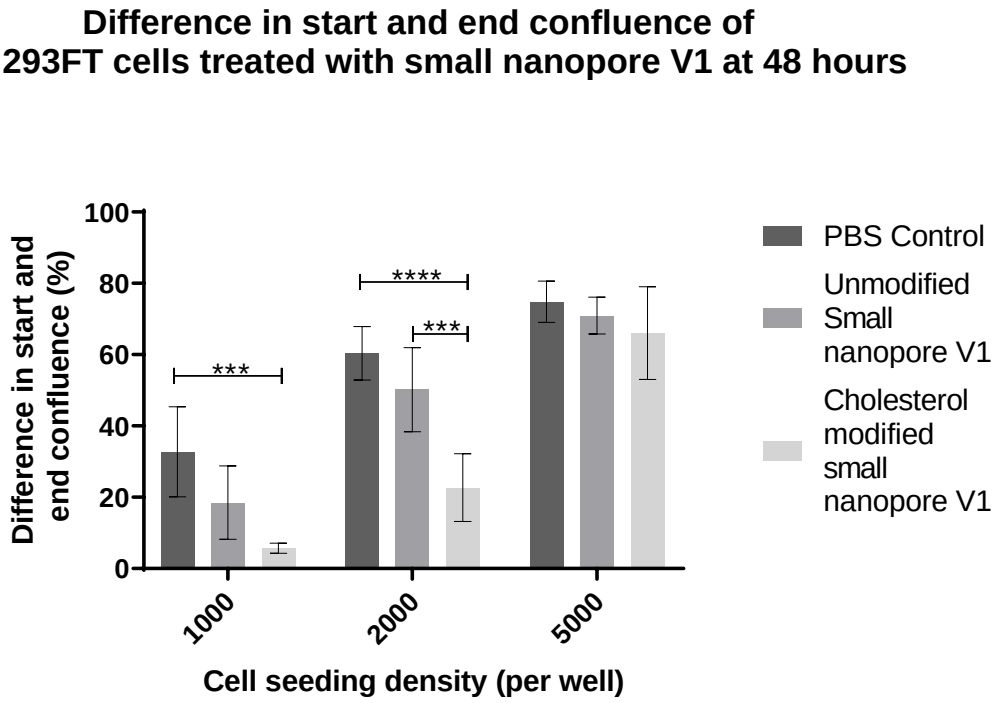

Figure 51 A decrease in change in confluence was observed in HEK293FT cells treated with 0.5 µM cholesterol modified small nanopore V1 at both seeding densities 1000 and 2000 cells per well whereas no change was seen at the higher seeding density of 5000 cells per

well. N=4 SD error shown. Statistically significant $p<0.05$, two-way ANOVA corrected for multiple comparisons using Tukey's method.

At 5000 cells per well it can be seen that the cells treated with PBS showed a change in confluence of 75% which was very similar to that seen by the cells treated with nanopores, both unmodified and modified, which showed changes of 71 and 66% respectively. Although a mean 9% difference was observed between the control and the cholesterol modified small nanopore V1, the standard deviation error bars were shown to overlap indicating that this small difference was not significant. However, at just under half the seeding density (2000 cells per well), the gap between the two treatments widened to a 37% difference which proved to be a significant difference when analysed by a two way ANOVA and Tukey's test. This trend was further observed when cells were seeded at 1000 cells per well where the difference in change in confluence between the two treatments was 27% which was also seen to be significant. This therefore indicated that the cholesterol modified small nanopore V1 was negatively affecting the proliferation of HEK293FT cells seeded at low densities such as 2000 and 1000 cells per well.

Although the unmodified small nanopore V1 was seen to also give lower values than that of the PBS control treated samples, it was not significantly so in all cases. Therefore this indicated that the unmodified nanopore did not have a significant effect on the growth of the cells.

These tests showed us that the number of cells seeded for the experiment had a large impact on the toxicity of the cholesterol modified nanopores. It was hypothesised that this could be due to several reasons. Firstly, the more cells that were seeded, the higher the ratio of cells to nanopore. It is not known how many nanopores would be needed to create a large enough disruption to the cell membrane. However, the more that are available to each cell, the more likely they are to cause disruption to the cell membrane. Also, it is well known that HEK293FT cells are very fast growing cells, therefore if the mechanism of action of the nanopores was not fast working, the cells may have proliferated and it would be difficult to see the true effect of nanopores.

4.3 Cytotoxicity of non-covalent modifications and small nanopore V1

Planar molecules are known to intercalate into DNA through base stacking[128-130]. It was suggested that the hydrophobic compounds that are theorised to insert the nanopore into the cell membrane may not need to be covalently attached to produce the cytotoxic effect of the nanopore. It was suggested that they may simply intercalate with the nanopore and provide enough of an anchoring effect. This would reduce synthesis times and open up the field to using a wider variety of compounds. Therefore, two different planar molecules were used to test this theory: methylene blue (MB) and 2-(1-hexyloxyethyl)-2-devinyl pyropheophorbide-a (HPPH). These compounds were

chosen as they have the phototoxic properties which could be utilised for photodynamic therapy[95, 131] in later tests.

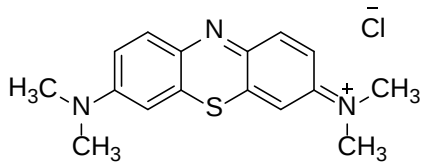

Methylene Blue
(MB)

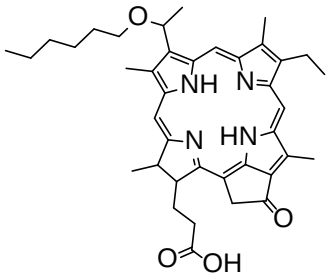

2-(1-hexyloxyethyl)-2-devinyl pyropheophorbide-a
(HPPH)

Figure 52 Chemical structures of methylene blue (MB) and2-(1-hexyloxyethyl)-2-devinyl pyropheophorbide-a (HPPH).

Three different concentrations of the compounds were used (0.5, 1 and 2 µM) and mixed with a constant concentration of 0.5 µM unmodified nanopore in cell media.

These concentrations were chosen so that if future experiments were conducted with the compounds they could be compared to these results. Although it could not be guaranteed that the compounds would intercalate to a specific ratio, 0.5 µM would simulate one modification, 1 µM would simulate 2 modifications and 2 µM would indicate four modifications.

Using the positive results from previous experiments detailed above, HEK293FT cells were seeded at 2000 cells per well in a 96 well plate and left to proliferate for 48 hours before a media change was performed including the treatment groups. The cells were then observed over a 66 hour time period using an IncuCyte before an end point MTS assay was conducted. Experiments were conducted with technical duplicates and three biological repeats.

A disadvantage of this proposal was the solubility of the hydrophobic compounds. When conjugated to DNA, the solubility of the compounds is increased and therefore the presence of organic solvents is not needed. Whereas, with the unconjugated compounds being hydrophobic, they were problematic to dissolve in aqueous media and needed organic solvents to form a solution. Therefore, the compounds were dissolved in dimethylsulphoxide (DMSO), a solvent commonly used in cell culture for freezing of cells, at a percentage volume of 0.1%. Although MB was slightly soluble in water it was also dissolved in DMSO. This was to allow comparisons between MB and HPPH which was insoluble in water.

Suitable controls were included in the experiments to ensure that the true effects of the treatments could be observed. Firstly, cells were treated with PBS using the same volume as that used to

dissolve the nanopores. This ensured that all the cells had access to the same amount of growth factors and nutrients. Secondly, cells were treated with a DMSO PBS mixture to ensure that any effect of the DMSO alone was noted. It was ensured that all the cells had the same amount of media supplied at the same concentration and the treatment volume was kept consistent at 250 µL.

It must first be stated that due to the low starting confluences, a small change in confluence led to a large difference in behaviour. Therefore, combining all data sets and applying standard deviation led to large errors being observed. The proliferation graphs could only be used for observation of trends (similarly to the data shown in further sections). For this reason, the difference in start and end confluence was plotted.

4.3.1 Non-covalent methylene blue

The first evaluation that had to be made was the effect of DMSO on the proliferation of cells. Therefore, a vehicle control was included in the experiment where 0.1% DMSO was included in the Media 60% PBS 39.9% control treatment mix.

The MTS assay, **Figure 53**, shows the data normalised to the cells treated with PBS. It can be seen that the cells treated with 0.1% DMSO showed a value of 104% indicating that there was very little difference in cell viability to those only treated with PBS and therefore the DMSO had little effect on the cells. Similarly, the cells treated with unmodified nanopore in DMSO showed an average value of 103% which also indicated no effect on cell viability. This was expected as no hydrophobic compounds had been added to the nanopores to provide anchors for the pores. This was also supported by the graph shown in **Figure 54** which shows the difference in starting and final confluence. Although showing slightly different values, the trend was the same as DMSO 0.1% and unmodified small nanopore & DMSO 0.1% showed similar changes in confluence of 76% and 75% respectively and the PBS control 85%. This suggested that these three treatment groups all had very similar effects on cell proliferation and viability.

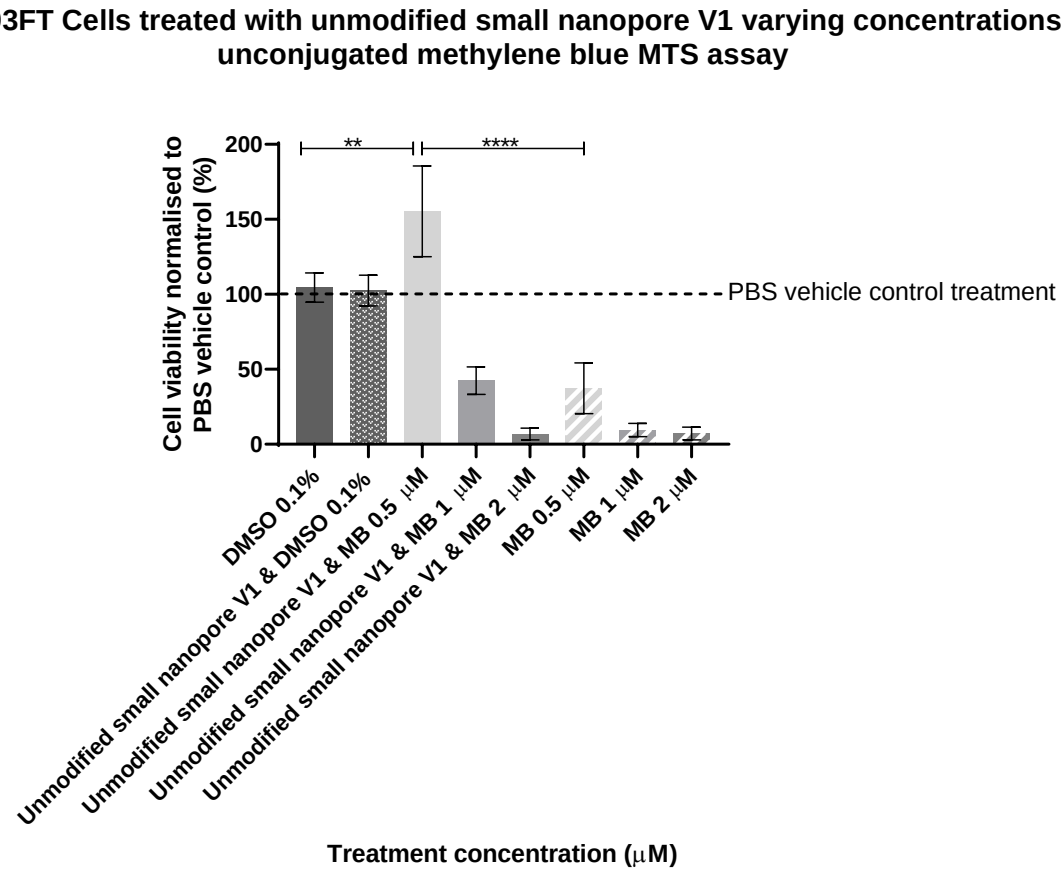

Figure 53 Methylene blue was shown to have a negative effect on cell viability at 1 µM and 2µM concentration with and without the unmodified small nanopore V1 in HEK293FT cells. At 0.5 µM the negative effect was negated by the addition of the nanopore. Statistically significant $p<0.05$, two-way ANOVA corrected for multiple comparisons using Tukey's method.

At the higher concentrations of MB used (1 and 2 µM) both with and without the unmodified small nanopore V1 showed a decrease in cell viability.

Cells treated with 1µM MB with the nanopore, showed an average value of 42% compared to cells treated with PBS alone. However, the cells treated with MB alone at 1 µM showed an average value of 10% compared to PBS treated cells. This was a 32% decrease from the mixed treatment. This indicated that at the addition of the nanopore to the MB treatment negated some of the effect of the methylene blue however this was not found to be significant through statistical analysis.

This trend was also seen when comparing the treatment of only 0.5 µM MB to 0.5 µM MB with nanopore. In the case of 0.5 µM MB with nanopore, no decrease in cell viability was observed. In fact, a significant increase (mean value 155%) was observed. Whereas the 0.5 µM MB showed a decrease with an average value of 37% which was also found to be significant.

However, this trend was no longer observed in the 2 μM treatments where both the methylene blue alone and together with the nanopore gave average values of 7% compared to the PBS control.

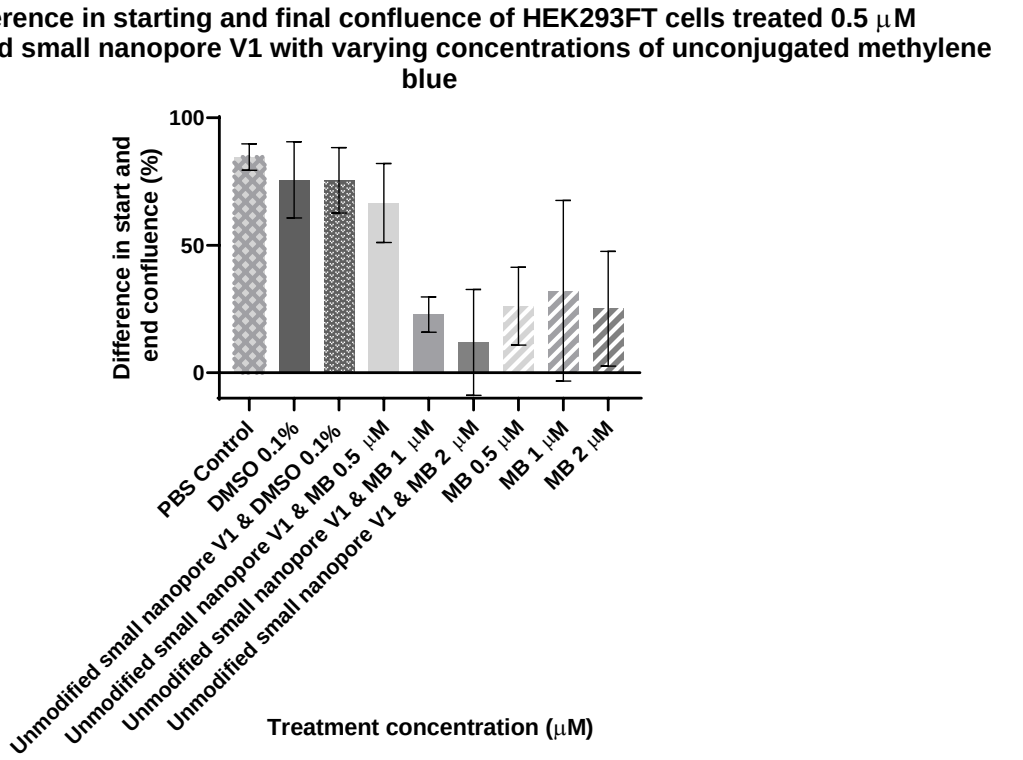

Figure 54 Methylene blue was shown to have a negative effect on change in proliferation of HEK293FT cells, both with and without unmodified small nanopore V1. This indicated a negative effect on cell viability. No difference in effectiveness was seen upon addition of the nanopore.

This was also observed in the confluence difference data apart from the trend seen with the 1 μM methylene blue treatment. Here it is shown to be higher than that of the treatment combined with the nanopore, however large error bars prove that this average value was not accurate.

These results indicated that the nanopore played a key role in these experiments but not in the way originally hypothesised. It was hypothesised that the methylene blue would allow the insertion of the nanopore into the cell membrane and therefore cause cell toxicity. However, these results indicate this hypothesis to be false.

Due to the trends seen where a change in concentration of methylene blue when mixed with a constant concentration of nanopore resulted in different cytotoxicity, it can be deduced that the nanopore is interacting with the methylene blue in some way. It has been postulated that the nanopore acted as a sink for the methylene blue so that rather than allowing the methylene blue to interact with the cellular DNA, it was held in the DNA nanopore.

4.3.2 Non-covalent HPPH

Similarly to the methylene blue data shown in the section above, the DMSO and DMSO and unmodified nanopore controls had no negative effect on cell viability or proliferation. This is shown in **Figure 55** where very similar values to the untreated cells were observed (107 and 113%) for the singular and joint treatments. This was also observed in **Figure 56** where the change in start and end confluences was not seen to change drastically between the three treatment groups.

As the concentration of HPPH was increased the cell viability was shown to decrease in both the treatments with and without the addition of the nanopore. At all concentrations of HPPH the addition of the nanopore to the treatment had no significant effect on the cell viability or change in proliferation.

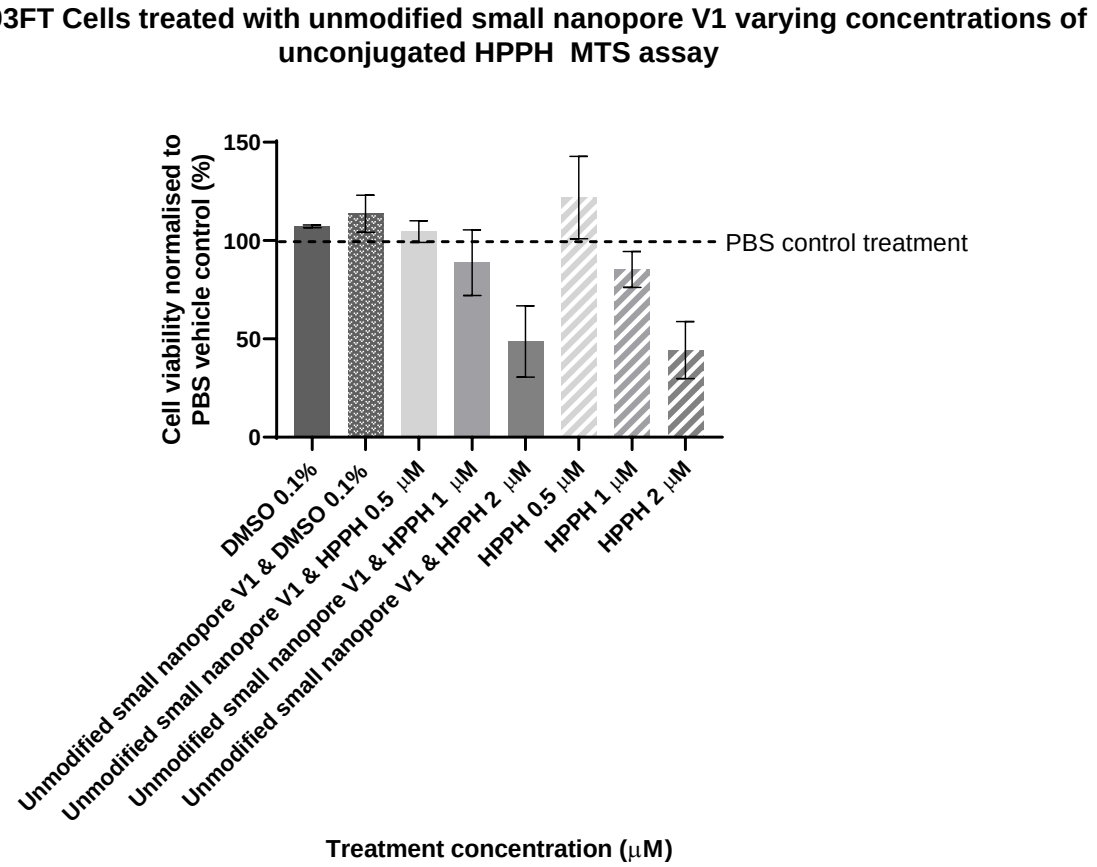

Figure 55 HPPH was shown to have a negative effect on cell viability at 1 and 2 µM concentration with and without the 0.5 µM unmodified small nanopore V1 in HEK293FT cells. No significant difference was seen between the treatments with and without the nanopore.

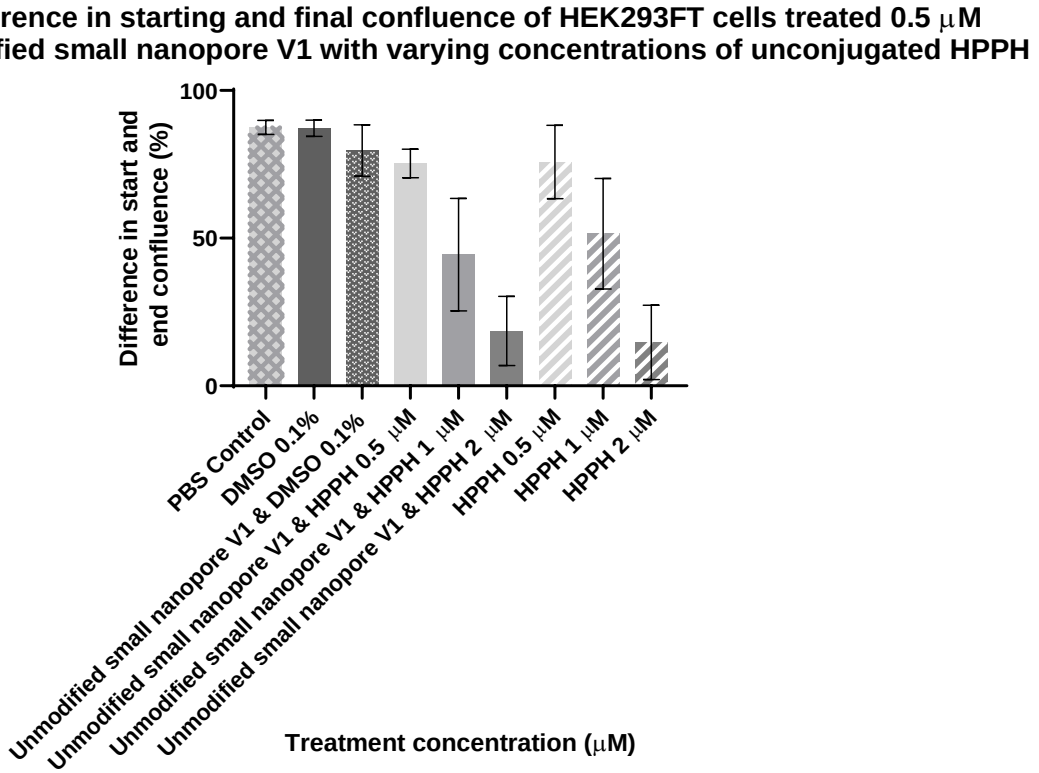

Figure 56 HPPH was shown to have a negative effect on proliferation at 1 and 2 μM concentration with and without the 0.5 μM unmodified small nanopore V1 in HEK293FT cells. No significant difference was seen between the treatments with and without the nanopore.

4.3.3 Conclusion

These results showed the hypothesis presented, that the introduction of unconjugated intercalators into the unmodified nanopore treatments would have negative effect on cell viability, to be invalid. The addition of the compounds did not act as predicted and induce a cytotoxic effect. The opposite of this was observed for low concentrations of methylene blue where the addition of the unmodified nanopore reduced the cytotoxic effect of the methylene blue.

At high concentrations the methylene blue was more detrimental to cell proliferation than HPPH. This information could be utilised for future works. These experiments were done with no light excitation therefore the toxicity is classed as dark toxicity. The ideal treatment would only cause cell death when exposed to the appropriate wavelength of light. This would introduce more control into the therapy and therefore reduce any off-target effects.

From these experiments it was concluded that the hydrophobic compound needed to be covalently attached to the DNA nanopore for further nanopore cytotoxicity experiments.

4.4 Cytotoxicity of small and large nanopores in HEK293T cells

The second set of cell experiments took place in 2019 under the supervision of Professor David Leavesley in the Skin Research Institute of Singapore (SRIS) A*STAR. Knowledge from the initial cell tests was applied to further experiments, working with a variety of cell lines: Human embryonic kidney cells 293T (HEK293T), a murine melanoma cell line (B16-F10), and a human melanoma cell line (FM55-P). The two nanopores used in this work are shown in sections 2.3.1 and 2.3.2.

Experiments were conducted on HEK293T cells by varying the size of the nanopore, type of modification on the nanopore and the concentration of the nanopores. A concentration of 0.5 μM was chosen as the only literature available at the time of experiment design was that produced by Burns *et al*.[2] They used a concentrations of 100 μg/mL, 60 μg/mL and 30 μg/mL, and found significant cytotoxicity at 60 μg/mL which correlates to 0.5 μM of the small nanopore. Initially in this project a concentration was taken either side of this for experiments. This allowed the observation of the effect of concentration. The proliferation of cells was measured by IncuCyte and end point assays (alamar blue and crystal violet) were conducted at 72 hours.

HEK293T cells were seeded at a density of 2000 cells per well and left to settle for 24 hours before the treatments were applied. This differed slightly from the protocol used in the previous experiments detailed for HEK293FT cells in initial experiments as the settling time for the cells was halved from 48 hours. Due to the fast growth of the cells this was not deemed to be a problem however it must be noted that the results cannot be directly compared.

The experiments were all conducted with experimental triplicates and four biological repeats. The exception to this was the second biological repeat for the unmodified small nanopore at concentrations of 1, 0.5 and 0.25 μM. In this biological repeat only one technical repeat was conducted due to loss of sample during sterilisation.

For cell viability assays an average of the technical triplicates was taken and used as the value for each experiment and normalised using the result given by cells treated with 100% media. The mean of the biological repeats was then taken and the standard deviation from these values was used to calculate the error.

4.4.1.1 HEK293T cells treated with varying concentrations of small nanopore

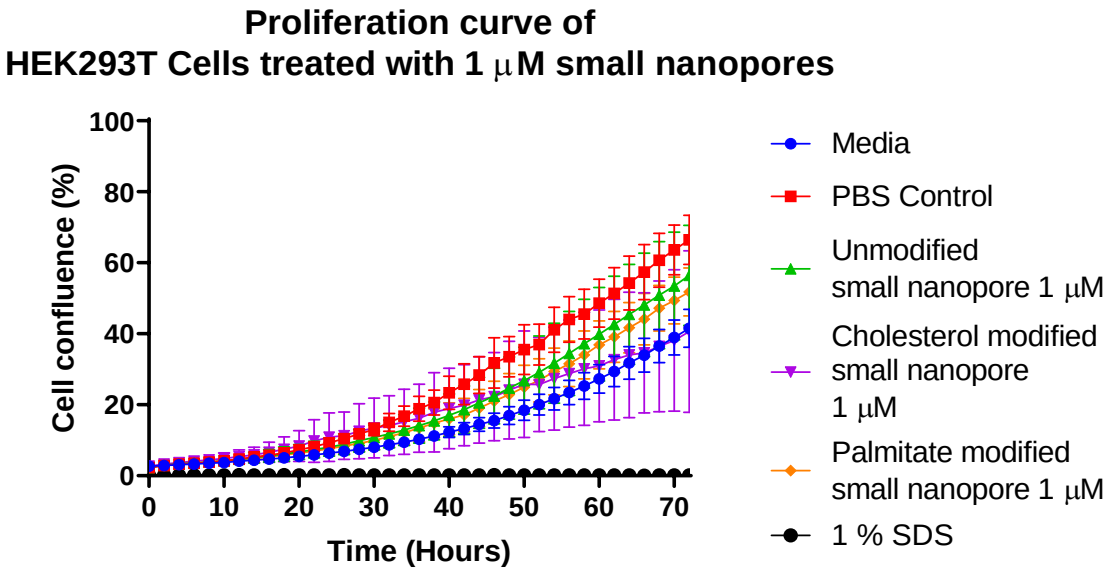

Figure 57 Graph showing HEK293T cells treated with small nanopore proliferation curve, N=4 mean and SD error shown. A similar increase in confluence of HEK293T cells was observed in all samples with large SD errors observed. Individual traces can be found in the appendix.

The proliferation curve of HEK293T cells treated with 1 μM cholesterol, palmitate and unmodified small nanopores can be seen in **Figure 57**. Due to large error bars it is difficult to see the trend that the treatment groups follow however a few things can be deduced. Firstly, it can be seen that the positive control of 1% Sodium dodecyl sulphate (SDS) was successful as there was no increase in the cell confluence. This was consistent with the images taken from the IncuCyte at time points where no cells can be seen.

Secondly, it can be seen that all other treatment groups showed an increase in cell proliferation, even those that were not expected. The final confluence measurement was taken at 72 hours followed by two further means of measurement: an alamar blue assay and crystal violet stain shown in **Figure 58** and **Figure 59** respectively.

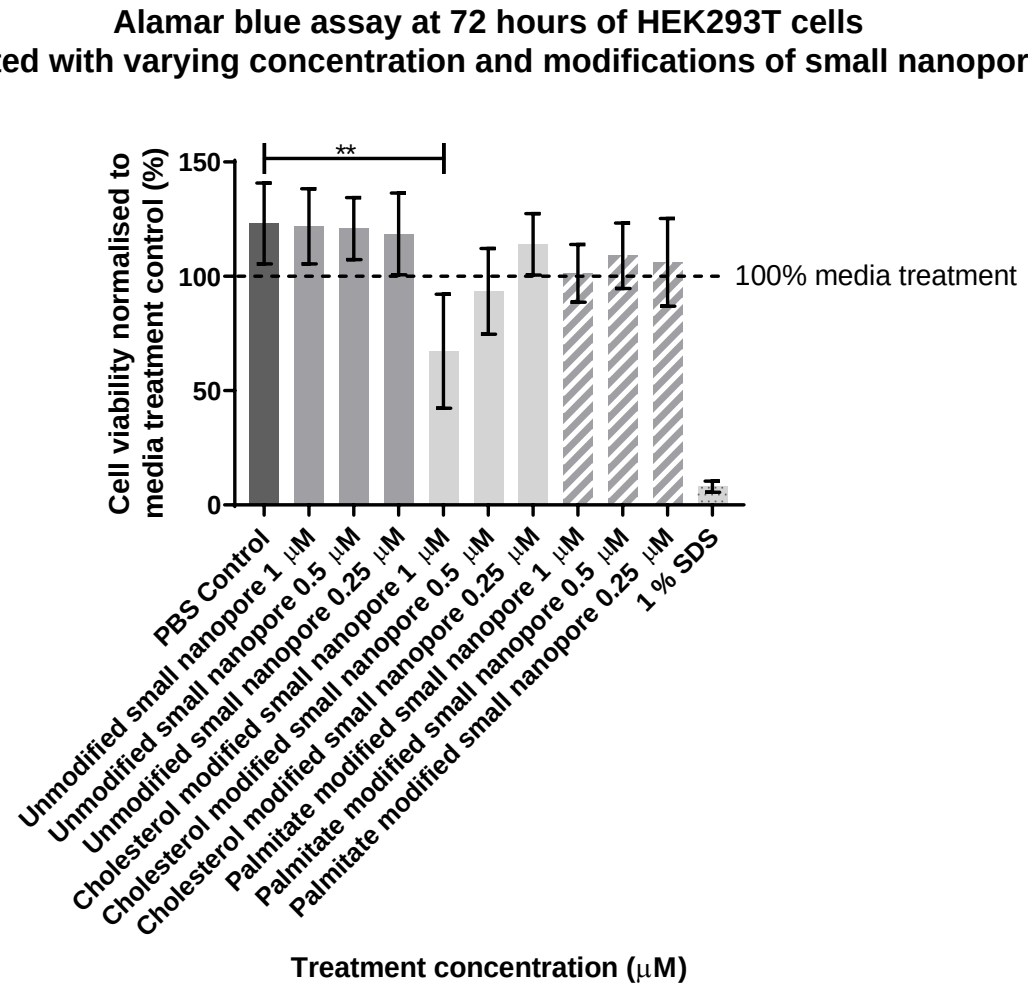

Figure 58 HEK293T cells treated with small nanopore alamar blue assay graph. N=4, mean and SD error shown, statistically significant $p<0.05$, one way ANOVA corrected for multiple comparisons using Tukey's method. A significant difference in cell viability was observed in HEK293T cells treated with 1 μM cholesterol modified small nanopore compared to those treated with the PBS control.

The alamar blue assay for this experiment can be seen in **Figure 58**. The PBS control showed a fluorescence read of 123% compared to the untreated cells, indicating that the cell viability was not negatively affected by the inclusion of PBS. Similarly, the 1 μM unmodified nanopore showed a read out of 122% indicating that it had a similar activity to the vehicle control and therefore can be classed as inactive. Conversely, the cholesterol modified nanopore and palmitate modified nanopore at 1 μM showed lower values of 67% and 101% respectively. This indicated less cells in the samples and therefore greater activity of the pores. This difference was found to be statistically significant when comparing the 1 μM cholesterol modified nanopore to the PBS control. However, no statistical significance was seen for the palmitate sample at this concentration.

This trend is also present between nanopores at 0.5 µM. As seen in the 1 µM treatments, the 0.5 µM unmodified nanopore measuring 121% gave a very similar value to that of the PBS control which measured 123%. Again, the cholesterol modified nanopore was seen to measure lower than the palmitate modified nanopore although neither differences were statistically significant compared to the vehicle control.

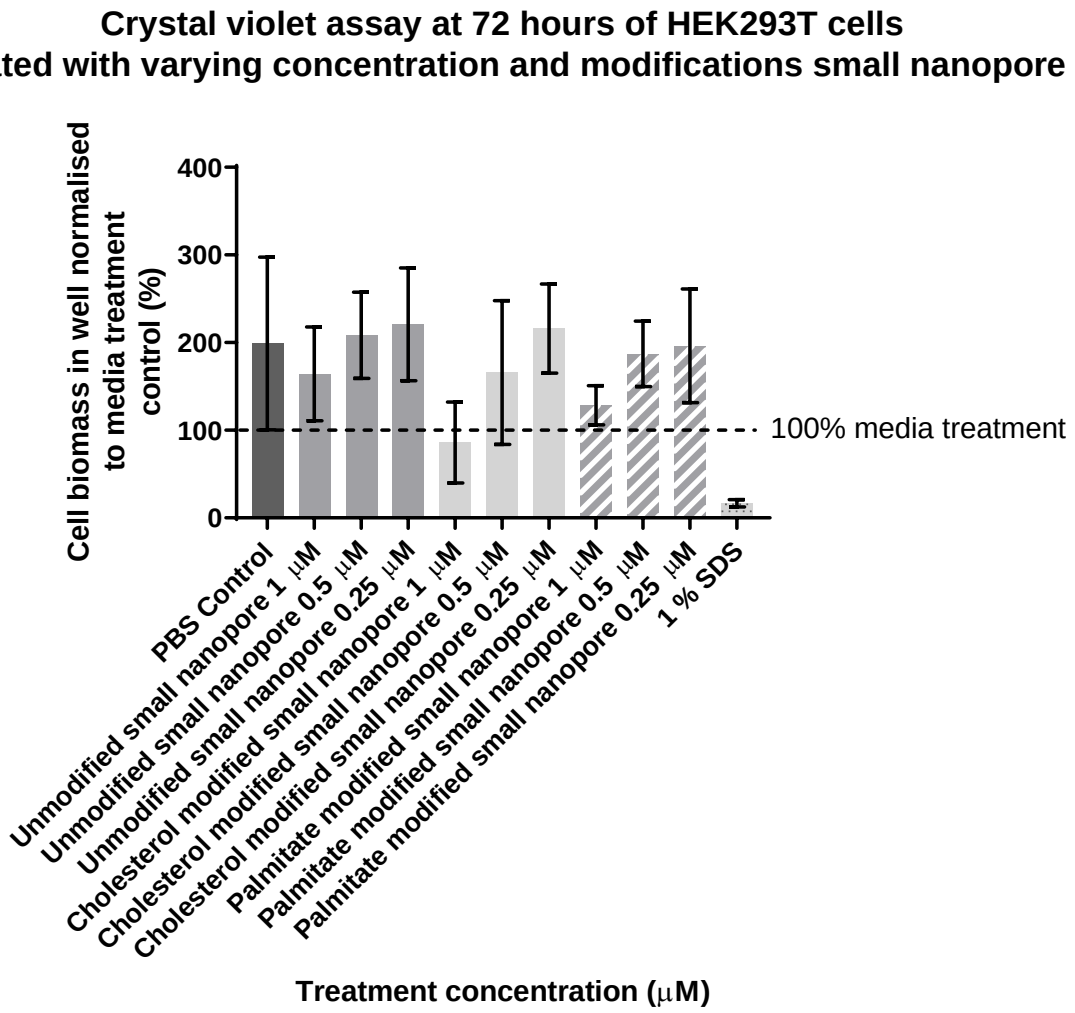

Figure 59 HEK293T cells treated with small nanopore crystal violet assay, N=4 mean and SD error shown. Although no significant differences were seen in the data due to large SD errors a decrease in cell biomass in well was observed in cells treated with 1 µM cholesterol modified small nanopore.

The crystal violet assay for this experiment can be seen in **Figure 59**. Although the percentage compared to untreated cells differed from that seen in **Figure 58**, the trend shown was the same. The PBS control and 1 µM unmodified nanopore showed similarly high values of 199% and 164% respectively and the hydrophobically modified pores lower values at 86% and 129% for cholesterol and palmitate modifications at 1 µM. However it must be noted that the error in these values was

high and no statistical significance could be found when applying a one way ANOVA corrected for multiple comparisons using Tukey's method.

At low concentrations of 0.25 µM this trend was no longer seen. It can be seen in both **Figure 58** and **Figure 59** which show the alamar blue and crystal violet assay data that the average values remained largely the same throughout treatment types. This indicated that at low concentrations the nanopores had no effect on cell viability.

Although, in **Figure 57**, the cells treated with 100% media solution and the cholesterol modified nanopore samples look to have are very similar final confluences (41.5% and 40.7% respectively), they show very different trends in the alamar blue assay. **Figure 58** shows that the cell viability from the cholesterol treated cells was 67.3% of that shown by the untreated cells indicating that there was a different number of cells in the sample at 72 hours. Therefore, further investigation into the IncuCyte images was conducted.

The IncuCyte first takes an image of the cells and the processes the images using a 'cell mask'. This is an algorithm which lets you define the area of the cell and the background. However, this must be applied throughout the whole experiment. Therefore, if there is a picture which is out of focus, or if there is cell debris in the well which doesn't fit the parameters set at the start of the experiment, this can lead to inaccurate results. **Figure 60** shows the cell mask applied to cells in one of the biological repeats. It can be seen that the program is accurately defining the cell confluence at 0 hours and 24 hours in all samples. However, at 48 hours and 72 hours cells the images of the cells treated with the cholesterol modified nanopore, show that the program was identifying the background as cells, therefore giving a higher confluence reading than was present. This therefore explains the inconsistences between the proliferation curve and the alamar blue assay.

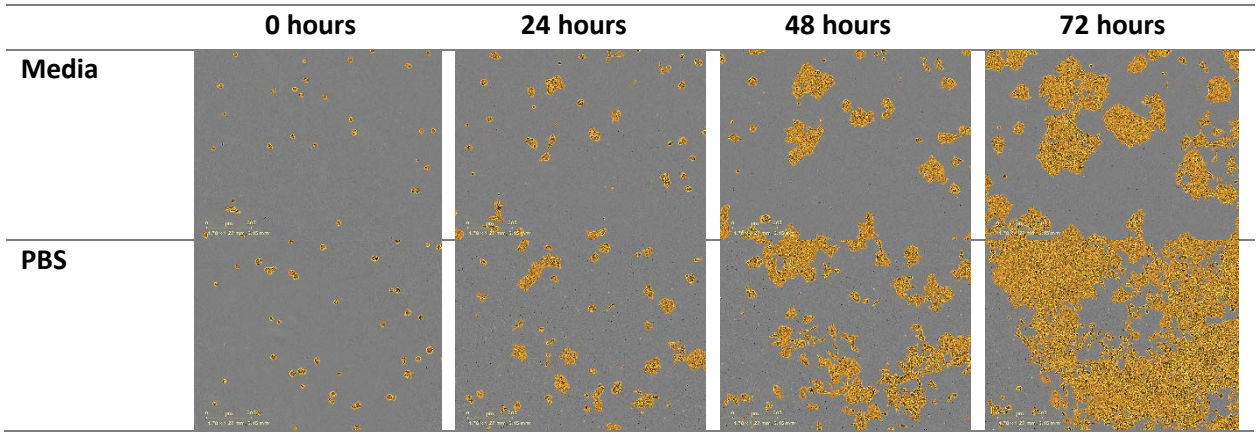

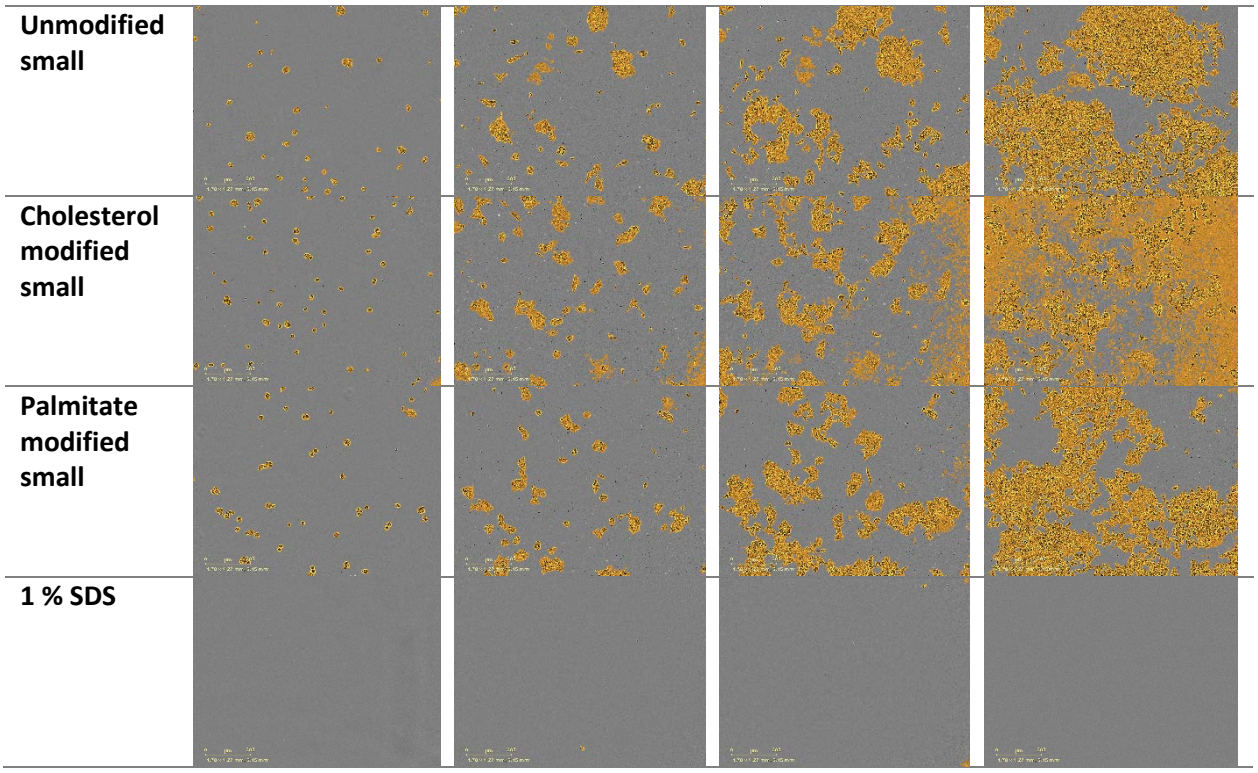

Figure 60 Example images taken from the IncuCyte with cell mask applied taken from 3rd biological repeat of experiment (EB_n=3_t3_image1). In the images taken at 48 and 72 hours in the samples treated with cholesterol and palmitate modified small nanopores it can be seen that the cell mask was also applying to the background and not only the cells. This led to misrepresentation of the confluence in these samples.

This occurrence was also seen in other wells with different concentrations therefore the proliferation curves taken directly from the IncuCyte could not be directly used for this experiment. However, the images were further processed using ImageJ[132] (computer software for scientific imaging). Using the overlay function, the cells were manually outlined and the area they occupied calculated. The overall area of the image was also measured and the confluence calculated using this data. An example of this is shown in **Figure 61** where the cells are clearly outlined and the measurements shown to the right.

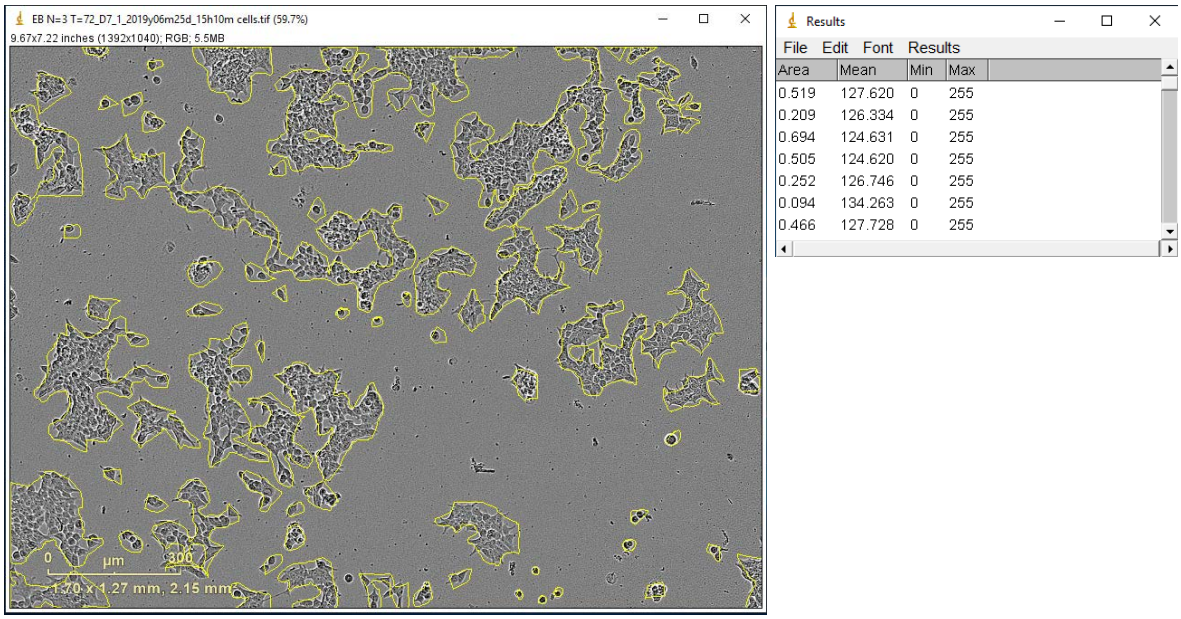

Figure 61 Image of HEK293T cells treated with 1 µM cholesterol modified small nanopore (EB_n=3_D7_1) analysed manually using Image J. The confluence calculated using this method was 27%.

Four images were taken for in each well and as the cell mask did not apply incorrectly for all of them the images were sifted through and sorted into those that needed the manual measurements and those where the cell mask was adequate. Due to the number of images taken in the experiments (36 wells, 4 images per well, 37 time points and 4 biological repeats) this was only done on the time point 72 hours and the difference measured between it and 0 hours (when the images where adequately analysed using the cell mask function). An example of this is shown in **Figure 61** and **Figure 62** which shows the confluence difference between using the cell mask analysis and the manual image J analysis. This showed a difference of 43% and although this value was not consistent throughout all of the images and therefore could not be applied to all images as a correction factor, it did give an indication that there were significant differences between the incucyte cell mask data, and the values calculated through Image J analysis.

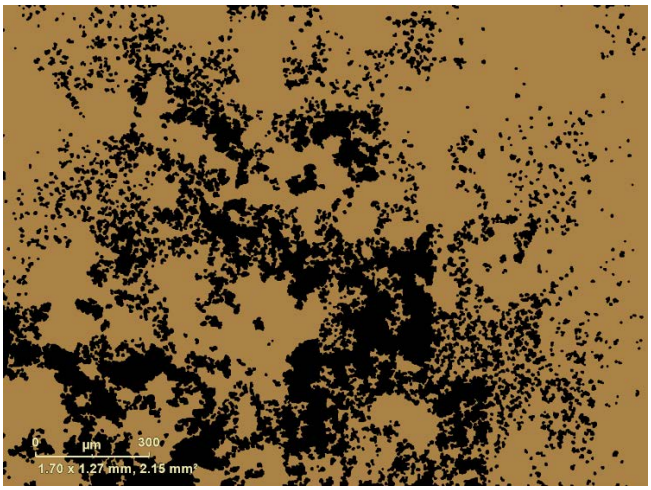

Figure 62 Image of HEK293T cells treated with 1 µM cholesterol modified small nanopore (EB_n=3_D7_1) showing the cell mask applied by the IncuCyte. Theconfluence calculated using this method was 70%.

The difference between the starting confluence and final confluence was calculated and shown as a percentage of the negative 100% media control. This showed a more accurate representation of the IncuCyte data than the proliferation curves shown in **Figure 57**.

The data, both ImageJ and IncuCyte depending on cell mask, was combined to form the graph seen in **Figure 63** which supported the same conclusions drawn from the assays data shown in **Figure 58** and **Figure 59**. A larger difference in confluence at 0 and 72 hours indicated that the cells continued to grow and therefore the treatment did not have a negative effect on the cell proliferation. A decrease of 33% in proliferation was observed between the PBS vehicle control and 1 µM cholesterol modified small nanopore. This mirrors the decrease in cell viability seen in **Figure 58**, supporting the evidence that when treated with 1 µM cholesterol modified small nanopore, the cells were negatively affected.

Similarly a smaller decrease of 15% was observed between the PBS vehicle control and 1 µM palmitate modified small nanopore. This was also seen in the alamar blue assays, also a smaller decrease than that of the cholesterol modification. This would indicate that at 1 µM the cholesterol modification was more potent than the palmitate modification.

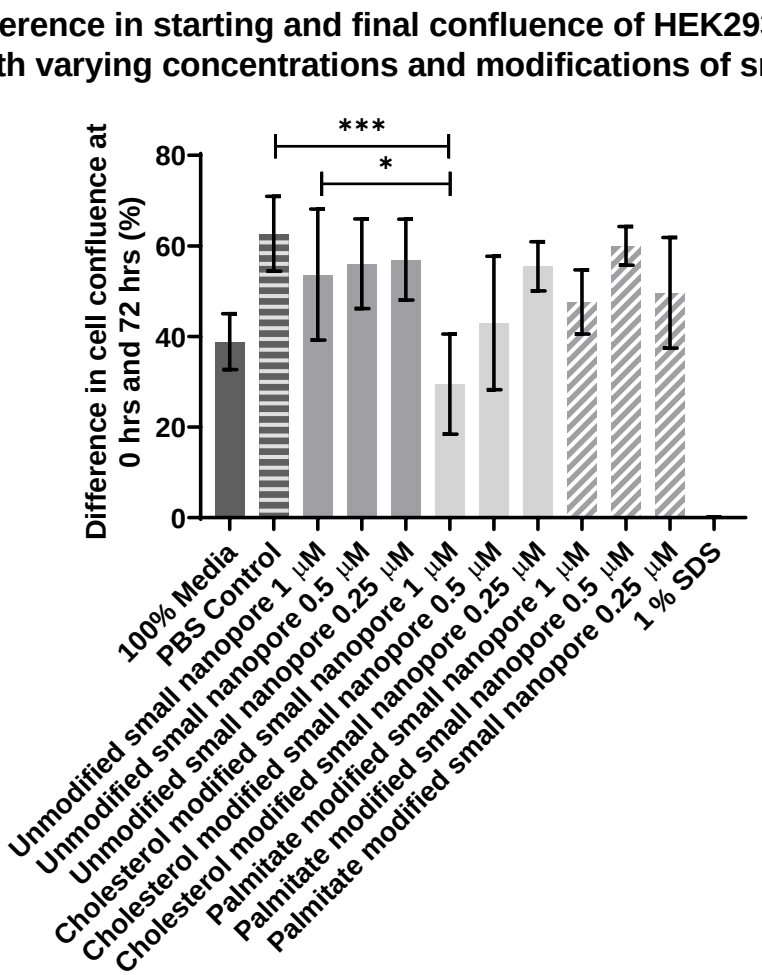

Figure 63 Graph showing difference in confluence at 0 hours and 72 hours of HEK293T cells treated with varying concentrations and modifications of small nanopore. N=4, mean and SD error shown. Statistically significant $p<0.05$, one way ANOVA corrected for multiple comparisons using Tukey's method. Treatment with 1 µM cholesterol modified small nanopore resulted in a significant decrease in change in start and end confluence compared to cells treated with the PBS control and the equivalent concentration of unmodified nanopore. This indicated that at 1 µM, the cholesterol modified small nanopore had a statistically significant negative effect on cell proliferation.

4.4.1.2 HEK293T cells treated with varying concentrations of large nanopores

The experiments detailed above with the small nanopore were repeated but with the large nanopore structure, using unmodified, cholesterol modified, and palmitate modified treatments. Experiments were conducted with 3 technical triplicates and 3 biological repeats. It was hypothesised that the large nanopores that were modified with hydrophobic moieties would have a negative effect on HEK293T cell viability.

Cells were seeded at a density of 2000 cells per well and left for 24 hours before the relevant treatments were applied and monitored for 72 hours by IncuCyte and finally by alamar blue and crystal violet assays. However, similarly to the small nanopore experiments, the cell mask did not apply correctly to all wells therefore the data could not be used. However, the images could still be used to monitor cell morphology throughout the experiment.

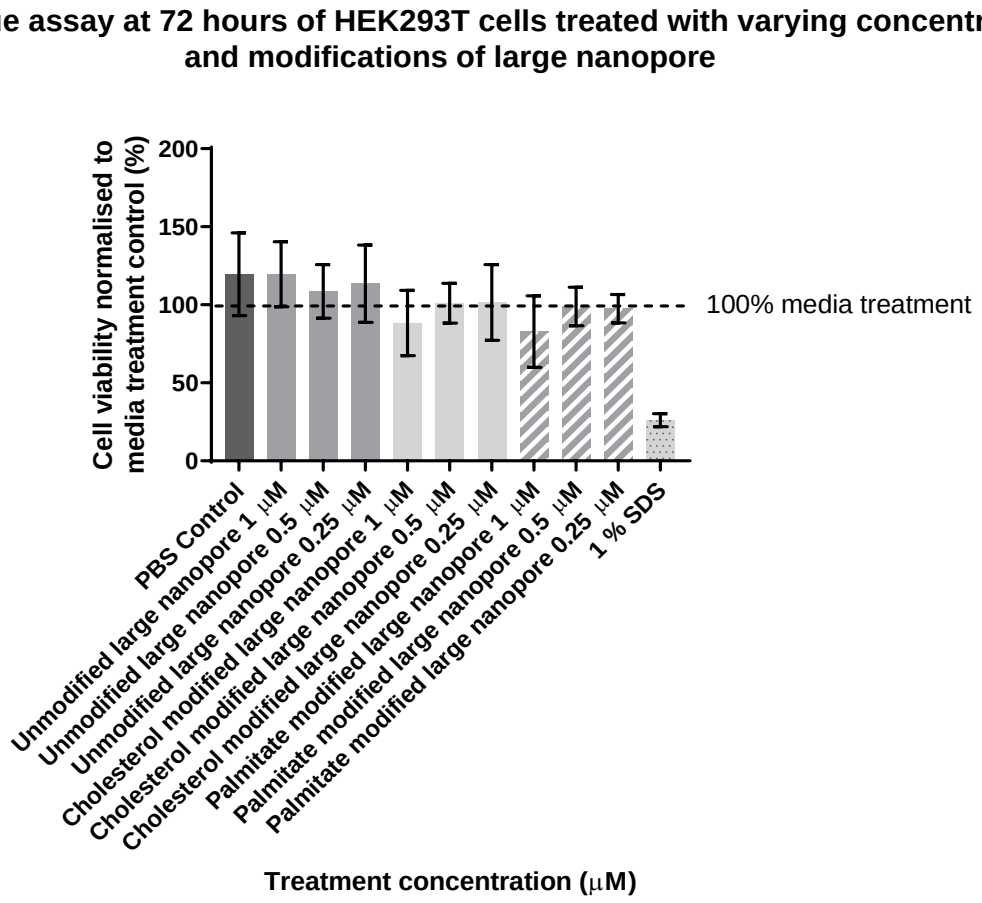

Figure 64 Graph showing the alamar blue assay at 72 hours of HEK293T cells treated with varying concentration and modifications of large nanopore. N=3, mean and SD error shown. Statistically significant $p<0.05$, one way ANOVA corrected for multiple comparisons using Tukey's method. No significant difference in cell viability was noted between treatments compared to the PBS control.

There is no large difference between PBS vehicle control and the unmodified nanopores at all concentrations. As seen in the cell viability data in Figure 64 the PBS vehicle control showed a value of 120% and the unmodified samples showed values of 120, 108 and 114% at 1, 0.5 and 0.25 µM with standard deviation error bars overlapping therefore showing no significance in the small differences. This was also seen in the crystal violet assay data in Figure 65, which showed a PBS value of 213% and unmodified large nanopore values of 155, 164 and 197% at 1, 0.5 and 0.25 µM respectively as a percentage of the cells treated with media only. This indicated that that the

unmodified nanopore had no negative effect on the cell viability of the HEK293T cells at concentrations 1, 0.5 and 0.25 µM.

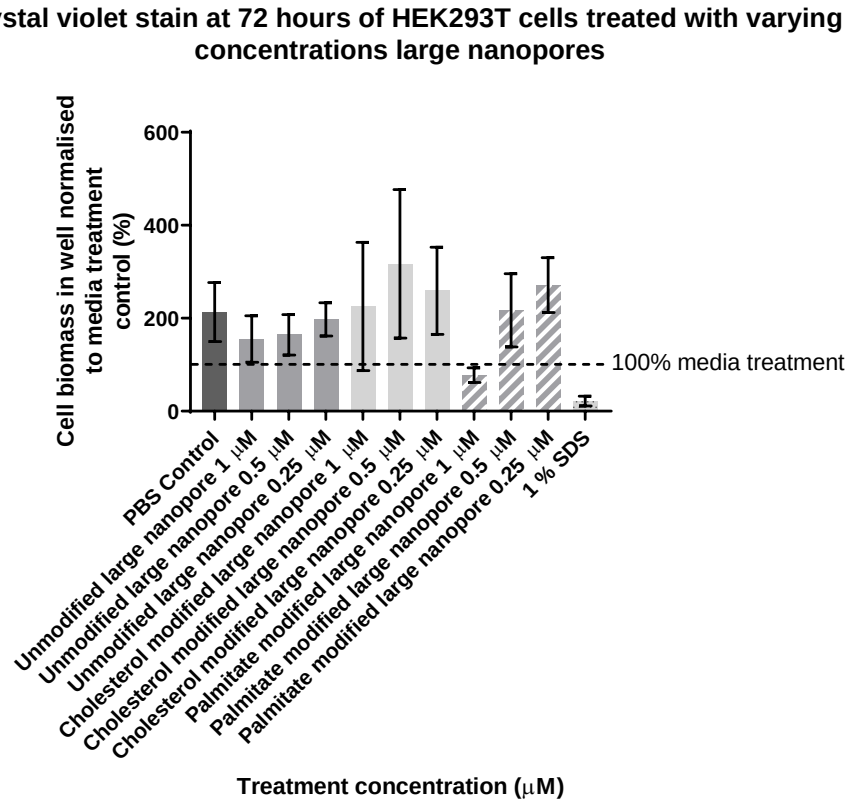

Figure 65 Graph showing the crystal violet stain at 72 hours of HEK293T cells treated with varying concentrations of large nanopores. N=3, mean and SD error shown. Statistically significant $p<0.05$, one way ANOVA corrected for multiple comparisons using Tukey's method. No significant difference in cell biomass was noted between treatments compared to the PBS control.

There was no difference observed in cell viability in cells treated with cholesterol modified large nanopores at the lower concentrations of 0.5 and 0.25 µM. In the alamar blue assay shown in Figure 64 it can be seen that the values at these concentrations were both 100%. However, at the higher concentration of 1 µM the average value reduced to 88%. Compared to the PBS vehicle control of 120% this shows a decrease of 32% in cell viability however upon statistical analysis it was seen that this was not statistically significant.

This trend was also noted in the palmitate modified large nanopore where the two lowest concentrations tested showed a similar cell viability of 99 and 98% at 0.5 and 0.25 µM and a lower cell viability again at 1 µM 83%. The similarity in values indicated that the modification type did not play a part in the efficacy of these treatments on HEK293T cells.

4.4.1.3 HEK293 cells conclusion

Working with both HEK293FT and HEK293T cells proved to be educating but also provided some difficulty. One of the main difficulties was the attachment of the cells to the wells. They are weakly adherent cells therefore the removal of media and addition of the treatment caused disturbance to the cells. The protocol applied tried to reduce the effect of this on the results by ensuring that all of the treatments were premixed before applying to the cells. This was to reduce pipette pressure into the wells through multiple applications of the different fractions of the treatment. The cell seeding density was therefore difficult to be accurate with as upon removal of the original media the cells were also disturbed.

This also caused an issue with the crystal violet assays as although the cells were fixed with formalin before staining, the cells had undergone multiple steps which were likely to have an effect on cell attachment. The alamar blue assay was first conducted on the cells which involved the removal of the treatment containing media and replaced with media containing alamar blue solution which was then transferred to a plate capable of allowing fluorescence readings. The cells were then washed with PBS. This washing step was only conducted once, whereas with both B16-F10 and FM55-P lines (Sections 4.2.3 and 4.2.4) this was repeated 3 times. This was to try and reduce disruption to the cells before finally fixing with 10% neutral buffered formalin. This would explain the large error bars in the crystal violet data shown in Figure 59 and **Figure 65**.

Overall it can be seen that the cholesterol modified small nanopore has a negative effect on cell viability at 1 µM. This effect was concentration dependant where the cytotoxicity decreases as concentration decreased. The palmitate modified small nanopore was also seen to be active at these concentrations but to a lesser degree than that seen with cholesterol modification.

4.5 Cytotoxicity of small and large nanopores in B16-F10 cells

B16-F10 cells are a mouse melanoma cell line commonly used for investigations with melanoma. They are fast growing, robust cell line. Unless otherwise specified the cells were grown in culture at 37 °C, 5% CO_2 until 70% confluence before passaging.

4.5.1 B16-F10 cells treated with varying concentrations of small nanopore

B16-F10 cells were first seeded at 2000 cells per well and treated with 1µM, 0.5 µM and 0.25 µM of varying modifications of small nanopore. Three plates were seeded so that three time points after cells were treated (24, 48 and 72 hours) could be used to run assays. This was to allow the

cells to be observed at different time points as the IncuCyte was not available at the location that these tests took place in.

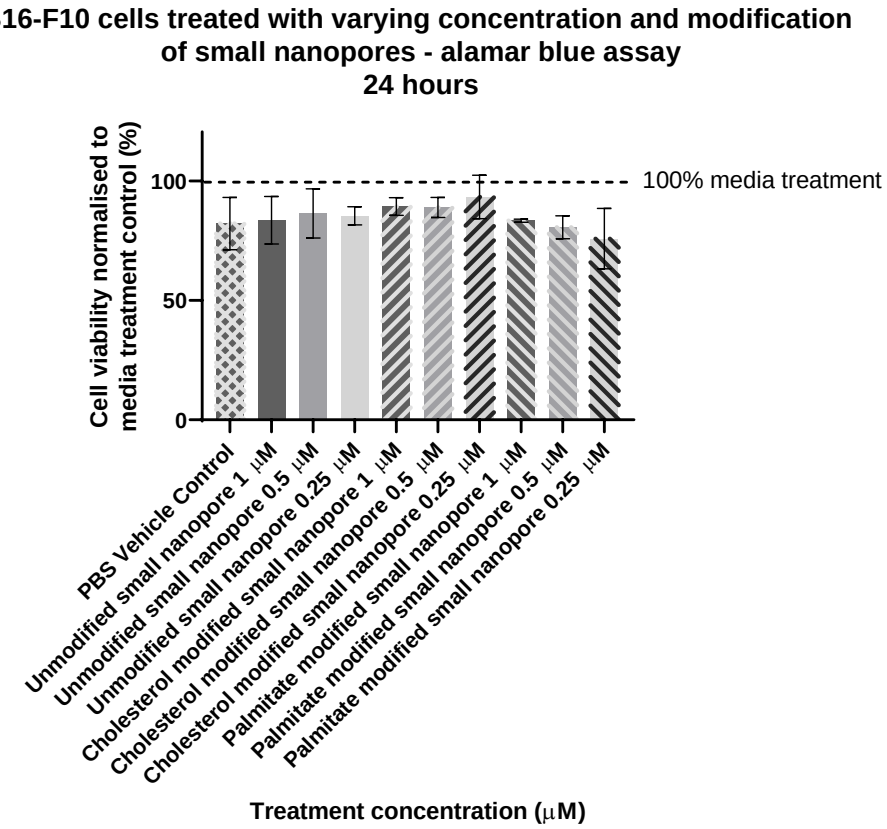

Figure 66 Graph showing alamar blue assay of B16-F10 cells treated with varying concentrations at 24 hours. N=3, mean and SD error shown. Not statistically significant $p<0.05$, one way ANOVA corrected for multiple comparisons using Tukey's method. No significant difference in cell viability was noted between treatments compared to the PBS control.

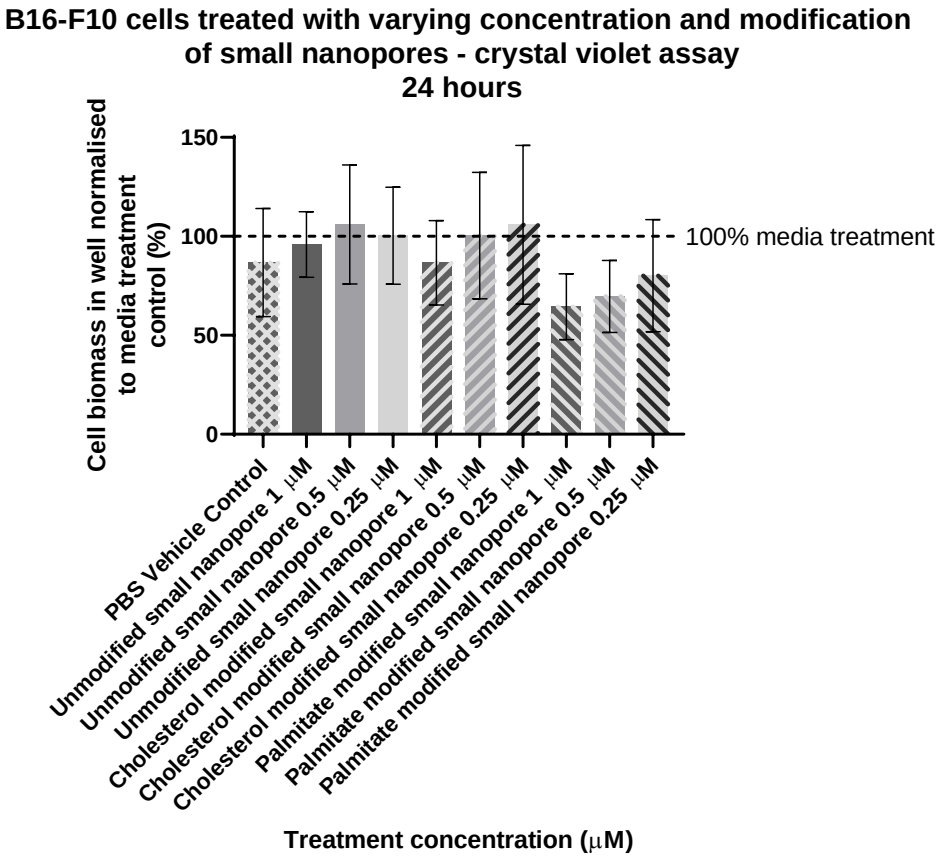

Figure 67 Graph showing crystal violet assay of B16-F10 cells treated with varying concentrations at 24 hours. N=3, mean and SD error shown. Not statistically significant $p<0.05$, one way ANOVA corrected for multiple comparisons using Tukey's method. No significant difference in cell biomass was noted between treatments compared to the PBS control.

Results were normalised and plotted as a percentage of the result given by cells treated with 100% cell media in each experiment and averages taken from these values. This ensured that any small differences in the experiment such as time the alamar blue was incubated for were nullified.

At 24 hours it can be seen that, according to the alamar blue assay in **Figure 66**, there was little change between the viability of the cells compared to the PBS treated cells at all concentrations. The unmodified nanopore was expected to show a similar result to the PBS vehicle control as it contained no hydrophobic modifications, and this was proven to be true at 24 hours with average values ranging between 83 and 85% compared to the 82% shown by the PBS control. Similar values between small ranges was also seen for the modified nanopores throughout the concentrations. However, they did not show any decrease compared to the PBS control or unmodified nanopore. The cholesterol modified small nanopore showed results in the small range of 89 to 93% between concentrations and the Palmitate modified nanopore between 76 and 83%. This was also consistent with the data shown in the crystal violet assay, **Figure 67**, that showed the amount of biological

material in the wells. Although the crystal violet values were seen to vary slightly between types of nanopores, the standard deviation of these values showed this to be insignificant. This indicated that at 24 hours no effect of the nanopores at any concentrations tested was observed.

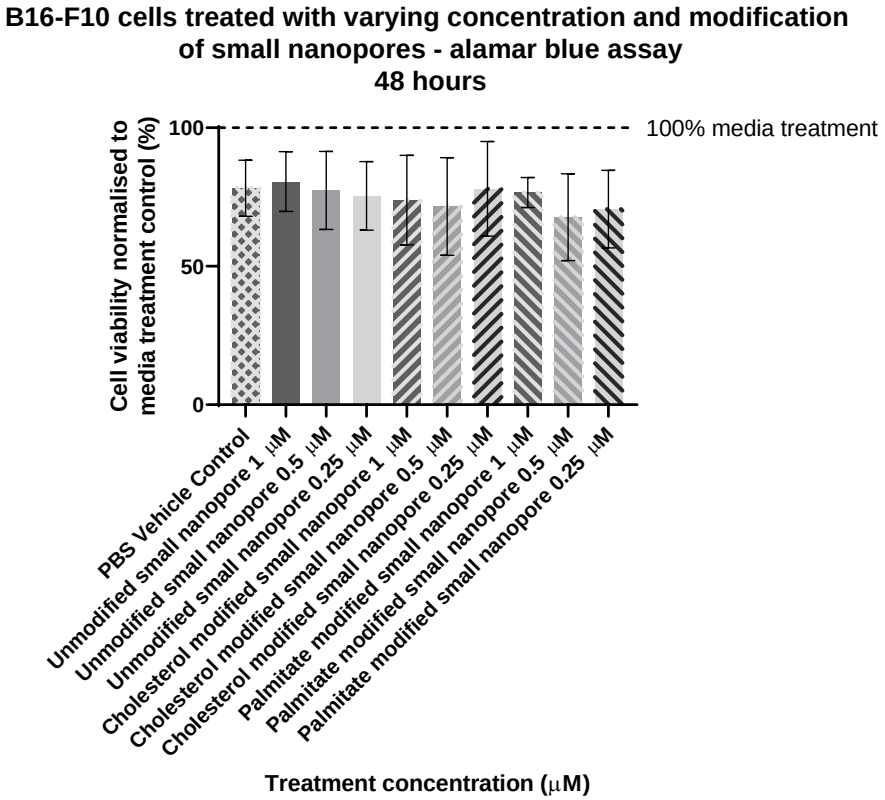

Figure 68 Graph showing cell viability assay of B16-F10 cells treated with varying concentration and modification of small nanopores at 48 hours. N=3, mean and SD error shown. Not statistically significant $p<0.05$, one way ANOVA corrected for multiple comparisons using Tukey's method. No significant difference in cell viability was noted between treatments compared to the PBS control.

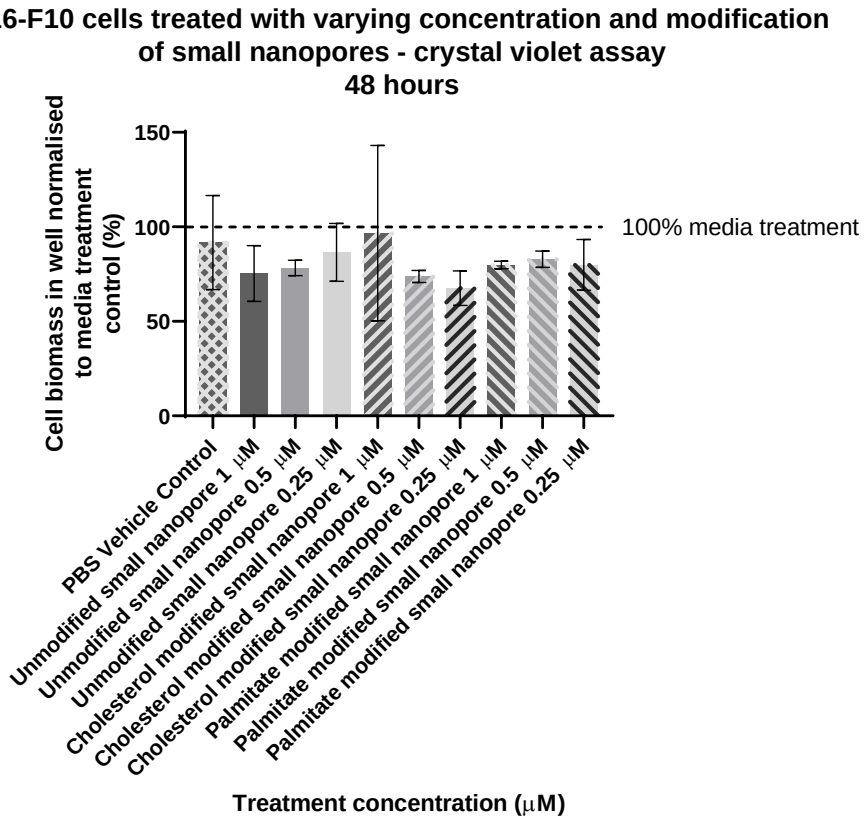

Figure 69 Graph showing crystal violet assay of B16-F10 cells treated with varying concentration and modification of small nanopores at 48 hours. N=3, mean and SD error shown. Not statistically significant $p<0.05$, one-way ANOVA corrected for multiple comparisons using Tukey's method. No significant difference in cell biomass was noted between treatments compared to the PBS control.

This trend was also observed at 48 hours, **Figure 68** and **Figure 69**. The PBS control had a larger effect than seen at 24 hours. However, this was expected as the longer the experiments ran, the more cell media would have been used up and as the PBS mixture only contained 50% media it would be expected that the compounds used for cell growth would diminish faster than in cells treated with media alone. This line of thought was further supported by the data given at 72 hours, **Figure 70** and **Figure 71**, which showed a further decrease in cell viability of cells treated with media alone.

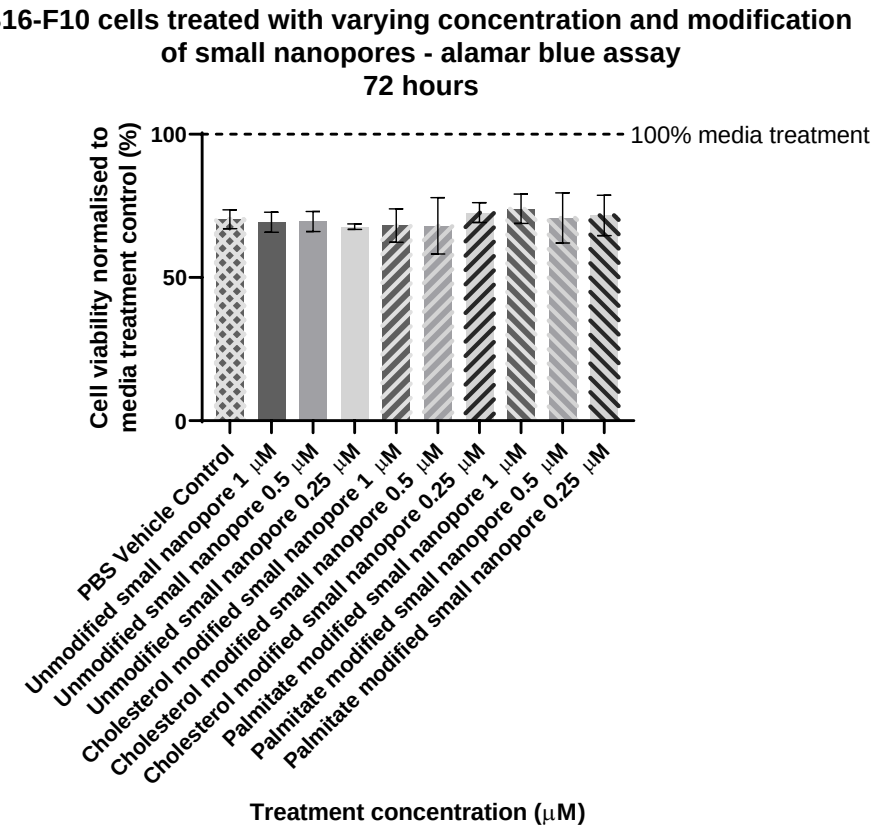

Figure 70 Graph showing cell viability assay of B16-F10 cells treated with varying concentration and modification of small nanopores at 72 hours. N=3, mean and SD error shown. Not statistically significant $p<0.05$, one-way ANOVA corrected for multiple comparisons using Tukey's method. No significant difference in cell viability was noted between treatments compared to the PBS control.

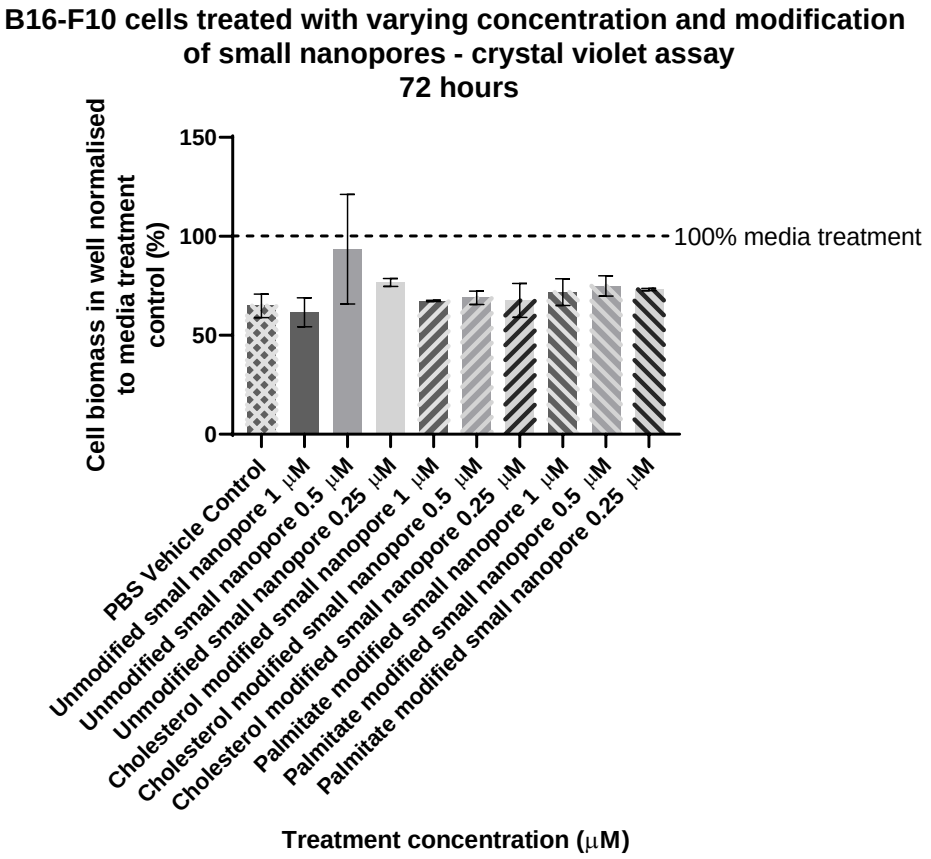

Figure 71 Graph showing crystal violet assay of B16-F10 cells treated with varying concentration and modification of small nanopores at 72 hours. N=2, mean and SD error shown. Not statistically significant $p<0.05$, one-way ANOVA corrected for multiple comparisons using Tukey's method. No significant difference in cell biomass was noted between treatments compared to the PBS control.

This trend also was seen in the cells observed at 72 hours after treatment. There was no significant difference seen in cells treated with PBS control and all other treatment groups at varying concentrations. In the alamar blue assay, **Figure 70**, it was shown that, where PBS control showed an average result of 72%, all other treatment groups fell in the small range of 68 to 74% compared to cells treated with 100% media.

After consideration of previous work with HEK293FT cells which showed a decrease in starting confluence to have an effect on the efficacy of the nanopores, Chapter 3, it was decided to reduce the seeding density of the B16-F10 cells to 1000 cells per well. This experiment was only conducted with the median of concentrations used, 0.5 μM nanopore, and can be seen in **Figure 72**.

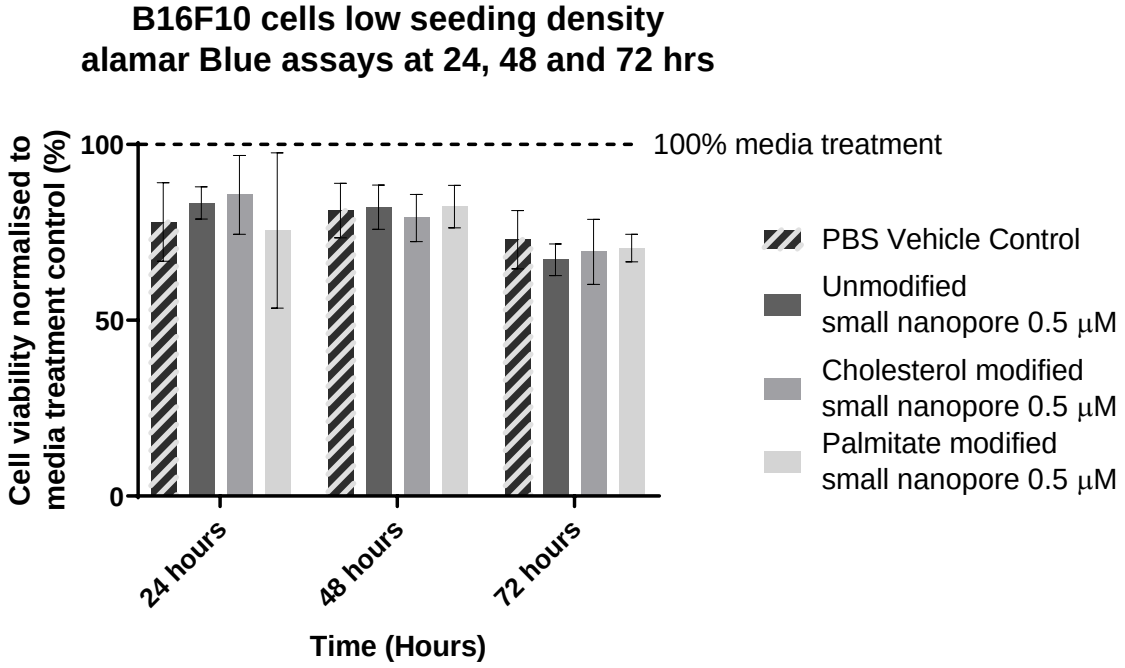

Figure 72 Graph showing treatment of B16-F10 cells at a seeding density of 1000 cells per well with 0.5 μM small nanopores measured by alamar blue assays at 24, 48 and 72 hours. N=3, mean and SD error shown. Not statistically significant $p<0.05$, two-way ANOVA corrected for multiple comparisons using Tukey's method. No differences were seen between treatments at 24, 48 or 72 hours.

However, this showed very similar results to those seen at the higher seeding density of 2000 cells per well. The vehicle control showed less of an effect over time compared to the previous experiment. At 24 hours the PBS control showed result of 78% similar to that seen at 72 hours which was 73%. This was expected as there were less cells competing for cell media throughout the experiment therefore the effect would not be seen until later time points if the experiment was continued. No statistically significant differences were found when comparing treatments with a two way ANOVA with Tukey's correction.

4.5.2 B16-F10 cells treated varying concentrations of large nanopore

It was thought that time window that we were looking into may have been too long and therefore the observation time was shortened for some experiments. Time points at 1 hour and 24 hours were used for alamar blue and crystal violet assays.

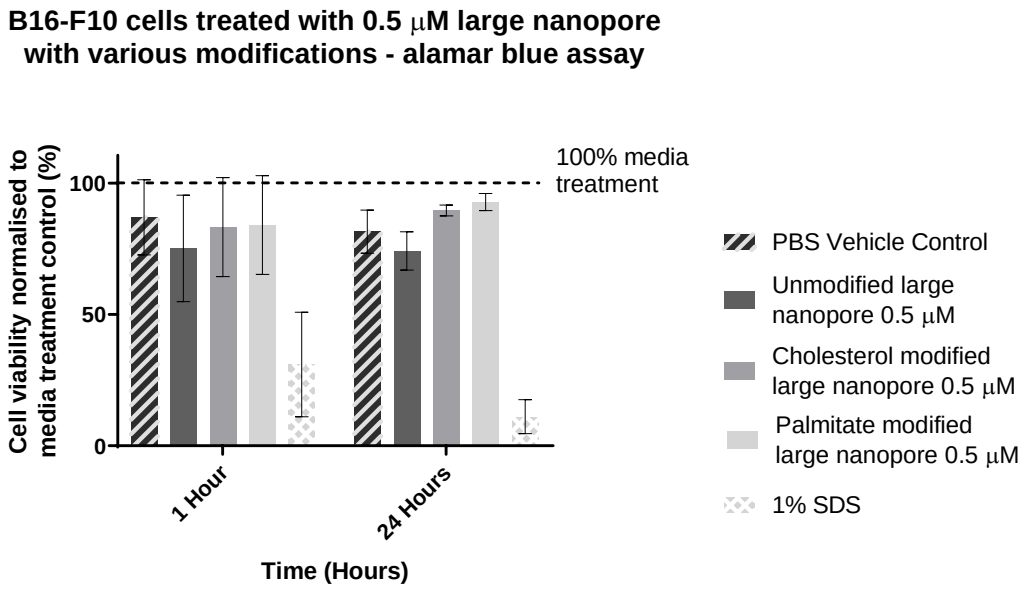

Figure 73 Graph showing alamar blue assay of B16-F10 cells treated with 0.5 μM large nanopores with various modifications. N=3, mean and SD error shown. No differences were seen between treatments at both 1 and 24 hours apart from the positive SDS control where a decrease in cell viability was seen as expected.

At 1 hour it can be seen that the error involved is a lot larger than that at 24 hours in the alamar blue assays. This made it difficult to ascertain any change. However, any changes observed at 24 hours were also insignificant. The crystal violet data shown in **Figure 74** also corroborated with the alamar blue results, showing no significant changes at either 1 or 24 hours.

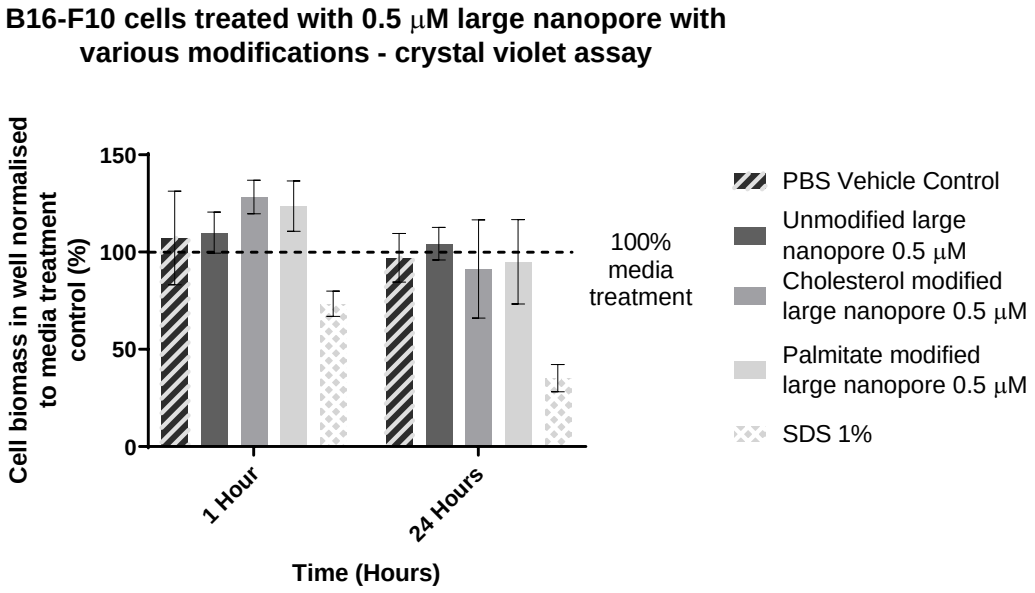

Figure 74 Graph showing crystal violet assay of B16-F10 cells treated with 0.5 μM large nanopores with various modifications. N=3, Mean and SD error. No differences were seen

between treatments at 1 or 24 hours apart from the positive SDS control which showed a decrease in cell biomass in the well.

Therefore, the protocol of monitoring was changed back to 72 hours, but additional monitoring through an IncuCyte was introduced. However as previously discussed with the HEK293T cells, the cell masks used gave unpredictable results therefore these results have not been included in this report for the further B16-F10 experiments.

B16-F10 cells were seeded at a density of 2000 cells per well and left to settle for 24 hours before treatments were applied. Cells were then observed over the course of 72hours before an alamar blue and crystal violet assay were conducted.

It can be seen from the alamar blue assay at 72 hours in **Figure 75** that there was no significant change within treatment groups. All concentrations of the unmodified nanopore gave values between the small range of 77 and 80% cell viability compared to untreated cells. This was also very similar to the cell viability shown of cells treated with varying concentrations of cholesterol modified nanopore and palmitate modified nanopores. These showed cell viabilities ranging between 71 to 77% and 69 to 77% respectively. These values and their error bars all fell within or overlapped with that of the cells treated with the vehicle control PBS.

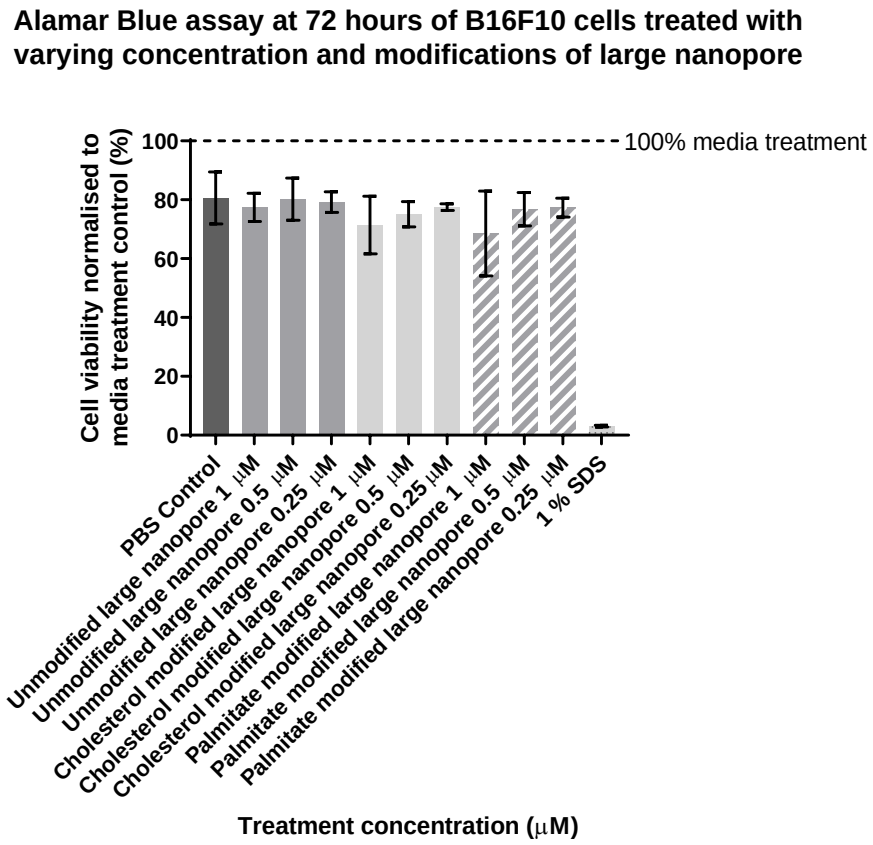

Figure 75 Graph showing alamar blue assay at 72 hours of B16-F10 cells treated with varying concentrations and modifications of large nanopore. N=3, mean and SD error shown. Statistically significant $p<0.05$, one-way ANOVA corrected for multiple comparisons using Tukey's method. No differences were seen between treatments apart from the positive control which showed a decrease in cell viability as expected.

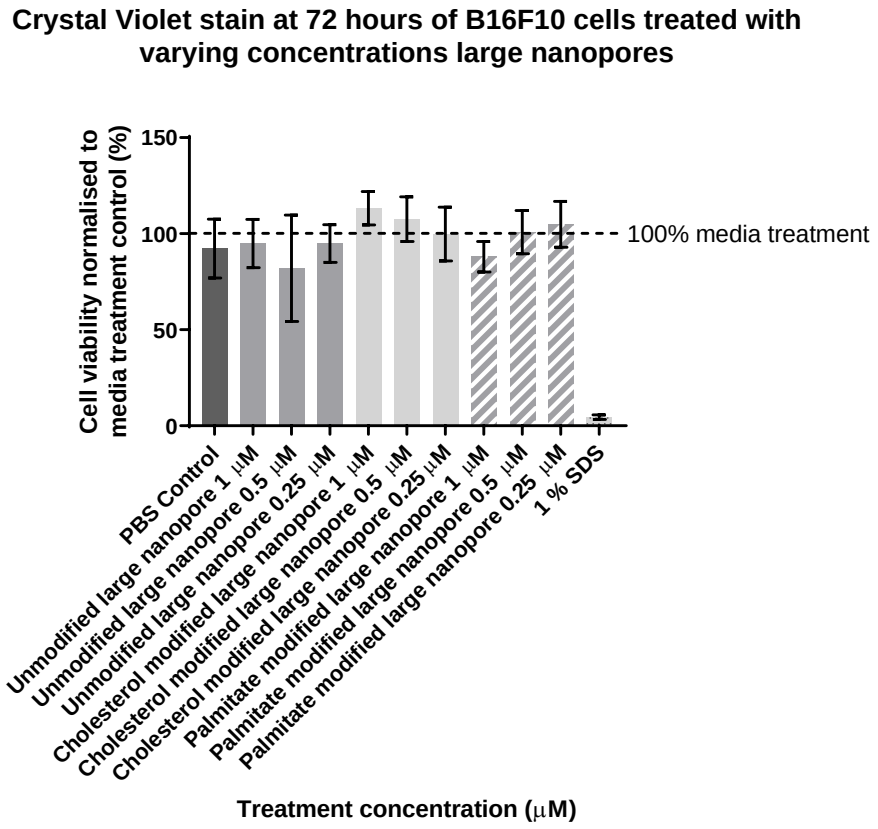

Figure 76 Graph showing crystal violet assay at 72 hours of B16-F10 cells treated with varying concentrations and modifications of large nanopore. N=3, mean and SD error shown. Statistically significant $p<0.05$, one-way ANOVA corrected for multiple comparisons using Tukey's method. No differences were noted between treatment groups apart from the positive SDS control.

This indicated that none of the modified nanopores had an effect on cell viability at any concentration. This was also supported by the crystal violet data shown in **Figure 76** which showed similar values throughout treatment groups.

From all this data it can be deduced that, at the conditions used in these experiments, neither the small or large nanopores had a negative effect on cell viability. This was seen with both unmodified pores and the hydrophobically modified pores; cholesterol and palmitate modified.

4.5.3 B16-F10 conclusion

No negative effect on cell viability was seen in B16-F10 cells with either small or large nanopore treatment. One thing that must be noted in these results is the difference in activity of the 1% SDS positive controls in these experiments as they vary slightly between experiments. This was due to a different stock of SDS being used. An older solution was used for the first experiments shown in **Figure 73** and **Figure 74** and a newer solution for **Figure 75** and **Figure 76**.

4.6 Cytotoxicity of small and large nanopores in FM55-P cells

FM55-P cells are an adherent human melanoma cell line established from a primary malignant melanoma therefore were highly relevant to this project. They are commonly used for modelling melanoma cell assays and were readily available for use. Unless otherwise stated cells were cultured at 37 °C, 5% CO_2 in RPMI with 10% FBS, 1% Pen/strep.

4.6.1 FM55-P cells treated with varying concentrations of small nanopore

The data shown in **Figure 77** used different cell culture conditions and cell media to the rest of the FM55-P experiments. FM55-P cells were first seeded at a density of 5000 cells per well and left to adhere to the plate for 24 hours at 37 °C, 8% CO_2. It must be noted that the media used contained 1% sodium pyruvate whereas further tests did not. Small nanopore treatments were then applied to the cells at 0.5 µM. Time points of 1 hour and 24 hours, mimicking that of published experiments[2], were used to monitor the cell viability with alamar blue (**Figure 77**) and crystal violet assay (**Appendix 1**). For the cell viability assay, fluorescence emission at 590 nm was measured when exciting at 560 nm and compared to that of cells treated with 100% media alone for each experiment. This was conducted with technical triplicates and three biological repeats. The mean of these values is show in **Figure 77** with standard deviation error.

It can be seen clearly, in **Figure 73**, that at one hour there is little difference between all treatments with averages ranging between 88 and 96% compared to non-treated cells apart from the positive control which measured a 75% decrease in cell viability. This trend was seen to continue at 24 hours. Although the difference of the positive control compared to all other samples was found to be statistically significant when analysed with a two-way ANOVA with Tukey's test to correct for multiple comparisons, no other statistical differences were found.

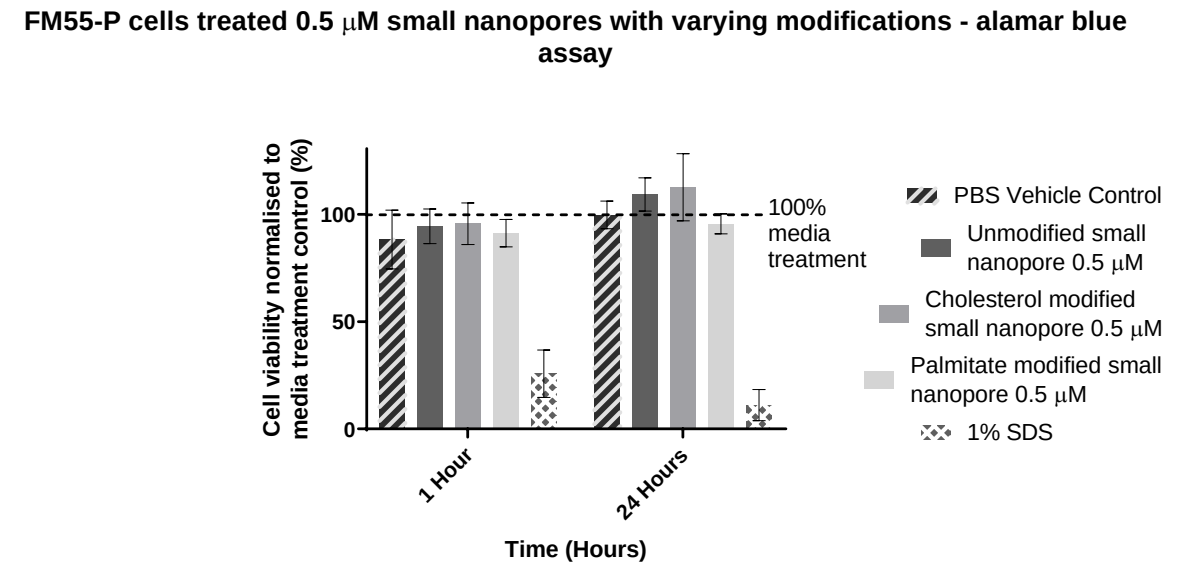

Figure 77 Graph showing FM55-P cells treated with 0.5 μM small nanopores with varying modifications cell viability assay. N=3 mean and SD error shown. No differences were seen between treatments at both 1 hour and 24 hours apart from the SDS positive control.

The protocol was then altered slightly. The settling time for the cells after passaging was increased from 24 to 48 hours as it was noted that better adhesion to the well plate occurred after 48 hours. Cells were cultured under the conditions previously mentioned of 37 °C, 5% CO_2. The observation time was increased to 72 hours when an alamar blue assay and crystal violet assay was used to calculate cell viability. The IncuCyte was also used in these experiments to monitor cell proliferation as the cell mask applied accurately to these experiments.

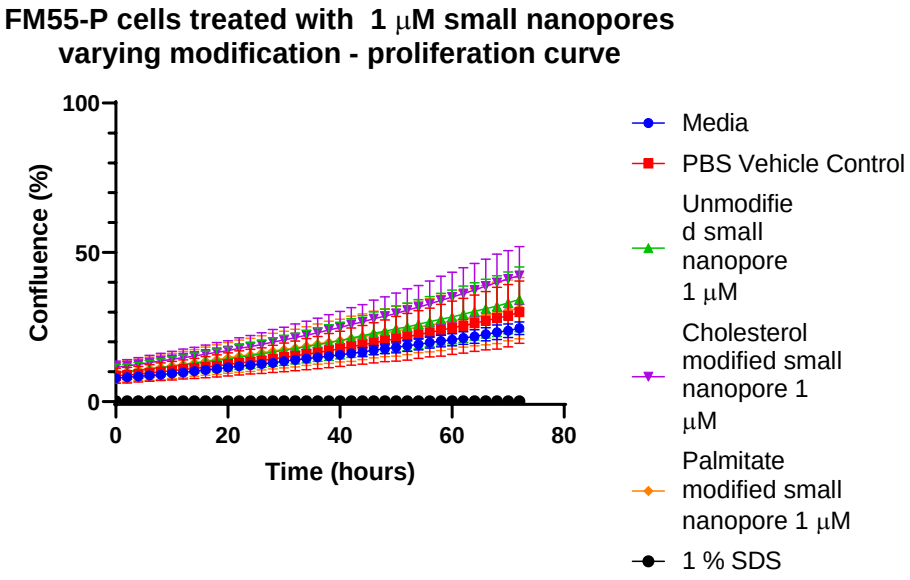

Figure 78 Graph showing proliferation of FM55-P cells treated with 1 μM small nanopores with varying modifications. N=3, mean and SD error shown. All treatments were seen to have very similar proliferation curves with overlapping SD error which indicated no treatment had a negative effect on proliferation. Individual traces can be found in the appendix.

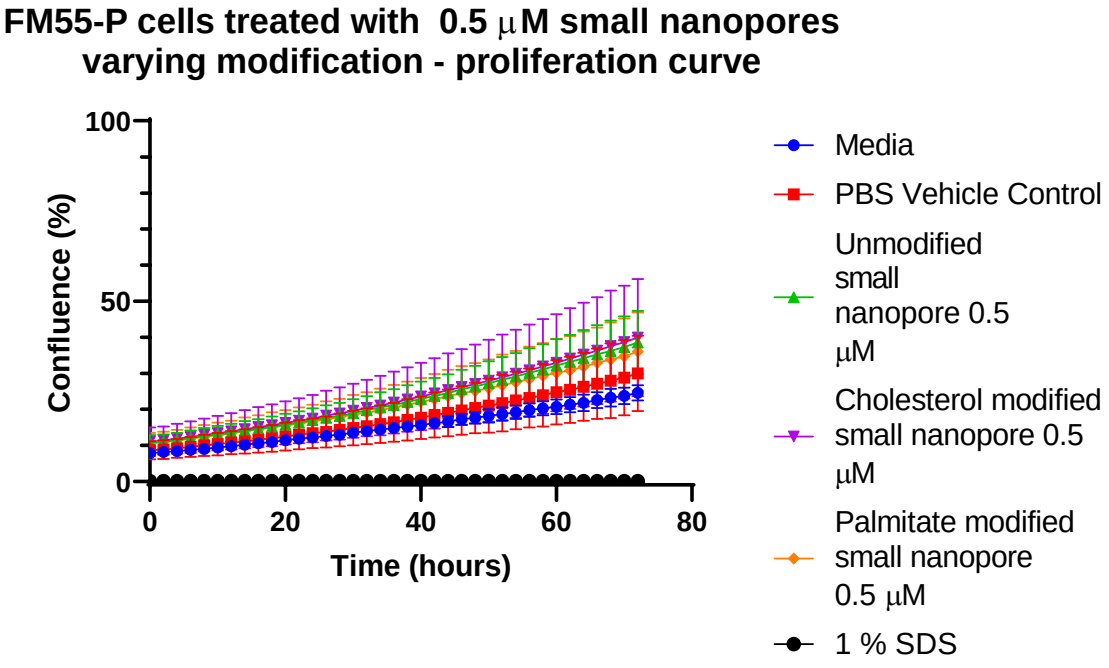

Figure 79 Graph showing proliferation of FM55-P cells treated with 0.5 μM small nanopores with varying modifications. N=3, mean and SD error shown. All treatments were seen to have very similar proliferation curves with overlapping SD error which indicated no

treatment had a negative effect on proliferation. Individual traces can be found in the appendix.

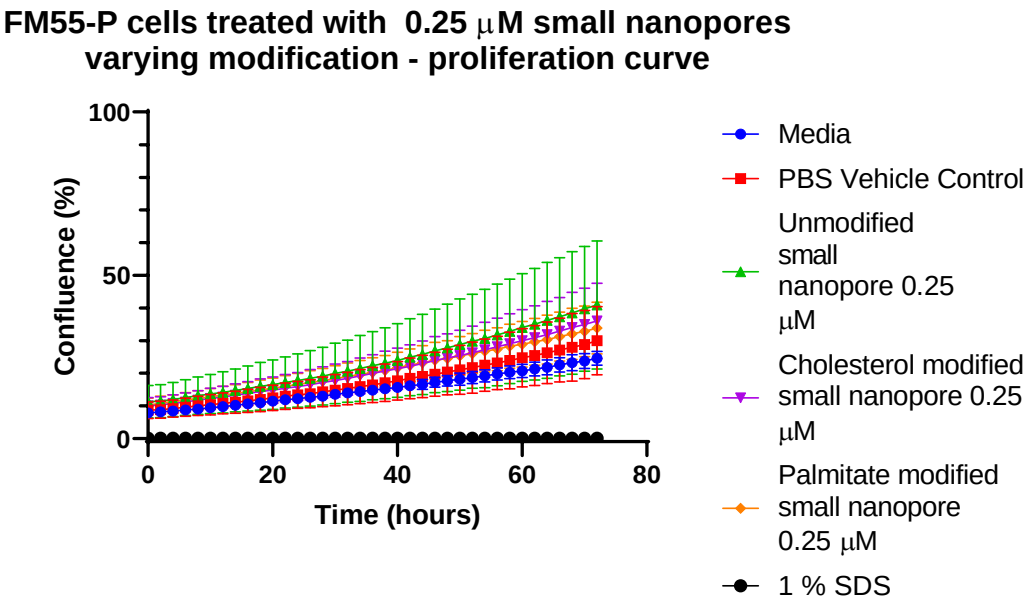

Figure 80 Graph showing proliferation of FM55-P cells treated with 0.25 μM small nanopores with varying modifications. N=3, mean and SD error shown. All treatments were seen to have very similar proliferation curves with overlapping SD error which indicated no treatment had a negative effect on proliferation. Individual traces can be found in the appendix.

The proliferation curves have been split into three figures showing different concentrations for ease of viewing; **Figure 78**, **Figure 79** and **Figure 80**. Due to small differences in the average confluences observed, the graphs at all concentrations were convoluted therefore the data was also plotted as change in start and end confluence shown in **Figure 81**. This also highlighted the large standard deviation errors bars involved with this method of data collection. However, it can be deduced that this data indicated that there was no significant change in cell proliferation between treatment groups.

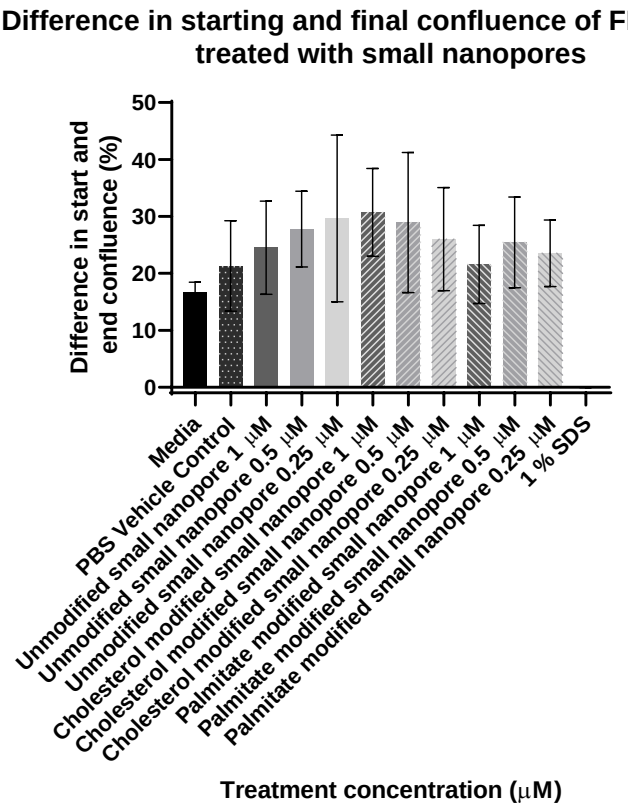

Figure 81 Graph showing difference in starting and end confluence of FM55-P cells treated with small nanopores with varying concentration and modifications. N=3, mean and SD error shown. Statistically significant $p<0.05$, one-way ANOVA corrected for multiple comparisons using Tukey's method. No significant differences were seen between treatment groups.

This deduction was also supported by the terminal assays that were run at 72 hours. The alamar blue assay shown in **Figure 82** showed no significant change in cell viability among the treatment groups when compared to the untreated cells.

The cell viability ranged between 109 and 115% for all concentrations of unmodified nanopore which was similar to that of the cholesterol and palmitate modified nanopores which measured between 108 to 120% and 94 to 109% respectively. This was mirrored in the crystal violet results in **Figure 83**.

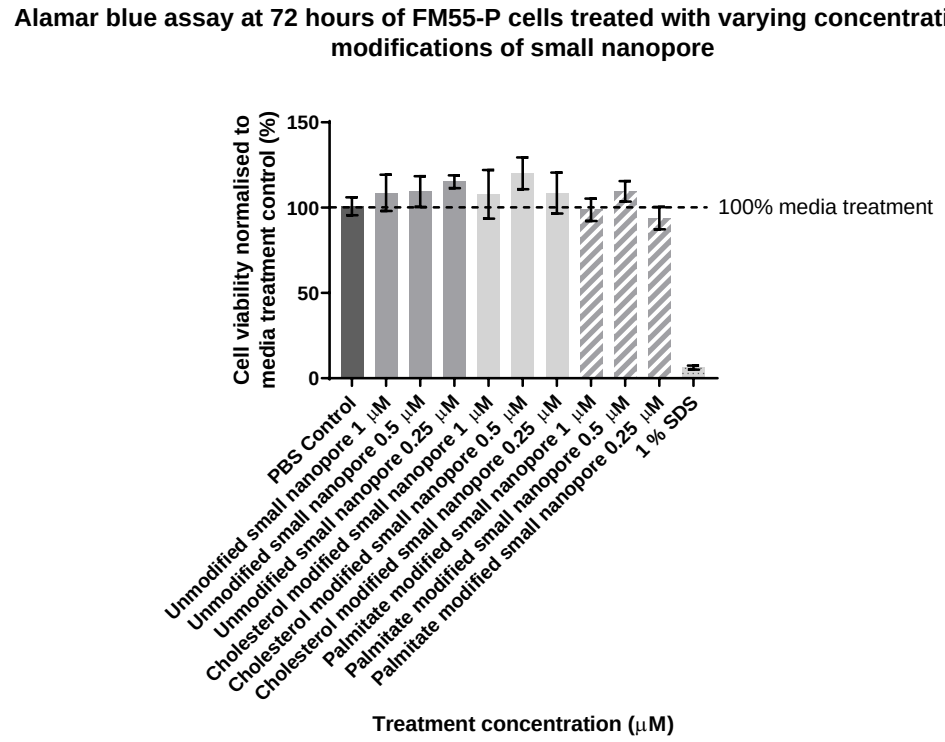

Figure 82 Graph showing alamar blue assay at 72 hours of FM55-P cells treated with varying concentration and modifications of small nanopore. N=3, mean and SD error shown. Statistically significant $p<0.05$, one-way ANOVA corrected for multiple comparisons using Tukey's method. All samples maintained a cell viability near to 100% apart from the positive control, which indicated no difference in efficacy of treatments.

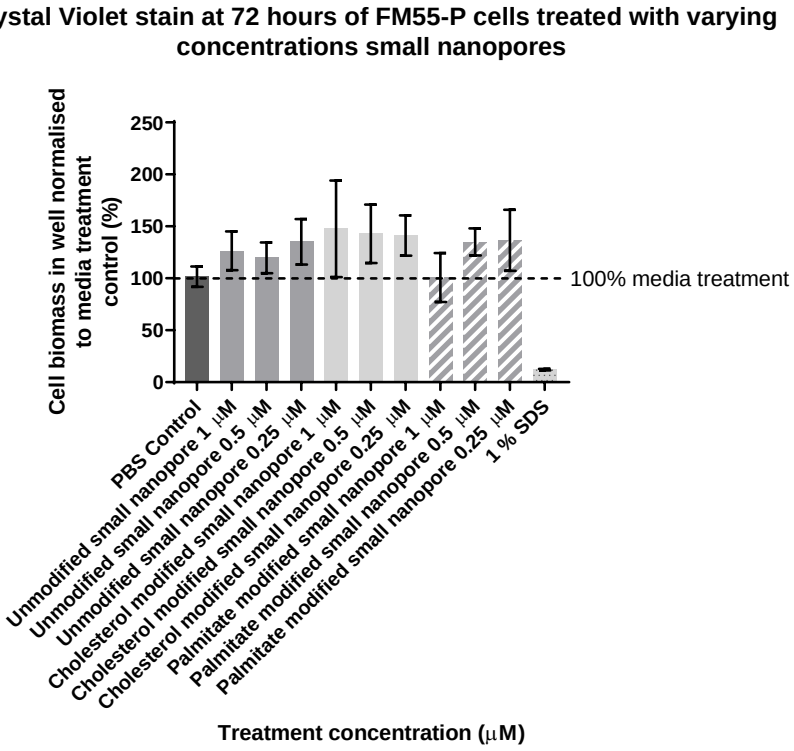

Figure 83 Graph showing crystal violet assay at 72 hours of FM55-P cells treated with varying concentration and modifications of small nanopore. N=3, mean and SD error shown. Statistically significant $p<0.05$, one-way ANOVA corrected for multiple comparisons using Tukey's method. All samples, apart from the positive control, maintained a value similar to the PBS control indicating no difference in efficacy of treatments.

4.6.2 FM55-P cells treated with varying concentrations of large nanopore

In parallel to the experiments in section 4.4.1 the same experiments were conducted with the large nanopore. Again, the FM55 – P cells were first seeded at a density of 5000 cells per well and left to adhere to the plate for 24 hours at 37 °C, 8% CO_2. Large nanopore treatments were then applied to the cells and time points of 1 hour and 24 hours were used to monitor the cell viability with alamar blue and crystal violet assays.

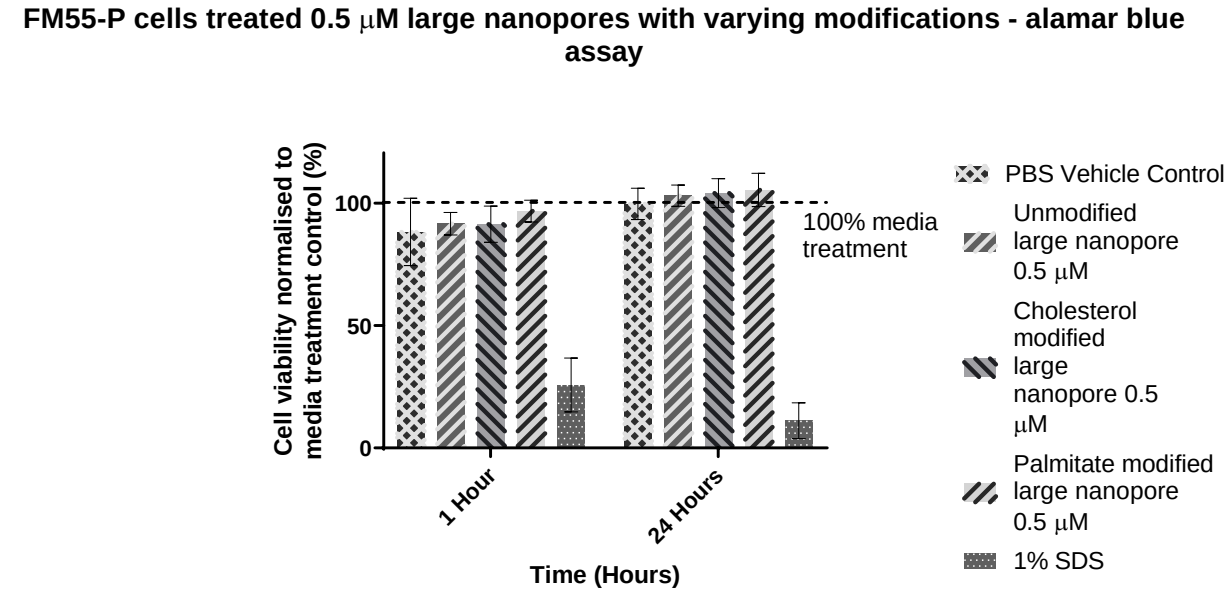

Figure 84 Graph showing alamar blue assay of FM55-P cells treated with 0.5 μM large nanopores with varying modifications. N=3, mean and SD error shown. Statistically significant $p<0.05$, two-way ANOVA corrected for multiple comparisons using Tukey's method. Only the 1% SDS positive control was seen to reduce the cell viability.

As seen with the small nanopore treatments, no effect was seen at 1 hour post treatment apart from that of the positive control which showed a 74% decrease in cell viability. This was also seen at 24 hours.

Further experiments were conducted with a wider range of concentrations and a few modifications to the protocol. Cells were cultured under 37 °C, 5% CO_2 conditions in RPMI, 10% FBS 1% P/S. Cells were left to adhere for 48 hours as opposed to 24 hours and the cells were monitored by IncuCyte and by a terminal alamar blue and crystal violet assay at 72 hours.

Upon inspection, it was noted that the cell mask on the IncuCyte did not apply correctly therefore proliferation curves could not be obtained. However, cell morphology could still be monitored. The cell viability assay, **Figure 85** showed that the treatment groups all showed very similar activity to the PBS vehicle control. This was supported by the crystal violet assay shown in **Figure 86**.

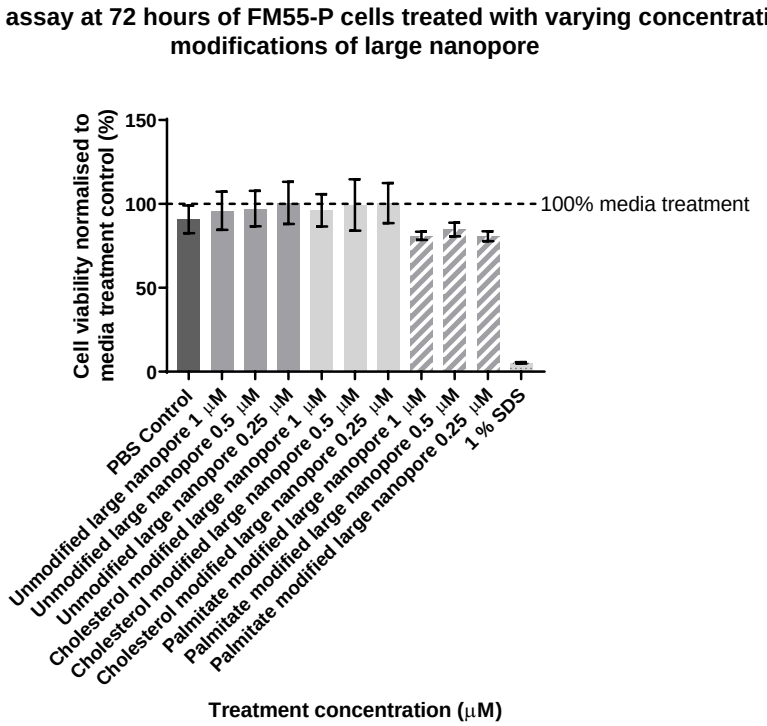

Figure 85 Graph showing alamar blue assay at 72 hours of FM55-P cells treated with varying concentration and modifications of large nanopore. N=3, mean and SD error shown. Statistically significant $p<0.05$, one-way ANOVA corrected for multiple comparisons using Tukey's method. No significant decreases in cell viability were observed apart from the positive control treatment of 1% SDS.

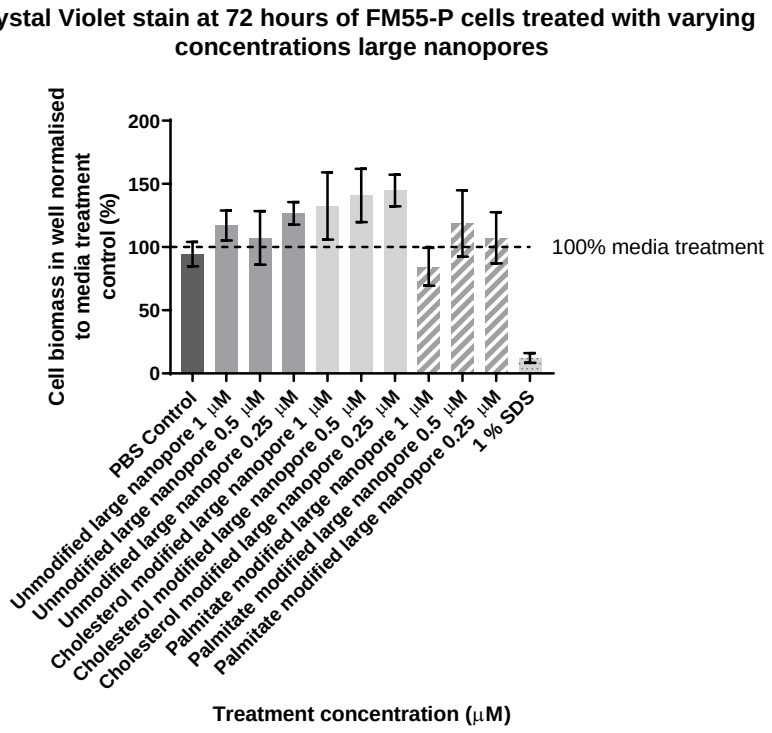

Figure 86 Graph showing crystal violet assay at 72 hours of FM55-P cells treated with varying concentration and modifications of large nanopore. N=3, mean and SD error shown. Statistically significant $p<0.05$, one-way ANOVA corrected for multiple comparisons using Tukey's method. No significant decreases in cell biomass in the well were observed apart from the positive control treatment of 1% SDS.

4.6.3 FM55-P conclusion

From all this data it can be deduced that, at the conditions used in these experiments, both the small and large nanopores had no effect on cell viability. This was seen with both unmodified nanopores and the hydrophobically modified nanopores (cholesterol and palmitate modified).

4.7 Phototoxicity studies of porphyrin modified small and large nanopores in FM55-P cells

An LED light device that delivered 12 watts of light at a wavelength of 630 - 660 nm was used for treatments. These wavelengths were used to target the Q -bands in the tetraphenyl porphyrin modified DNA rather than the soret band due to the evidence that has shown that the melanin produced by melanoma can compete for the absorption of light at lower wavelengths[68]. Eumelanin and pheomelanin, two compounds that are part of the melanin family and readily expressed by melanocytes, are shown to have lower absorption in this region[133].

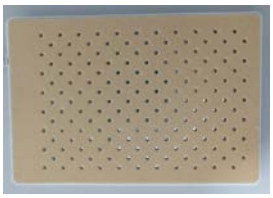

Figure 87 LED Light device that was used for light treatments. The relevant 96- well plate was removed from the IncuCyte and placed in the laminar flow hood. The device was placed on top of the lid of the 96 well plate and wrapped in foil to avoid light leakage before being turned on to the highest setting.

FM55-P cells were first plated and left to culture for 48 hours in 5% CO_2 at 37 °C. Two plates were set up so that one group of cells could be irradiated with light and the other kept in darkness. This showed the dark toxicity of the porphyrin modified nanopore and acted as a control for the light experiments. Experiments were conducted with technical triplicates and three biological replicates.

The light treatments were applied for 5 minutes at 1, 2 and 3 hours on day 0 after initial treatment and the cycle repeated on day 1 and day 2 before assays were conducted. Cell proliferation and viability were monitored by IncuCyte, alamar blue assay and crystal violet assay.

This was conducted with both the small and large nanopore and multiple controls were used. 100% media was used as treatment of 'untreated cells' to show the effect of the vehicle control on the cells. A PBS vehicle control was used as the nanopore was in a 1 x PBS solution and at the highest concentrations this accounted for 50% of the treatment solution. Single strands of both unmodified and porphyrin DNA were used to ensure that any effect from the porphyrin nanopores could be accredited to the nanopore as well as the porphyrin. This was done at a 2x concentration of the nanopore treatments as the nanopores were made with a 2x excess of modified strands. A positive control of 1% SDS was used to ensure that the cells could be killed and that the assays were working.

4.7.1 FM55-P cells treated with porphyrin modified small nanopore

Experiments were done in parallel with two different seeding densities of cells, 5000 and 20,000 cells per well. First discussed are the cells seeded at 5000 cells per well.

The proliferation curves generated by the IncuCyte shown are unclear due to the heavy overlap of the standard deviation error bars. This is common in IncuCyte proliferation data where low starting confluences are used. Therefore, although all were conducted within the same experiment, the proliferation curves have been spilt into concentrations with their control experiments for clarity.

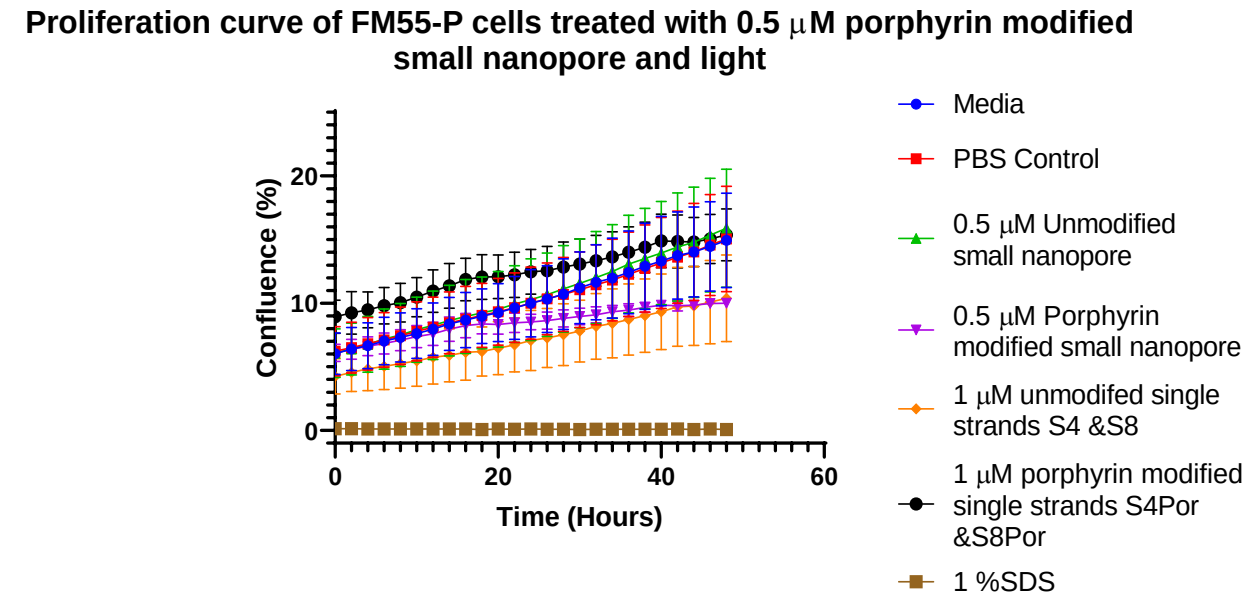

Figure 88 Proliferation curves of FM55-P cells treated with 0.5 μM porphyrin modified small nanopore and light. The treatment curves and SD errors heavily overlap yet differences in proliferation trajectory can be seen between the 0.5 μM porphyrin modified small nanopore and the PBS control indicating that the porphyrin modified small nanopore negatively affected FM55—P proliferation when combined with light. Individual traces can be found in the appendix.

The proliferation curves of the cells treated with the highest concentration used, 0.5 μM porphyrin nanopore can be seen in **Figure 88**. Although all points and their SD errors overlap, a trend can be seen to emerge as the trajectory of the proliferation curves differ. The treatments containing porphyrin have a less steep gradient than that seen by treatments without it, indicating that the cells were not proliferating at the same rate. This was different to the curves shown in the dark control experiment, **Figure 89**, at the same concentrations where all the treatments show very similar proliferation curves. This indicated no dark toxicity.

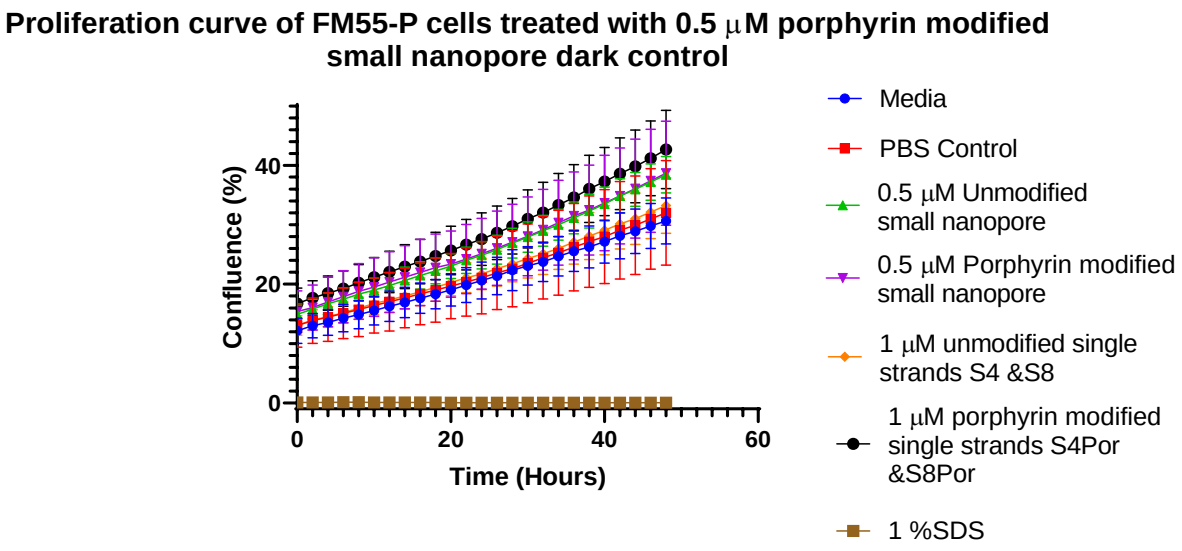

Figure 89 Proliferation curve of FM55-P cells treated with 0.5 μM porphyrin modified small nanopore dark control. All treatment groups were seen to follow a similar proliferation trajectory. This indicated that the light was needed for the porphyrin to disrupt FM55-P proliferation. Individual traces can be found in the appendix.

This was also seen at lower concentrations of 0.25 μM shown in **Figure 90** with light where the porphyrin modified nanopore showed a clear plateau in proliferation. However, the porphyrin modified single strands treated cells behaved similarly to that of their unmodified counterparts indicating that at this concentration, the single strands are not active. All treatments behaved similarly to each other in the dark control experiments, **Figure 91**, indicating no dark toxicity of treatments.

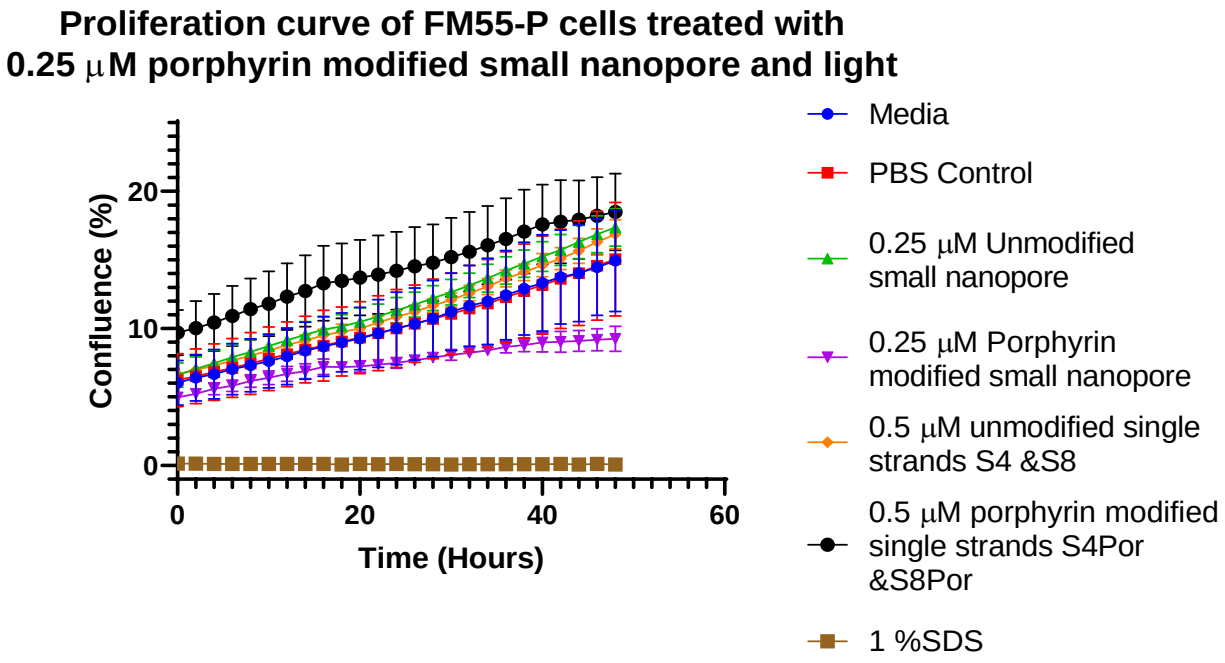

Figure 90 Proliferation curve of FM55-P cells treated with 0.25 μM porphyrin modifid small nanopore and light. The proliferaton of cells treated with 0.25 μM porphyrin modified small nanopore was seen to plateau 9% confluence from 40 hours compard to the continually increasing proliferation seen in other treatments groups. Individual traces can be found in the appendix.

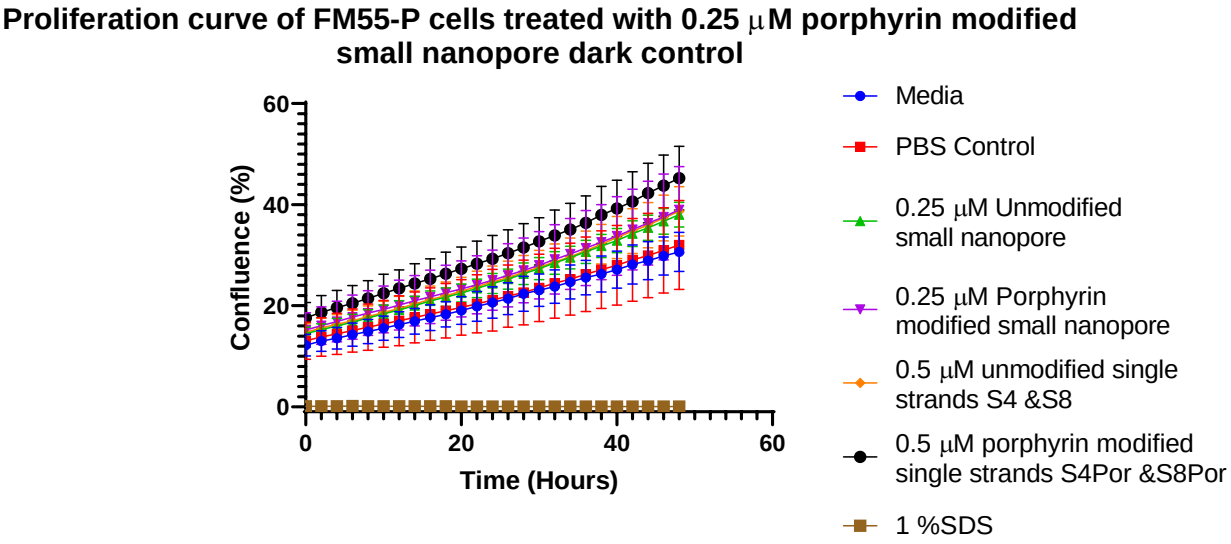

Figure 91 Proliferation curve of FM55-P cells treated with 0.25 μM porphyrin modified small nanopore dark control. Treatments all followed a similar proliferation curve indicating that light in combination with porphyrin modified nanopore was needed to negatively effect proliferation at 0.25 μM. Individual traces can be found in the appendix.

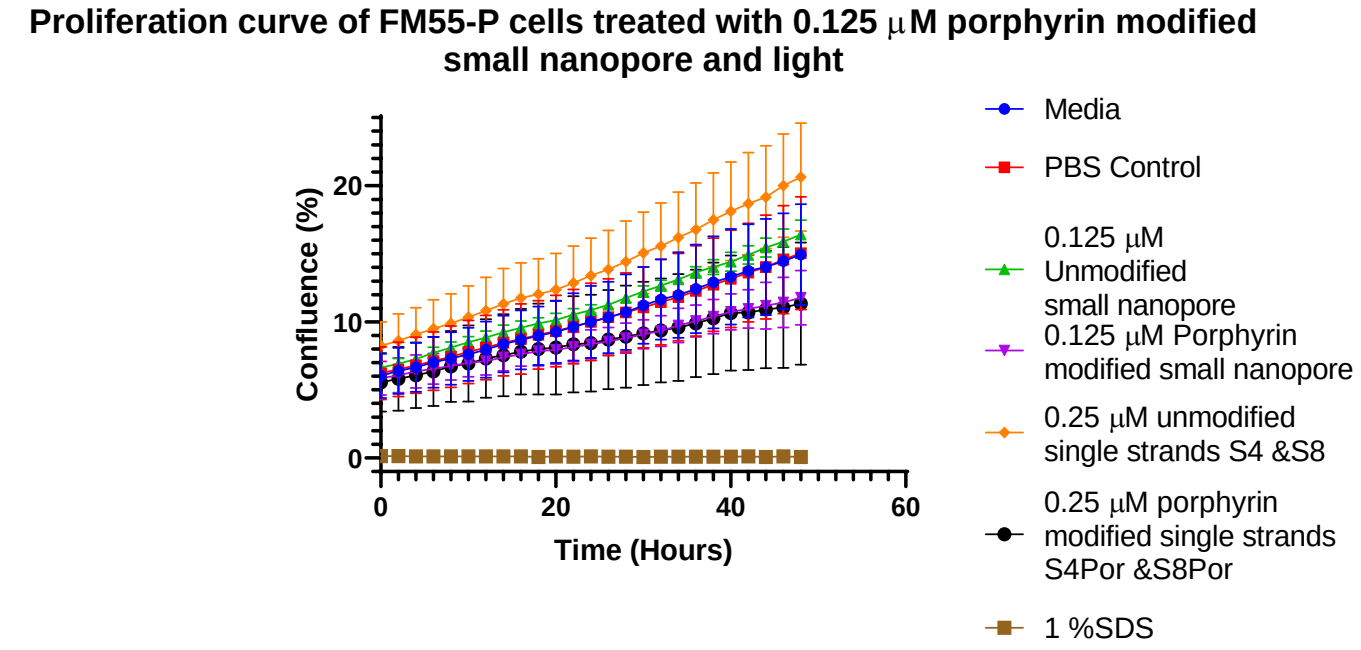

Figure 92 Proliferation curve FM55-P cells treated with 0.125 μM porphyrin modified small nanopore and light. All treatments followed a similar proliferation trajectory indicating that at 0.125 μM, the porphyrin modified small nanopore combined with light, had no negative effect on FM55-P proliferation. Individual traces can be found in the appendix.

At the lowest concentrations tested, the graph becomes even more congested and the main difference between the light and dark experiments is the spread of the curves. It can be seen that the range of the proliferation curves in the light experiments, **Figure 92**, is much wider than that seen in the dark experiments, **Figure 93**, indicating that there may have been some activity in the light treatments but the trend was not clear.

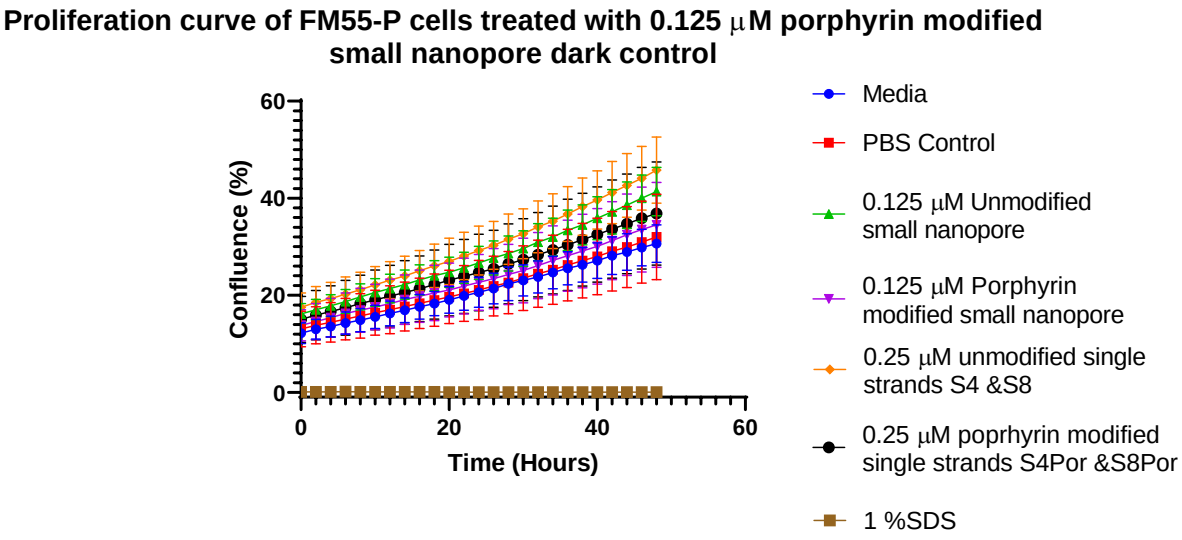

Figure 93 Proliferation curve FM55-P cells treated with 0.125 μM porphyrin modified small nanopore dark control. All treatments followed a similar proliferation trajectory indicating that at 0.125 μM, the porphyrin modified small nanopore in the dark, had no negative effect on FM55-P proliferation. Individual traces can be found in the appendix.

Therefore, the start and end confluences were plotted of all concentrations which, as 100% confluence was not reached on all samples, gave a useful view of the change in proliferation. This is shown in **Figure 94**. This shows the changes in proliferation more clearly. Both the cells treated with 100% media and PBS vehicle control showed very similar changes in confluence of 9%. This was similar to changes seen with the unmodified nanopores and unmodified single strands which all showed changes in confluence ranging between 10 and 12%. This indicated that the unmodified nanopores had no effect on the cells. Conversely the porphyrin modified small nanopore at 0.5 μM showed a significant decrease in change in proliferation compared to the PBS control. A small average change in confluence of 4% was observed in this treatment group. However, this was by no means conclusive. Therefore the assays must be also be analysed.

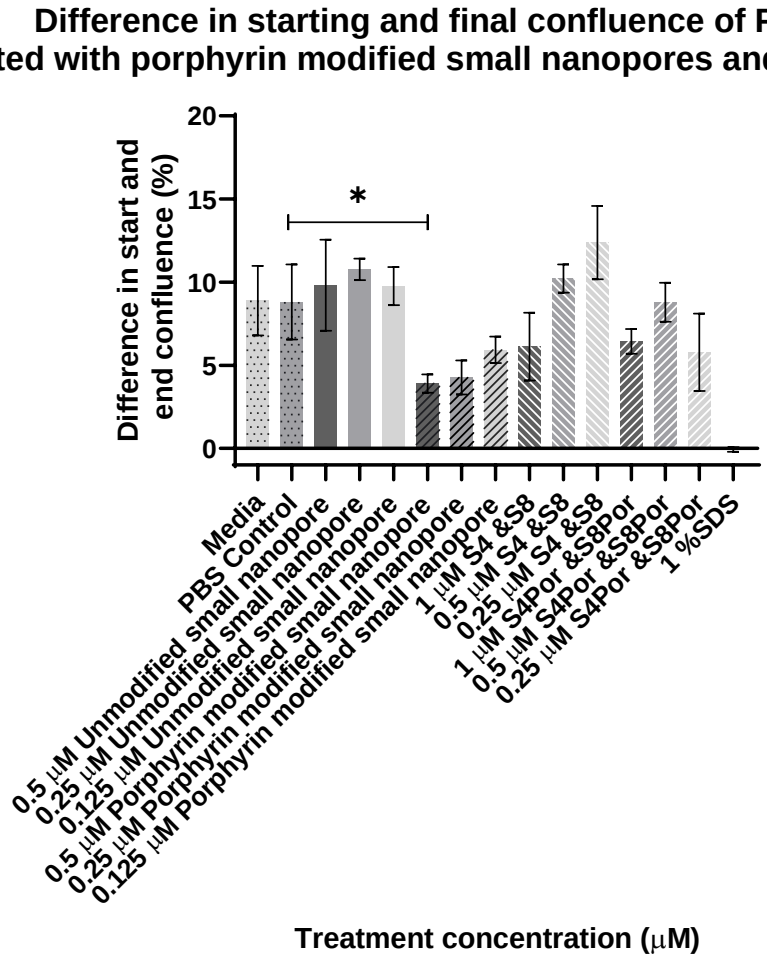

Figure 94 Graph showing the difference in starting and end confluence of FM55-P cells treated with prophyrin modified small nanopores and treated with light. N=3, mean and SD error shown, statistically significant $p<0.05$, one way ANOVA corrected for multiple comparisons using Tukey's method. A statistically significant difference between between the PBS control and 0.5 μM porphyrin modified small nanopore was observed.

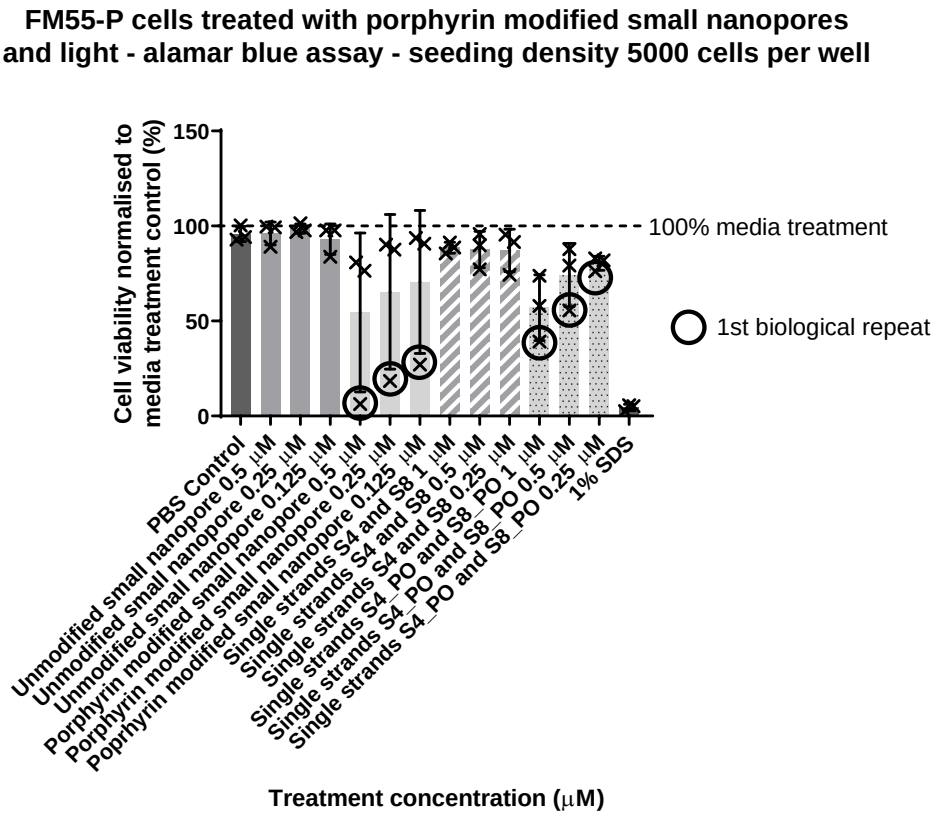

Figure 95 FM55-P cells treated with porphyrin modified nanopore and light. Circled values shown are results from 1st biological repeat. N=3, mean and SD error shown, statistically significant $p<0.05$, one way ANOVA corrected for multiple comparisons using Tukey's method. All biological repeat data points are shown. The first biological repeat was shown to produce a much bigger negative effect on poliferation in the porphyrin treatments.

The results for the alamar blue assay can be seen in **Figure 95**. Averages of technical replicates were taken as the result for one biological repeat. This was then used to generate an overall average for the three biological replicates and the standard deviation error for the experiments. Measurements were also normalised to cells treated with 100% media of each biological repeat.

The first thing that can be noted in this data is the large error seen in the porphyrin modified small nanopore treatments. Therefore, all data points were shown on this graph. This could have been due to a couple of reasons. This may have been an anomaly of the reaction however no difference to the experimental method was used and there was little variation in treatments that did not contain porphyrin in all biological repeats. The more likely possibility was the porphyrin in the DNA may have degraded. These experiments were done over the course of ~14 days therefore the degradation of the DNA was not thought to be an issue. However, the results indicate it may have been a factor. Ideally this experiment would be repeated with new porphyrin DNA where the DNA

was aliquoted after initial dilution. However due to material and time constraints this was not possible.

The controls used in the experiment must also be discussed. The PBS vehicle control had little to no effect on the cell viability with an average decrease in 4% of cell viability compared to the untreated cells. At the other end of the scale the positive control of 1% SDS showed a 96% decrease in cell viability showing that the alamar blue assay was working correctly.

Similarly to previous experiments conducted with unmodified small nanopores, at all concentrations tested, there was no effect on cell viability. This indicated that any negative effect on cell viability seen in the cells treated with porphyrin modified nanopores was due to the porphyrin modification. The single strands of unmodified DNA also showed no effect on cell viability. This indicated that the decrease in cell viability observed in the porphyrin modified single strands was due to the inclusion of the porphyrin.

It can be seen that the first biological repeat of this experiment (the data points circled) showed much more drastic results that that of the second and third repeats which show more consistent results. 0.5 µM porphyrin modified small nanopore first biological repeat showed a decrease in cell viability of 94% compared to untreated cells. For the second and third biological repeats they averaged a decrease of 21% cell viability. Although very different they both still showed a decrease which would indicate that the 0.5 µM porphyrin modified small nanopore treatment when combined with light caused a detriment to cell viability.

The advantage of using the IncuCyte was that the cell morphology could be observed throughout the experiments. Table 4 and Table 5 show an example of the images taken from treatment groups, PBS control, porphyrin modified small nanopore and porphyrin single strands. Zoomed in images are shown on the right-hand side of the table for ease of viewing. Table 4 shows the first biological repeat whereas Table 5 shows the third biological repeat to help ascertain the large differences in in cell viability measured in **Figure 95**.

Table 4 Images taken by the IncuCyte of FM55-P cells seeded at 5000 cells per well at 48 hours after various treatments and light – first biological repeat (left) standard image (right) zoomed image. In porphyrin treated samples the cell morphology has changed to a rounded shape indicating cell death.

PBS Control
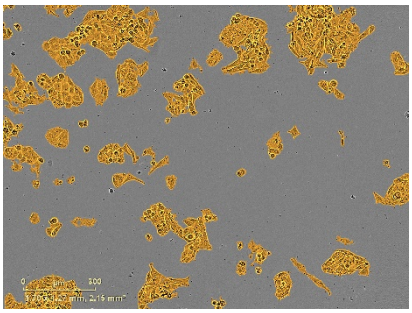 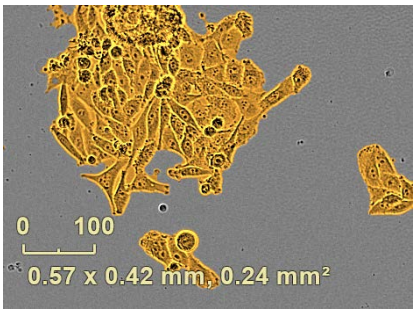
Porphyrin modified small nanopore 0.5 µM
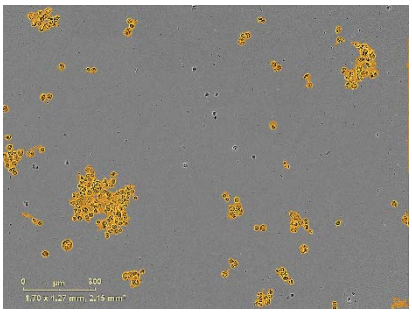 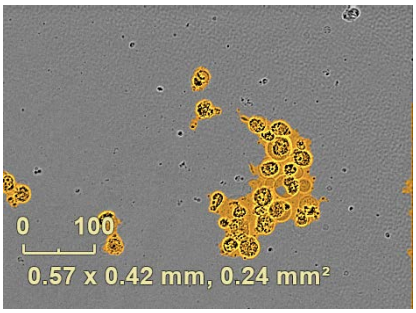
Porphyrin single strands
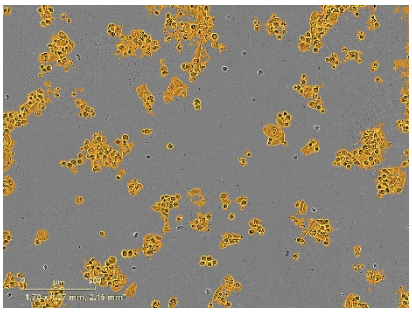 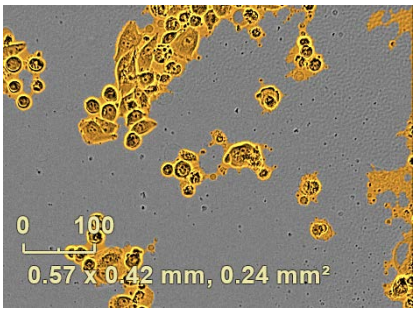

Primarily looking at the first biological repeat it can be seen that the cell morphology differs greatly between the PBS control and both treatment groups. Where the cells are flat and irregular shapes when treated with the PBS control, they are all small and rounded when treated with the porphyrin modified small nanopore and light. This indicated that the cells had dissociated from the surface which in turn indicated cell death. Interestingly the cells treated with the porphyrin modified single strands alone, showed a mixture of cell morphology indicating some live and some dead cells. This is in line with the cell viability assay which showed some activity yet not as much as the nanopore

system. This also suggested that the nanopore structure increased the efficacy of the PDT treatment.

Table 5 Images taken by the IncuCyte of FM55-P cells seeded at 5000 cells per well at 48 hours after various treatments and light – Third biological repeat (left) standard image (right) zoomed image.

PBS Control	
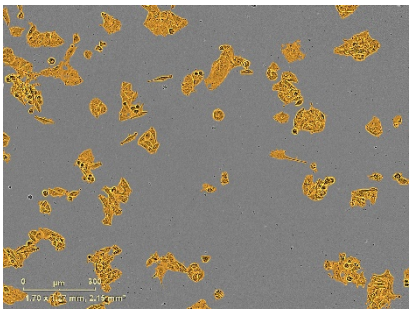	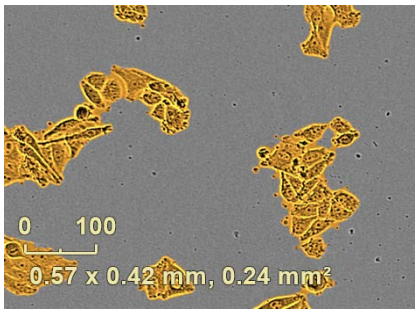
Porphyrin modified small nanopore 0.5 µM	
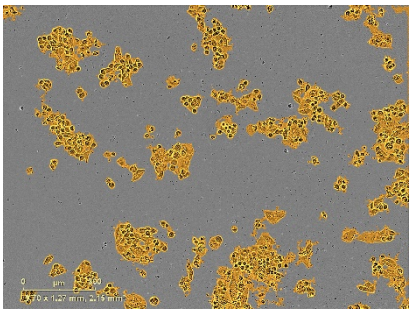	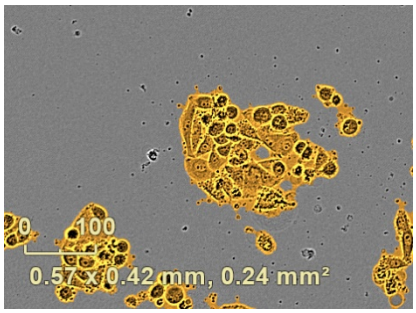
Porphyrin single strands 1 µM	
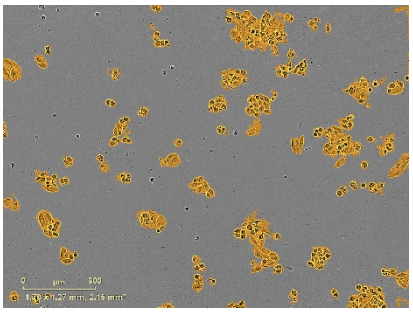	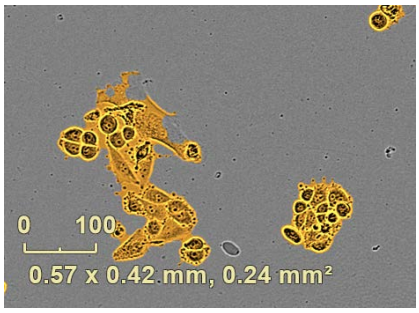

Now looking at the third biological repeat images, Table 5, it can be seen that again the PBS control treated cells were of healthy morphology. Whereas, both the treatment groups of porphyrin modified nanopore and porphyrin single strands showed cells of mixed morphology. Again, this was in agreeance with the cell viability data where the later experiments showed some activity yet less than the first biological repeat.

A trend can be seen that as the concentration of the porphyrin nanopore treatments decreased, so did the negative effect on cell viability. This was also observed to a lesser degree in the samples treated with the porphyrin modified single strands. This indicated that the concentration of porphyrin influenced cell viability.

Comparing the light experiments to the dark experiments was key to understand if the predicted PDT occurred.

Applying the previous hypothesis that a hydrophobically modified nanopore would have a negative effect on the cell viability and proliferation, even the cells treated with porphyrin modified nanopore in the dark should have a negative effect on cell viability. However, due to the dual therapy of the PDT in the light treated cells, less of a negative effect was expected to be seen in the cells treated in the dark.

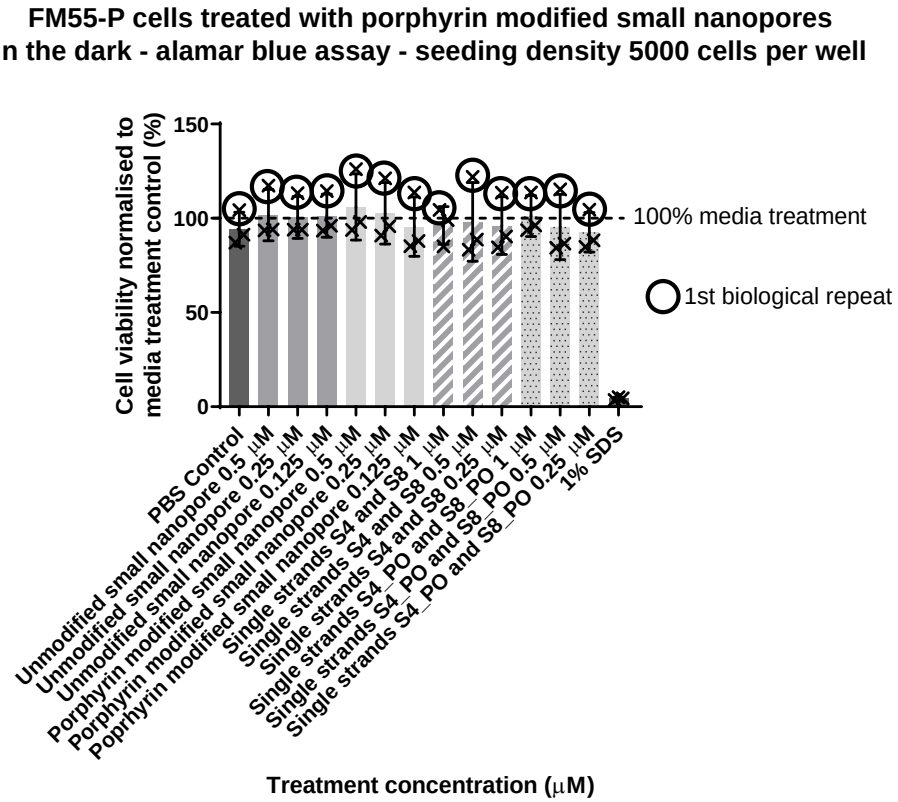

Figure 96 FM55-P cells treated with porphyrin modified nanopore in the dark. Circled values shown are results from 1st biological repeat. N=3, mean and SD error shown, statistically significant $p<0.05$, one-way ANOVA corrected for multiple comparisons using Tukey's method. All treatments were shown to have no negative effect on cell viability which indicated that treatments including porphyrin had no dark toxicity.

As previously discussed above, the proliferation curve of FM55-P cells treated with porphyrin modified small nanopores showed little variation in proliferation between all the treatment groups

apart from the positive 1% SDS control. This was supported by the alamar blue data in **Figure 96** where it can clearly be seen in a single glance that the cell viability was not affected by any of the treatment groups apart from the positive control. This indicated that the porphyrin modified small nanopore had no dark toxicity.

This was analogous to the experiments in Chapter 4 which showed that the cholesterol and palmitate modified small nanopores had no negative effect on cell viability or proliferation of FM55-P cells. This also indicated that the light treatment did effect cell viability and proliferation.

In parallel to the above, the experiment was repeated with a higher confluence of cells where 20,000 cells were initially seeded. It was hypothesised that the higher seeding density of cells would not be affected as much as the lower seeding densities.

Unfortunately, due to space and time constraints in the IncuCyte only the 2nd and 3rd biological repeats were recorded.

Similarly to the lower seeding density experiment above, the first biological repeat showed higher activity than any of the other repeats. This meant that there was a larger spread in the data making it difficult to analyse. This also supported the above theory that the porphyrin DNA degraded over time.

If only looking at the first biological repeat, a clear trend relating concentration of porphyrin to activity can be observed. However, little difference between the nanopore and single strands was observed. Any activity seen was to a lesser degree than that seen in the first biological repeat in the lower seeding density experiment. This was expected as the ratio of nanopore to cell was decreased.

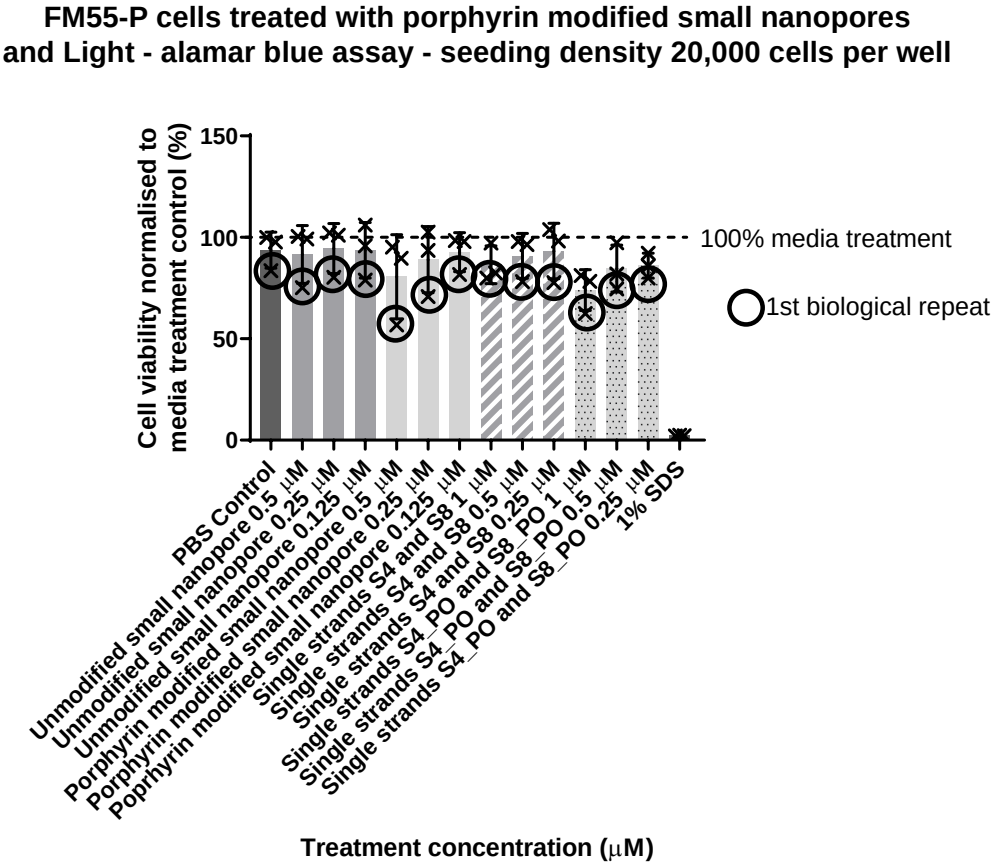

Figure 97 Alamar blue assay data of FM55-P cells treated with porphyrin modified small nanopores and light. Seeding density 20,000 cells per well. N=3, SD error shown, statistically significant $p<0.05$, one-way ANOVA corrected for multiple comparisons using Tukey's method. Although the 1st biological repeat treatments were shown to be more active, there was no significant change in cell viability between treatment groups.

The dark control in these experiments shown in **Figure 98** showed no activity throughout the treatment groups apart from the positive 1% SDS control. This was in line with the dark control data in **Figure 96** which also showed no dark toxicity for the porphyrin treatments.

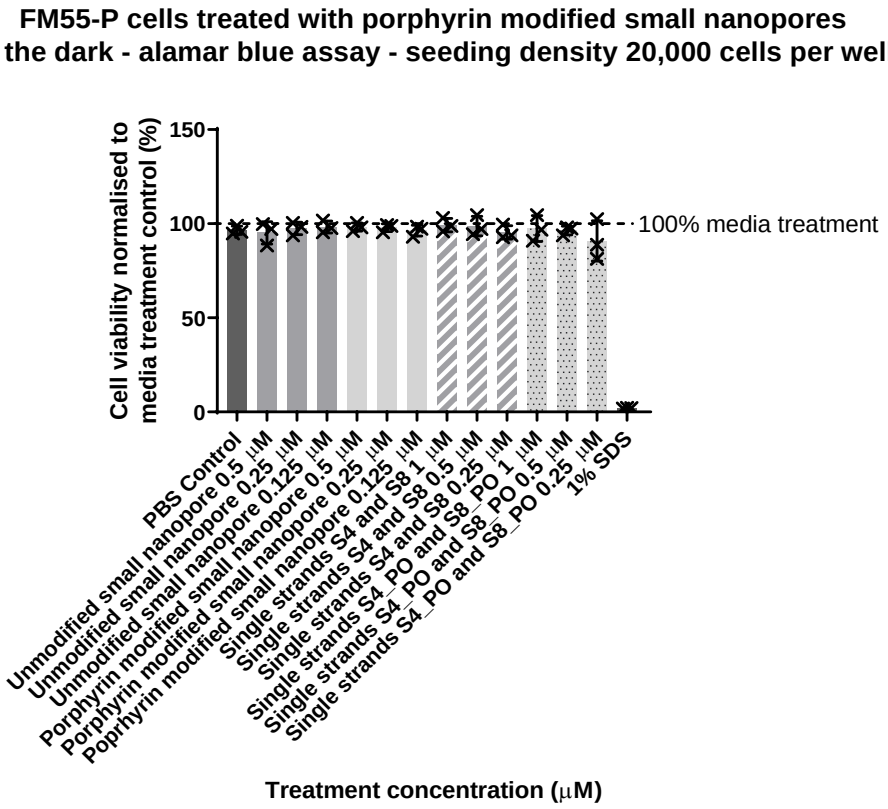

Figure 98 Alamar blue assay data of FM55-P Cells treated with porphyrin modified small nanopores in the dark. Seeding density 20,000 cells per well. N=3, SD error shown, statistically significant $p<0.05$, one way ANOVA corrected for multiple comparisons using Tukey's method. No differences in cell viability were observed between treatment groups indicating no dark toxicity.

4.7.2 FM55-P cells treated with porphyrin modified large nanopores

The large nanopore system was also applied as a treatment for the light experiments. However due to material and time limitations only the lower seeding density of 5000 cells per well was used.

Due to the crowded proliferation data not being clear the difference in starting and end confluence was plotted and shown in **Figure 99**. Although it can be seen that there was a large variation in data, it does indicate that there was some porphyrin activity. Looking purely at the average change in confluence, a 7% decrease in change in proliferation can be seen between the PBS control and cells treated with 0.5 µM porphyrin modified nanopore. This effect was further confirmed when observing the cell viability assay. Although not statistically significant, a decrease of 56% in average cell viability was noted between the PBS control and 0.5 µM porphyrin modified nanopore treated cells. This effect was also noted in the singular strands of porphyrin modified DNA in **Figure 99** where the change in confluence was between 5 and 6% at all concentrations.

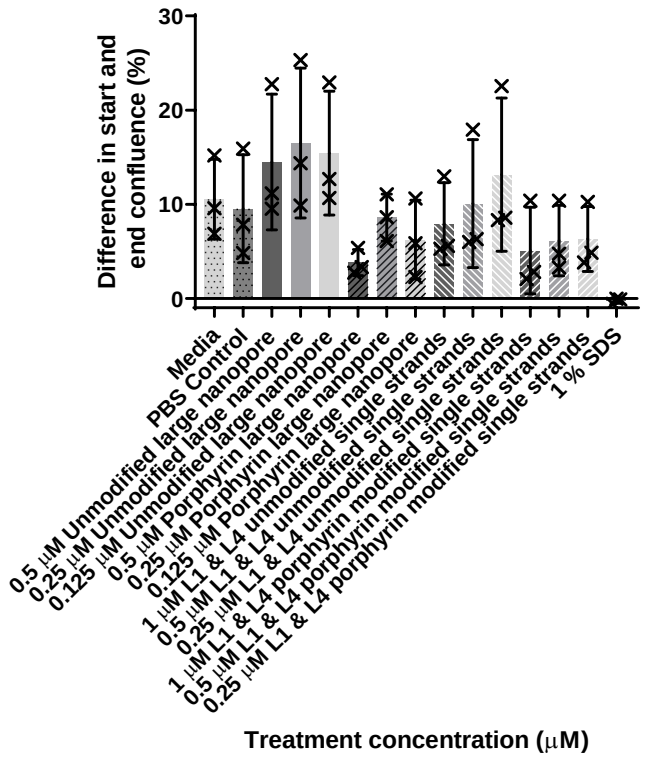

Figure 99 Graph showing the difference in starting and final confluence of FM55-P cells plotted using data gathered from the IncuCyte. N=3 SD error shown, statistically significant $p<0.05$, one-way ANOVA corrected for multiple comparisons using Tukey's method. No significant differences were seen I the data due to large SD errors.

This was supported by the cell viability data shown in **Figure 100** which showed decreased cell viability in treatments containing porphyrin when also treated with light. Again, similar to the treatments with the small nanopore, the first biological repeat was most potent. As previously described this could be due to porphyrin DNA degradation. However, this was to a smaller degree than seen with the small nanopore.

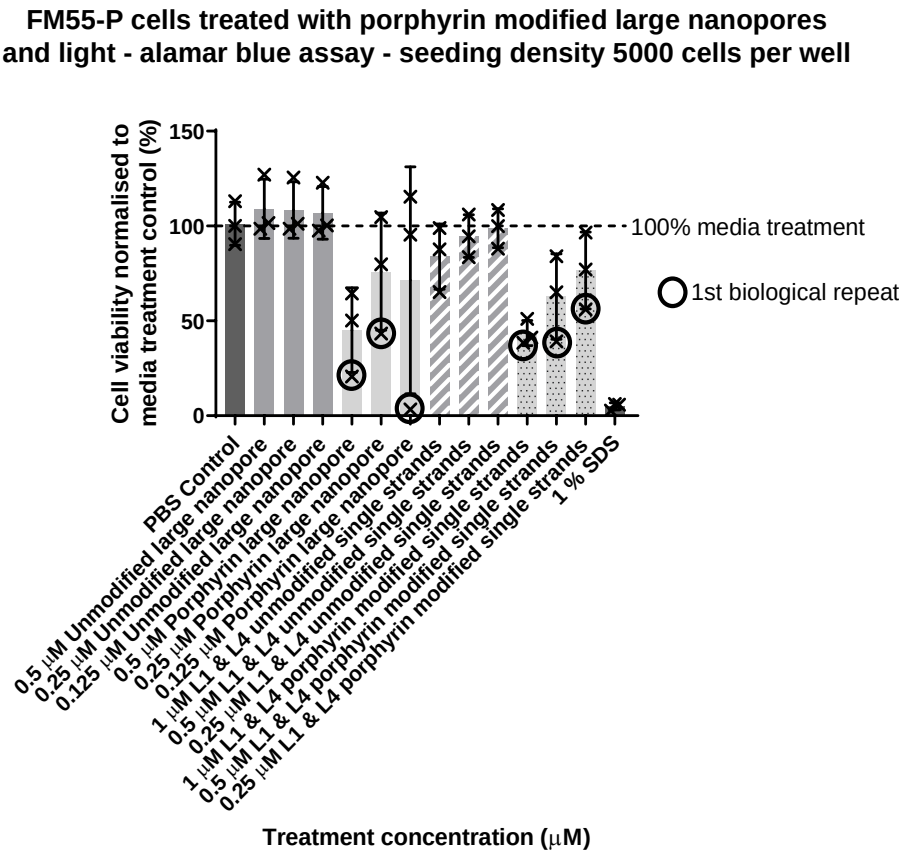

Figure 100 Graph showing cell viability of FM55-P cells with porphyrin modified large nanopores and light. N=3 mean and SD error shown. Statistically significant $p<0.05$, one way ANOVA corrected for multiple comparisons using Tukey's method. The first biological treatments including porphyrin DNA, marked by the circled (x), were shown to be more active than the second and third repeats. Little difference was observed between the activity of the porphyrin modified nanopores and the single strands of DNA modified with porphyrin.

Looking at the average values of cell viability it can be seen that there was a 56% decrease in average cell viability between the PBS control and the porphyrin modified large nanopore at 0.5 μM concentration. This was seen to decrease as the concentration of porphyrin modified large nanopore was decreased indicating that cytotoxicity was related to concentration. However, this was also observed in the single strands of porphyrin DNA which, at 1 μM, showed a decrease of 57% compared to the PBS control. This indicated that the full nanopore structure was not needed for the cytotoxic effect.

Both the data generated from the IncuCyte and the cell viability assay indicated that the porphyrin modified large nanopore had no dark toxicity. **Figure 101** showed the difference in start and end confluence of the experiment. This enabled the comparison of the proliferation between treatment groups. The vehicle control showed little difference in change in confluence compared to the cells

treated with 100% media. Therefore, if the values remained roughly the same as the vehicle control then it would indicate that the cell proliferation was not affected by the treatment. This is the case in **Figure 101**. Similarly, in the alamar blue assay (shown in Figure 102), little difference in cell viability between treatments was observed. This all confirmed the lack of dark toxicity of the porphyrin modified large nanopore.

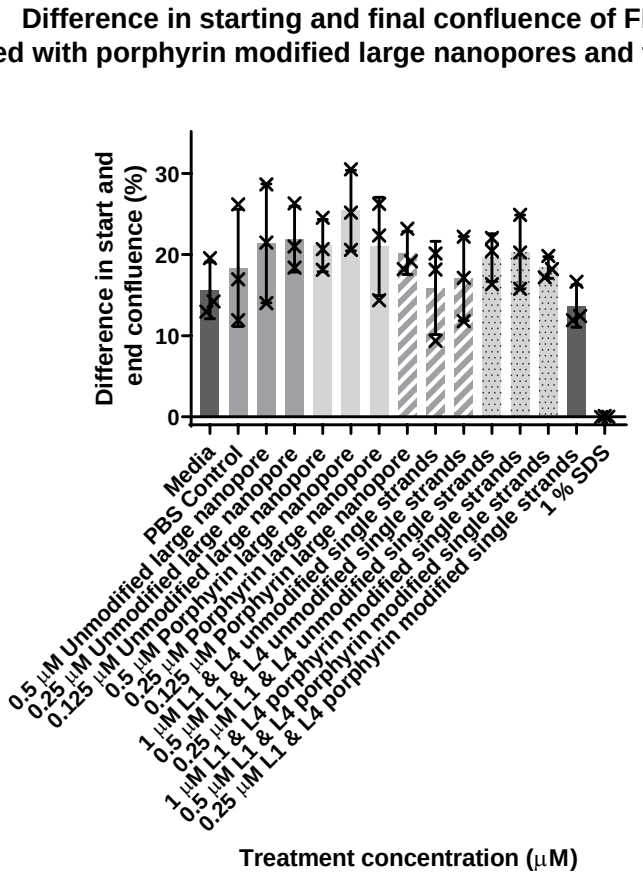

Figure 101 Graph showing difference in starting and final confluence of FM55-P cells threated with porphyrin modified large nanopore treated in the dark. N=3, mean and SD error shown. statistically significant $p<0.05$, one way ANOVA corrected for multiple comparisons using Tukey's method. No significant differences were seen between the the treatments.

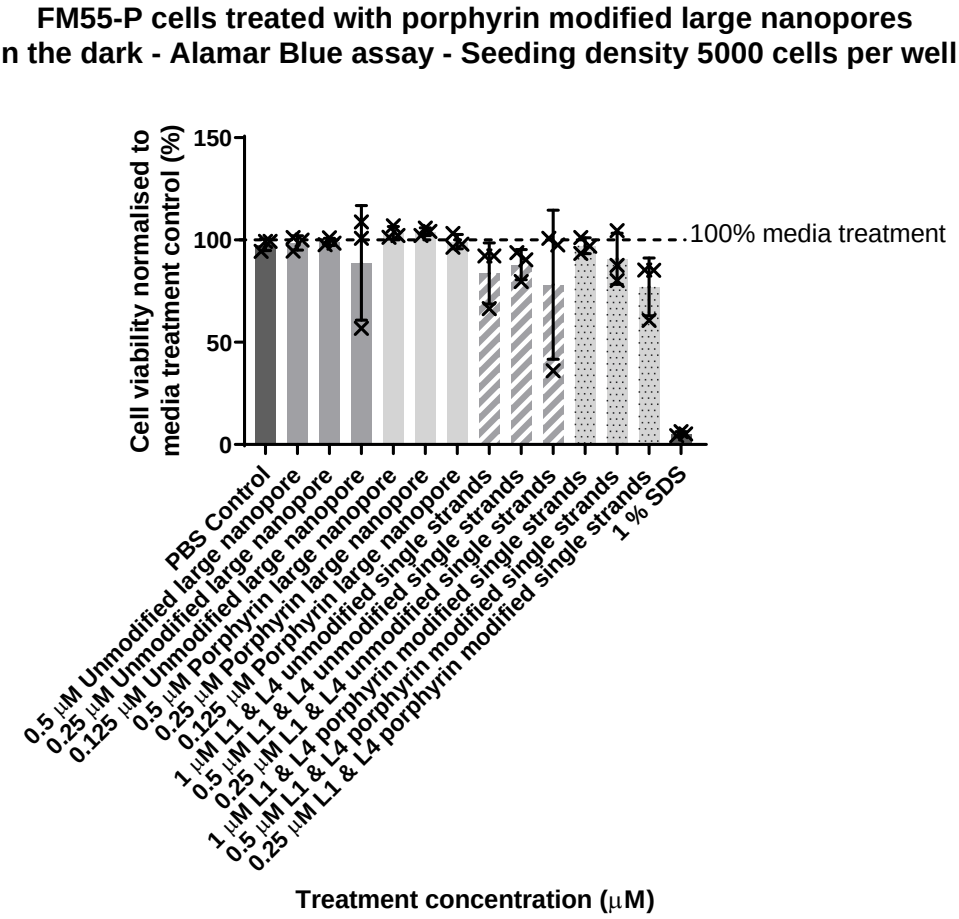

Figure 102 Graph showing FM55-P cells treated with porphyrin modified large nanopores in the dark. N=3, mean and SD error shown. statistically significant $p<0.05$, one way ANOVA corrected for multiple comparisons using Tukey's method. No significant differences were seen between the the treatments.

4.7.3 Phototoxicity study conclusion

The stability of the porphyrin DNA was greatly underestimated and this has affected the results of this experiment greatly. The start of this experiment showed great promise as the porphyrin nanopore was seen to be highly toxic to the FM55-P cells in the first biological repeat with light and both the large and small nanopore. However, the second and third biological repeats showed a decrease in activity in all experiments. This indicated that the porphyrin DNA had degraded over the short period of time that the experiments took place. Therefore, it would be highly recommended that these experiments be repeated with samples that are aliquoted and dried straight after synthesis.

The main hypothesis of this project was that a hydrophobic modification to the nanopores would cause cell toxicity. Due to the additional PDT effect seen in the light experiments the best results to look at to test this hypothesis are those in the dark.

No dark toxicity was observed for either the small or large porphyrin modified nanopore in FM55-P cells. This did not support the hypothesis and was analogous to the results seen with the cholesterol and palmitate modified small and large nanopores in FM55-P cells.

Chapter 5 Discussion

This discussion is split into two main sections: the chemical synthesis of the porphyrin modified DNA that took place at the University of Southampton, and the cell testing that took place in Singapore.

5.1 DNA porphyrin synthesis

The porphyrin DNA synthesis was a limiting step in this project. The synthesis of the monosubstituted porphyrin is well known to be a low yielding reaction and decreases further upon attachment to DNA. Due to the time limiting nature of this project moving between Southampton and Singapore it was of upmost importance that this step was optimised to produce the large quantities of DNA needed for the cell experiments.

The standard practise in the Stulz group for making porphyrin DNA has been to conjugate the porphyrin to a nucleobase (through a Sonogashira reaction) followed by forming a phosphoramidite. This has the advantage of making the modification anywhere on the strand, however the cost of this is a low yield. This is due to two reasons. Firstly, the phosphoramidite is sensitive to air and moisture therefore degrades quickly which decreases the yield. Secondly if the coupling reaction is unsuccessful then this stops the strand from growing any further due to the capping step which therefore results in a lower yield. Another disadvantage to this method is that the strands require extensive purification through either HPLC or PAGE. With this in mind, a plan was devised to reduce these issues.

Both small and large nanopores were designed with the modification at the 3' terminus. Therefore, two main methods of attachment were investigated, a post synthetic modification and a pre synthetic modification.

The post synthetic modification studied in this project was conducted using an amine modified DNA strand. This utilised a simple reaction regularly used in peptide science; an activated carboxylic acid forming an amide bond with an amine. Firstly, a mono substituted carboxylic acid of tetraphenyl porphyrin was synthesised. This was done using the method described in Chapter 2 where a ratio of pyrrole, benzaldehyde and methyl-p-formybenzoate (6:6:1) was mixed in chloroform, under argon with the Lewis acid borondifluoride diethyl etherate followed by oxidation with DDQ. This formed a mono substituted methyl ester of tetraphenyl porphyrin (TPP) which was then hydrolysed to the acid using a strong base. The acid was then activated with an NHS group which provides a better leaving group than the proton for the reaction with the amine.

However, the amine NHS reaction takes place in aqueous buffer between pH 7.2 and 9 to ensure that the competing hydrolysis reaction of the N-hydoxysuccinimide (NHS) ester does not occur. Due to the highly hydrophobic nature of the porphyrin, the compound was unable to dissolve in the solvent for the reaction.

Therefore, this project focussed on the pre synthetic modification of oligonucleotide synthesis. A porphyrin compound was conjugated to a nucleobase, **Figure 103**.

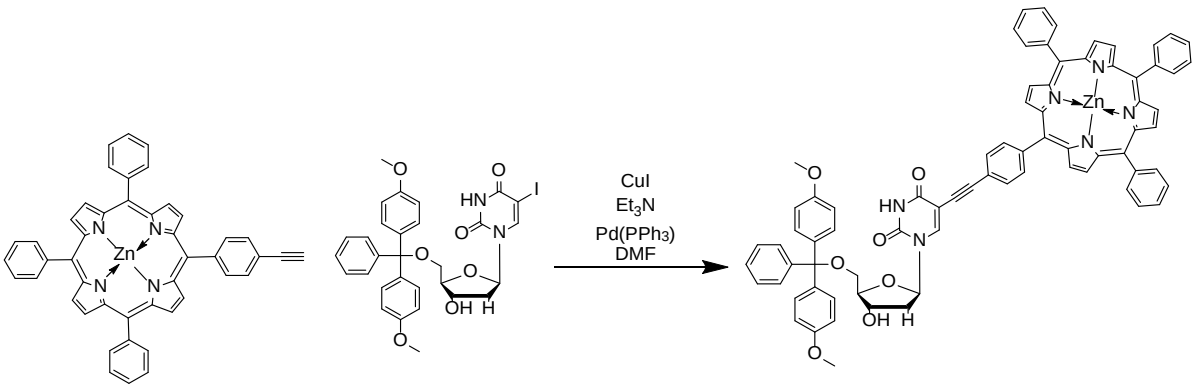

Figure 103 Sonogashira reaction between substitted porphyrin and 5' DMT-iododeoxyuridine.

Firstly, an asymmetric porphyrin was formed containing a functional group capable of crosslinking the porphyrin with the DNA. Therefore, the first stage in the synthesis was the formation of a benzaldehyde modified with a protected alkyne group which yielded 37% product. This was used in the synthesis of the porphyrin which was done using an established protocol[45].

Benzaldehyde, pyrrole and 4-(3-hydroxy-3-methylbut-1-ynyl)benzaldehyde were mixed in degassed chloroform at a specific ratio of (6:6:1) with the addition of boron trifluoride dietyletherate. The reaction was left to run for 1 hour forming the porphyrinogen structure the mechanism of which is shown in Figure 104. It was then oxidised using DDQ, Figure 105. Although this only resulted in a reaction yield of 11%, this was still a significant yield for the formation of the asymmetric porphyrin. Tetraphenyl porphyrin was also made in significant amounts as a side product in the reaction.

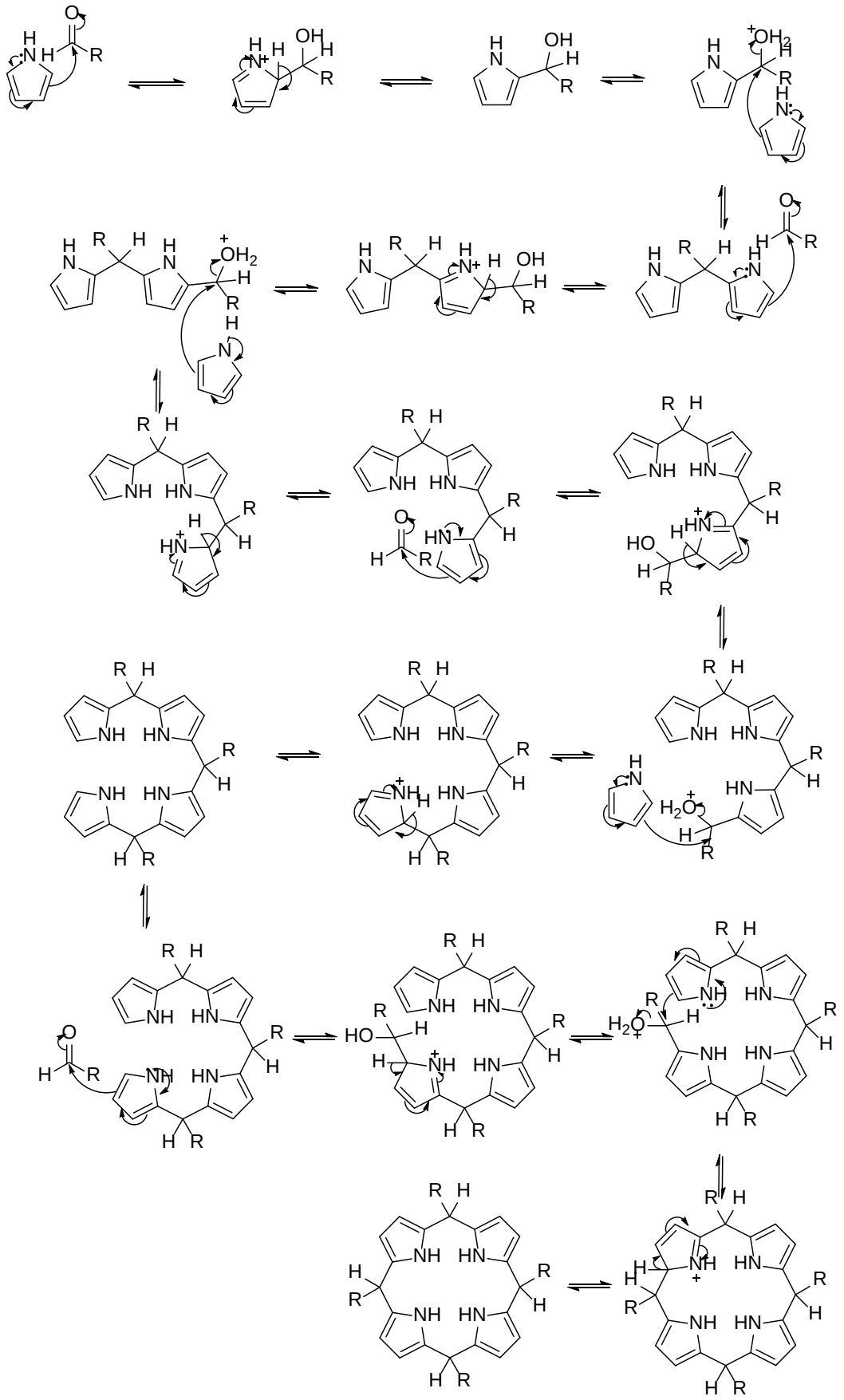

Figure 104 Porphyrinogen formation mechanism

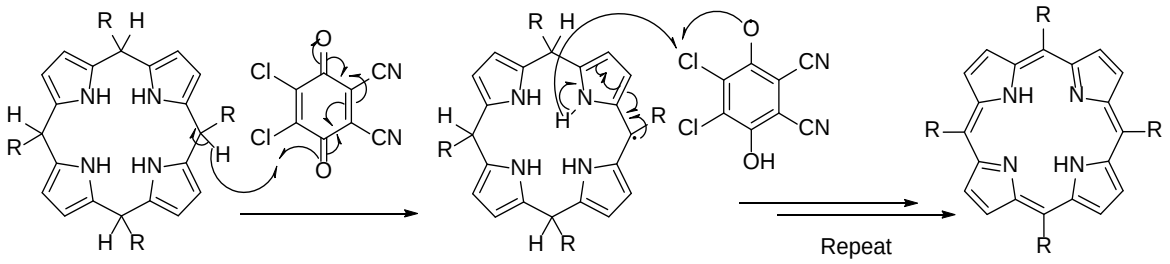

Figure 105 Oxidation of porphyrinogen with DDQ mechanism

This was then metallated using a high temperature and zinc acetate resulting in a high yield of 93%. The small amount of loss here was expected to be from the column purification of the compound. Metallation was clearly shown by the disappearance of the peak at -2.78 δ in the proton nuclear magnetic resonance (NMR) which represented the hydrogens in the porphyrin ring. The next step was the deprotection of the alkyne group through refluxing in toluene overnight.

In parallel to the porphyrin synthesis, the 5’ hydroxyl group of an iodeoxyuridine (dU) base was protected using dimethyoxy trityl chloride (DMT). This would allow it to be used in DNA synthesis in later steps. It is known that DMT reacts more readily with the 5’ primary hydroxyl group than the secondary 3’ hydroxyl group due to the bulkiness of the compound and therefore steric hindrance at the 3’ group. However, the addition at the 3’ hydroxyl can still occur, therefore, the addition of the DMT was made in small portions to ensure that only the 5’ hydroxyl group was protected. Any compound that was protected at both the 5’ and 3’ hydroxyl groups was easily removed in purification by column chromatography. Neutral conditions were used throughout the synthesis to ensure that the reaction was not reversed through acidic conditions as the DMT protecting group is labile in acidic conditions.

The two monomers, alkyne modified porphyrin and DMT-dU were then used in a Sonogashira reaction; a coupling reaction between an aryl halide and a terminal alkyne to form a carbon-carbon bond. This reaction took place under argon and used a copper and a palladium catalyst. Molecular sieves were also used in the reaction to ensure no water entered the reaction. This was to ensure undesirable reactions with the copper iodide did not occur such as a Glayserhay coupling. The purification of this reaction was problematic as the coupled and uncoupled nucleoside had very close retardation factor (RF) values therefore several columns were run slowly to purify the material. ^{1}H NMR was conducted on each of the fractions and the ratio between the nucleoside and the porphyrin was compared to determine the amount of uncoupled nucleoside in the sample. This product was used in two different methods, phosphoramidite method and resin functionalisation, to form porphyrin modified DNA.

The first methodology used converted the nucleobase-porphyrin to a phosphoramidiate,

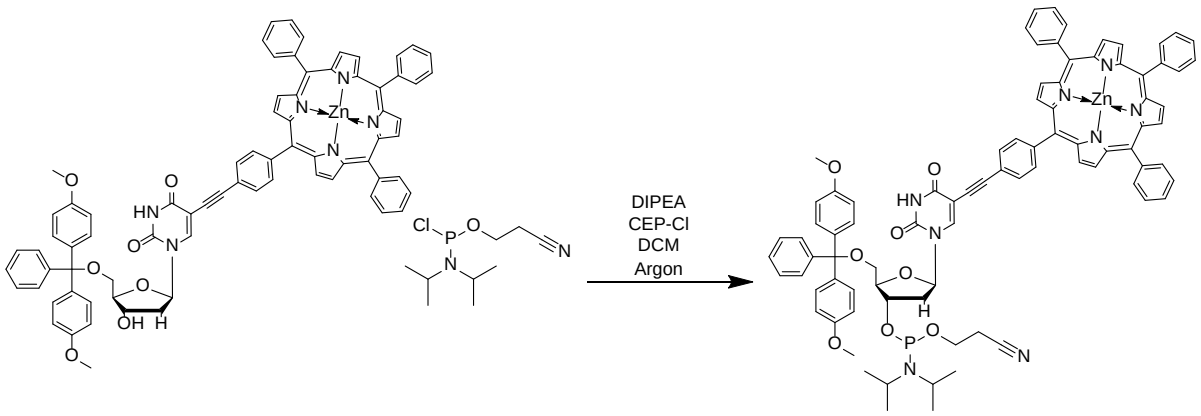

Figure 106 Phophoramidite reaction of porphyrin nucleobase.

This allowed the modification to be placed at any position in the strand which was to a great advantage. However, this method produced very low yields of modified DNA and also needed lots of timely purification.

The second method was conducted by modifying the resin of the beads used in solid phase synthesis. There are a few methods found in literature leading to the functionalisation of resin[134-136]. The protocol selected[137] was carried out by **4th year undergraduate student Andrew Peddie**.

Amino-SynBase™ CPG (1000/110) (LCAA) beads were purchased from Link technologies, which contained a free amine group. Succinic anhydride was first reacted with the amine modified beads to give a free carboxylic acid. This was then coupled with the porphyrin modified nucleoside, **Figure 107**. Loading of the beads was calculated by treating with deblock solution and measuring the trityl yield through absorbance at 505 nm. The beads were then used in standard solid phase synthesis to form 3' modified porphyrin DNA strands.

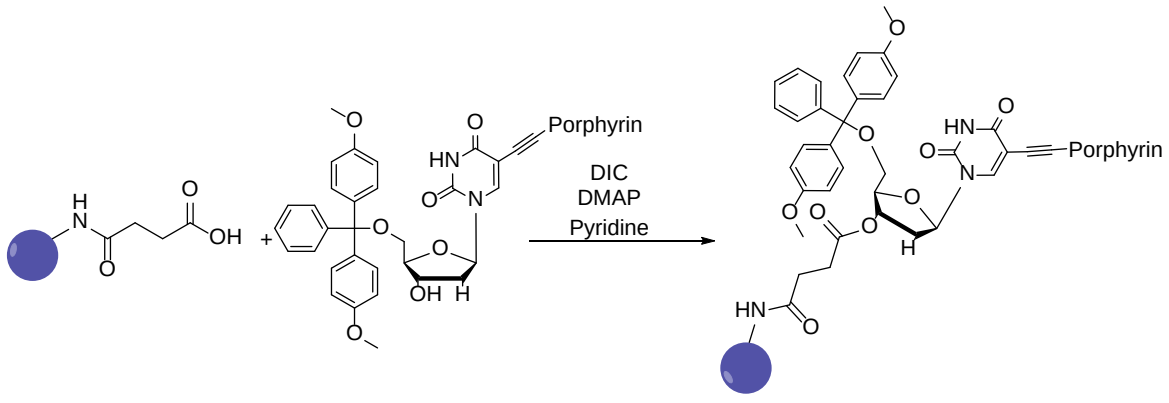

Figure 107 Attachment of porphyrin nucleobase to solid phase synthesis support.

This method led to the successful modification of DNA with porphyrin which was used in the photodynamic therapy treatments seen in section 4.7.

5.2 Cell discussion

The cell experiments conducted in this project have taken us on a journey of enlightenment and have highlighted a number of issues to address in future experiments. As with every project there were limitations that although they inhibited the results of this project, the can valuably inform future research.

Although concentration was varied in some experiments in this thesis it did have an upper limit. It was limited by the well volume and that the cells also needed some media to survive and proliferate. The maximum amount of media that can be replaced without affecting the cells is unknown. However, the inclusion of the PBS vehicle control in the experiments insured that any effects were noted. Comparing the nanopore treatments to the PBS control gave the best indication of the effect of treatments. All experiments were conducted in 96 well plates and the overall well volume was taken to be 200 µL to stop spillages (first experiments on HEK293FT used 250 µL volume however this increased handling errors). Half the well volume was used for media and half the media was substituted for PBS which the nanopores were formed in. The nanopores were formed at 2 µM concentration in a 100 µL of PBS therefore the highest concentration treatment for cells could be 1 µM. Higher nanopore formation concentrations were not attempted due to the fear of aggregation. Literature procedures[4] formed the nanopore at 1µM concentration, however used a higher excess of cholesterol modified strands (4x excess). Due to the formation concentration being double to 2 µM in this thesis the hydrophobic strands were used at a 2x excess. This mimicked the same concentration of hydrophobic strands used in literature and also preserved material and reduced the potential for aggregation. Increasing the size of the well plate would give more opportunity to treat with higher concentrations however this would need more DNA material which is a limiting factor itself when using hydrophobically modified nanopores.

The first set of experiments conducted on HEK293FT cells (section 4.2) proved that the seeding density, and therefore starting confluence, was of great importance for seeing an effect of cholesterol modified small nanopore V1. This was evident from the decrease in cell proliferation when the cells were seeded at 2000 and 1000 cells per well compared to no decrease seen when cells were seeded at 5000 cells per well.

Experiments using HEK293T cells (section 4.4), a slightly different variant to HEK293FT cells as they grow slower than their FT counterpart, were seeded at a density of 2000 cells per well. This seeding density was used opposed to 1000 cells per well as the cells were left to settle for a shorter time and therefore had less time to grow before the treatment application.

B16-F10 cells were also seeded at 2000 cells per well as they had a similar rate of growth. FM55-P cells were seeded at a higher density as they were smaller cells and therefore a higher seeding density led to a similar starting confluence as seen with the HEK293 and B16-F10 cells. The FM55-P cells also grew much slower than the other cell lines.

Seeding at a lower density encourages the cells to proliferate. At this point the cell membrane is dividing and is therefore more fluid and actively looking to collect lipids to form new membranes. It could therefore be argued that they are more likely to take up the lipid modified nanopores. As previously stated HEK293 cells are fast proliferating therefore this could be why they are affected more than the slower proliferating FM55-P cells. However, B16-F10 cells proliferate at a similar rate therefore this premise may be false.

From the experiments conducted on the three different cell groups it can be proposed that the DNA nanopores effect different cell lines differently. Activity was seen in HEK293FT as a decrease in cell viability of 56% when treated with 1 µM cholesterol modified small nanopore compared to cells treated with PBS. This is similar activity to that seen in literature with a larger nanopore in HeLa cells[2]. However no activity was seen in FM55-P or B16-F10 cells under the same conditions. This hypothesis is supported by the authors of the literature discussed in section 1.1.2.2 who used a self-complementary cholesterol modified DNA duplex for cell toxicity[50, 51]. They found that out of a range of cell lines their treatment was only active for select cell lines. What cannot be ignored is that in this thesis the cells that were susceptible to treatment, the HEK293FT and HEK293T cells, are cells that are regularly used for transfection. Cell membranes are made up of a composition of various lipids, proteins, and sugars and each of these varies depending on cell type. These variations give cell membranes different properties one of which would be their susceptibility to allow charged compounds, such as DNA, to pass through them making them suitable for transfection. It would make sense that these cells would also be most susceptible to a treatment that uses DNA to penetrate the membrane. This opens the question as to whether a wider range of cell lines should be tested with the nanopore treatments. However, there are also other things to consider, discussed below, before this could take place.

Throughout this project different methods of monitoring cells have been used, some of which have proved to be more successful than others. In the initial cell tests on HEK293FT cells with small nanopore V1 only the IncuCyte was used and in later experiments (including methylene blue and HPPH) an MTS assay was also included to gain more knowledge on cell viability. This was carried through to the secondary experiments where, depending on availability, the IncuCyte was used along with an alamar blue and crystal violet assay, when testing HEK293T, B16-F10 and FM55-P cells.

The IncuCyte is a very useful machine as it allows the cells to be monitored without disturbing them from cell culture conditions. For confluence measurements it takes a set number of photos in a well (four for a 96 well plate) and applies a specified cell mask which recognises cell material and calculates the area covered by cells in the photo. However, the camera does not image the well edge which in a larger plate does not provide so much of a problem, yet in a 96 well plate it can account for a large proportion of well area. This can especially be a problem at low seeding densities as when seeding the cells, the pressure of the pipetting can push the cells to the edges of the well. This can normally be combatted by moving the plate in a figure of eight to ensure an even spread of cells across the surface. However, this is less effective in smaller 96 well plates. Therefore, when using low seeding densities this can mean that the majority of the cells are pushed to the well edge. This was especially evident when staining with crystal violet as it highlighted a lot of cells around the outside of the well. This can therefore mean that the IncuCyte does not always capture the true number of cells in the well. However, it can monitor the proliferation profile of the cells that it does capture and cell morphology.

The other main issue with this equipment is when the camera is out of focus. This cannot be predicted therefore care must be taken when large jumps are observed in data. Throughout the secondary cell tests the cell mask application caused many issues throughout the experiments. It was considered that the issue was contamination of cells due to a move to a new lab however the problem was not consistent within plates or cell types. The cell mask only failed to apply correctly to wells which contained hydrophobically modified DNA.

All nanopore treatments were sterilised using the same method with a 0.22 µm Millex® -GV hydrophilic Durapore® membrane filter. The PBS used was also sterilised through a 0.2 µm Minisart hydrophilic filter before use. The PBS couldn't be contaminated as the vehicle control cells showed no sign of anything untoward in the cells. The unmodified DNA was used both in the unmodified nanopores and relevant strands in the modified nanopores. As no discrepancies were seen in the unmodified nanopore treatments it would indicate that these were not the source of the problem. Therefore this would indicate that the problem, if any, lay with the modified DNA strands. However, this was not consistent through different cell types therefore it did not lead to the conclusion that contamination was the problem. It is hypothesised that this could possibly be due to aggregation of the DNA nanostructures with the proteins in the cell media used, however this was not confirmed. The other hypothesis lay with the machine itself. As it was a newly set up IncuCyte, there could have been a machine error because the treatments were always applied in the same area of wells throughout the experiments. Therefore there may have been a problem with imaging in that section. Again, this was not confirmed due to time constraints.

The cell mask and focusing issues could be addressed by utilising the fluorescence function now readily available in the IncuCyte. It is possible to use live cell assays that use fluorescent dyes to label dead and live cells therefore making the cell distinction clearer in images and give a more accurate representation of the cell population within a well.

Although a widely used method for staining cells, the crystal violet assay did present some drawbacks in this project. As previously discussed in section 4.4.1.3, the HEK293T cells presented the most difficulty due to the weakly adherent nature of the cells and the multiple washing steps involved before the assay. Although every attempt was made to conduct washing steps gently it is believed that this, the small number of seeded cells, and low sensitivity of the assay led to the high error seen in throughout the assays.

Therefore, when interpreting results, although the IncuCyte and crystal violet assays data provided valuable insights and evidence, the most accurate results in this project are presented by the alamar blue assays.

Although not addressed in this project due to the previous success seen using DMEM in HeLa cells, an important factor that has recently been discussed in literature is the stability of the nanopores in cell media. Burns and Howorka conducted a study which showed their 6 duplex nanopores (both unmodified and with three cholesterol modifications) stability in various solutions[138]. Although the melting temperature of the structure was slightly decreased (lowered by approximately 6 °C in PBS) in solutions not specifically containing magnesium ions, it did not lower it more than temperatures used in cell culture. This supported our methods of forming the nanopore in PBS rather than in the typical 1 x TAE magnesium supplemented buffer to prevent any off-target effects of magnesium on the cells.

Interestingly the study[138] also showed that the presence of FBS in cell media was highly detrimental to the uptake of both cholesterol and unmodified nanopores in GUVs. They suggest that when using FBS in media, the nanopores are not exposed to the serum for prolonged periods of time. This may suggest changing the way the samples were prepared in this thesis. In this thesis the standard procedure for application of nanopore treatment was, samples were prepared at a 2 µM concentration by adding an equimolar concentration of each DNA strand to an Eppendorf. Concentrated PBS (10X PBS) (10 µL) was added and the volume was made up to 100 µL. Depending on the volume needed for the experiments this was repeated with multiple Eppendorf's. They were then placed in the PCR machine and annealed. All same samples were combined so that any error in pipetting in each of the samples was the same in all wells throughout the experiment. The samples were then sterilised through a 0.22 µm filter. The filter used, a GV Millipore filter, was

selected as it had a low hold up volume, therefore reducing the amount of sample lost during the sterilising process.

The treatments were then prepared in a clear 96 well plate for ease of use and to reduce human error in pipetting. This involved mixing the appropriate volume of nanopore with 100 µL of cell media and then using 1 X PBS to make the volume up to 200 µL in the well. This ensured that all cells, apart from the 100 % media control treated cells, had access to the same amount of media and therefore growth factors.

This protocol may have caused a problem with aggregation. The cell media used contained FBS, a serum that provides growth factors for cell growth. As stated above Burns and Howorka[138] showed that serum in the media can led to the aggregation of their DNA nanostructures. However, this could either be seen as a positive or a negative action. On the negative note, the aggregation may have caused the nanostructures to join together in a way that stopped them interacting with the cell membrane. The hydrophobically charged modifications to the structures would interact strongly with the FBS therefore they may have been masked in a way that they would not be able to insert into the membrane. On the other hand, the FBS may cause a positive interaction. When aggregated the nanopores may create large holes in the membrane therefore increasing potency. In another publication by the same research group[53], they conducted experiments with DMEM with FBS yet still found that the nanopores were taken up by the cells. However, it must be noted that they did not find cell toxicity in their study. This study also questioned the main assumption in this project; that the nanopores insert into the cell membrane. They have shown through confocal microscopy of HeLa cells that they do not only sit in the cell membrane but also end up inside of the cell. This may, of course, differ for different cell lines, but it does bring up the question of locality and action of the treatment. However, it could be argued that by being inside the cell, the nanopores, at some point, have interacted with the cell membrane. Cells sense when their membranes are compromised through actions such as ion flows in the cells such as calcium ions, when the flows become unbalanced the cell enacts mechanisms to fix the breach in the membrane. This can be through endo or exocytosis. Endocytosis involves the cell consuming the offending compound in the membrane, therefore it only makes sense that investigators would in fact find hydrophobically modified nanostructures inside the cells as well as in the membranes. Ways of ensuring the nanopore stays in the cell membrane would be of interest in future works. The proposal regarding attachment of targeting peptides, discussed in chapter 6, to the nanopore for surface membrane receptors may encourage the anchoring effect of the nanopore to stay in the membrane. However, this would have to be thoroughly investigated.

An important note on the work discussed above is the number of cholesterol modifications used on the nanopores. They highlighted that an increase from one to three modifications impacted the interaction of the nanopores with the cells. This thesis only used nanopores with two hydrophobic modifications. Therefore, the amount of modifications on the nanopore may also have played a role in the efficacy of the treatments. Studies conducted by Burns *et al.* with the large nanopore used digestion enzymes to show that as the number of modifications increased on the nanopore, the nanopore interacted with the artificial bilayer more strongly[139]. However, arguably, the more modifications on the nanostructures, the more likely they are to interact with the cell media and aggregate. Therefore, there must be a fine balance between these two factors.

This thesis also looked at the difference between pore size and modification as an effect on cells. The most significant and therefore compelling data was provided by the small nanopore with two cholesterol modifications. This would be expected as cholesterol is more hydrophobic than palmitate and therefore would act as a better anchor for the nanopores. It was hypothesised that the large nanopore would be more virulent than its small counterpart due to it being able to allow larger cell components to flow through. However this was not seen to be the case. This could be due to the overall size of the nanostructures. Both nanopores used only contained two hydrophobic modifications. Therefore the ratio of hydrophobic compound to helical domains, (four for the small nanopore and six for the large) differed. Perhaps if the amount of hydrophobic modifications was increased on the large pore, stronger data would have been gathered.

Perhaps the most interesting data gathered from this thesis was that gained from the phototoxicity experiments. Although with large errors the data does show that the combination of porphyrin modified nanopore and light therapy had a negative effect on cell viability. These pilot experiments showed great promise yet could be optimised in several fashions.

Light treatment times could easily be modified and optimised in the procedure. After consideration of the discussion of the stability of nanopores in cell media it may be more suitable to apply multiple light irradiations straight after nanopore application. For example, increasing the frequency of treatments from three five-minute treatments over three hours for three days, to six five-minute treatments every 30 minutes directly after nanopore application for three hours. Alternatively, the light irradiation time could be extended to 10 minutes. However, care must be taken to make sure that the cells are not overly disturbed and effected by the change in temperature and CO_2 concentration when removed for the treatments.

Chapter 6 Summary and outlook

This chapter summarises the work shown in this thesis and discusses the possible next stages to further this research.

It was found that the cholesterol modified small nanopore at a concentration of 1 μM reduced the cell viability of HEK293T cells by 56%. Although decreases in cell viability were seen at lower concentrations, no significance was seen. This was also the case with the palmitate modified nanopores and hydrophobically modified large nanopores where effects were seen but no significance found. Neither the hydrophobically modified large nanopore or small nanopore was seen to have any effect on the murine (B16-F10) or human (FM55-P) melanoma cell lines.

Photodynamic therapy using a porphyrin modified nanopore initially showed promising results with large reductions in cell viability however results were hindered by porphyrin stability and limited material. Therefore, no solid conclusions could be drawn.

Looking forward this work could be taken in many different directions. Firstly, the narrowing down of which nanopore to use. I would suggest further experiments being carried on with the small nanopore. It is cheaper to form than the large nanopore and the modified strands are shorter making them easier to make in high yields or cheaper to buy commercially. It has also shown the most promising results in this thesis.

Further experiments with different cell types could be explored. As discussed, cell type has shown to play a role in the efficacy of treatments therefore although not providing a treatment for melanoma, different cancer cell lines could be assayed. However, caution must be taken: as proven with in this thesis, experimental design, such as seeding density, also plays a role in effectiveness.

Another element of experimental design would be the exploration of experiments with serum free media. Although in this work we have shown activity of cholesterol modified DNA nanopores in HEK293T cells, the drawbacks of using serum in media became increasingly evident. Therefore this requires further exploration.

When continuing work with melanoma treatment, targeting cell receptors should be of prime interest to prevent off target effects. As discussed previously this could be done using NAP-amide which targets the melanocortin 1 receptor which is over expressed on melanoma cells. One possible method to explore this conjugation would be using a linker molecule between DNA and NAP-amide as NHS ester modified DNA is not readily available commercially. The linker molecule proposed is

Dibenzocyclooctyne-PEG4-N-hydroxysuccinimidyl ester which contains a strained alkyne bond and a NHS ester at either end, **Figure 108**.

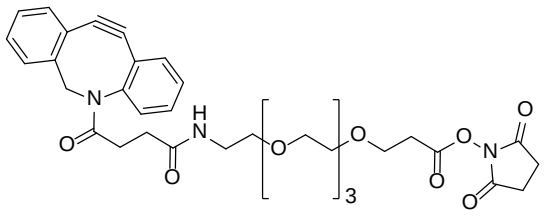

Figure 108 Linker molecule - Dibenzocyclooctyne-PEG4-N-hydroxysuccinimidyl ester.

An azide modified DNA strand would be included in the nanopore structure. This would then couple through a strain-promoted copper-free click reaction to the linker molecule. Finally, this coupled product would react to the NAP-amide through the free NHS ester. This conjugated structure would then be used in further PDT experiments. As previously discussed, the future PDT experiments need to be optimised for porphyrin DNA stability. Also, the frequency and duration of light treatments must be considered.

Finally, further investigations into the location of the nanopore treatments should be conducted through confocal microscopy and fluorescent tagging of the nanopores. This would be of great interest in the HEK293T cells where cytotoxicity was observed, thus allowing a comparison to other cell types where cytotoxicity was not seen.

Appendix A

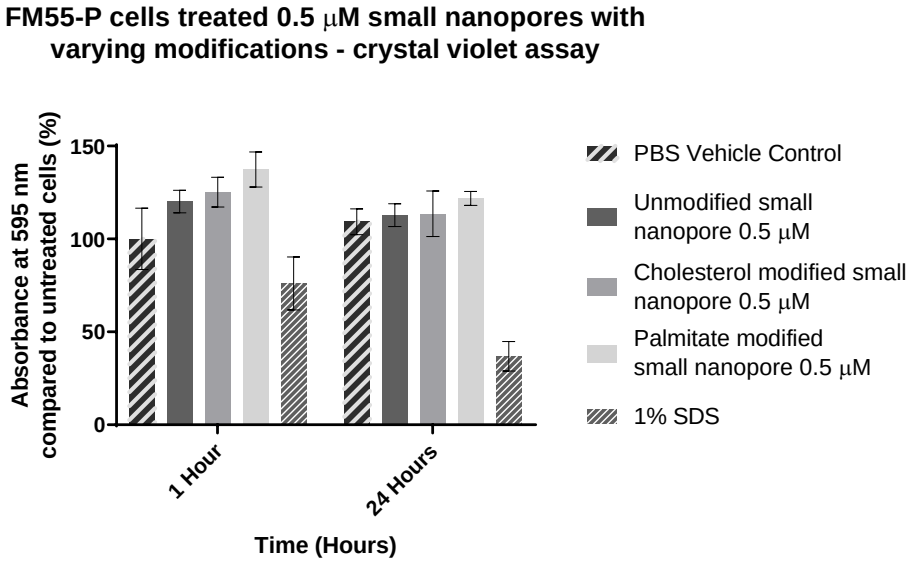

Appendix 1 Graph showing FM55-P cells treated with 0.5 μM small nanopores with varying modifications cell viability assay. N=3 mean and SD error shown. No significant differences were seen between samples.

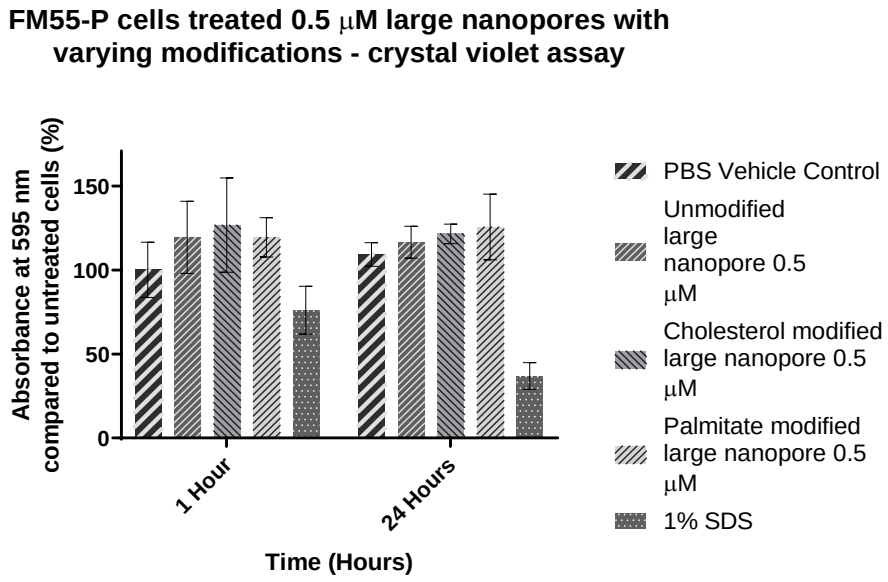

Appendix 2 Graph showing FM55-P cells treated with 0.5 μM large nanopores with varying modifications cell viability assay. N=3 mean and SD error shown. No significant differences were seen between samples.

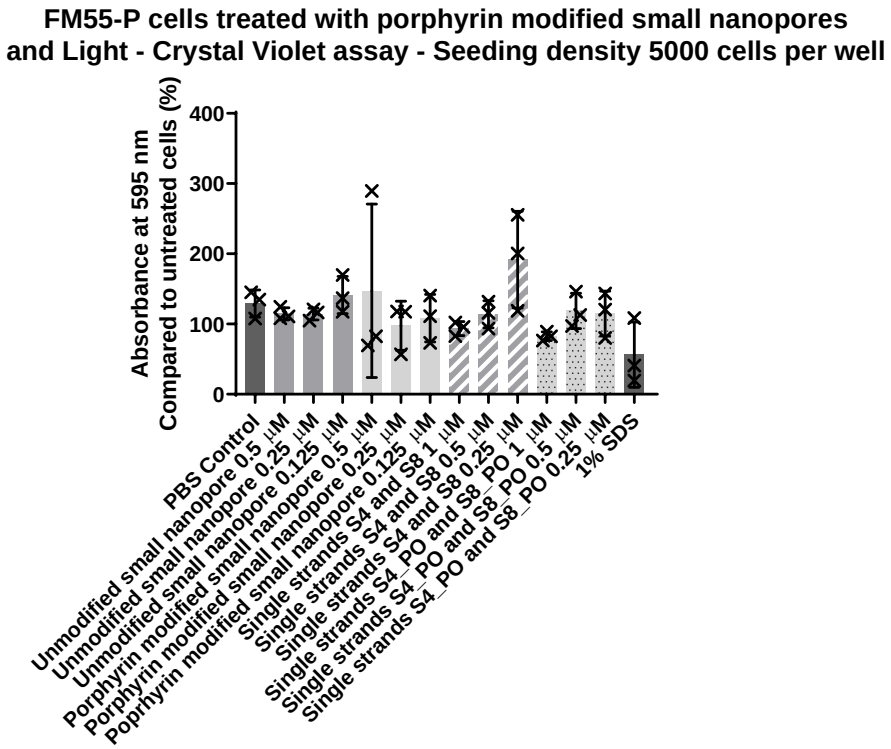

Appendix 3 Graph showing FM55-P cells treated with 0.5 µM porphyrin modified small nanopores and light cell viability assay. N=3 mean and SD error shown. No significant differences were seen between samples.

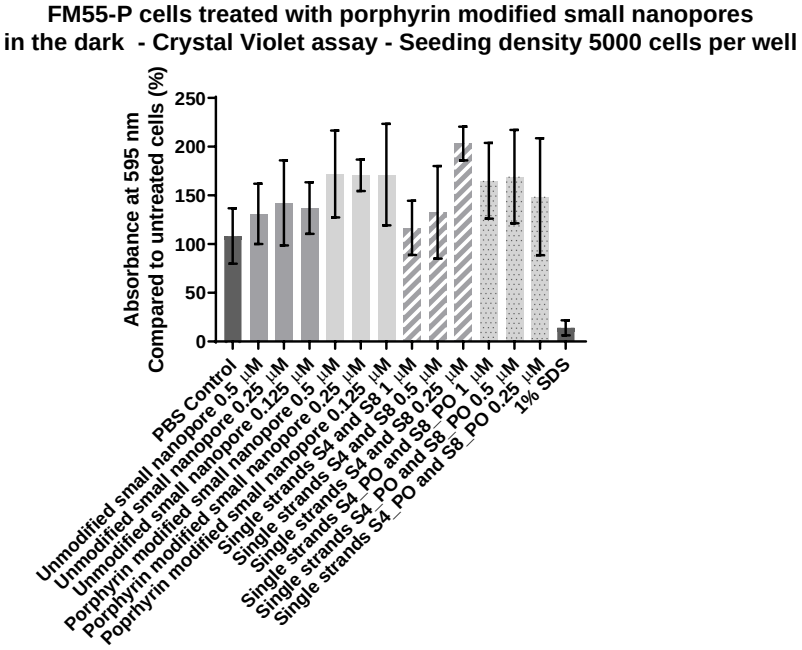

Appendix 4 Graph showing FM55-P cells treated with 0.5 µM porphyrin modified small nanopores dark control cell viability assay. N=3 mean and SD error shown. No significant differences were seen between samples.

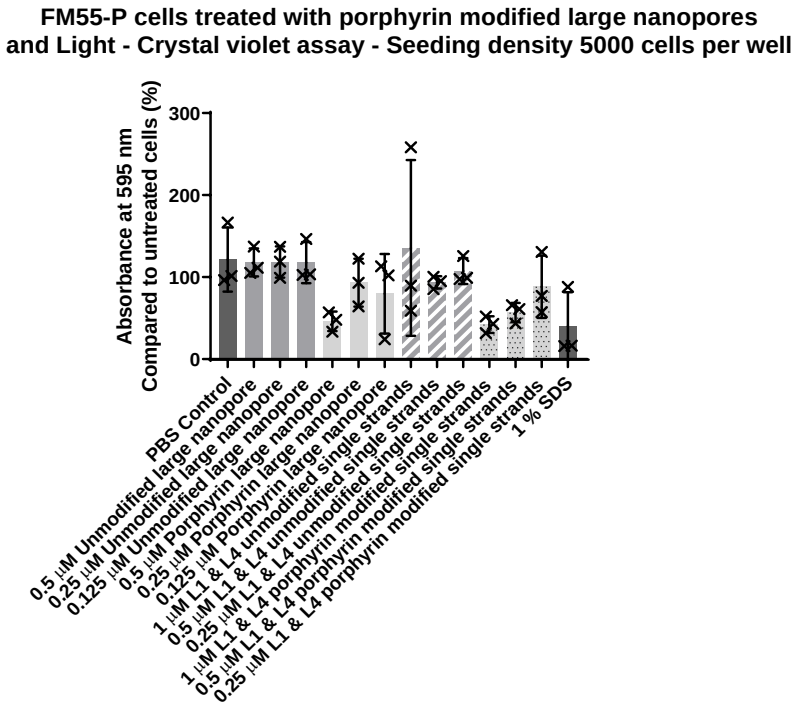

Appendix 5 Graph showing FM55-P cells treated with 0.5 µM porphyrin modified large nanopores and light cell viability assay. N=3 mean and SD error shown. No significant differences were seen between samples.

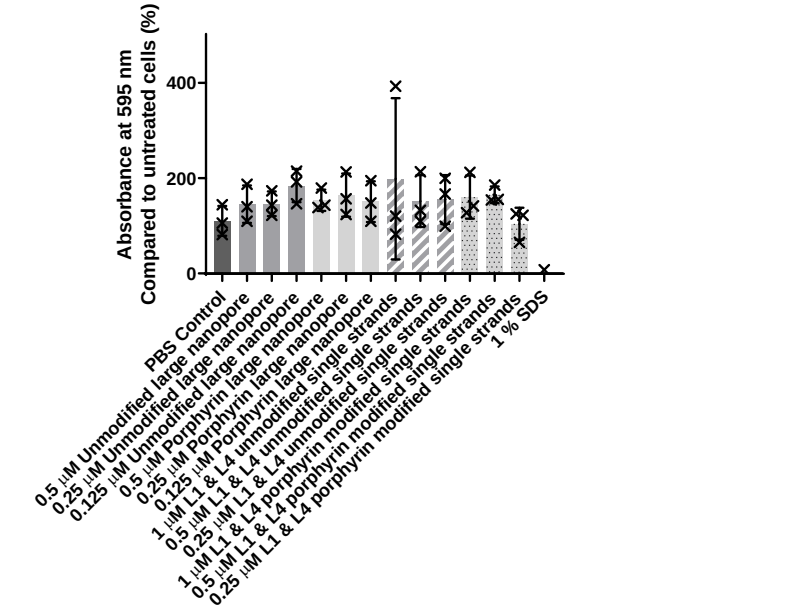

Appendix 6 Graph showing FM55-P cells treated with 0.5 µM porphyrin modified large nanopores dark control cell viability assay. N=3 mean and SD error shown. No significant differences were seen between samples.

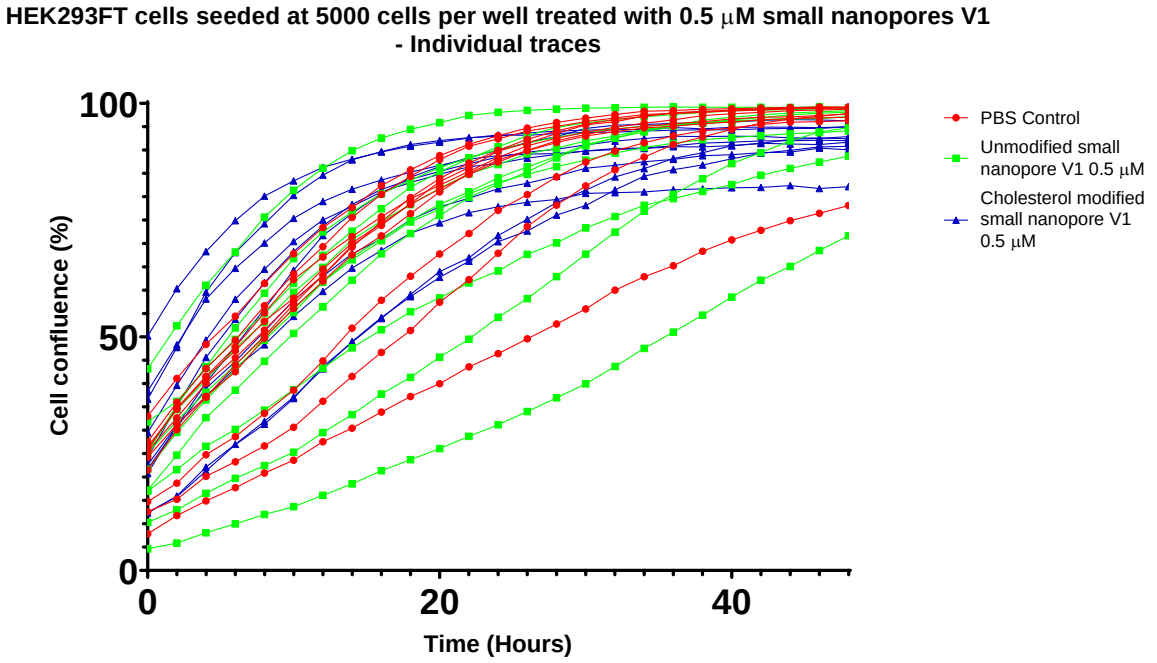

Appendix 7 Individual traces of experiment shown in **Figure 48** (Left) At high seeding densities of 5000 cells per well the proliferation of HEK293FT cells was not negatively affected by the cholesterol modified small nanopore V1. (Right) Omitting the 3rd biological repeat had no effect on the high seeding density results.**Figure 48** of cells seeded at 5000 cells per well treated with 0.5 μM small nanopores V1. Most traces follow a similar proliferation curve. Each line represents a technical duplicate of the four biological repeats.

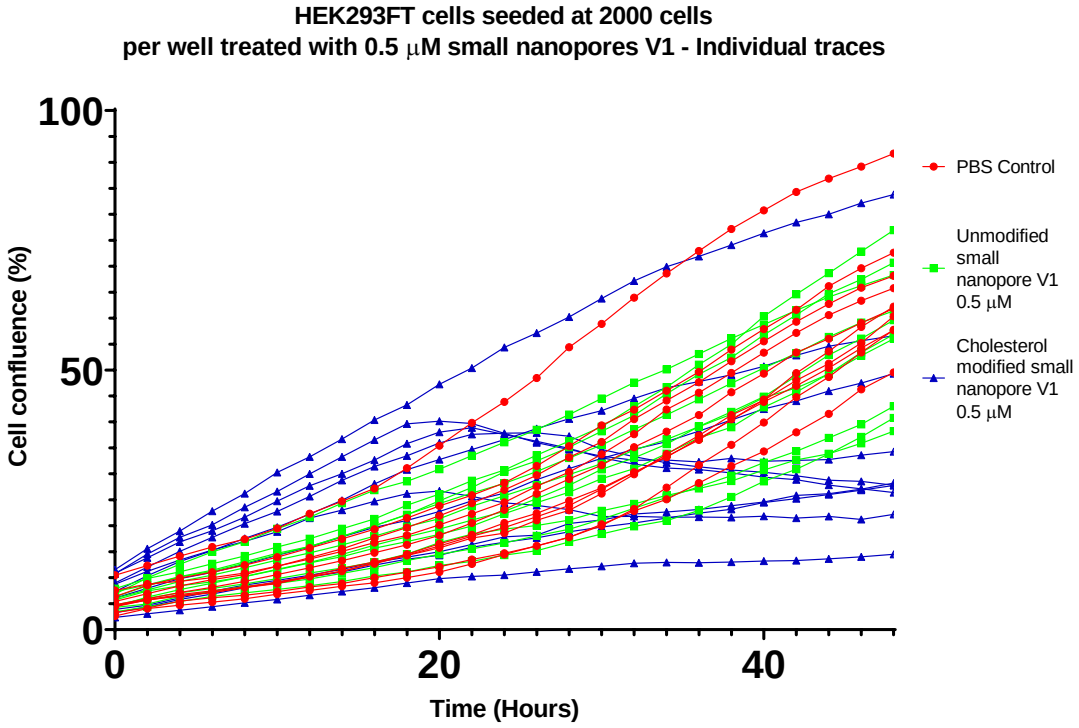

Appendix 8 Individual traces of experiment shown in **Figure 49** of cells seeded at 2000 cells per well treated with 0.5 μM small nanopores V1. All but one trace in the cells treated with the cholesterol modified nanopore V1 plateaued at 20 hours indicating the treatment resulted in a negative effect on proliferation. Each line represents a technical duplicate of the four biological repeats.

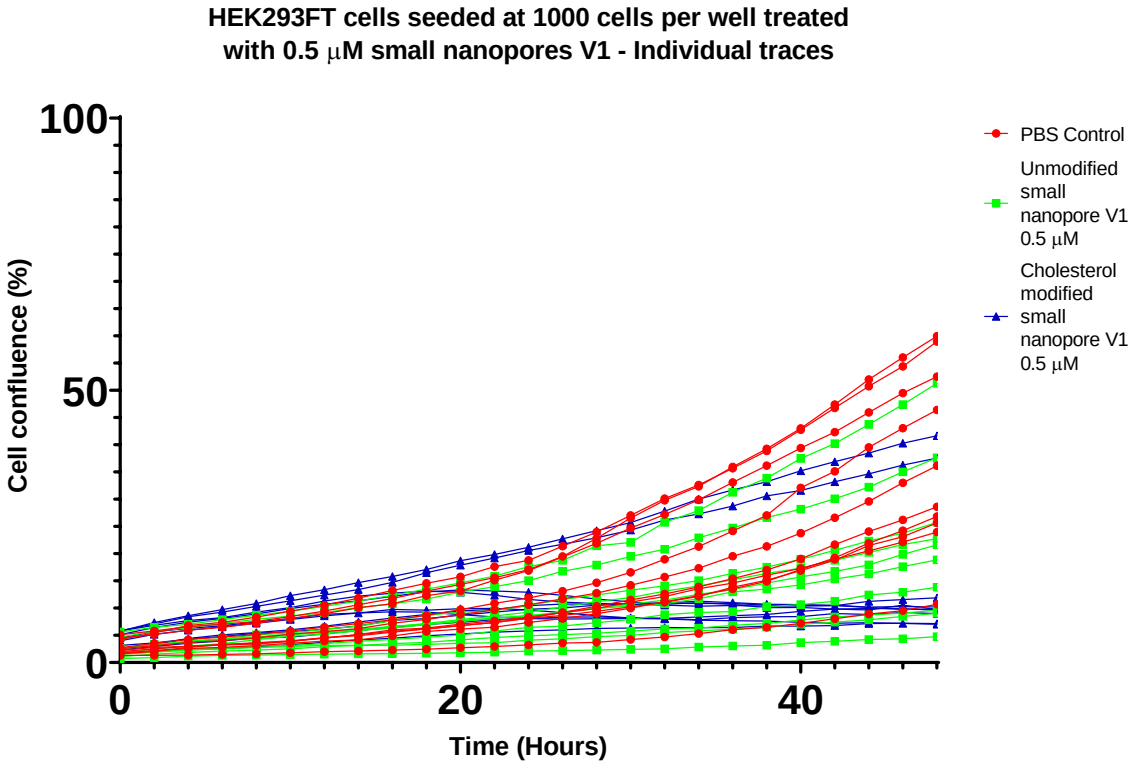

Appendix 9 Individual traces of experiment shown in **Figure 50** of cells seeded at 1000 cells per well treated with 0.5 μM small nanopores V1. All but two traces in the cells treated with the cholesterol modified nanopore V1 plateaued at 20 hours indicating the treatment resulted in a negative effect on proliferation. Each line represents a technical duplicate in the four biological repeats.

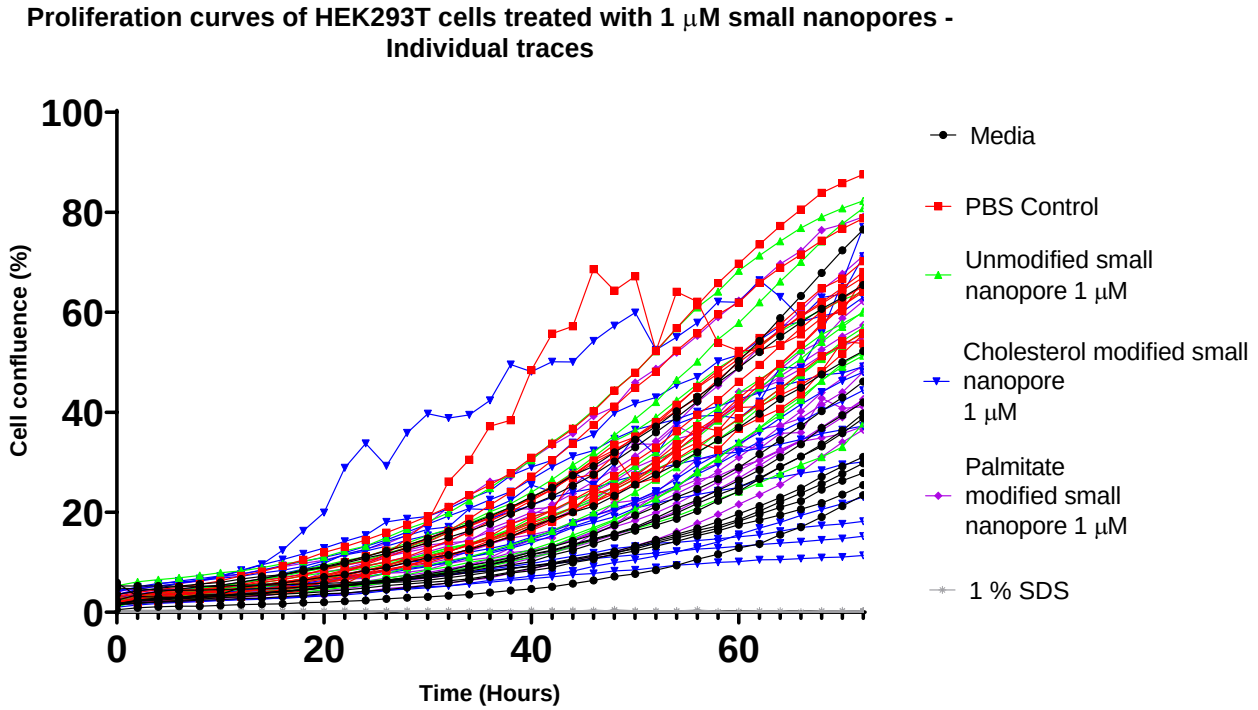

Appendix 10 Individual traces of proliferation experiment shown in **Figure 57** of HEK293T cells treated with 1 μM small nanopores. Erratic traces can be seen in various samples which explained the large SD error bars seen in **Figure 57**. Each line represents a technical triplicate of the four biological repeats.

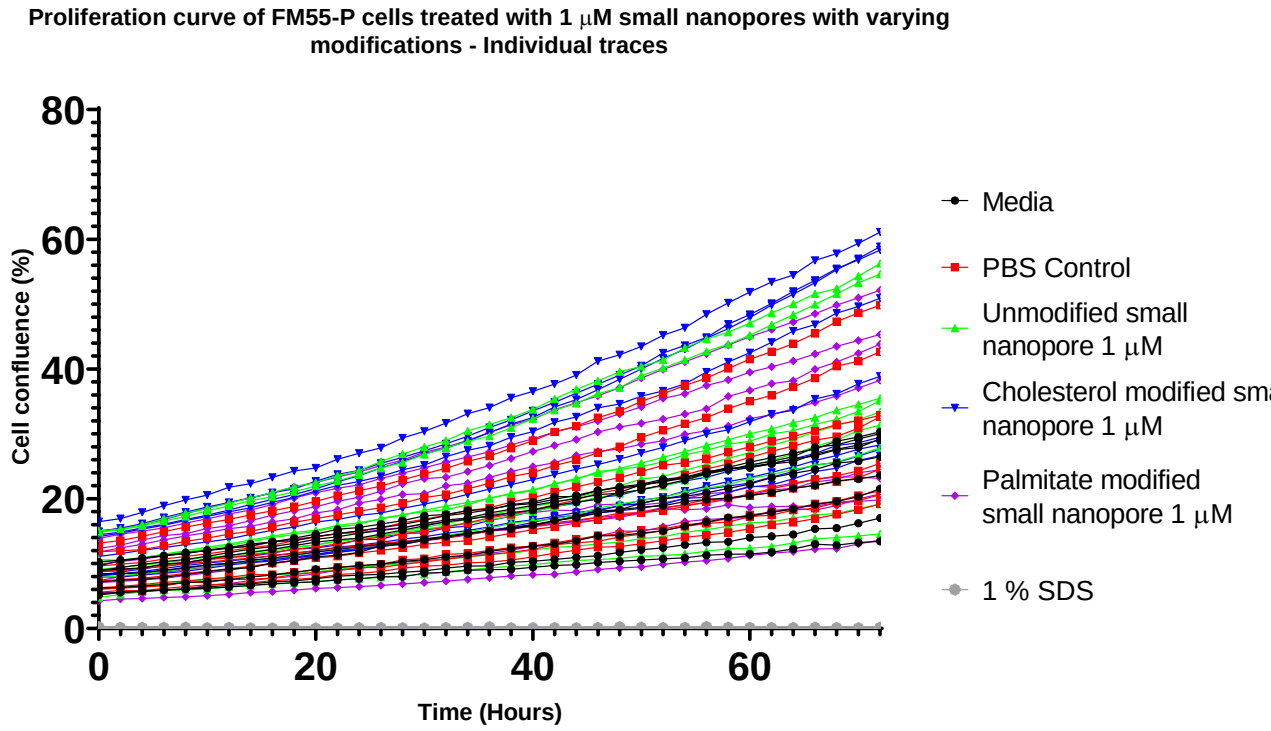

Appendix 11 Individual traces of proliferation experiment shown in **Figure 78** of FM55-P cells treated with 1 μM small nanopores. A small difference in starting confluence was seen

to have an effect on proliferation rate. Each line represents a technical triplicate of the four biological repeats.

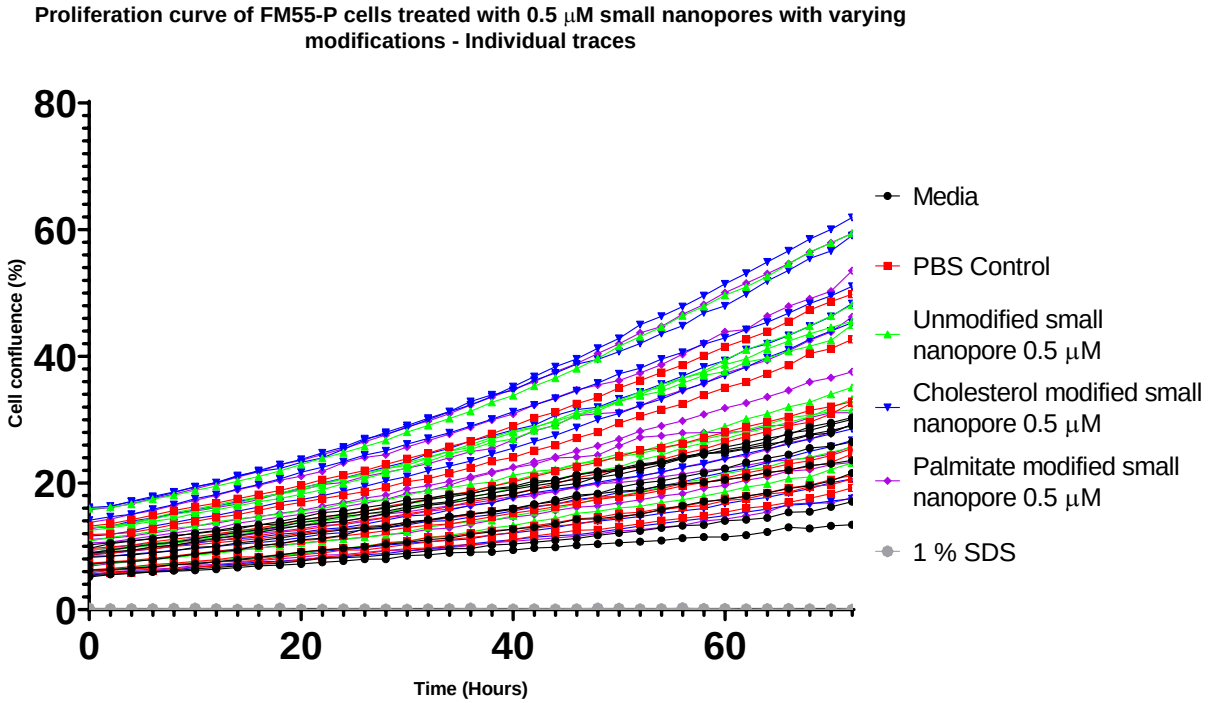

Appendix 12 Individual traces of proliferation experiment shown in **Figure 79** of FM5-P cells treated with 0.5 μM small nanopores. A small difference in starting confluence was seen to influence proliferation rate. Each line represents a technical triplicate of the four biological repeats.

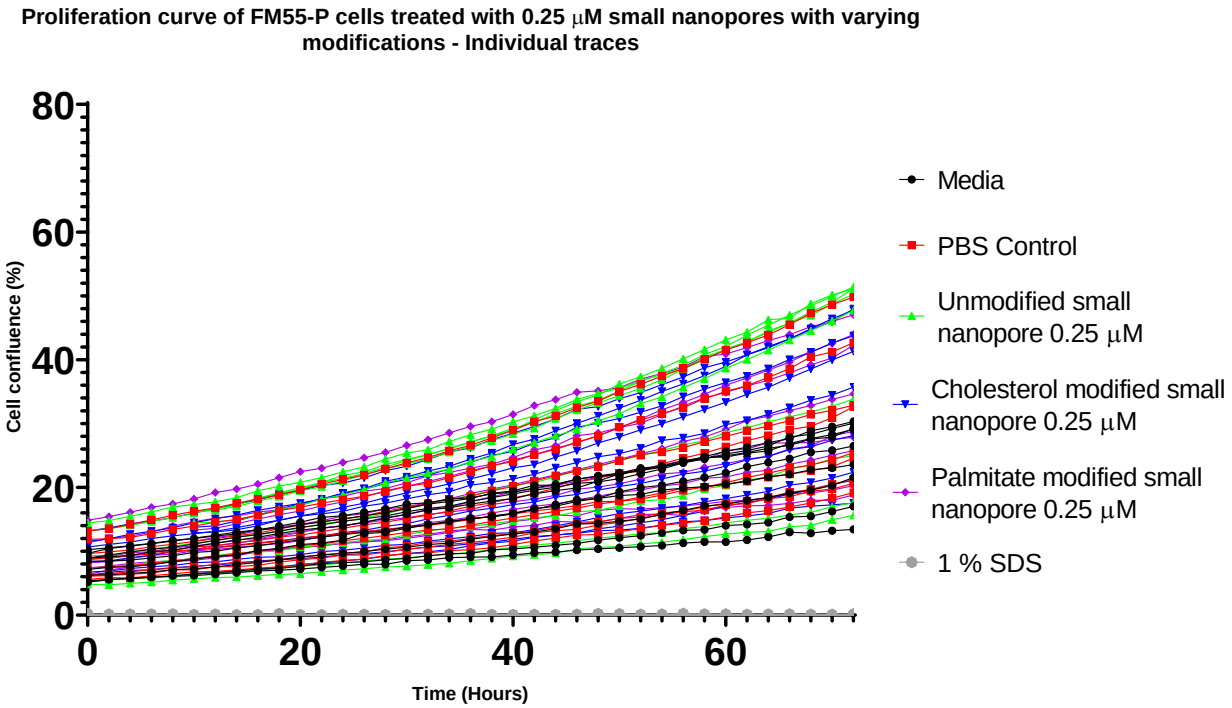

Appendix 13 Individual traces of proliferation experiment shown in **Figure 80** of FM5-P cells treated with 0.25 μM small nanopores. A small difference in starting confluence was seen to

influence proliferation rate. Each line represents a technical triplicate of the four biological repeats.

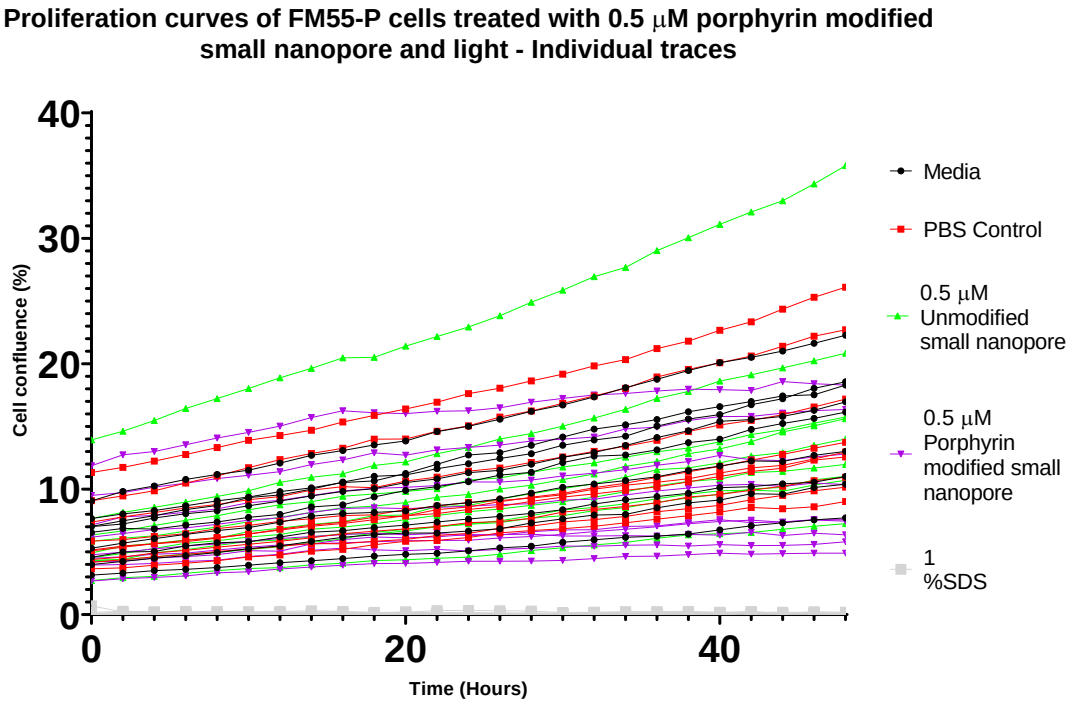

Appendix 14 Individual traces of the nanopore samples in the phototoxicity proliferation experiment shown in **Figure 88** of FM55-P cells treated with 0.5 μM porphyrin modified small nanopore and light. Each line represents the technical repeats of each biological repeat.

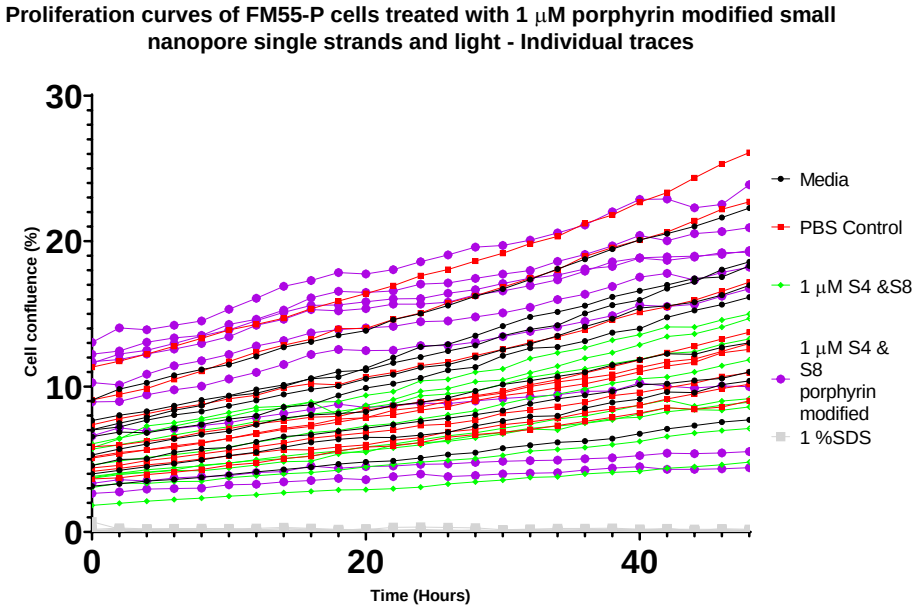

Appendix 15 Individual traces of the single DNA strand samples in the phototoxicity proliferation experiment shown in **Figure 88** of FM55-P cells treated with 1 μM porphyrin modified

single strands of DNA and light. Each line represents the technical repeats of each biological repeat.

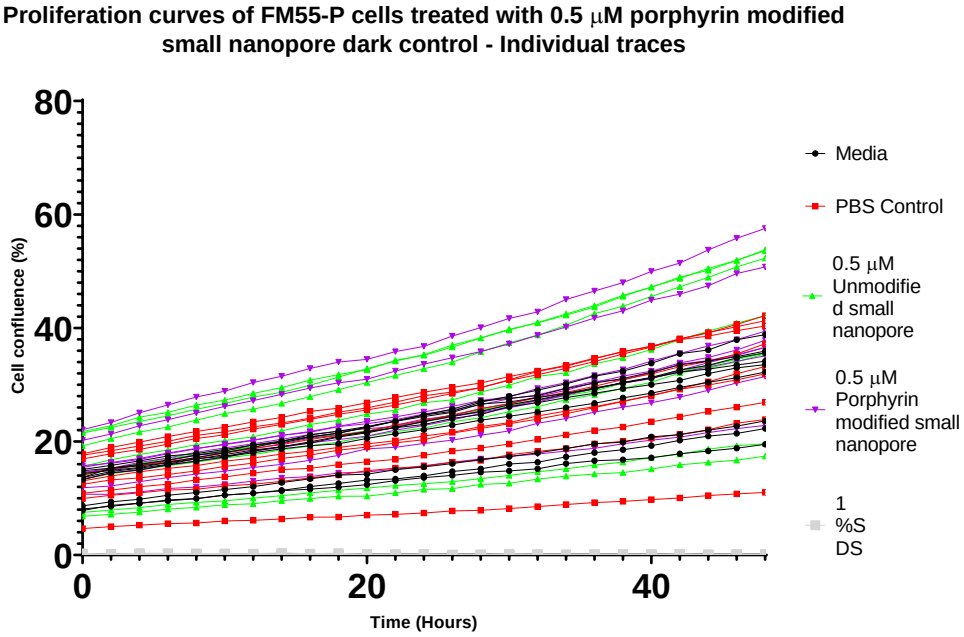

Appendix 16 Individual traces of the nanopore samples in dark control experiment shown in **Figure 89** of FM55-P cells treated with 0.5 μM porphyrin modified small nanopore. Each line represents the technical repeats of each biological repeat.

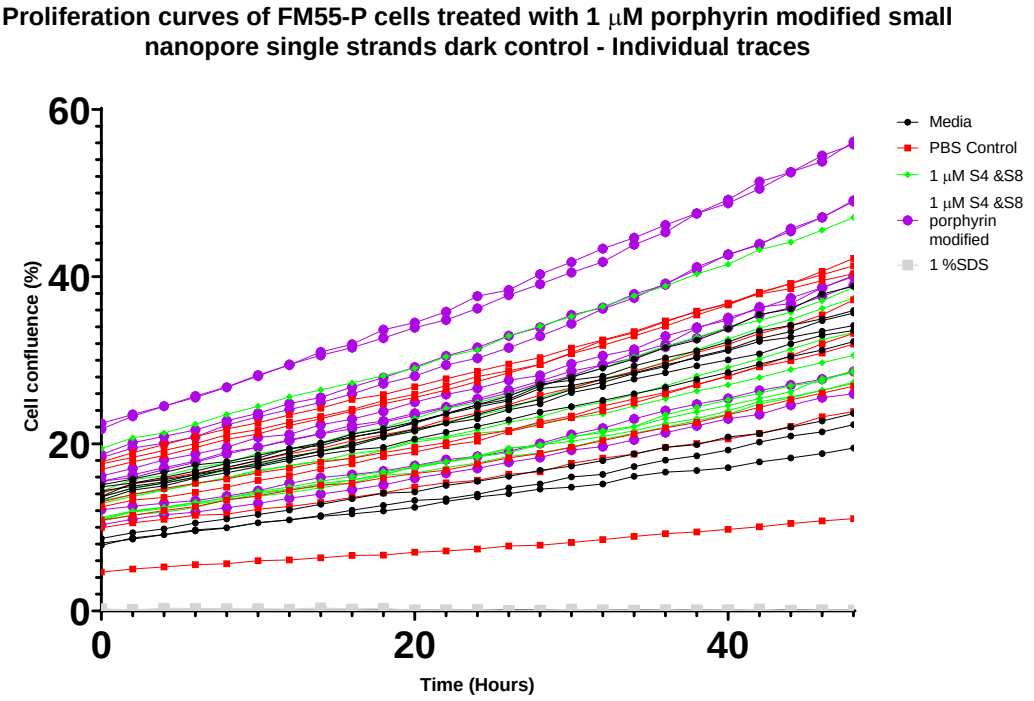

Appendix 17 Individual traces of the single DNA strand samples in the dark control proliferation experiment shown in **Figure 89** of FM55-P cells treated with 1 μM porphyrin modified small nanopore. Each line represents the technical repeats of each biological repeat.

Proliferation curves of FM55-P cells treated with 0.25 μM porphyrin modified small nanopore and light - Individual traces

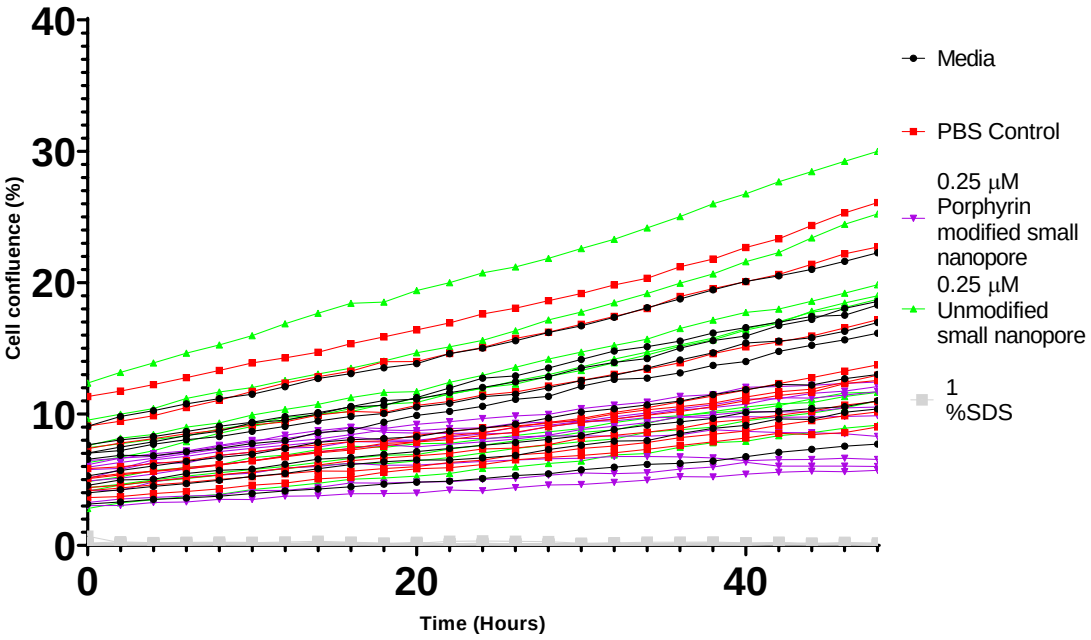

Appendix 18 Individual traces of the single DNA strand samples in the phototoxicity proliferation experiment shown in **Figure 90**. of FM55-P cells treated with 0.25 μM porphyrin modified single strands of DNA and light. Each line represents the technical repeats of each biological repeat.

Proliferation curves of FM55-P cells treated with 0.5 μM porphyrin modified small nanopore single strands and light - Individual traces

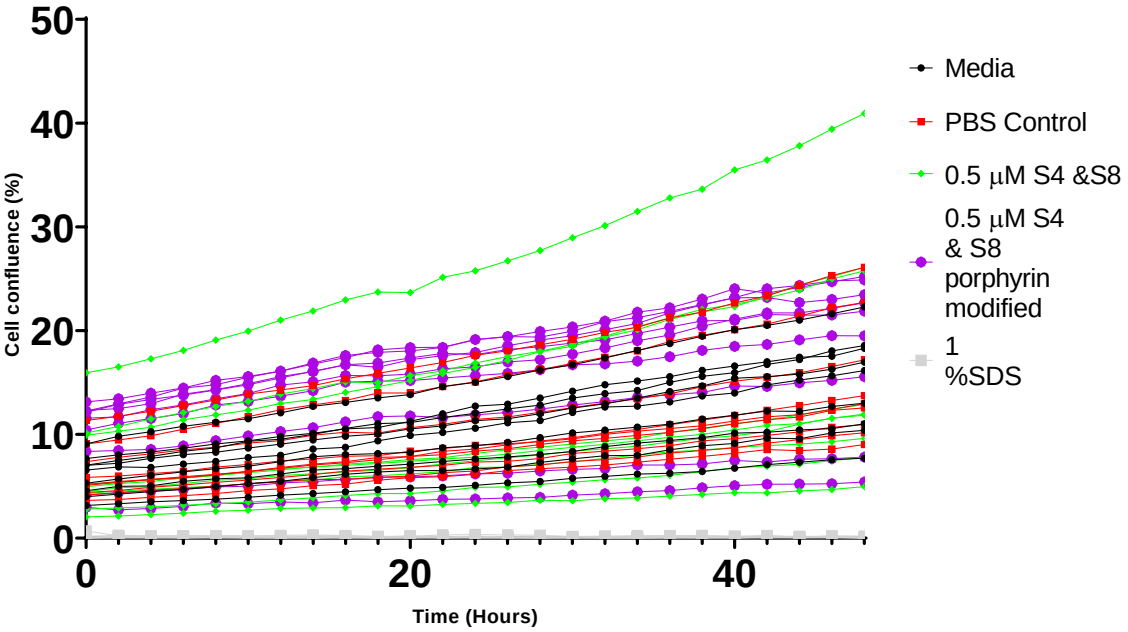

Appendix 19 Individual traces of the single DNA strand samples in the phototoxicity proliferation experiment shown in **Figure 90** of FM55-P cells treated with 0.5 μM porphyrin

modified single strands of DNA and light. Each line represents the technical repeats of each biological repeat.

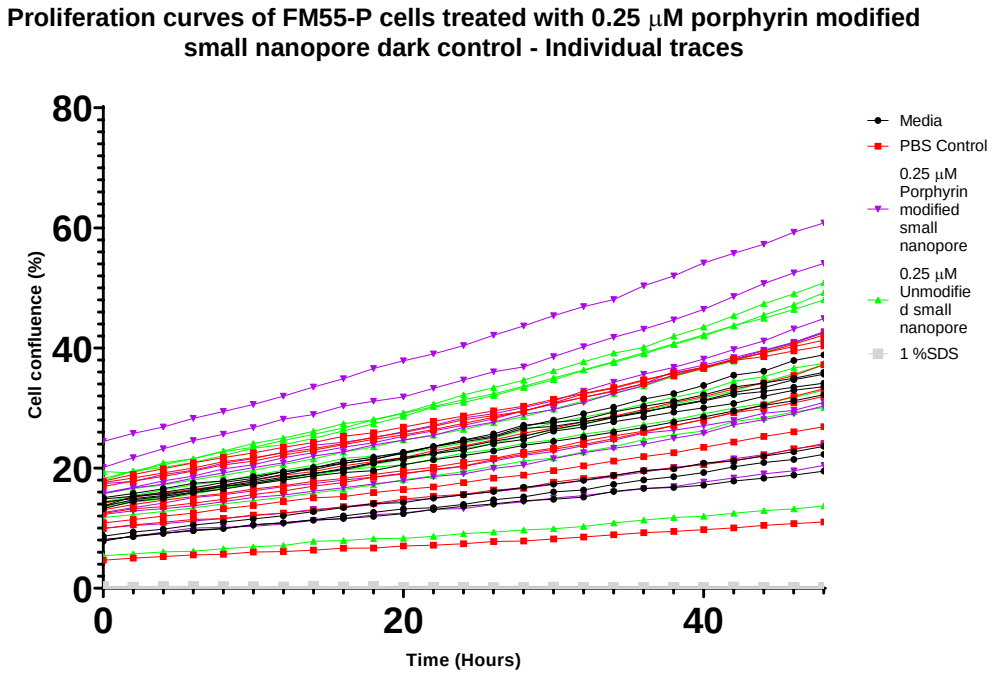

Appendix 20 Individual traces of the nanopore samples in dark control experiment shown in **Figure 91** of FM55-P cells treated with 0.25 μM porphyrin modified small nanopore. Each line represents the technical repeats of each biological repeat.

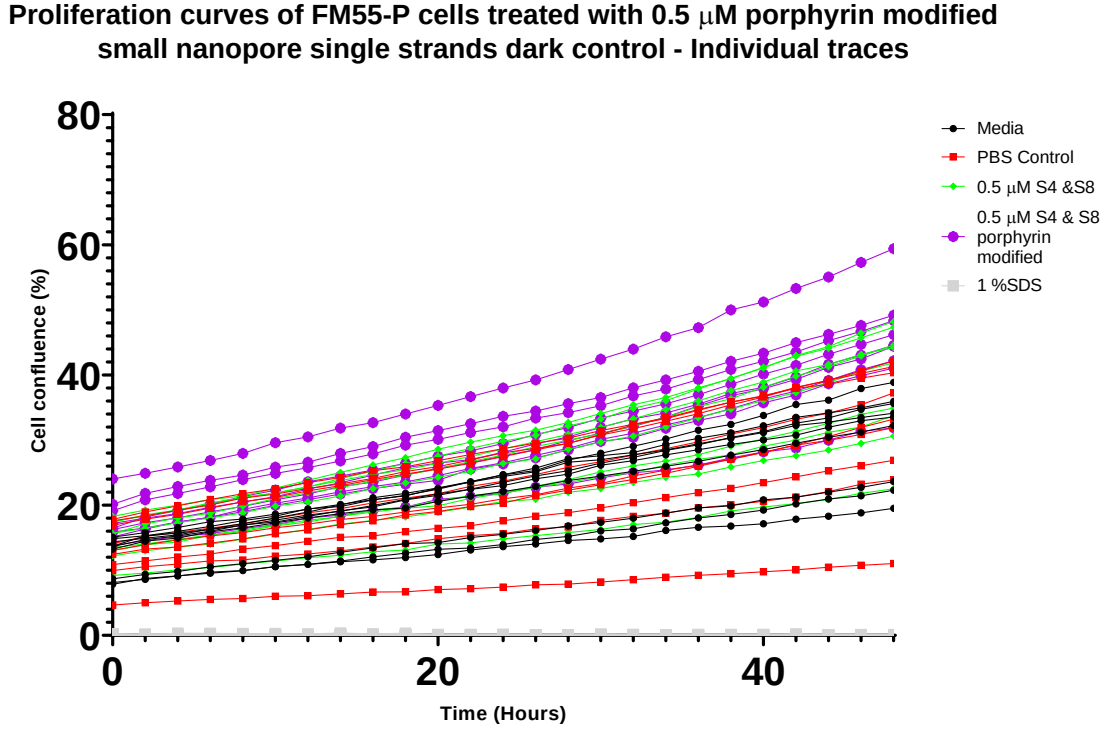

Appendix 21 Individual traces of the single DNA strand samples in the dark control proliferation experiment shown in **Figure 91** of FM55-P cells treated with 0.5 μM porphyrin

modified small nanopore. Each line represents the technical repeats of each biological repeat.

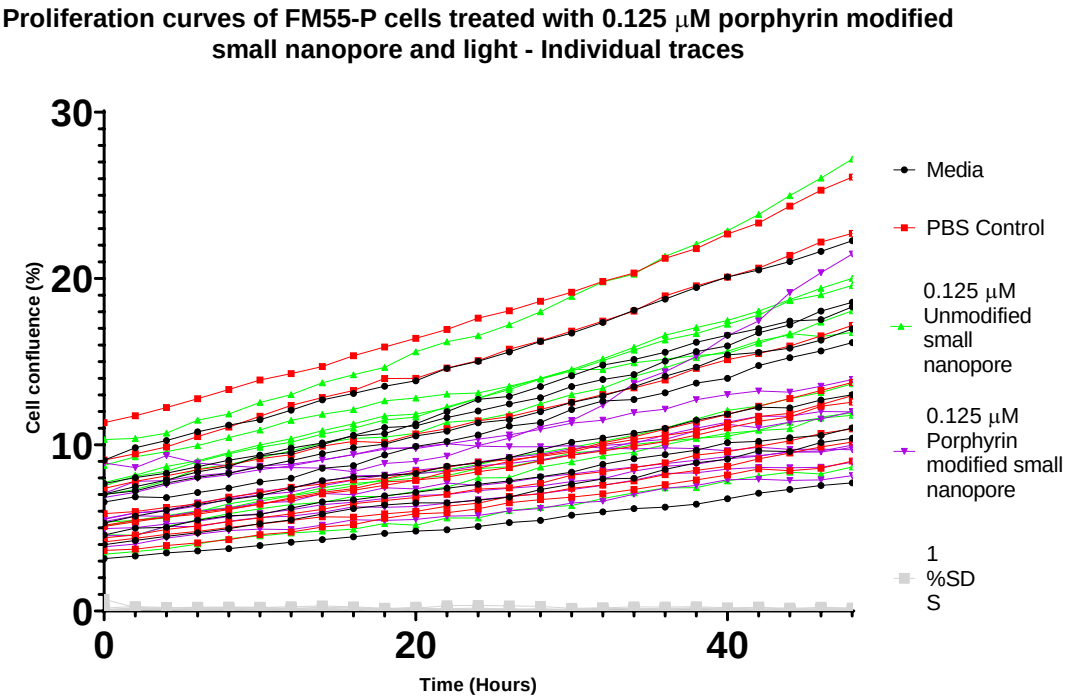

Appendix 22 Individual traces of the nanopore samples in the phototoxicity proliferation experiment shown in **Figure 92** of FM55-P cells treated with 0.125 μM porphyrin modified small nanopore and light. Each line represents the technical repeats of each biological repeat.

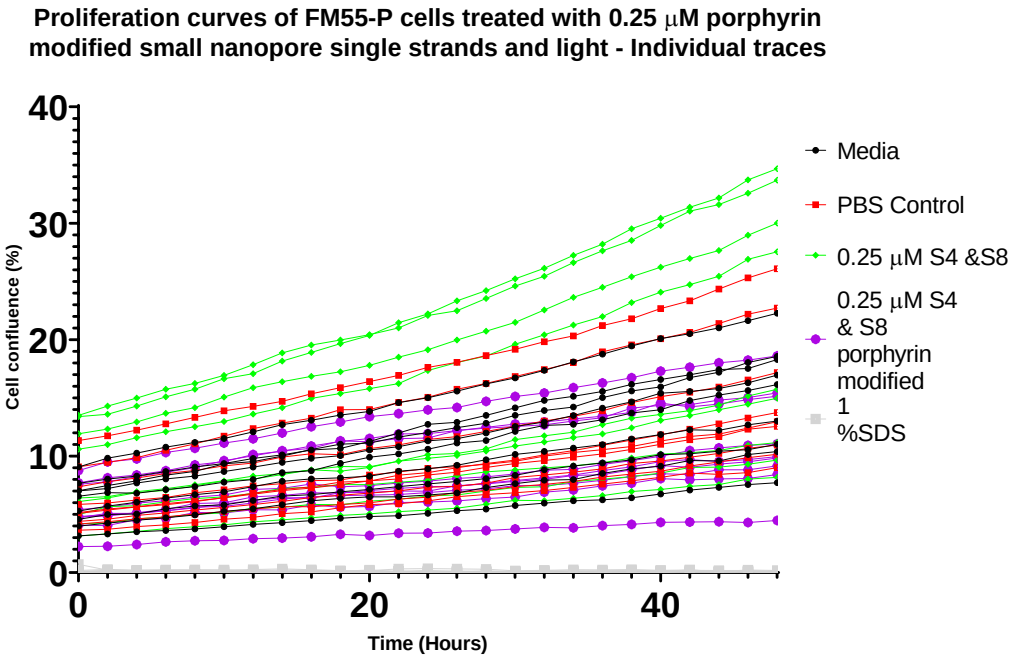

Appendix 23 Individual traces of the single DNA strand samples in the phototoxicity proliferation experiment shown in **Figure 92** of FM55-P cells treated with 0.25 μM porphyrin

modified single strands of DNA and light. Each line represents the technical repeats of each biological repeat.

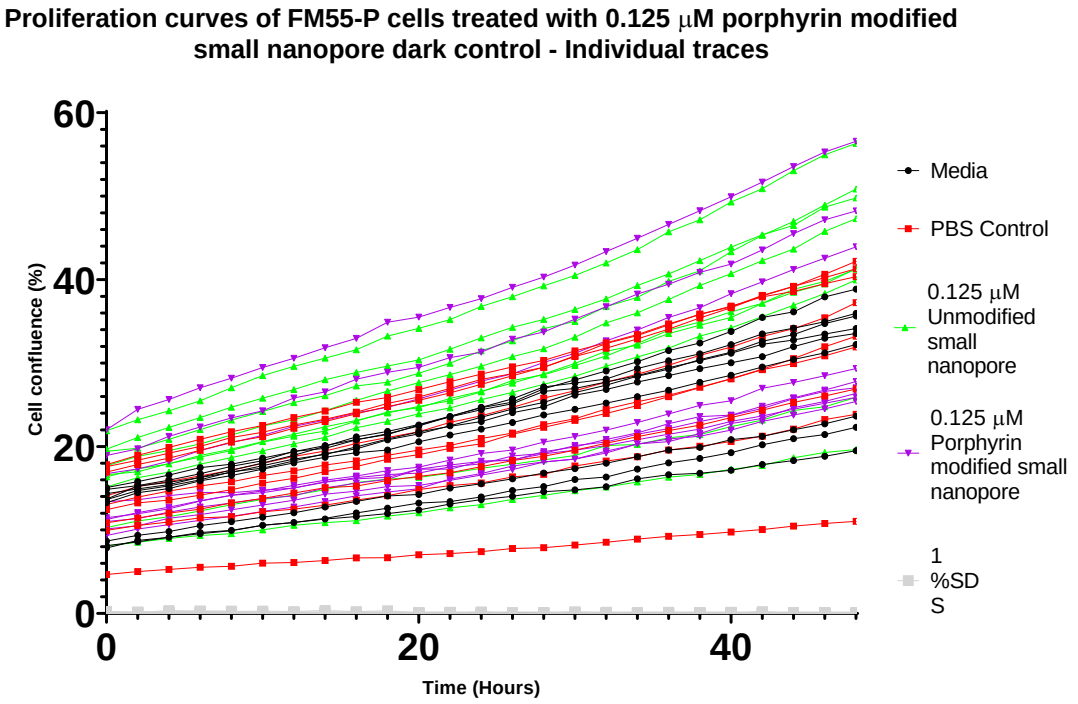

Appendix 24 Individual traces of the nanopore samples in dark control experiment shown in **Figure 93** of FM55-P cells treated with 0.125 μM porphyrin modified small nanopore. Each line represents the technical repeats of each biological repeat.

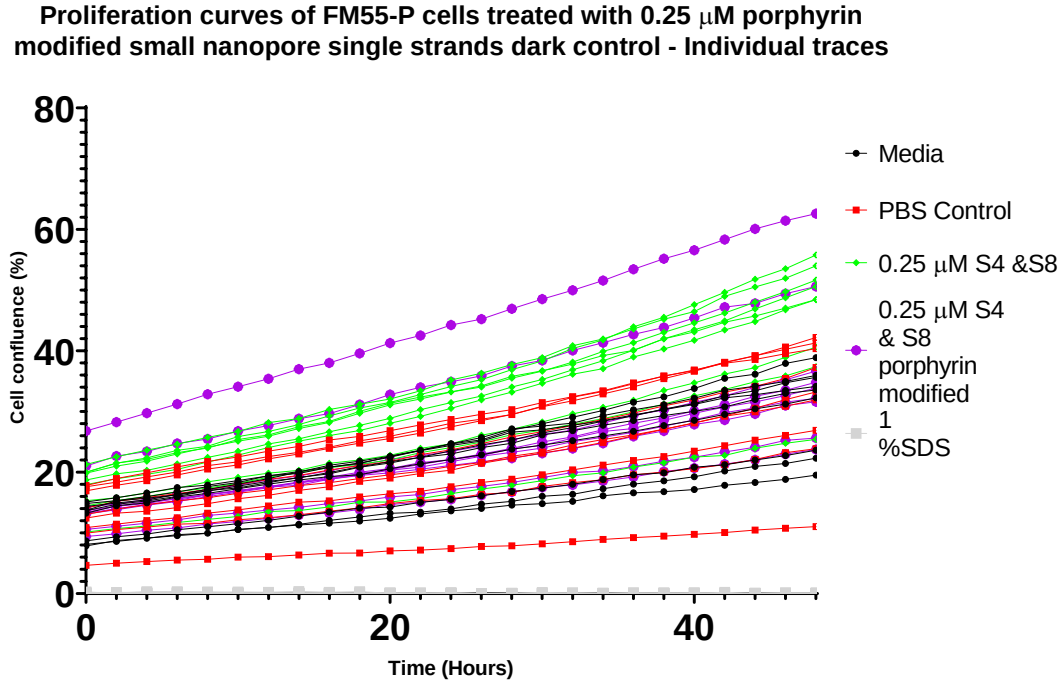

Appendix 25 Individual traces of the single DNA strand samples in the dark control proliferation experiment shown in **Figure 93** of FM55-P cells treated with 0.25 μM porphyrin

modified small nanopore. Each line represents the technical repeats of each biological repeat.

Bibliography

1. CancerResearchUK Melanoma skin cancer statistics. https://www.cancerresearchuk.org/health-professional/cancer-statistics/statistics-by-cancer-type/melanoma-skin-cancer#heading-Zero (accessed 01/02/2019).

2. Burns, J. R.; Al-Juffali, N.; Janes, S. M.; Howorka, S., Membrane-Spanning DNA Nanopores with Cytotoxic Effect. *Angewandte Chemie-International Edition* **2014,** *53* (46), 12466-12470.

3. Burns, J. R.; Seifert, A.; Fertig, N.; Howorka, S., A biomimetic DNA-based channel for the ligand-controlled transport of charged molecular cargo across a biological membrane. *Nature Nanotechnology* **2016,** *11* (2), 152-156.

4. Göpfrich, K.; Zettl, T.; Meijering, A. E. C.; Hernández-Ainsa, S.; Kocabey, S.; Liedl, T.; Keyser, U. F., DNA-Tile Structures Induce Ionic Currents through Lipid Membranes. *Nano Letters* **2015,** *15* (5), 3134-3138.

5. Dahm, R., Friedrich Miescher and the discovery of DNA. *Developmental Biology* **2005,** *278* (2), 274-288.

6. NobelMediaAB Albrecht Kossel - Facts. (accessed 08/11/2016).

7. Pray, L., Discovery of DNA Structure and Function: Watson and Crick. *Nature Education* **2008,** *1* (1), 100.

8. Vischer, E.; Chargaff, E., THE SEPARATION AND QUANTITATIVE ESTIMATION OF PURINES AND PYRIMIDINES IN MINUTE AMOUNTS. *Journal of Biological Chemistry* **1948,** *176* (2), 703-714.

9. Chargaff, E., Chemical specificity of nucleic acids and mechanism of their enzymatic degradation. *Experientia* **1950,** *6* (6), 201-9.

10. Astbury, W. T.; Bell, F. O., SOME RECENT DEVELOPMENTS IN THE X-RAY STUDY OF PROTEINS AND RELATED STRUCTURES. *Cold Spring Harbor Symposia on Quantitative Biology* **1938,** *6*, 109-121.

11. Furberg, S., On the structure of nucleic acids. *Acta Chemica Scandinavica* **1952,** *6*, 634-640.

12. Watson, J. D.; Crick, F. H. C., Molecular Structure of Nucleic Acids: A Structure for Deoxyribose Nucleic Acid. *Nature* **1953,** *171* (4356), 737-738.

13. Bhagavan, N. V.; Ha, C.-E., Chapter 21 - Structure and Properties of DNA. In *Essentials of Medical Biochemistry (Second Edition)*, Bhagavan, N. V.; Ha, C.-E., Eds. Academic Press: San Diego, 2015; pp 381-400.

14. Brown, T.; Brown, T. Nucleic Acids Book. (accessed 06/11/2019).

15. Seeman, N. C.; Kallenbach, N. R., DNA BRANCHED JUNCTIONS. *Annual Review of Biophysics and Biomolecular Structure* **1994,** *23*, 53-86.

16. Seeman, N. C.; Kallenbach, N. R., DESIGN OF IMMOBILE NUCLEIC-ACID JUNCTIONS. *Biophysical Journal* **1983,** *44* (2), 201-209.

17. Kallenbach, N. R.; Ma, R.-I.; Seeman, N. C., An immobile nucleic acid junction constructed from oligonucleotides. *Nature* **1983,** *305* (5937), 829-831.

18. Chen, J.; Seeman, N. C., Synthesis from DNA of a molecule with the connectivity of a cube. *Nature* **1991,** *350* (6319), 631-633.

19. Fu, T. J.; Seeman, N. C., DNA double-crossover molecules. *Biochemistry* **1993,** *32* (13), 3211-3220.

20. Shih, W. M.; Quispe, J. D.; Joyce, G. F., A 1.7-kilobase single-stranded DNA that folds into a nanoscale octahedron. *Nature* **2004,** *427* (6975), 618-621.

21. Rothemund, P. W. K., Folding DNA to create nanoscale shapes and patterns. *Nature* **2006,** *440* (7082), 297-302.

22. Zadegan, R. M.; Jepsen, M. D. E.; Thomsen, K. E.; Okholm, A. H.; Schaffert, D. H.; Andersen, E. S.; Birkedal, V.; Kjems, J., Construction of a 4 Zeptoliters Switchable 3D DNA Box Origami. *ACS Nano* **2012,** *6* (11), 10050-10053.

23. Douglas, S. M.; Dietz, H.; Liedl, T.; Hogberg, B.; Graf, F.; Shih, W. M., Self-assembly of DNA into nanoscale three-dimensional shapes. *Nature* **2009,** *459* (7245), 414-418.

24. Douglas, S. M.; Marblestone, A. H.; Teerapittayanon, S.; Vazquez, A.; Church, G. M.; Shih, W. M., Rapid prototyping of 3D DNA-origami shapes with caDNAno. *Nucleic Acids Research* **2009,** *37* (15), 5001-5006.

25. Sun, W.; Jiang, T.; Lu, Y.; Reiff, M.; Mo, R.; Gu, Z., Cocoon-Like Self-Degradable DNA Nanoclew for Anticancer Drug Delivery. *Journal of the American Chemical Society* **2014,** *136* (42), 14722-14725.

26. Jiang, Q.; Song, C.; Nangreave, J.; Liu, X.; Lin, L.; Qiu, D.; Wang, Z.-G.; Zou, G.; Liang, X.; Yan, H.; Ding, B., DNA Origami as a Carrier for Circumvention of Drug Resistance. *Journal of the American Chemical Society* **2012,** *134* (32), 13396-13403.

27. Halley, P. D.; Lucas, C. R.; McWilliams, E. M.; Webber, M. J.; Patton, R. A.; Kural, C.; Lucas, D. M.; Byrd, J. C.; Castro, C. E., Daunorubicin-Loaded DNA Origami Nanostructures Circumvent Drug-Resistance Mechanisms in a Leukemia Model. *Small* **2016,** *12* (3), 308-320.

28. Yan, J.; Hu, C.; Wang, P.; Zhao, B.; Ouyang, X.; Zhou, J.; Liu, R.; He, D.; Fan, C.; Song, S., Growth and Origami Folding of DNA on Nanoparticles for High-Efficiency Molecular Transport in Cellular Imaging and Drug Delivery. *Angewandte Chemie International Edition* **2015,** *54* (8), 2431-2435.

29. Zhang, Q.; Jiang, Q.; Li, N.; Dai, L.; Liu, Q.; Song, L.; Wang, J.; Li, Y.; Tian, J.; Ding, B.; Du, Y., DNA Origami as an In Vivo Drug Delivery Vehicle for Cancer Therapy. *ACS Nano* **2014,** *8* (7), 6633-6643.

30. Timm, C.; Niemeyer, C. M., Assembly and Purification of Enzyme-Functionalized DNA Origami Structures. *Angewandte Chemie International Edition* **2015,** *54* (23), 6745-6750.

31. Linko, V.; Eerikainen, M.; Kostiainen, M. A., A modular DNA origami-based enzyme cascade nanoreactor. *Chemical Communications* **2015,** *51* (25), 5351-5354.

32. Fu, Y.; Zeng, D.; Chao, J.; Jin, Y.; Zhang, Z.; Liu, H.; Li, D.; Ma, H.; Huang, Q.; Gothelf, K. V.; Fan, C., Single-Step Rapid Assembly of DNA Origami Nanostructures for Addressable Nanoscale Bioreactors. *Journal of the American Chemical Society* **2013,** *135* (2), 696-702.

33. Fu, J.; Liu, M.; Liu, Y.; Woodbury, N. W.; Yan, H., Interenzyme Substrate Diffusion for an Enzyme Cascade Organized on Spatially Addressable DNA Nanostructures. *Journal of the American Chemical Society* **2012,** *134* (12), 5516-5519.

34. Marras, A. E.; Zhou, L.; Su, H.-J.; Castro, C. E., Programmable motion of DNA origami mechanisms. *Proceedings of the National Academy of Sciences* **2015,** *112* (3), 713-718.

35. Liber, M.; Tomov, T. E.; Tsukanov, R.; Berger, Y.; Nir, E., A Bipedal DNA Motor that Travels Back and Forth between Two DNA Origami Tiles. *Small* **2015,** *11* (5), 568-575.

36. Ke, Y.; Douglas, S. M.; Liu, M.; Sharma, J.; Cheng, A.; Leung, A.; Liu, Y.; Shih, W. M.; Yan, H., Multilayer DNA Origami Packed on a Square Lattice. *Journal of the American Chemical Society* **2009,** *131* (43), 15903-15908.

37. Busch, W.; Saier, M. H., Jr., The transporter classification (TC) system, 2002. *Critical reviews in biochemistry and molecular biology* **2002,** *37* (5), 287-337.

38. Luckey, M., Membrane structural biology : with biochemical and biophysical foundations. **2008**.

39. Jap, B. K.; Walian, P. J., Structure and functional mechanism of porins. *Physiological Reviews* **1996,** *76* (4), 1073-1088.

40. Parker, M. W.; Feil, S. C., Pore-forming protein toxins: from structure to function. *Progress in Biophysics and Molecular Biology* **2005,** *88* (1), 91-142.

41. Freedman, J. C., Chapter 4 - Ionophores in Planar Lipid Bilayers. In *Cell Physiology Source Book (Fourth Edition)*, Sperelakis, N., Ed. Academic Press: San Diego, 2012; pp 61-66.

42. Novilla, M. N., Chapter 29 - Ionophores. In *Reproductive and Developmental Toxicology*, Gupta, R. C., Ed. Academic Press: San Diego, 2011; pp 373-384.

43. Langecker, M.; Arnaut, V.; Martin, T. G.; List, J.; Renner, S.; Mayer, M.; Dietz, H.; Simmel, F. C., Synthetic Lipid Membrane Channels Formed by Designed DNA Nanostructures. *Science* **2012,** *338* (6109), 932-936.

44. Burns, J. R.; Stulz, E.; Howorka, S., Self-Assembled DNA Nanopores That Span Lipid Bilayers. *Nano Letters* **2013,** *13* (6), 2351-2356.

45. Burns, J. R.; Gopfrich, K.; Wood, J. W.; Thacker, V. V.; Stulz, E.; Keyser, U. F.; Howorka, S., Lipid-Bilayer-Spanning DNA Nanopores with a Bifunctional Porphyrin Anchor. *Angewandte Chemie-International Edition* **2013,** *52* (46), 12069-12072.

46. Arnott, P. M.; Howorka, S., A Temperature-Gated Nanovalve Self-Assembled from DNA to Control Molecular Transport across Membranes. *ACS Nano* **2019,** *13* (3), 3334-3340.

47. Kocabey, S.; Kempter, S.; List, J.; Xing, Y.; Bae, W.; Schiffels, D.; Shih, W. M.; Simmel, F. C.; Liedl, T., Membrane-Assisted Growth of DNA Origami Nanostructure Arrays. *ACS Nano* **2015,** *9* (4), 3530-3539.

48. Conway, J. W.; Madwar, C.; Edwardson, T. G.; McLaughlin, C. K.; Fahkoury, J.; Lennox, R. B.; Sleiman, H. F., Dynamic Behavior of DNA Cages Anchored on Spherically Supported Lipid Bilayers. *Journal of the American Chemical Society* **2014,** *136* (37), 12987-12997.

49. Gopfrich, K.; Li, C. Y.; Mames, I.; Bhamidimarri, S. P.; Ricci, M.; Yoo, J.; Mames, A.; Ohmann, A.; Winterhalter, M.; Stulz, E.; Aksimentiev, A.; Keyser, U. F., Ion Channels Made from a Single Membrane-Spanning DNA Duplex. *Nano Letters* **2016,** *16* (7), 4665-4669.

50. Zhou, J. H.; Pai, B. S.; Reed, M. W.; Gamper, H. B.; Lukhtanov, E.; Podyminogin, M.; Meyer, R. B.; Cheng, Y.-c., Discovery of Short, 3′-Cholesterol-modified DNA Duplexes with Unique Antitumor Cell Activity. *Cancer Research* **1994,** *54* (22), 5783-5787.

51. Reed, M. W.; Lukhtanov, E.; Gorn, V.; Lucas, D. D.; Zhou, J. H.; Pai, S. B.; Cheng, Y.-c.; Meyer, R. B., Structure-Activity Relationships of Cytotoxic Cholesterol-Modified DNA Duplexes. *Journal of Medicinal Chemistry* **1995,** *38* (22), 4587-4596.

52. Seifert, A.; Göpfrich, K.; Burns, J. R.; Fertig, N.; Keyser, U. F.; Howorka, S., Bilayer-Spanning DNA Nanopores with Voltage-Switching between Open and Closed State. *ACS Nano* **2015,** *9* (2), 1117-1126.

53. Whitehouse, W. L.; Noble, J. E.; Ryadnov, M. G.; Howorka, S., Cholesterol Anchors Enable Efficient Binding and Intracellular Uptake of DNA Nanostructures. *Bioconjugate Chemistry* **2019**.

54. Juarranz, A.; Jaen, P.; Sanz-Rodriguez, F.; Cuevas, J.; Gonzalez, S., Photodynamic therapy of cancer. Basic principles and applications. *Clinical & Translational Oncology* **2008,** *10* (3), 148-154.

55. Sylvain, I.; Zerrouki, R.; Granet, R.; Huang, Y. M.; Lagorce, J. F.; Guilloton, M.; Blais, J. C.; Krausz, P., Synthesis and biological evaluation of thioglycosylated porphyrins for an application in photodynamic therapy. *Bioorganic & Medicinal Chemistry* **2002,** *10* (1), 57-69.

56. Allison, R. R.; Moghissi, K., Photodynamic Therapy (PDT): PDT Mechanisms. *Clin Endosc* **2013,** *46* (1), 24-9.

57. Castano, A. P.; Demidova, T. N.; Hamblin, M. R., Mechanisms in photodynamic therapy: part one—-photosensitizers, photochemistry and cellular localization. *Photodiagnosis Photodyn Ther* **2004,** *1* (4), 279-93.

58. Kinsella, T. J.; Colussi, V. C.; Oleinick, N. L.; Sibata, C. H., Photodynamic therapy in oncology. *Expert Opinion on Pharmacotherapy* **2001,** *2* (6), 917-927.

59. Alonso, C.; Boyle, R. W., Bioconjugates of porphyrins and Related Molcules for Photodynamic Therapy. In *Handbook of Porphyrin Science with Applications to Chemistry, Physics, Materials Science, Engineering, Biology and Medicine*, Kadish, K.; Smith, K.; Guilard, R., Eds. World Scientific: 2010; Vol. Volume 4 Phototherapy, Radioimmunotherapy and Imaging.

60. Chen, X.; Hui, L.; Foster, D. A.; Drain, C. M., Efficient synthesis and photodynamic activity of porphyrin-saccharide conjugates: Targeting and incapacitating cancer cells. *Biochemistry* **2004,** *43* (34), 10918-10929.

61. Temizel, E.; Sagir, T.; Ayan, E.; Isik, S.; Ozturk, R., Delivery of lipophilic porphyrin by liposome vehicles: preparation and photodynamic therapy activity against cancer cell lines. *Photodiagnosis Photodyn Ther* **2014,** *11* (4), 537-45.

62. Smith, K.; Malatesti, N.; Cauchon, N.; Hunting, D.; Lecomte, R.; van Lier, J. E.; Greenman, J.; Boyle, R. W., Mono- and tri-cationic porphyrin–monoclonal antibody conjugates: photodynamic activity and mechanism of action. *Immunology* **2011,** *132* (2), 256-65.

63. Woodburn, K. W.; Fan, Q.; Kessel, D.; Luo, Y.; Young, S. W., Photodynamic therapy of B16F10 murine melanoma with lutetium texaphyrin. *J Invest Dermatol* **1998,** *110* (5), 746-51.

64. Zilberstein, J.; Schreiber, S.; Bloemers, M. C.; Bendel, P.; Neeman, M.; Schechtman, E.; Kohen, F.; Scherz, A.; Salomon, Y., Antivascular treatment of solid melanoma tumors with bacteriochlorophyll-serine-based photodynamic therapy. *Photochem Photobiol* **2001,** *73* (3), 257-66.

65. Barbazetto, I. A.; Lee, T. C.; Rollins, I. S.; Chang, S.; Abramson, D. H., Treatment of choroidal melanoma using photodynamic therapy. *Am J Ophthalmol* **2003,** *135* (6), 898-9.

66. Sheleg, S. V.; Zhavrid, E. A.; Khodina, T. V.; Kochubeev, G. A.; Istomin, Y. P.; Chalov, V. N.; Zhuravkin, I. N., Photodynamic therapy with chlorin e(6) for skin metastases of melanoma. *Photodermatol Photoimmunol Photomed* **2004,** *20* (1), 21-6.

67. Mroz, P.; Huang, Y. Y.; Szokalska, A.; Zhiyentayev, T.; Janjua, S.; Nifli, A. P.; Sherwood, M. E.; Ruzie, C.; Borbas, K. E.; Fan, D.; Krayer, M.; Balasubramanian, T.; Yang, E.; Kee, H. L.; Kirmaier, C.; Diers, J. R.; Bocian, D. F.; Holten, D.; Lindsey, J. S.; Hamblin, M. R., Stable synthetic bacteriochlorins overcome the resistance of melanoma to photodynamic therapy. *Faseb j* **2010,** *24* (9), 3160-70.

68. Nelson, J. S.; McCullough, J. L.; Berns, M. W., Photodynamic therapy of human malignant melanoma xenografts in athymic nude mice. *J Natl Cancer Inst* **1988,** *80* (1), 56-60.

69. Huang, Y.-Y.; Vecchio, D.; Avci, P.; Yin, R.; Garcia-Diaz, M.; Hamblin, M. R., Melanoma resistance to photodynamic therapy: new insights. *Biol Chem* **2013,** *394* (2), 239-250.

70. Sharma, K. V.; Bowers, N.; Davids, L. M., Photodynamic therapy-induced killing is enhanced in depigmented metastatic melanoma cells. *Cell Biology International* **2011,** *35* (9), 939-944.

71. Hadjur, C.; Richard, M. J.; Parat, M. O.; Jardon, P.; Favier, A., Photodynamic effects of hypericin on lipid peroxidation and antioxidant status in melanoma cells. *Photochem Photobiol* **1996,** *64* (2), 375-81.

72. Ali, H.; van Lier, J. E., Porphyrins and Phthalocyanines as Photosensitizers and Radiosensitizers. In *Handbook of Porphyrin Science with Applications to Chemistry, Physics, Materials Science, Engineering, Biology and Medicine*, Kadish, K.; Smith, K.; Guilard, R., Eds. World Scientific: 2010; Vol. Volume 4 Phototherapy, Radioimmunotherapy and Imaging.

73. Luksiene, Z., Photodynamic therapy: mechanism of action and ways to improve the efficiency of treatment. *Medicina (Kaunas)* **2003,** *39* (12), 1137-50.

74. Burge, S.; Wallis, D., Oxford Handbook of Medical Dermatology. 'Oxford University Press': Oxford, UK.

75. Graham-Brown, R.; Burns, T., *Dermatology*. 9 th ed.; Blackwell Publishing 2007.

76. CancerReseachUK What is skin cancer? https://www.cancerresearchuk.org/about-cancer/skin-cancer/about-skin-cancer (accessed 24/03/2020).

77. SEER Training Modules, Layers of the Skin. https://training.seer.cancer.gov/melanoma/anatomy/layers.html (accessed 11/10/2016).

78. Rubin, A. I.; Chen, E. H.; Ratner, D., Basal-Cell Carcinoma. *New England Journal of Medicine* **2005,** *353* (21), 2262-2269.

79. Alam, M.; Ratner, D., Cutaneous Squamous-Cell Carcinoma. *New England Journal of Medicine* **2001,** *344* (13), 975-983.

80. Burton, K. A.; Ashack, K. A.; Khachemoune, A., Cutaneous Squamous Cell Carcinoma: A Review of High-Risk and Metastatic Disease. *American Journal of Clinical Dermatology* **2016,** *17* (5), 491-508.

81. Wong, C. S. M.; Strange, R. C.; Lear, J. T., Basal cell carcinoma. *BMJ* **2003,** *327* (7418), 794-798.

82. Zhang, N.; Yin, Y.; Xu, S.-J.; Chen, W.-S., 5-Fluorouracil: mechanisms of resistance and reversal strategies. *Molecules* **2008,** *13* (8), 1551-1569.

83. Gold, M. H.; Goldman, M. P., 5-aminolevulinic acid photodynamic therapy: where we have been and where we are going. *Dermatol Surg* **2004,** *30* (8), 1077-83; discussion 1083-4.

84. Gupta, A. K.; Ryder, J. E., Photodynamic Therapy and Topical Aminolevulinic Acid. *American Journal of Clinical Dermatology* **2003,** *4* (10), 699-708.

85. Society, A. C. Key Statistics for Melanoma Skin Cancer. https://www.cancer.org/cancer/melanoma-skin-cancer/about/key-statistics.html (accessed 13/11/2019).

86. Rigel, D. S.; Carucci, J. A., Malignant melanoma: Prevention, early detection, and treatment in the 21st century. *CA: A Cancer Journal for Clinicians* **2000,** *50* (4), 215-236.

87. Bhatia, S.; Tykodi, S. S.; Thompson, J. A., Treatment of metastatic melanoma: an overview. *Oncology (Williston Park)* **2009,** *23* (6), 488-496.

88. Institute, N. C. Melanoma Treatment (PDQ) - Patient Version. https://www.cancer.gov/types/skin/patient/melanoma-treatment-pdq (accessed 13/11/2019).

89. Jiang, J.; Sharma, S. D.; Fink, J. L.; Hadley, M. E.; Hruby, V. J., Melanotropic peptide receptors: membrane markers of human melanoma cells. *Exp Dermatol* **1996,** *5* (6), 325-33.

90. Ghanem, G. E.; Comunale, G.; Libert, A.; Vercammen-Grandjean, A.; Lejeune, F. J., Evidence for alpha-melanocyte-stimulating hormone (alpha-MSH) receptors on human malignant melanoma cells. *Int J Cancer* **1988,** *41* (2), 248-55.

91. Siegrist, W.; Solca, F.; Stutz, S.; Giuffre, L.; Carrel, S.; Girard, J.; Eberle, A. N., Characterization of receptors for alpha-melanocyte-stimulating hormone on human melanoma cells. *Cancer Res* **1989,** *49* (22), 6352-8.

92. Bagutti, C.; Oestreicher, M.; Siegrist, W.; Oberholzer, M.; Eberle, A. N., alpha-MSH receptor autoradiography on mouse and human melanoma tissue sections and biopsies. *J Recept Signal Transduct Res* **1995,** *15* (1-4), 427-42.

93. Froidevaux, S.; Calame-Christe, M.; Tanner, H.; Sumanovski, L.; Eberle, A. N., A Novel DOTA-α-Melanocyte–Stimulating Hormone Analog for Metastatic Melanoma Diagnosis. *Journal of Nuclear Medicine* **2002,** *43* (12), 1699-1706.

94. Froidevaux, S.; Calame-Christe, M.; Schuhmacher, J.; Tanner, H.; Saffrich, R.; Henze, M.; Eberle, A. N., A Gallium-Labeled DOTA-α-Melanocyte- Stimulating Hormone Analog for PET Imaging of Melanoma Metastases. *Journal of Nuclear Medicine* **2004,** *45* (1), 116-123.

95. Bigliardi, P. L.; Rout, B.; Pant, A.; Krishnan-Kutty, V.; Eberle, A. N.; Srinivas, R.; Burkett, B. A.; Bigliardi-Qi, M., Specific Targeting of Melanotic Cells with Peptide Ligated Photosensitizers for Photodynamic Therapy. *Scientific Reports* **2017,** *7* (1), 15750.

96. Wood, J. The structural analysis of porphyrin modified DNA and the construction of a molecular wire University of Southampton, 2015.

97. Stillwell, W., Chapter 5 - Membrane Polar Lipids. In *An Introduction to Biological Membranes (Second Edition)*, Stillwell, W., Ed. Elsevier: 2016; pp 63-87.

98. Chaltin, P.; Margineanu, A.; Marchand, D.; Van Aerschot, A.; Rozenski, J.; De Schryver, F.; Herrmann, A.; Müllen, K.; Juliano, R.; Fisher, M. H.; Kang, H.; De Feyter, S.; Herdewijn, P., Delivery of Antisense Oligonucleotides Using Cholesterol-Modified Sense Dendrimers and Cationic Lipids. *Bioconjugate Chemistry* **2005,** *16* (4), 827-836.

99. Alahari, S. K.; Dean, N. M.; Fisher, M. H.; Delong, R.; Manoharan, M.; Tivel, K. L.; Juliano, R. L., Inhibition of expression of the multidrug resistance-associated P-glycoprotein of by phosphorothioate and 5' cholesterol-conjugated phosphorothioate antisense oligonucleotides. *Molecular Pharmacology* **1996,** *50* (4), 808-819.

100. Gusachenko, O.; Kravchuk, Y.; Konevets, D.; Silnikov, V.; Vlassov, V. V.; Zenkova, M. A., Transfection Efficiency of 25-kDa PEI–Cholesterol Conjugates with Different Levels of Modification. *Journal of Biomaterials Science, Polymer Edition* **2009,** *20* (7-8), 1091-1110.

101. Yang, J.; Chen, C.; Tang, X., Cholesterol-Modified Caged siRNAs for Photoregulating Exogenous and Endogenous Gene Expression. *Bioconjugate Chemistry* **2018,** *29* (4), 1010-1015.

102. Carta, G.; Murru, E.; Banni, S.; Manca, C., Palmitic Acid: Physiological Role, Metabolism and Nutritional Implications. *Front Physiol* **2017,** *8*, 902-902.

103. Stillwell, W., Chapter 4 - Membrane Lipids: Fatty Acids. In *An Introduction to Biological Membranes (Second Edition)*, Stillwell, W., Ed. Elsevier: 2016; pp 49-62.

104. Huang, X.; Nakanishi, K.; Berova, N., Porphyrins and metalloporphyrins: versatile circular dichroic reporter groups for structural studies. *Chirality* **2000,** *12* (4), 237-55.

105. Rita, G., *The Use of Spectrophotometry UV-Vis for the Study of Porphyrins*. INTECH Open Access Publisher: 2012.

106. Spellane, P. J.; Gouterman, M.; Antipas, A.; Kim, S.; Liu, Y. C., Porphyrins. 40. Electronic spectra and four-orbital energies of free-base, zinc, copper, and palladium tetrakis(perfluorophenyl)porphyrins. *Inorganic Chemistry* **1980,** *19* (2), 386-391.

107. Gouterman, M., Study of the Effects of Substitution on the Absorption Spectra of Porphin. *The Journal of Chemical Physics* **1959,** *30* (5), 1139-1161.

108. Maiti, N. C.; Mazumdar, S.; Periasamy, N., J- and H-Aggregates of Porphyrin−Surfactant Complexes: Time-Resolved Fluorescence and Other Spectroscopic Studies. *The Journal of Physical Chemistry B* **1998,** *102* (9), 1528-1538.

109. PÜNtener, A. G.; Schlesinger, U., 9 - Natural Dyes. In *Colorants for Non-Textile Applications*, Freeman, H. S.; Peters, A. T., Eds. Elsevier Science: Amsterdam, 2000; pp 382-455.

110. Rothemund, P., FORMATION OF PORPHYRINS FROM PYRROLE AND ALDEHYDES. *Journal of the American Chemical Society* **1935,** *57* (10), 2010-2011.

111. Rothemund, P., A New Porphyrin Synthesis. The Synthesis of Porphin1. *Journal of the American Chemical Society* **1936,** *58* (4), 625-627.

112. Rothemund, P.; Menotti, A. R., Porphyrin Studies. IV.1 The Synthesis of α,β,γ,δ-Tetraphenylporphine. *Journal of the American Chemical Society* **1941,** *63* (1), 267-270.

113. Adler, A. D.; Longo, F. R.; Finarelli, J. D.; Goldmacher, J.; Assour, J.; Korsakoff, L., A simplified synthesis for meso-tetraphenylporphine. *The Journal of Organic Chemistry* **1967,** *32* (2), 476-476.

114. Lindsey, J. S.; Hsu, H. C.; Schreiman, I. C., Synthesis of tetraphenylporphyrins under very mild conditions. *Tetrahedron Letters* **1986,** *27* (41), 4969-4970.

115. Lindsey, J. S.; Schreiman, I. C.; Hsu, H. C.; Kearney, P. C.; Marguerettaz, A. M., Rothemund and Adler-Longo reactions revisited: synthesis of tetraphenylporphyrins under equilibrium conditions. *The Journal of Organic Chemistry* **1987,** *52* (5), 827-836.

116. Bouamaied, I.; Stulz, E., Synthesis and Spectroscopic Properties of Porphyrin-Substituted Uridine and Deoxyuridine. *Synlett* **2004,** *2004* (09), 1579-1583.

117. Bouamaied, I.; Stulz, E., Porphyrin-Substituted Dinucleotides: Synthesis and Spectroscopy. *CHIMIA International Journal for Chemistry* **2005,** *59* (3), 101-104.

118. Fendt, L.-A.; Bouamaied, I.; Thöni, S.; Amiot, N.; Stulz, E., DNA as Supramolecular Scaffold for Porphyrin Arrays on the Nanometer Scale. *Journal of the American Chemical Society* **2007,** *129* (49), 15319-15329.

119. Bouamaied, I.; Nguyen, T.; Rühl, T.; Stulz, E., Supramolecular helical porphyrin arrays using DNA as a scaffold. *Organic & Biomolecular Chemistry* **2008,** *6* (21), 3888-3891.

120. Nguyen, T.; Brewer, A.; Stulz, E., Duplex Stabilization and Energy Transfer in Zipper Porphyrin–DNA. *Angewandte Chemie International Edition* **2009,** *48* (11), 1974-1977.

121. Brewer, A.; Siligardi, G.; Neylon, C.; Stulz, E., Introducing structural flexibility into porphyrin–DNA zipper arrays. *Organic & Biomolecular Chemistry* **2011,** *9* (3), 777-782.

122. Oka, Y.; Nakajima, K.; Nagao, K.; Miura, K.; Ishii, N.; Kobayashi, H., 293FT cells transduced with four transcription factors (OCT4, SOX2, NANOG, and LIN28) generate aberrant ES-like cells. *J Stem Cells Regen Med* **2010,** *6* (3), 149-156.

123. O'Brien, J.; Wilson, I.; Orton, T.; Pognan, F., Investigation of the Alamar Blue (resazurin) fluorescent dye for the assessment of mammalian cell cytotoxicity. *European Journal of Biochemistry* **2000,** *267* (17), 5421-5426.

124. Rampersad, S. N., Multiple applications of Alamar Blue as an indicator of metabolic function and cellular health in cell viability bioassays. *Sensors (Basel)* **2012,** *12* (9), 12347-12360.

125. Feoktistova, M.; Geserick, P.; Leverkus, M., Crystal Violet Assay for Determining Viability of Cultured Cells. *Cold Spring Harbor Protocols* **2016,** *2016* (4), pdb.prot087379.

126. Thomas, P.; Smart, T. G., HEK293 cell line: A vehicle for the expression of recombinant proteins. *Journal of Pharmacological and Toxicological Methods* **2005,** *51* (3), 187-200.

127. Dumont, J.; Euwart, D.; Mei, B.; Estes, S.; Kshirsagar, R., Human cell lines for biopharmaceutical manufacturing: history, status, and future perspectives. *Critical Reviews in Biotechnology* **2016,** *36* (6), 1110-1122.

128. Li, W.-Y.; Xu, J.-G.; He, X.-W., Characterization of the Binding of Methylene Blue to DNA by Spectroscopic Methods. *Analytical Letters* **2000,** *33* (12), 2453-2464.

129. Tuite, E.; Norden, B., Sequence-Specific Interactions of Methylene Blue with Polynucleotides and DNA: A Spectroscopic Study. *Journal of the American Chemical Society* **1994,** *116* (17), 7548-7556.

130. Nafisi, S.; Saboury, A. A.; Keramat, N.; Neault, J.-F.; Tajmir-Riahi, H.-A., Stability and structural features of DNA intercalation with ethidium bromide, acridine orange and methylene blue. *Journal of Molecular Structure* **2007,** *827* (1), 35-43.

131. Monro, S.; Colón, K. L.; Yin, H.; Roque, J.; Konda, P.; Gujar, S.; Thummel, R. P.; Lilge, L.; Cameron, C. G.; McFarland, S. A., Transition Metal Complexes and Photodynamic Therapy from a Tumor-Centered Approach: Challenges, Opportunities, and Highlights from the Development of TLD1433. *Chemical Reviews* **2019,** *119* (2), 797-828.

132. Schneider, C. A.; Rasband, W. S.; Eliceiri, K. W., NIH Image to ImageJ: 25 years of image analysis. *Nature Methods* **2012,** *9* (7), 671-675.

133. Ou-Yang, H.; Stamatas, G.; Kollias, N., Spectral Responses of Melanin to Ultraviolet A Irradiation. *Journal of Investigative Dermatology* **2004,** *122* (2), 492-496.

134. Winkler, J.; Urban, E.; Losert, D.; Wacheck, V.; Pehamberger, H.; Noe, C. R., A novel concept for ligand attachment to oligonucleotides via a 2'-succinyl linker. *Nucleic Acids Res* **2004,** *32* (2), 710-8.

135. Damha, M. J.; Giannaris, P. A.; Zabarylo, S. V., An improved procedure for derivatization of controlled-pore glass beads for solid-phase oligonucleotide synthesis. *Nucleic Acids Res* **1990,** *18* (13), 3813-21.

136. Pon, R. T.; Yu, S.; Sanghvi, Y. S., Rapid esterification of nucleosides to solid-phase supports for oligonucleotide synthesis using uronium and phosphonium coupling reagents. *Bioconjug Chem* **1999,** *10* (6), 1051-7.

137. Pon, R. T., Attachment of Nucleosides to Solid-Phase Supports. *Current Protocols in Nucleic Acid Chemistry* **2000,** *00* (1), 3.2.1-3.2.23.

138. Burns, J. R.; Howorka, S., Structural and Functional Stability of DNA Nanopores in Biological Media. *Nanomaterials (Basel)* **2019,** *9* (4).

139. Burns, J. R.; Howorka, S., Defined Bilayer Interactions of DNA Nanopores Revealed with a Nuclease-Based Nanoprobe Strategy. *ACS Nano* **2018,** *12* (4), 3263-3271.